Characterising the Phenotype and Impact of Adipose in Idiopathic Intracranial Hypertension

By

Connar Stanley James Westgate

A thesis submitted to the University of Birmingham for the degree of DOCTOR OF PHILOSOPHY

Institute of Metabolism and Systems Research

College of Medical and Dental Sciences

University of Birmingham

April 2019

Abstract

Idiopathic intracranial hypertension (IIH) is a rare disease that primarily affects obese women of reproductive age, characterised by raised intracranial pressure (ICP) and papilloedema that drives chronic debilitating headache and visual loss. The aetiology of IIH is uncertain, however it is clear that weight loss is therapeutic and reduces ICP, headache, and visual morbidity. Novel data has highlighted that female IIH patients have an androgen excess phenotype. However the role of adipose tissue and androgens in the pathogenesis of IIH remains unclear.

Utilising RNA-sequencing, NMR-based metabolomics and secretomic techniques, it has been identified that *ex vivo* subcutaneous adipose tissue from female IIH patients has features of glucocorticoid excess including increased lipolysis, ribosomal subunit depletion and a preference for lipid synthesis, driven by intra-adipose cortisol accumulation. Moreover, this phenotype is driving hyperleptinaemia in IIH patients. Additionally, a novel *in vitro* Na^+/K^+ ATPase activity assay was developed, which demonstrated that testosterone increases Na^+/K^+ ATPase activity, suggesting capacity to increase ICP.

Together, these data highlight that adipose tissue in IIH has characteristics of glucocorticoid excess, contributing to a specific metabolic phenotype and that testosterone could be driving raised intracranial pressure, highlighting routes for the development of novel therapeutics and treatments for IIH.

Acknowledgments

A PhD is a journey, as such I wish to thank those who have joined me on this journey. Firstly I want to convey my heart felt gratitude to my supervisors, firstly Alex Sinclair for her guidance and mentorship which has helped me grow as a scientist, and for her help in keeping me motivated when things were not going according to plan. Secondly, to Gareth Lavery, for his calming influence, experience and oversight in guiding this work.

I also wish to thank members past and present of the metabolic neurology group who have helped enrich my PhD. In particular, I wish to thank Hannah Botfield who taught me pretty much everything in the lab and for being an excellent mentor. I also wish to thank James Mitchell for his critical mind and our stimulating conversations about science and beyond.

I also which to thank members of the IMSR for their collective scientific companionship, I however wish to specifically thank David Hodson and Nick Fine for the their assistance with live cell microscopy, Dean Larner for conferring his sage wisdom of histology and Mick O'Reilly for his advice on all things adipose and androgens. I wish to thank the lunchtime group, especially the 'Coup' team of Haydn, Rob, Nick and *ρ*-dog who helped keep me sane with the immortal words '3 coins as the duke'.

I want to thank the Danish Headache Centre for being welcoming during my time there. I also want to thank the bariatric team at Heartlands hospital, especially Mr Singhal and Mr Super for their exemplary efforts in recruiting

patients and providing me with precious tissue samples. Without these, my thesis would look very different.

Thanks with all my heart go to my family for their continuous and unwavering support during my PhD, especially during my write-up. You have always believed in me and encouraged me to succeed.

To Ola, who has been at my side during the highs and lows of my PhD, I want to thank you for your continuous support, encouragement and patience.

For Daniel, Elliott and Lillyanna

Declaration

I confirm that the data presented in this thesis is my own and that I have been involved in the design, conduct, data analysis and the preparation of the thesis. The following aspects of this thesis were undertaken as part of collaboration:

1) Mark Walsh and Daniel Hebenstreit of the University of Warwick and Ildem Akerman and Gabrielle Smith of the University of Birmingham carried out bioinformatic analysis of RNA sequencing data.

2) Christian Ludwig acquired NMR spectra within the study.

3) William Scotton and Hannah Botfield carried out surgeries on a portion of the animals in the *in vivo* ICP experiments.

I undertook all other experiments and statistical analyses within this thesis

Publications and presentations

Peer reviewed papers directly from this doctoral research

- O'Reilly MW*, **Westgate CSJ***, Hornby C*, Botfield HF*, Taylor AE, Markey K, Mitchell JL, Scotton WJ, Mollan SP, Yiangou A, Jenkinson C, Gilligan LC, Sherlock M, Gibney J, Tomlinson JW, Hodson DJ, Arlt W and Sinclair A. *A unique androgen excess signature in idiopathic intracranial hypertension is linked to cerebrospinal fluid dynamics*. Journal of Clinical Investigation Impact, 2019; 4(6): e125348. Portions of this paper appear in chapters 5 and 6.
- Scotton WJ, Botfield HF, **Westgate CSJ**, Mitchell JL, Yiangou A, Uldall MS, Jensen RH, Sinclair A. *Topiramate is more effective than acetazolamide at lowering intracranial pressure*. Cephalalgia, 2018. Portions of this paper are in chapter 5.
- Botfield HF, Uldall M, **Westgate CSJ**, Mitchell JL, Hagen SM, Gonzalez AM, Hodson DJ, Jensen RH, Sinclair A. *A glucagon-like peptide-1 receptor agonist reduces intracranial pressure in a rat model of hydrocephalus*. Science Translational Medicine, 2017; 9(404), eaan0972. None of this work appears in this thesis.
- Hornby C, Botfield HF, O'Reilly MW, **Westgate CSJ**, Mitchell JL, Mollan SP, Manolopoulos K, Tomlinson J, Sinclair A. *Evaluating the Fat Distribution in Idiopathic Intracranial Hypertension Using Dual-Energy X-ray Absorptiometry Scanning*. Neuro-Ophthalmology, 2018; 42 (2),99-104. None of this work appears in this thesis.

Conference abstracts and talks

- ‘Subcutaneous adipose tissue from patients with idiopathic intracranial hypertension displays distinct metabolic features’ at Society for Endocrinology BES meeting , Glasgow, November 2018
- ‘Subcutaneous adipose tissue from patients with idiopathic intracranial hypertension displays unique transcriptomic and metabolic features’ at Migraine Trust international symposium, London, September 2018
- ‘Evaluating the role of testosterone in cerebrospinal fluid secretion’ at the Society for Endocrinology BES meeting, Harrogate, November 2017
- ‘Characterising the role of androgens in cerebrospinal fluid secretion’ Invited talk at the UK CSF day, Birmingham, September 2017
- ‘Developing a cerebrospinal fluid secretion assay using a genetically encoded biosensor to evaluate therapeutic and pathogenic molecules in idiopathic intracranial hypertension’ at International Headache Society congress, Vancouver September 2017 (Poster of distinction)

Table of Contents

List of Figures

List of tables

List of abbreviations

3β-HSD – 3β Hydroxysteroid dehydrogenase

11β-HSD – 11β Hydroxysteroid dehydrogenase

17β-HSD – 17β Hydroxysteroid dehydrogenase

A4 – Androstenedione

AKR1C3 – Aldo-ketoreductase type 1C3

BCAA – Branched chain amino acids

BMI – Body mass index

cDNA – Copy deoxyribose nucleic acid

CA – Carbonic anhydrase

CP – Choroid plexus

CPe – Choroid plexus epithelial

CSF – Cerebrospinal Fluid

D_2O – Deuterium

DHEA – Dehydroepiandrosterone

DHT – Dihydrotestosterone

DMEM – Dulbecco's modified Eagle medium

DSS – 4,4-dimethyl-4-silapentane-1-sulfonic acid

ELISA – Enzyme linked immunosorbent assay

FDR – False discovery rate

FPKM – Fragments per Kilobase Million

GC – Glucocorticoid

ICP – Intracranial pressure

IIH – Idiopathic intracranial hypertension

IIH:DT – Idiopathic intracranial hypertension drug trial

IIH:WT – Idiopathic intracranial hypertension weight trial

HRP – Horseradish Peroxidase

IL – Interleukin

LP – Lumbar puncture

LP-Opp- Lumbar puncture opening pressure

MCP-1 – Monocyte chemoattractant protein 1

MND – Mixed neurological diseases

MNOD – Mixed neuro-ophthalmic diseases

mRNA – Message ribose-nucleic acid

N – Number

NES – Net enrichment score

NMR – Nuclear magnetic resonance

OD – Optical density

OM – Omental

OMHO – Otherwise medically healthy obese

PBS – Phosphate buffered saline

PCOS – Polycystic ovary syndrome

REC – Research ethic committee

RT-qPCR – Quantitative (real-time) polymerase chain reaction

RNA – Ribose nucleic acid

RNA-Seq – RNA sequencing

SC – Subcutaneous

SD – Standard deviation

SEM – Standard error of the mean

T – Testosterone

TNFα – Tumour necrosis factor alpha

Chapter 1 General Introduction

1.1 Idiopathic intracranial Hypertension

Idiopathic intracranial hypertension (IIH) is a neurological condition whose diagnostic criteria were formalised in 1937 by Walter Dandy and termed *pseudotumor cerebri* (Dandy, 1937). IIH is a disease of unknown aetiology where patients present with raised intracranial pressure (ICP) and papilloedema, whereby diagnosis is that of excluding secondary causes for raised ICP according to the modified Dandy criteria (see table 1) (Mollan et al., 2018b). In the general population the incidence of IIH is 4.69 individuals per 100,000 and is rising in line with the obesity epidemic (Mollan et al., 2018a). However in its main patient group, obese women of childbearing age, the incidence is raised to 20 per 100,000 (Markey et al., 2016a). Furthermore 82% of all IIH patients are female (Mollan et al., 2018a).

IIH patients present with chronic debilitating headaches caused by raised ICP which is thought to be derived from disrupted cerebrospinal fluid dynamics (Mollan et al., 2016). The raised ICP drives papilloedema which causes visual defects and in 25% of cases, can lead to permanent visual loss (Corbett et al., 1982).

The raised ICP and subsequent papilloedema and headache are symptoms of an underlying condition that is of unknown aetiology, as such there is a need to understand the pathogenesis of IIH.

1.1.1 Idiopathic intracranial hypertension diagnosis

IIH is primarily a diagnosis of exclusion, where raised ICP secondary to other causes is excluded, as based on the modified Dandy criteria (table 1.1) (Mollan et al., 2018b). A diagnostic lumbar puncture must have a lumbar puncture opening pressure (LP Opp) over 25cmCSF, where cerebrospinal fluid (CSF) is essentially acellular, and falls into normal biochemical parameters. Papilloedema, swelling of the optic disk, must also be present. Suspected IIH patients have neuro-anatomical abnormalities excluded with the exception of an empty sella. Furthermore, patients must have a normal cranial nerve examination with the exception of a 6th cranial nerve palsy (Mollan et al., 2018b).

IIH Diagnostic criteria
Papilloedema
Normal neurological exam except 6th cranial nerve palsy
Evidence of normal neuroanatomy
Normal CSF composition
Raised lumbar puncture opening pressure, >25cm CSF

Table 1.1 Diagnostic criteria for IIH

Table modified from Mollan et al 2018b.

1.1.2 Epidemiology of idiopathic intracranial hypertension

IIH is a rare disease with an incidence in the general population of 4.69 per 100,000 in 2016, up from 2.2 per 100,000 individuals in 2002 (Mollan et al., 2018a). When divided into patient groups IIH has an incidence of 1.6 per 100,000 in men and affects 7.69 per 100,000 women in the UK where women represent 82% of all IIH patients in the UK (Mollan et al., 2018a). The incidence of IIH is greatest in obese women of reproductive age, at 20 in 100,000 (Markey et al., 2016a). The incidence of IIH is increasing in both men and women in line with the obesity epidemic and, as such, is projected to further increase in line with obesity (Mollan et al., 2018a). In the UK, IIH is associated with socio-economic deprivation, a factor also linked with obesity in high income countries (McLaren, 2007; Mollan et al., 2018a).

1.1.3 Idiopathic intracranial pressure and co-morbidities

1.1.3.1 Headache in IIH

IIH has several co-morbidities that affect the quality of life for the patients. The most common co-morbidity is chronic debilitating headache that presents in up to 93% of IIH patients at diagnosis that is often migrainous in phenotype (Jensen et al., 2016). Although raised ICP is thought to be the primary driver of this, IIH headache often persists after resolution of raised ICP and visual defects, highlighting long term quality of life issues for IIH patients (Yri et al., 2014b). Headache was highlighted as the primary determinant of quality of life in IIH (Mulla et al., 2015). Importantly, weight loss improves headache morbidity in IIH (Sinclair et al., 2010a).

1.1.3.2 Visual loss in IIH

Perhaps the most concerning co-morbidity in IIH is visual loss linked to papilloedema, where the retinal artery is occluded, causing retinal ischaemia. It has been demonstrated that visual loss is progressive in IIH, even with therapeutic intervention (Hatem et al., 2018). This visual loss is permanent in 25% IIH patients (Corbett et al., 1982). Due to papilloedema being an obligate symptom in IIH, the potential visual loss represents significant morbidity and a focus of treatment.

1.1.3.3 IIH as a metabolic syndrome

Female IIH patients have an increased incidence of polycystic ovary syndrome (PCOS), ranging from 15%-53%, compared to the general population (8.7%), dependent on the BMI of the IIH population (Avisar et al., 2012; Glueck et al., 2005, 2003; March et al., 2010). This increased incidence of PCOS could be linked to a novel phenotype of androgen excess elucidated in female IIH patients (Appendix 1) (O'Reilly et al., 2019). Conversely, hypoandrogenism is associated with IIH in males (Fraser et al., 2010). Furthermore, recent unpublished work demonstrates that IIH patients have an increased HOMA2-IR score, suggesting insulin resistance. This portfolio of work supports the hypothesis that IIH is a distinct metabolic syndrome as well as a neuro-ophthalmic disease, increasing the need to understand the biochemical and metabolic perturbations in IIH to facilitate more effective long term treatment of IIH (Hornby et al., 2018b).

1.1.3.4 IIH and cognition

Female IIH patients have diminished cognitive ability, with deficits in reaction speed, verbal fluency and executive function. These cognitive deficits persist following improvements in headache and reduction of ICP, thus cognitive deficit represents serious morbidity in IIH (Yri et al., 2014a). Perhaps linked to the chronic headache, IIH patients also present with an increased risk of depression and anxiety that contributes to reduced quality of life (Kleinschmidt et al., 2000; Mulla et al., 2015).

1.1.4 Economic burden of IIH

The comorbidities, particularly the cognitive defects, debilitating chronic headache, associated mental health issues and visual loss contribute to IIH economic burden: in 2011, it was estimated that IIH costs around $444 million in the United States (Friesner et al., 2011). This economic burden of IIH will only increase as the incidence and prevalence of IIH increases in line with the obesity epidemic (Mollan et al., 2018a). Indeed, IIH is projected to cost English health services £462.7 million by 2030, rising from the current hospital cost of £49.9 in 2014 (Mollan et al., 2018a). The total economic cost of IIH in the UK will be much higher due to lost working days and reduced productivity owing to severe headache and depressive episodes. As such there is a need understand the pathogenesis and improve the treatment of IIH for both IIH patients and for the benefit of society.

1.2 Intracranial pressure and cerebrospinal fluid dynamics

Although the aetiology of IIH is unknown, it is apparent that ICP homeostasis is perturbed due to the presence of raised ICP. According to the anatomists Monro and Kellie, ICP is determined by three parameters; the volume of the brain, cerebral blood volume and CSF volume, where cerebral blood volume and CSF are homeostatically controlled and compensate for acute changes in ICP (Kim et al., 2012). Indeed, it is clear that changes in cerebral blood volume, through changes in cerebral blood vessel calibre alters ICP rather than cerebral blood pressure (Dunn, 2002). When any of these three parameters are altered outside physiological parameters, intracranial hypotension or hypertension occurs. CSF leakages are known to cause intracranial hypotension leading to brain slump and significant morbidity. More common are conditions of intracranial hypertension, hydrocephalus, brain tumours and intracranial haemorrhage. In the case of IIH, gross anatomical alterations are excluded in diagnosis, excluding altered brain volume and to a lesser extent alterations in cerebral blood volume (Mollan et al., 2018b). Moreover there is little evidence for altered cerebral perfusion pressure, cerebral blood pressure and systemic blood pressure in IIH, compared to obese controls. Consequently it is likely that altered CSF dynamics in IIH are contributing to the raised ICP, whereby the contribution of CSF to ICP is a balance between CSF secretion and CSF drainage (Mollan et al., 2016).

1.2.1 Anatomy and physiology of CSF

The brain and the spinal cord are enclosed within the rigid cranium and vertebral column respectively, in an anatomical compartment termed the central

nervous system (CNS). Due to being enclosed in this rigid compartment, the brain, blood and CSF exert a pressure. Here the brain and spinal cord are bathed in CSF, a biofluid that has several functions. CSF provides the brain with buoyancy, making the 1.5 kg brain weigh ~45g (Spector et al., 2015). Furthermore the CSF acts as a hydraulic cushion, reducing forces that the brain may endure.

Besides its mechanical properties, the CSF also serves to remove waste, such as amyloid-β, from the brain (Iliff et al., 2012). Furthermore, CSF facilitates the delivery of nutrients, hormones and neurotransmitters such as folate and vitamin C to the brain, where the CSF is the sole source of these nutrients for the brain (Hammarström, 1966; Spector and Johanson, 2014). Within the brain, CSF resides in the cerebral ventricles and parenchymal aqueducts; outside of the brain CSF resides in the cisterna magna and the subarachnoid spaces (Fig 1.1). The subarachnoid spaces are part of the meninges, layers of tissue that line the brain, spinal cord and the internal bony surfaces of the CNS. The deepest meningeal layer is the pia mater, a thin membrane that lines the brain. The arachnoid mater is the intermediate meningeal layer that provides space for CSF to flow. The dura mater is the most superficial meningeal layer and lines the internal ossified surface of the CNS. Together, the meninges provide the brain and spinal cord with structural support.

1.2.2 CSF flow

Traditional teaching dictates that CSF produced in the lateral ventricles flows through the foramina of Monro (intraventricular foramina) reaching the third ventricle where it traverses the aqueduct of Sylvius (cerebral aqueduct) to the

fourth ventricle. From the fourth ventricle, CSF flows through the foramen of Magendie (median aperture) to the cisterna magna, and from the foramina of Luschka (lateral aperture) to the subarachnoid space (Cushing, 1925). CSF also flows through the central canal of the spinal cord. When in the CSF spaces, CSF flows around the brain and spinal cord and is drained through several routes (Fig1.1). CSF flow is not simply a feature of a pressure differential between the ventricles and the CSF spaces. Instead, it is aided by action of motile cilia on the ependymal cells that line the cerebral ventricles and the intra-parenchymal aqueducts, whereby the knockout and dysfunction of said cilia causes a communicating hydrocephalus (Ibañez-Tallon et al., 2004). In humans, CSF flow is pulsatile and displays net movement from the ventricular system to the subarachnoid space (Wagshul et al., 2011).

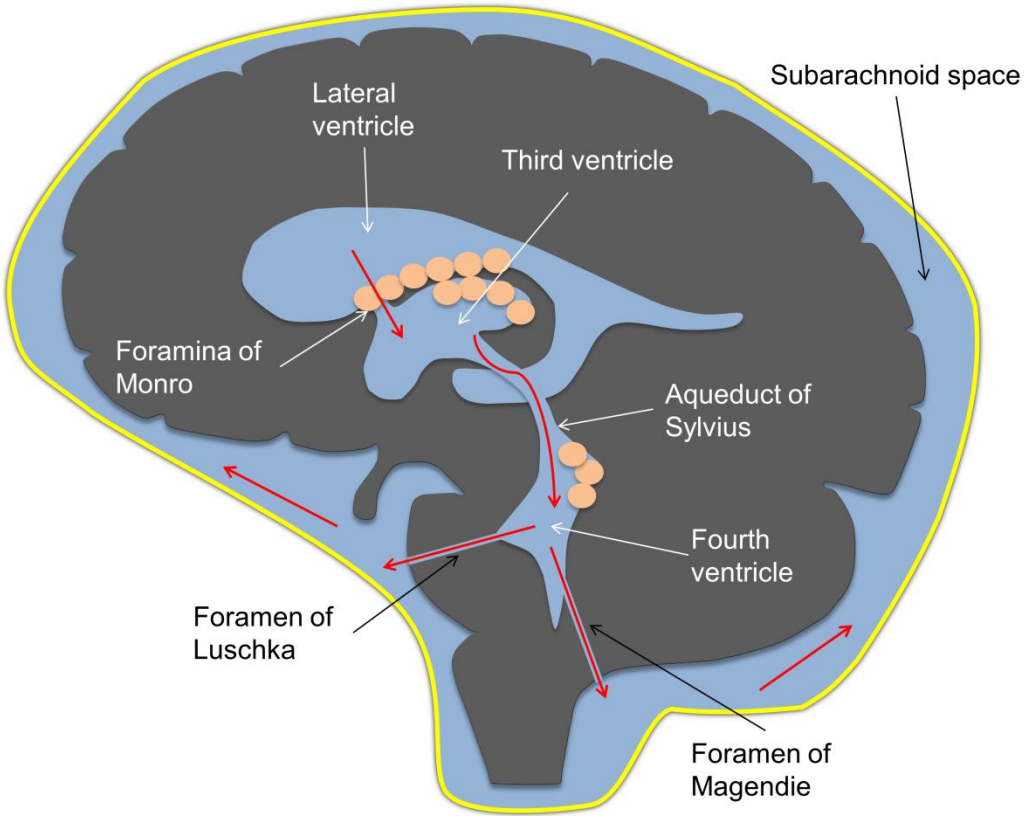

Figure 1.1 Anatomy of the CSF spaces

A diagram in the sagittal plane detailing the anatomy of the CSF spaces in the human central nervous system. Red arrows represent the net flow of CSF, blue represents CSF spaces. Beige circles represent choroid plexus.

1.2.3 CSF production

Humans produce around 500ml of CSF a day, filling the CSF spaces to a total volume of 120-150ml, indicating that the CSF is replaced several times a day with an average production rate of around 20 ml per hour (Nilsson et al., 1992). CSF is produced with diurnal variation, where more CSF is produced during sleeping hours and less produced in waking hours (Nilsson et al., 1992). A portion of CSF is generated from the brain interstitial fluid via the ependymal lining of the ventricles and the pia mater, perhaps through hydrostatic forces.

However the majority of CSF (80%) is generated via the choroid plexus (Brinker et al., 2014).

1.2.3.1 The choroid plexus

CSF is primarily produced by choroid plexus, organs that reside in the lateral, third and fourth ventricles. Histologically the choroid plexus comprises of villi, the functional unit of the choroid plexus. These villi comprise of central, fenestrated capillaries that are surrounded by a monolayer of cells residing on a basement membrane, the choroid plexus epithelial (CPe) cells. These CPe cells are the functional cell of the choroid plexus, whose apical membrane faces the ventricular space and are continuous with the ependymal cells that line the cerebral ventricles (Fig1.2a). CPe cells have been demonstrated to have apical microvilli in non-human primates and rodents (Fig1.2b) (Cornford et al., 1997; Keep and Jones, 1990). These provide a brush border and have been proposed to increase the surface area for both the transportation of nutrients and for the cardinal role of the choroid plexus: CSF secretion (Brown et al., 2004; Cornford et al., 1997).

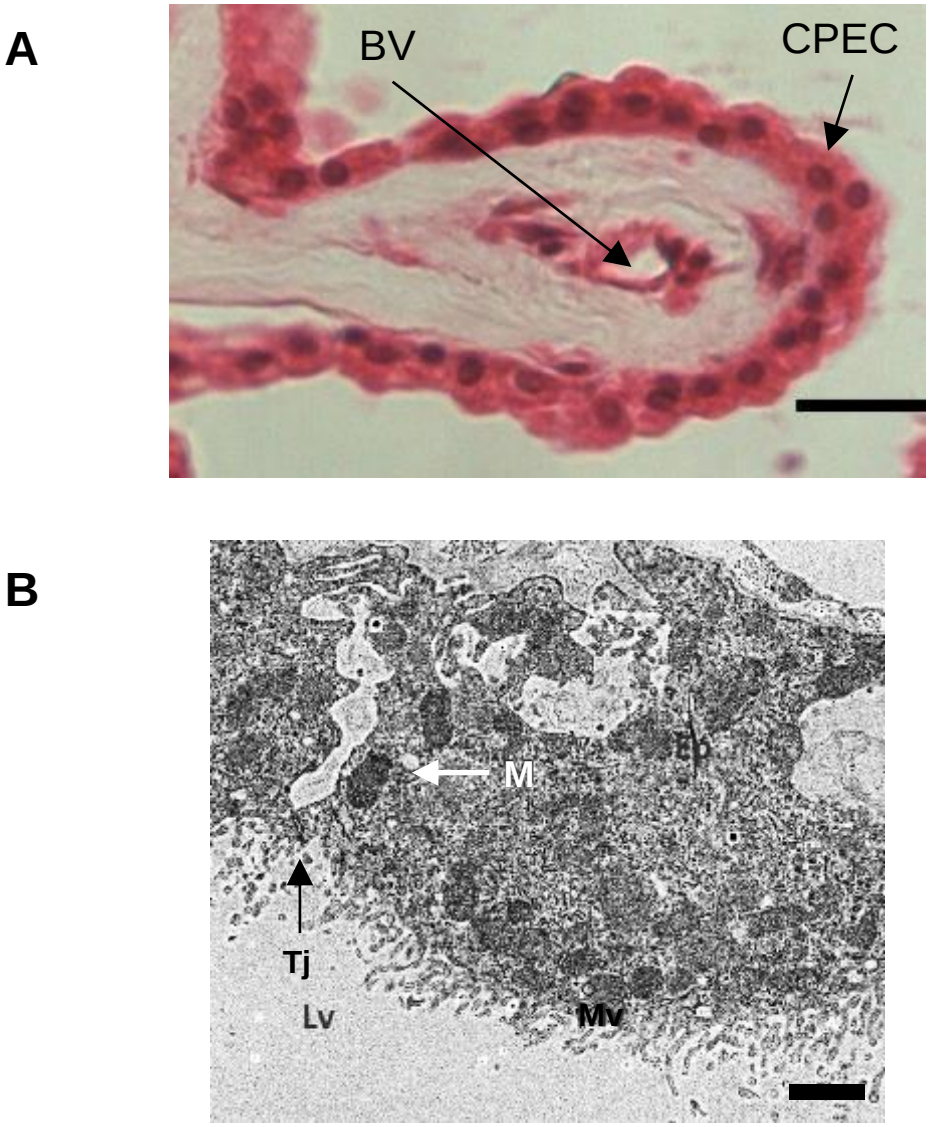

Figure 1.2 Choroid plexus villus

A) A haematoxylin and eosin stain of a human choroid plexus displaying a choroid plexus villus comprising a monolayer of choroid plexus epithelial cells (CPEC) surrounding a central blood vessel (BV). B) Electron micrograph of a Wistar rat choroid plexus epithelial cell, highlighting stereotypic features such as microvilli (Mv), mitochondria (M) and tight junction(Tj). Lateral ventricle (LV) Scale bar=20 microns for A and 1000nm for B. Electron micrograph courtesy and copyright of Zerin Alimajstorovic.

The choroid plexus are the primary organs of the blood-cerebrospinal-fluid-barrier (BCSFB), whereby the CPe cells form a barrier sufficient enough to make it impermeable to the diffusion of molecules, through the formation of tight junctions (Brown et al., 2004). As such, choroid plexus function dictates the molecular composition of the CSF through selective trans-epithelial movement of nutrients and macro-molecules. This is exemplified by the hormone leptin, where the choroid plexus expresses the OB-Ra slice variant of the leptin receptor, which is the transporting splice variant (Fei et al., 1997). Here the selective transport of leptin via the OB-Ra splice variant facilitates the saturatable transport of leptin from the blood to the CSF (Schwartz et al., 1996; Zlokovic et al., 2000). The strength of the BCSFB is further demonstrated by the ionic and protein composition of the CSF, if the barrier between the blood and CSF were a weak barrier, it stands to reason that the two compartments would have a similar composition. However the CSF has a distinct ionic and protein composition which further highlights the strength of the BCSFB (Table 1.2). The choroid plexus has a putative role in monitoring the composition of the CSF. The choroid plexus has been demonstrated to express many receptors at a functional level, including glucagon-like 1 receptor, somatostatin receptors, serotonin receptors and olfactory receptors, amongst others. (Botfield et al., 2017; Conn et al., 1986; Gonçalves et al., 2016; Katz et al., 2002). Together these suggest the choroid plexus can sense the composition of the CSF, as well as alter its function to modulate either the CSF composition or even alter CSF secretion to hormonal ques, however more work is required to fully assess the properties of these receptors.

	CSF	Plasma
Na^+ (mM)	151	155
K^+ (mM)	3.0	4.6
Mg^{2+} (mM)	1.0	0.7
Ca^{2+} (mM)	1.4	2.9
Cl^- (mM)	133	121
HCO_3^- (mM)	25.8	26.2
Glucose (mM)	4.2	6.3
pH	7.4	7.4
Osmolality (mOsm/L)	305	300
Protein (mg/dL)	25	6500

Table 1.2 Composition of plasma and CSF

All values taken from dog CSF, except protein which comes from rabbit CSF.
Table adapted from Brown et al. 2004.

1.2.4 CSF secretion at the choroid plexus

CSF secretion at the choroid plexus is a complex and energy demanding process as exemplified by the rich mitochondrial content of CPe cells and a choroid plexus perfusion rate four times that of the brain (Cornford et al., 1997; Faraci et al., 1990). CSF secretion at the choroid plexus has been suggested to be partially under neuronal control, where sympathetic stimulation decreases CSF secretion by roughly 20% and parasympathomimetics increase CSF secretion (Hayw and Vogh, 1979). However, these experiments were carried out in felines, thus replication is required in more standard experimental animals to determine whether these are applicable to other species. Moreover, there is little understanding of how other physiological ques modulate CSF secretion,

perhaps due to the limited range of experimental techniques that are low throughput.

In its simplest terms the choroid plexus has been thought to function like an inverted renal tubule cell, whereby the asymmetric localisation of ion transporters facilitates the movement of sodium ions from the blood to the cerebral ventricles (Botfield et al., 2017). However, the ionic gradients present across the choroid plexus, roughly 5mOmol greater in the CSF from the serum, are insufficient to generate the volumes of CSF that are produced (MacAulay and Zeuthen, 2010). Indeed CSF can be generated against an osmotic gradient (Heisey et al., 1962). Furthermore, knockout of the molecular water pore aquaporin 1 (AQP1) does not ameliorate CSF secretion, rather it reduces CSF secretion by roughly 25%, further suggesting that CSF secretion is not entirely dependent on osmosis (Oshio et al., 2004).

1.2.4.1 Ion transport at the choroid plexus

Although osmosis does not appear to be the primary driver of CSF secretion, it is clear that ionic gradients and transport are fundamental to the secretion of CSF (Fig1.3). Inhibition of the carbonic anhydrases, generators of bicarbonate ions, via acetazolamide decreases CSF secretion, perhaps through an indirect effect on the Na^+/K^+ ATPase though reduced activity of the basolateral bicarbonate exchangers, namely anion exchanger 2 (AE2), sodium bicarbonate cotransporter 1 (NBCn1) and the apical sodium hydrogen exchanger (HNE) or altered cellular pH (Damkier et al., 2009; Oshio et al., 2004; Sterling et al., 2001; Uldall et al., 2017). Indeed Na^+/K^+ ATPase activity had been proposed to contribute to CSF secretion (Vates et al., 1964). Several studies have

highlighted that selective inhibition of the Na^+/K^+ ATPase at the CP by the cardiotonic steroid ouabain diminishes production of CSF to up to 80% of basal levels, as such the activity of the Na^+/K^+ ATPase is used as an *in vitro* surrogate measure for CSF secretion (Pollay et al., 1985; Vates et al., 1964). However, whether the Na^+/K^+ ATPase activity directly contributes to CSF secretion or has an indirect effect through altering ion transport across CPe cells has yet to be elucidated. Regardless of this mechanistic uncertainty, it is clear Na^+/K^+ ATPase activity is linked to CSF secretion.

More recently it has been demonstrated that the NKCC1 symporter has a unique function in the choroid plexus. It is orientated to transport ions out of CPe cells rather than into the CPe cells as observed in other cell types, working against ionic chloride and sodium gradients to facilitate the production of CSF through moving potassium, sodium and chloride ions into the ventricular space, driven by a potassium gradient (Haas and Forbush III, 2000; Steffensen et al., 2018).

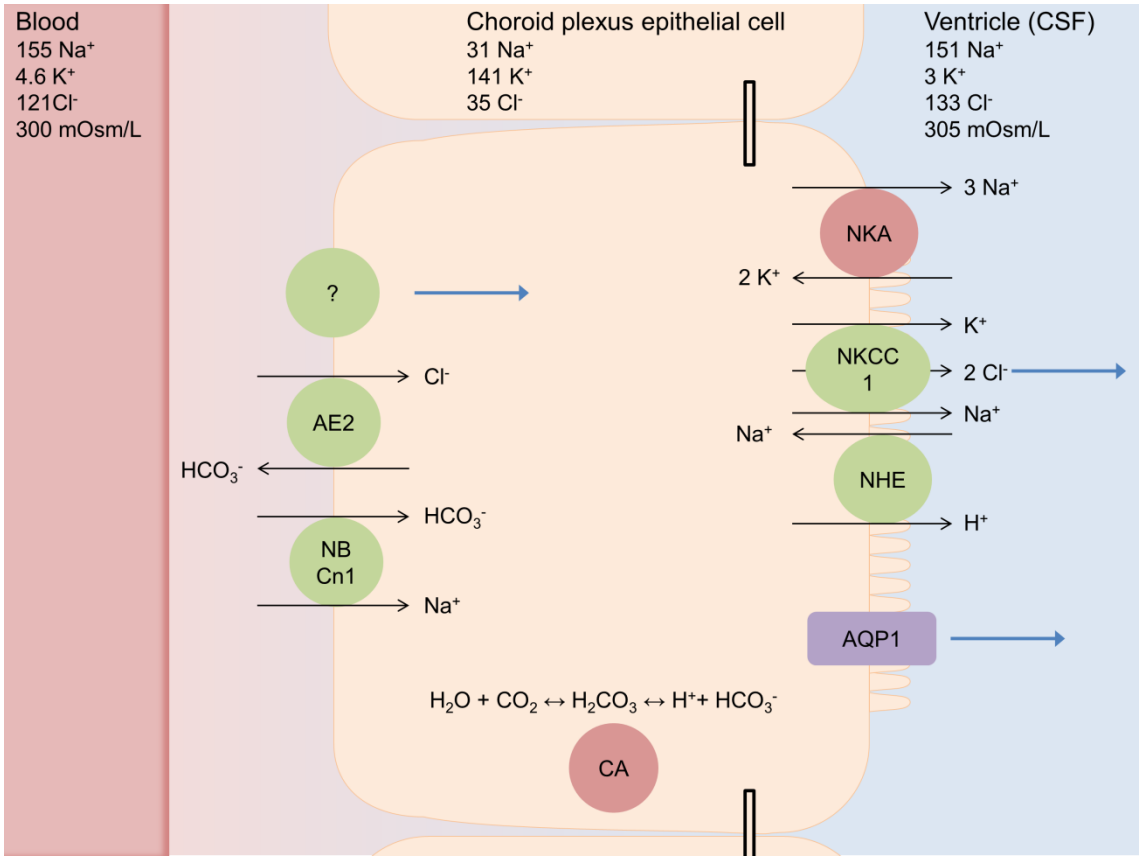

Figure 1.3 CSF secretion at the choroid plexus

A simplified schematic of CSF secretion in a choroid plexus epithelial (CPe) cell whereby the activity of carbonic anhydrase (CA) generates carbonic acid which dissociates to a proton and a bicarbonate ion, these drive the sodium/hydrogen exchanger (NHE) and anion exchanger (AE2) respectively, transporting sodium and chloride ions into CPe cells. Additionally the basolateral sodium bicarbonate transporter (NBCn1) transports bicarbonate and sodium ions into the cell .These provide the ionic gradients to drive both the Na^+/K^+ ATPase and the NKCC1 channel to transport sodium into the ventricular spaces, this facilitates the osmosis of water via aquaporin 1 (AQP1). Furthermore the action of NKCC1 independently draws water from the cytosol to the ventricular space. Values provided are in mM. Blue arrows represent the movement of water.

1.4.4.2 Water transport at the choroid plexus

Aquaporin 1 (AQP1) has long been hypothesised to facilitate osmosis in the choroid plexus, and thus contribute to CSF secretion. However the choroid plexus is relatively impermeable to water. This is perhaps explained by AQP1 localisation on CPe cells, however, this area is however controversial. Although it is clear that the majority of AQP1 is located on the apical membrane of CPe cells in both rodents and humans, some studies have also demonstrated diffuse basolateral localisation, although these are in the minority (Praetorius, 2007; Praetorius and Nielsen, 2006; Speake et al., 2003). However, given that CPe cells are relativity impermeable to water, it stands to reason an asymmetrical apical localisation of AQP1 is most likely (MacAulay and Zeuthen, 2010). Furthermore, as previously stated, AQP1 knockout reduces CSF secretion by roughly 25%, indicating that osmosis of water is not the primary method of transporting water through CPe cells (Oshio et al., 2004).

This however leaves the majority of CSF secretion to be carried out by unaccounted mechanisms. Interestingly, it was demonstrated that the sodium/potassium/chloride (NKCC1) transporter can directly facilitate the movement of water through action as a water channel (Hamann et al., 2010). This property, combined with the apical orientation of the NKCC1 transporter on CPe cells, it has been demonstrated that the NKCC1 transporter directly contributes roughly 50% of CSF secretion, driven by a potassium ion motive force (Steffensen et al., 2018). The current data does not account for the remainder of CSF secretion and more importantly does not account for water transport across the basolateral membrane of choroid plexus epithelial cells. It

has also been hypothesised that other transporters contribute to water transporter at the at the choroid plexus through ion mediated water co-transport on both the basolateral and apical membranes, however this requires further investigation within the context of the choroid plexus (MacAulay and Zeuthen, 2010).

1.2.5 CSF drainage

The drainage of CSF is vital in maintaining intracranial pressure; indeed, if CSF is produced it must also be removed from the CSF spaces at the rate it is produced. Considering CSF is produced with diurnal variation, drainage must be regulated to match the production rate, otherwise intracranial hypertension or hypotension would occur. Of note there is limited understanding of how CSF drainage is regulated in humans or rodents, and models do not currently exist to assess the molecular components of CSF drainage. Rather only physiological assessment CSF drainage via *in vivo* measurement of CSF drainage resistance, this technique has not been utilised to assess modulators of CSF drainage (Jones et al., 1987).

1.2.5.1 Arachnoid granulations

Classically, the arachnoid granulations that sit in the superior sagittal sinus are where CSF is thought to drain directly into the venous system and are the classic organ of CSF drainage (Cushing, 1925). The precise mechanism for CSF drainage at the arachnoid granulations is unknown and the contribution of arachnoid granulations to CSF drainage is unknown. It is hypothesised to be facilitated through either paracellular movement of water or the vacuolisation of CSF by the capsule cells of the arachnoid granulations (Pollay, 2010).

1.2.5.2 Glymphatics

Recent work has highlighted that cerebral perivascular spaces, Virchow-Robin spaces, structures formed by astrocytes, endothelial cells and pericytes within the brain parenchyma facilitate the drainage of CSF (Iliff et al., 2012). Functionally, subarachnoid CSF was demonstrated to enter the brain parenchyma via these perivascular spaces, 'glymphatics', where CSF is then follows these perivascular spaces where bulk flow occurs. It was demonstrated that aquaporin 4 at astrocytes was vital for this, where knock out reduced both bulk flow and solute clearance (Iliff et al., 2012)

1.2.5.3 Lymphatics

Two distinct branches of the lymphatic system have been demonstrated to drain CSF. Historically the lymphatics of the nasal cavity have been demonstrated to act as a drain of CSF through the cribriform plate in a variety of mammals including human and non-human primates (Johnston et al., 2004; Walter et al., 2006). More recently in a paradigm shift in CNS biology, lymphatic vessels have been shown in the CNS, indicating immune surveillance in the CNS (Aspelund et al., 2015; Louveau et al., 2015). Studies demonstrate that these lymphatic vessels, which are in intimate contact with the CSF in the dura mater, have the capability to drain CSF (Aspelund et al., 2015). More recently, it has been demonstrated that damaging these dural lymphatics impairs CSF flow and drainage (Da Mesquita et al., 2018).

1.2.6 CSF dynamics in IIH

CSF dynamics have been assessed to a limited capacity in IIH patients. Perhaps the largest piece of data suggesting altered CSF dynamics in IIH is the

fact that ICP is raised in IIH patients. Beyond this, there are limited studies that consist of low patient numbers. Several studies utilising a small cohorts of IIH patients identified an increased CSF flow rate through the cerebral aqueduct, thus increased CSF secretion (Akay et al., 2015; Donaldson, 1979; Gideon et al., 1994). Furthermore IIH patients have been identified to have larger ICP wave forms compared to headache controls, which could indicate reduced parenchymal compliance (Eide and Kerty, 2011). Additionally IIH patients have cortical astrogliosis, an inflammatory reactive state in astrocytes, and reduced AQP4 at the astrocyte end feet. This could be suggestive of reduced CSF clearance via the glymphatics but this has yet to be fully assessed (Eide et al., 2016). This astrogliosis may be linked to headache persistence, where astrocyte dysfunction is linked to headache episodes (Eide et al., 2016; Ricci et al., 2009). Additional evidence for IIH patients having reduced CSF drainage comes from small studies utilising isotope cisternography, which identify increased resistance to CSF drainage, however these findings are not universal across IIH patients and could be confounded by increased venous sinus pressure (Janny et al., 1981; Malm et al., 1992; Orefice et al., 1992). Of interest, IIH patients have a similar CSF osmolality to controls and CSF osmolality does not change following resolution of symptoms, suggesting that gross alterations in osmotic forces are not associated with disease activity in IIH (Wibroe et al., 2016), The current literature fails to conclusively elucidate whether IIH patients have CSF hypersecretion or reduced CSF drainage, confounded by low patient numbers in all studies, furthermore the studies do not address the aetiology of the alterations they describe, consequently further studies are required.

1.3 IIH pathogenesis

As its name suggests, the aetiology of IIH is unknown. However, there are differing phenotypes between genders and pubertal state, suggesting varied aetiologies for IIH. Consequently, the remainder of this thesis will focus on the syndrome associated with obese women of child bearing age, the population with the highest incidence of IIH. As the diagnostic criterion of IIH alludes to, the pathologic drive of IIH is presumed to be biochemical rather than a gross anatomical defect. A single genetic study has been carried out to determine any polymorphisms in genes associated with IIH, this small study was inconclusive and could not exclude or confirm genetic mutations as the pathological basis of IIH (Kuehn et al., 2018).

Several studies have attempted to delineate the potential cause of IIH where factors known to cause secondary intracranial hypertension have been investigated. Perhaps the longest held hypothesis for the pathogenic drive for IIH is altered retinoid metabolism.

1.3.1 Retinoids

Retinoids are vitamin A metabolites that have vital roles in the body such as acting as a chromophore for rhodopsin in retinal cells (Kiser and Palczewski, 2016). Retinoids have been known to cause secondary intracranial hypertension since the visits of explorers to the Arctic where consumption of polar bear liver, a rich source of vitamin A, caused hypervitaminosis A leading to IIH like symptoms (Rodahl and Moore, 1943). Furthermore patients receiving all-trans retinoic acid (ATRA) to treat malignancies can develop iatrogenic intracranial hypertension, which resolves temporally with withdrawal of ATRA,

suggesting secondary intracranial hypertension is a toxic effect of hypervitaminosis A (Anoop et al., 2014). As such it has been hypothesised that IIH is a disease of altered retinoid metabolism, perhaps through as of yet unelucidated transcriptomic effects on tissues in the CNS (Libien et al., 2017). However, IIH patients only have mildly altered retinoid metabolism compared to controls and is most likely clinically irrelevant, suggesting that altered retinoid metabolism is unlikely to be pathogenic in IIH (Libien et al., 2017; Warner et al., 2007).

1.3.2 Steroid hormones

Steroid hormones are pleotropic hormones derived from cholesterol and are hypothesised to be pathogenic in IIH, predominantly through altering CSF dynamics (Mollan et al., 2016).

1.3.2.1 Steroidogenesis

Steroid hormones are hormones derived from cholesterol and perform a multiplicity of functions and are named according to their function and organ of production. Mineralocorticoids such as aldosterone, and glucocorticoids such as cortisone fall under the corticosteroids group. Androgens such as testosterone, oestrogens such as oestrodiol and pregnanes such as progesterone fall into the sex steroid group (Miller and Auchus, 2011).

Steroid hormones are generated through sequential enzymatic reactions, whereby one steroid group acts as a precursor to another steroid species. This sequential generation of steroids is underpinned by expression of steroidogenic enzymes in a tissue, whereby absence of expression precludes the generation

of specific steroid species. The primary organ of steroidogenesis is the adrenal cortex, where it is split into discrete layers that produce specific steroid classes (Fig1.4). The most superficial layer, *zona glomerulosa*, generates the mineralocorticoid aldosterone from corticosterone via aldosterone synthase. The next layer is the *zona fasciculata* which generates glucocorticoids, where humans primarily generate cortisol. The most interior layer of the adrenal cortex is the *zona reticularis,* where androgens are generated. The production of steroid hormones is under the regulation of negative feedback loops unique to each steroid class. Furthermore, *de novo* synthesis of steroid hormones occur in the gonads, placenta and in the brain. Circulating steroid precursors undergo pre-receptor metabolism in target tissues, allowing them to elicit their effect (Miller and Auchus, 2011).

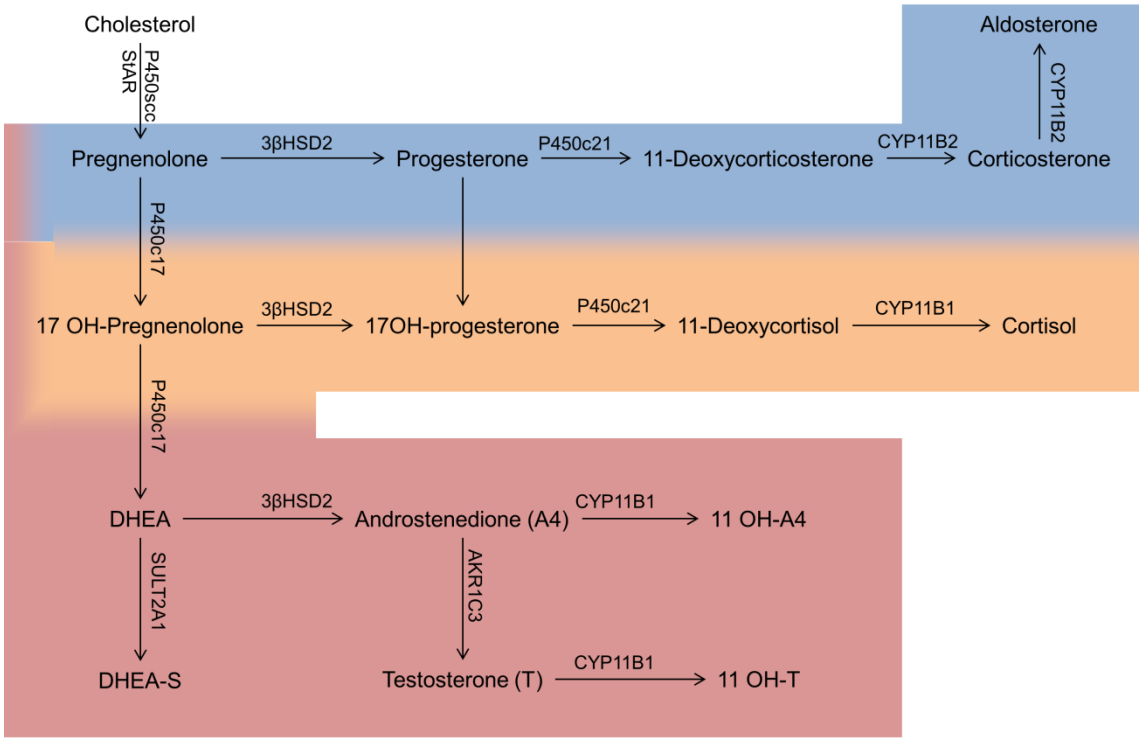

Figure 1.4 Human adrenal steroidogenesis

Steroid hormones are predominantly generated in the adrenal cortex, cholesterol is acted upon by cholesterol side chain cleavage enzyme (P450scc) generating pregnenolone. In the *zona glomerulosa* (blue), pregnenolone is converted to 11-deoxycorticosterone via sequential 3βHSD and P450c21 reactions. Aldosterone is generated via the enzyme aldosterone synthase (CYP11B2). In the *zona fasciculate* (orange), pregnenolone undergoes a P450C17 reaction prior to sequential 3βHSD and P450c21, generating 11-deoxycortisol. Cortisol is then generated via CYP11B1. In the *zona reticularis* (red) pregnenolone undergoes sequential generating dehydroepiandrostendione (DHEA), where the majority is sulphated via SULT2A1 generating DHEA-S. A proportion of DHEA undergoes a 3βHSD reaction, forming androstenedione (A4). Testosterone (T) is then generated via AKR1C3. Both A4 and T are converted to 11 OH-A4 and 11 OH-T via CYP11B1. Mixed colours represent common pathways. 11 OH = 11 hydroxy.

1.3.2.2 Steroid receptor signalling

Steroid hormones predominantly elicit their biological functions through cognate steroid receptors, where steroid hormone receptors namely glucocorticoid receptor (GR) mineralocorticoid (MR), androgen receptor (AR), progesterone receptor (PR) and oestrogen receptors (ERα and ERβ) form part of the class I nuclear receptor family. Upon binding of the cognate steroid in the cytoplasm, the steroid receptor unbinds from a chaperone proteins, such as heat-shock 90. This frees the receptor to form homodimers and heterodimers, where upon dimerization the receptors translocate from the cytoplasm to the nucleus via microtubules. Within the nucleus, the receptor dimer binds to hormone responsive elements (HRE), sequences of DNA specific to each receptor class, where co-regulatory proteins then bind to the receptor-HRE complex. These co-regulatory proteins promote DNA modification, either promoting or repressing gene transcription, where transcriptomic effects are the primary output of steroid receptor activation (Griekspoor et al., 2007).

1.3.3 Glucocorticoids

Glucocorticoids (GCs) are primarily produced in the *zona fasciculata* of the adrenal cortex where cortisol is the primary secreted GC in humans. Adrenal synthesis of GC is regulated by the hypothalamic-pituitary-adrenal (HPA) axis negative feedback loop. GCs are primarily carried in the circulation by transcortin and secondarily by albumin (Miller and Auchus, 2011).

The action of glucocorticoids in target tissues is gated by 11β-hydroxysteroid dehydrogenase (11β-HSD) enzymes within the mitochondria and the endoplasmic reticulum. In mineralocorticoid sensitive tissues such as the

kidney, circulating cortisol is inactivated to cortisone by 11β-HSD type 2 (11β-HSD2). This renal inactivation ensures the major circulating GC is cortisone. In glucocorticoid sensitive tissues, such as adipose tissue and the liver, 11β-HSD type 1 (11β-HSD1) is primarily expressed, which gates at the tissue level, active glucocorticoid exposure (Hewitt et al., 2005). This bi-directional enzyme preferentially converts the circulating GC cortisone to the active GC cortisol via an NADPH dependent oxo-reductase reaction within the endoplasmic reticulum, where NADPH is provided by the activity of the enzyme hexose-6-phosphate dehydrogenase (H6PDH) (Fig1.5) (Hewitt et al., 2005). Indeed, knockdown of H6PDH reverses the activity of 11β-HSD1, facilitating a dehydrogenase reaction (Hewitt et al., 2005). Glucocorticoids are deactivated via 5α or 5β reductase reactions followed by a 3α-HSD converting cortisol and cortisone to tetrahydrocortisol (THF) or 5αTHF and tetrahydrocortisone (THE) respectively and eliminated in the urine (Miller and Auchus, 2011).

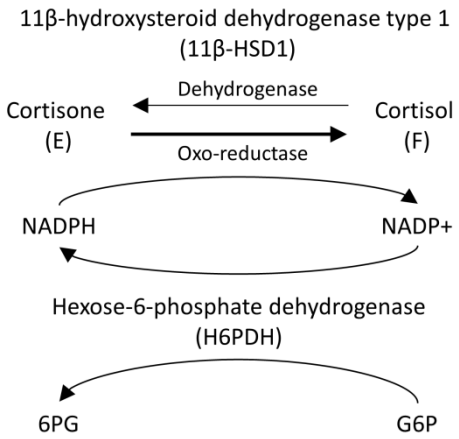

Figure 1.5 Glucocorticoid pre-receptor metabolism

The enzyme 11β-hydroxysteroid dehydrogenase type 1 (11β-HSD1) gates tissue level glucocorticoid exposure through converting the inactive circulating glucocorticoid cortisone to the active glucocorticoid cortisol via an NADPH cofactor mediated oxo-reductase reaction within the endoplasmic reticulum. Availability of NADH is provided by the action of hexose-6-phosphae dehydrogenase.

Glucocorticoids primarily act at the glucocorticoid receptor, where cortisol binding causes dimerization and nuclear translocation to the glucocorticoid response element. Functionally, glucocorticoids are catabolic hormones which have a plethora of actions. GCs are immunosuppressive and promote glucose sparing metabolic processes and elicit cognitive effects (Baxter and Forsham, 1972).

1.3.3.1 Glucocorticoids and IIH

Iatrogenic intracranial hypertension has been described upon prolonged treatment with GC's (Walker and Adamkiewicz, 1964). Interestingly the converse has been described; IIH has been demonstrated as a rare complication of Cushing's disease treatment where one study reported the incidence of IIH as 3% in treated Cushing's patients, a higher incidence of IIH

than in the general population (Zada et al., 2010). Together these reports highlight a causal relationship between altered GC exposure and IIH.

A comprehensive study assessing glucocorticoids in IIH patients has yet to be completed. However, weight loss in IIH is associated with reduced adrenal GC output and reduced systemic 11β-HSD1 activity, which correlates with reduction in ICP, linking active glucocorticoids to the disease activity of IIH (Sinclair et al., 2010b). The physiological rationale for the link between 11β-HSD1 activity and ICP is clear. Inhibition of 11β-HSD1 in the eye reduces intraocular pressure, most likely through altering sodium transport and reducing aqueous humour secretion, in a secretary system analogous to the choroid plexus (Rauz et al., 2001). With this data, in combination with the expression of functional 11β-HSD1 and glucocorticoid receptor at the choroid plexus, it has been hypothesised that glucocorticoids could alter ICP through modulating fluid secretory processes in a manner analogous to the ocular ciliary epithelium (Sinclair et al., 2010b). Indeed, unpublished PhD thesis work has demonstrated that glucocorticoids increase CSF secretion in rats (Alimajstorovic, 2016). A phase 2 clinical trial has closed that aimed to assess the role of GCs in modulating human ICP, results for this are eagerly awaited to shed light on this putative pathogenic mechanism in IIH (Markey et al., 2017). The current literature does not highlight whether there is an IIH specific GC phenotype. Indeed the marker for systemic GC activation, 5αTHF+THF/THE ratio, has not been assessed compared to controls, as such this needs to be assessed.

1.3.4 Oestrogens and progestogens

Due to IIH being a disease primarily affecting females of reproductive age, it is plausible that alterations in female sex hormones, namely oestrogens and progestogens, could be altered and associated with the pathogenesis of IIH (Mollan et al., 2016).

Progestogens are precursor steroid molecules to both androgens and corticosteroids and are primarily generated in thecal cells, and the placenta during pregnancy. Oestrogens are derived from both androstenedione and testosterone following aromatisation via aromatase (CYP19A1), where oestrogens are synthesised primarily in the ovarian granulosa cells. Similarly to androgens, oestrogens are anabolic hormones (Miller and Auchus, 2011).

1.3.4.1 Oestrogens, progestogens and IIH

Case studies have identified a potential causal relationship between oral contraceptives and intracranial hypertension, but no mechanism has been elucidated (Finsterer et al., 2006). Of interest, rodent experimentation has demonstrated that oestrogens and progesterone reduce Na^+/K^+ ATPase activity at the choroid plexus, thus assumed reduction in CSF secretion and ICP (Lindvall-Axelsson and Owman, 1989). Furthermore, a meta-analysis demonstrated that in female humans that short term oestrogen treatment reduces intraocular pressure (IOP) (Dewundara et al., 2016). This could suggest that a refractory increase in ICP following a reduction in systemic levels of hormone could contribute to the raised ICP in intracranial hypertension. However a recent longitudinal population based study highlights hormonal contraceptives do not increase the risk of developing IIH (Kilgore et al., 2018).

With relevance to IIH, evidence is mixed as to an oestrogen phenotype in IIH. The current studies contain small numbers of patients, are of low quality and present conflicting data, demonstrating an uncertain CSF oestrogen phenotype but an unaltered serum oestrogen phenotype (Donaldson and Horak, 1982; Toscano et al., 1991). Owing to the unique CSF and serum androgen phenotype in IIH, it would be prudent to assess IIH CSF and serum oestrogens in larger IIH cohorts (O'Reilly et al., 2019). Furthermore there is no apparent link between oestrogens and disease activity in IIH. There is no apparent evidence for progestogen abnormality in IIH (Klein et al., 2013).

1.3.5 Androgens

Androgens are primarily generated in the *zona reticularis* of the adrenal cortex where dehydroepiandrosterone–sulfate (DHEA-s) is the primary secreted adrenal androgen. Androgens undergo *de novo* synthesis in the gonads, where ovarian thecal cells and testicular leydig cells generate androgens, under the influence of luteinising hormone. Key peripheral androgen metabolising tissues include the skin, adipose tissue and the liver (Schiffer et al., 2018).

Androgens undergo a series of enzymatic reactions as part of their pre-receptor metabolism where circulating DHEAs is desulphated via steroid sulfatase (STS) to DHEA which is subsequently converted to androstenedione via 3β-HSD enzymes. A4 is subsequently converted to testosterone via 17-βHSD enzymes, namely 17β-HSD5 (AKR1C3) and 17β-HSD3. Testosterone is further activated by 5α-reductase enzymes (SRD5A1, SRD5A2) to dihydrotestosterone (DHT), the most potent androgen (Miller and Auchus, 2011). More recently it has been identified that 11-oxygenated androgens are potent agonists of the androgen

receptor, which are generated via the enzymatic reaction with 11β-hydroxylase (CYP11B1), these 11-hydroxy androgens are activated by 11β-HSD2 to form the more potent 11-keto androgens (Fig1.6) (Schiffer et al., 2018). Androgens are anabolic hormones, promoting skeletal muscle growth, the initiation of puberty, promoting virilisation and secondary sex characteristics and are male sex steroids. Androgens also elicit psychological effects, promoting aggression and libido. Androgens promote their effects primarily via the androgen receptor (Schiffer et al., 2018).

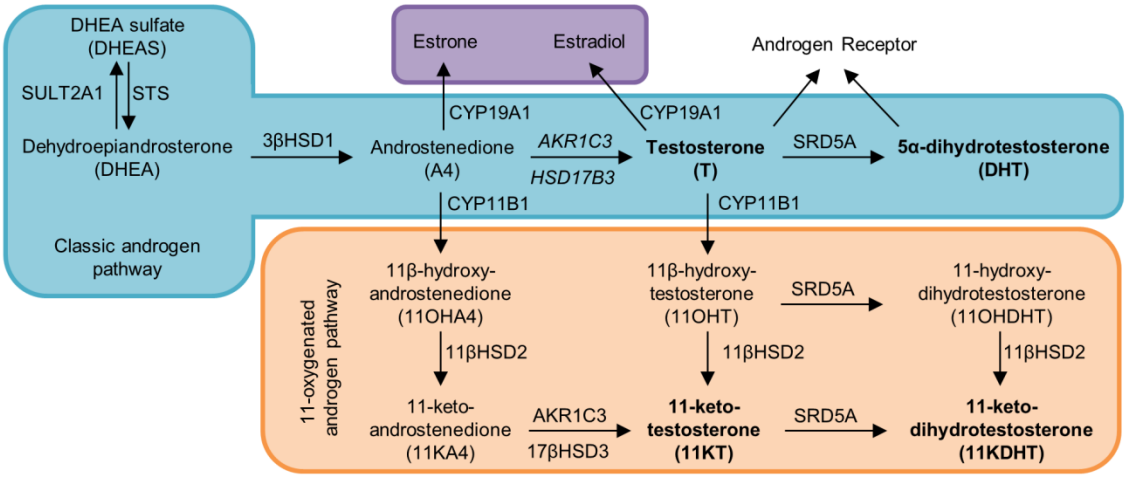

Figure 1.6 Pre-receptor androgen and oestrogen metabolism

A schematic describing the peripheral activation of androgens, hormones in bold are the most potent agonists of the androgen receptor. Note that CYP11B1 is only expressed in the adrenal gland.

1.3.5.1 IIH and androgens

Recently, novel work has identified that IIH patients have a distinct androgen profile, whereby they have raised serum and CSF testosterone but reduced serum androstenedione (Appendix 1) (O'Reilly et al., 2019). Furthermore, androgen production is reduced following weight loss in IIH patients (Sinclair et al., 2010b). Additionally, IIH presents earlier in those IIH patients who have androgen excess (Klein et al., 2013). This androgen excess phenotype perhaps explains the raised incidence of PCOS in IIH patients.

With relevance to disease activity, several case studies exist of female-to-male gender reassignment patients receiving therapeutic testosterone developing IIH symptoms. These symptoms resolve temporally with the withdrawal of testosterone, allowing intracranial hypertension to be defined as a 'possible' adverse drug reaction to testosterone (Hornby et al., 2017; Kapoor, 2015). Functionally, testosterone has been described to increase IOP in both rodents and humans, providing further evidence that testosterone has the potential to increase ICP (Kass and Sears, 1977; Toker et al., 2003). The current evidence surrounding testosterone in IIH highlights it as a putative pathogenic molecule in IIH, where testosterone could affect both ICP regulation and perturb metabolic function. This warrants further investigation to elucidate whether testosterone has the potential to alter ICP. This is especially important to evaluate considering other steroids that alter fluid secretory processes at the eye demonstrate a similar effect on CSF secretory processes, namely the activity of the Na^+/K^+ ATPase has been demonstrated to be fundamental in the secretion

of both CSF and aqueous humour secretion (Riley and Kishida, 1986) (table 1.3).

Hormone	IOP	CSF secretion	References
Progestogens	?	↓ Na^+/K^+ ATPase activity	(Lindvall-Axelsson and Owman, 1989)
Oestrogens	↓ IOP	↓ Na^+/K^+ ATPase activity	(Dewundara et al., 2016; Lindvall-Axelsson and Owman, 1989)
Glucocorticoids	Inhibition of 11β-HSD1 ↓ IOP	↑ CSF secretion	(Alimajstorovic, 2016; Rauz et al., 2001)
Androgens	↑ IOP	?	(Toker et al., 2003)

Table 1.3 Effects of steroid hormones on secretory systems

IOP=intraocular pressure. ↓= decrease, ↑=increase and ? = unknown.

1.3.6 Leptin

Leptin is a 16-kDa peptide hormone that is primarily secreted from adipose tissue and secondarily from the gastric mucosa. Leptin was among the first identified adipokines, hormones secreted from adipose tissue, whose secretion is modulated through dietary and physiological cues. Leptin has several functions within the body including immunomodulation, bone metabolism and initiation of puberty. However the classic function of leptin is the induction of satiety through signalling at the hypothalamus via the OB-Rb splice variant of the leptin receptor (Kelesidis et al., 2010).

1.3.6.1 Leptin and IIH

Leptin levels in IIH have been investigated due to the association of IIH with obesity. It has been demonstrated that IIH patients have raised serum leptin, independent of BMI (Ball et al., 2009; Lampl et al., 2002). Furthermore leptin has been shown to be raised in the CSF of unfasted IIH patients (Ball et al., 2009). However these data have not been corroborated by subsequent studies, perhaps due to differing methodologies between studies, including differences in fasting state, use of appropriate controls subjects and differences in IIH phenotypes (Behbehani et al., 2010; Dhungana et al., 2009; Samancl et al., 2017). Intriguingly, lumbar puncture opening pressure positivity correlates with CSF leptin values in control patients, indicating that leptin could be pathogenic in IIH through altering CSF dynamics (Ball et al., 2009). This hypothesis is plausible: chronic leptin exposure increases Na^+/K^+ ATPase activity in renal tubule cells, cells that function analogously to choroid plexus epithelial cells (Bełtowski et al., 2004; Botfield et al., 2017). Being as Na^+/K^+ ATPase activity is

a driver of CSF secretion at the choroid plexus, this highlights leptin as a putative pathogenic molecule in IIH. This necessitates *in vitro* and *in vivo* assessment of leptins capacity to modulate ICP, and Na^+/K^+ ATPase activity in CPe cells. Furthermore there is a need to replicate previous leptin studies in a larger homogenous IIH cohort with appropriate controls.

Although there are several putative pathogenic molecules in IIH, as discussed above there has been limited assessment of their capacity to modulate CSF secretion, functional surrogates such as Na^+/K^+ ATPase activity and CSF drainage. Indeed there has been limited *in vitro* assessment on how these molecules can alter the molecular processes at key tissues such as the choroid plexus, as such more work is required to assess these molecules in a variety of tissue and physiological processes.

1.4 IIH treatment

Although several hypotheses exist as to the cause of IIH, there is little understanding of how these putative factors are pathogenic in IIH. Consequently the treatment of IIH primarily focuses on resolving its symptoms, namely preserving vison through reducing papilloedema, achieved through reducing ICP. These are symptomatic treatments rather than disease modifying treatments.

1.4.1 Surgical interventions

Treatment for IIH primarily depends on the nature of the symptoms presented. Where there is an imminent risk of visual loss, surgical interventions are pursued and involve CSF diversion therapies (Mollan et al., 2018b).

Although primarily diagnostic, lumbar punctures and more commonly lumbar drains are used in IIH to drain excess CSF to reduce ICP and save eyesight where vision is at imminent risk. However, IIH patients report poor experience with lumbar punctures and often develop exacerbation of headache so these procedures are only temporary measures (Mollan et al., 2018b; Scotton et al., 2018b; Yiangou et al., 2018).

Subsequent to lumbar drainage, other more permanent CSF diversion procedures are utilised. These include optic nerve sheath fenestration and CSF shunting procedures. Although surgical interventions work acutely to save vision, there are often high revision rates, especially for shunting procedures. Furthermore, not every patient requires CSF diversion due to stable vision, as such, pharmaceutical and 'self-help' options are recommended (Mollan et al., 2018b).

1.4.2 Pharmaceutical interventions for IIH

Non-surgical interventions for IIH are often pharmacological and utilise the knowledge that choroid plexus secretes CSF to repurpose other drugs, known to modulate secretion at other secretory epithelia, to modulate ICP. The drug of choice in IIH is acetazolamide (Mollan et al., 2018b). Acetazolamide is a carbonic anhydrase inhibitor and has proven efficacy in both renal and ocular secretory epithelia as a diuretic and as an inhibitor of aqueous humour formation, through reducing Na^+/K^+ ATPase activity (Maus et al., 1997). Indeed, in rodents acetazolamide decreases both Na^+/K^+ ATPase activity at the choroid plexus and reduces CSF secretion, perhaps through altered bicarbonate transport thus altered ionic and pH balance (Oshio et al., 2004; Sterling et al.,

2001; Uldall et al., 2017) These data have provided the rationale for using acetazolamide to reduce ICP in humans.

The clinical evidence for acetazolamide use in IIH is unconvincing. In a recent large scale trial, acetazolamide conferred mild improvements in visual outcome compared to a placebo group, although the dose provided in this study is well above what most patients in a previous study would tolerate (Ball et al., 2011). Furthermore, the study failed to achieve its pre-defined treatment effect for clinically relevant change in visual outcomes, suggesting poor clinical efficacy for acetazolamide in IIH (Wall et al., 2014).

Other diuretic compounds such as furosemide, topiramate, amiloride, inhibitors of the NKCC1 channel, carbonic anhydrase and NHE channel respectively, and the somatostatin analogue octreotide are used to treat IIH on the assumption that they reduce CSF secretion in the choroid plexus, however efficacy is limited and high quality comparative studies do not exist (Çelebisoy et al., 2007; Corbett, 1983; Mollan et al., 2018b; Panagopoulos et al., 2007). Furthermore, diuretic drugs have an unfavourable side effect profile. The lack of true efficacy with these drugs was highlighted in a recent Cochrane review highlighting the need for more high quality randomised clinical trials in IIH (Piper et al., 2015). Interestingly, a recent *in vivo* study demonstrated a single dose of topiramate reduces ICP more than any of the other drugs described above in rats (Scotton et al., 2018a).

There is also a need for further preclinical studies and screening of potential therapeutic compounds with a reduced side effect profile. An open label trial

evaluating the effects of diuretic drugs in treating IIH, utilising ICP as an objective measure of treatment effect is currently underway (ISRCTN12678718). This trial is also evaluating the ability of glucagon-like peptide 1 receptor agonists to decrease ICP, which have shown promise in pre-clinical studies in reducing ICP in physiological and pathophysiological ranges (Botfield et al., 2017). Pharmaceutical interventions for IIH only provide symptomatic relief and do not treat the underlying pathology.

1.4.3 Weight loss and IIH

The only current intervention with true disease modifying efficacy is weight loss, whereby 15% weight loss provides IIH patients with reduced ICP and improved visual and headache outcomes (Sinclair et al., 2010a). As such, weight loss is the recommended conservative treatment for IIH (Mollan et al., 2018b). The effects of weight loss on IIH and its symptoms sheds light on the potential pathogenesis of IIH; it is hypothesised that the adipose tissue in IIH is driving the pathology of IIH (Hornby et al., 2018b).

1.5 Adipose tissue

Adipose tissue is a mesenchyme derived tissue that has three functional phenotypes: white adipose tissue which primarily acts as a store for excess calories; brown adipose is thermogenic and beige adipose displays an intermediate phenotype. Adipose tissue is comprised of adipocytes, the functional unit of adipose tissue, and supporting cells such as fibroblasts, macrophages, stomovascular preadipocyes and the newly discovered adipogenisis-regulatory cells (Rosen and Spiegelman, 2014; Schwalie et al., 2018).

1.5.1 Adipose distribution

White adipose tissue is distributed over several depots, where the depots can be grouped into either subcutaneous (SC) or visceral adipose depots. SC adipose tissue functions as a store of energy and provides thermal insulation, whilst visceral adipose, which resides in the body cavities, additionally provides mechanical cushioning for organs. The greater and lesser omentum reside in the abdominal cavity and comprised of omental (OM) adipose tissue, which are the visceral adipose of choice for *ex vivo* experimentation.

Two primary adipose distributions exist, this includes the gynaecoid adipose distribution whereby SC adipose tissue is found primarily in a gluteo-femeral distribution and is associated with the female sex and confers a protective metabolic phenotype (Manolopoulos et al., 2010). The second main adipose distribution is the android adipose distribution, where SC adipose is primarily deposited abdominally with an expansion in visceral adipose depot volume. The android adipose distribution is associated with males and an adverse metabolic risk (Manolopoulos et al., 2010). Increased visceral adipose mass is strongly associated with adverse metabolic risk and contributes to the android adipose distribution (Smith et al., 2001; Taksali et al., 2008).

1.5.2 The adipocyte

White adipocytes are the functional cell type in white adipose tissue; they are post-mitotic and their cell structure is dominated by a large central lipid droplet with an acentric cytoplasm and nucleus. The white adipocyte is exquisitely adapted for its classical role: the production and storage of triglycerides, and the liberation of free fatty acids from triglycerides in a state of fasting.

1.5.3 Lipid storage in adipose tissue

1.5.3.1 Adipocyte lipogenesis

Lipogenesis dominates the function of the adipocyte in the post-prandial state, where carbohydrates and amino acids contribute to *de novo* lipogenesis in adipocytes (Fig 1.7). The post-prandial insulin increase stimulates the uptake of glucose from the blood via the GLUT4 transporter (Huang and Czech, 2007). This glucose undergoes glycolysis, where pyruvate is generated. Pyruvate is also generated by non-ketogenic amino acid catabolism. Subsequently pyruvate is converted to acetyl-CoA, by the mitochondrial pyruvate dehydrogenase complex (PDH), which enters the tricarboxylic acid (TCA) cycle forming citrate. Amino acids also join the TCA cycle, either as TCA intermediates, or as acetyl-CoA in the case of ketogenic amino acids. Citric acid then enters the cytoplasm due to increased mitochondrial levels facilitated by increased glycolysis and TCA intermediate generation. This citrate is cleaved via ATP citrate lyase (ACLY), liberating oxaloacetate and acetyl-CoA. Acetyl-CoA is converted to malonyl-CoA by acetyl CoA carboxylate (ACACA), which is the precursor for fatty acid synthesis. Fatty acid synthesis is performed by the fatty acid synthase (FASN) enzyme complex, forming fatty acids from malonyl-CoA (Kersten, 2001). Interestingly, *de novo* fatty acid synthesis from BCAA backbones is highly efficient in adipocytes, contributing to roughly 25% of acetyl-CoA destined for fatty acid synthesis (Crown et al., 2015; Rosenthal et al., 1974).

Dietary and hepatic derived free fatty acids freely diffuse into an adipocyte whereas intestinal derived chylomicrons are acted upon by lipoprotein lipase, freeing fatty acids to diffuse into the adipocyte. Dietary free fatty acids and *de*

novo synthesised fatty acids are conjugated to glycerol-3-phosphate moieties, a product of glycolysis, to form triglycerides (Ameer et al., 2014).

1.5.3.2 Storage of triglycerides

Triglycerides form the basis of the central lipid droplet in adipocytes, where its structural integrity is maintained primarily by perilipin proteins, whose conformation prevents lipases from catabolising the lipid droplet (Brasaemle et al., 2009).

1.5.3.3 Lipolysis in adipocytes

In the fasting state, the adipocyte receives hormonal input, from glucagon and adrenaline, which stimulate lipolysis through activation of protein kinase A (PKA). PKA phosphorylates perilipins, facilitating a conformation change, allowing PKA phosphorylated lipases to cleave triglycerides, liberating fatty acids and glycerol following sequential reaction with adipocyte triglyceride lipase (ATGL), hormones sensitive lipase (HSL) and monacylglycerol lipase (MAG) (Fig 1.7) (Brasaemle et al., 2009). Free fatty acids freely diffuse into the circulation whereas glycerol diffusion is facilitated by aquaporin 7 (Hibuse et al., 2006). Free fatty acids are utilised in tissues as a respiratory substrate in β-oxidation, especially when musculo-heptatic glycogen stores are depleted, whereas glycerol is utilised in hepatic gluconeogenesis (Rui, 2014).

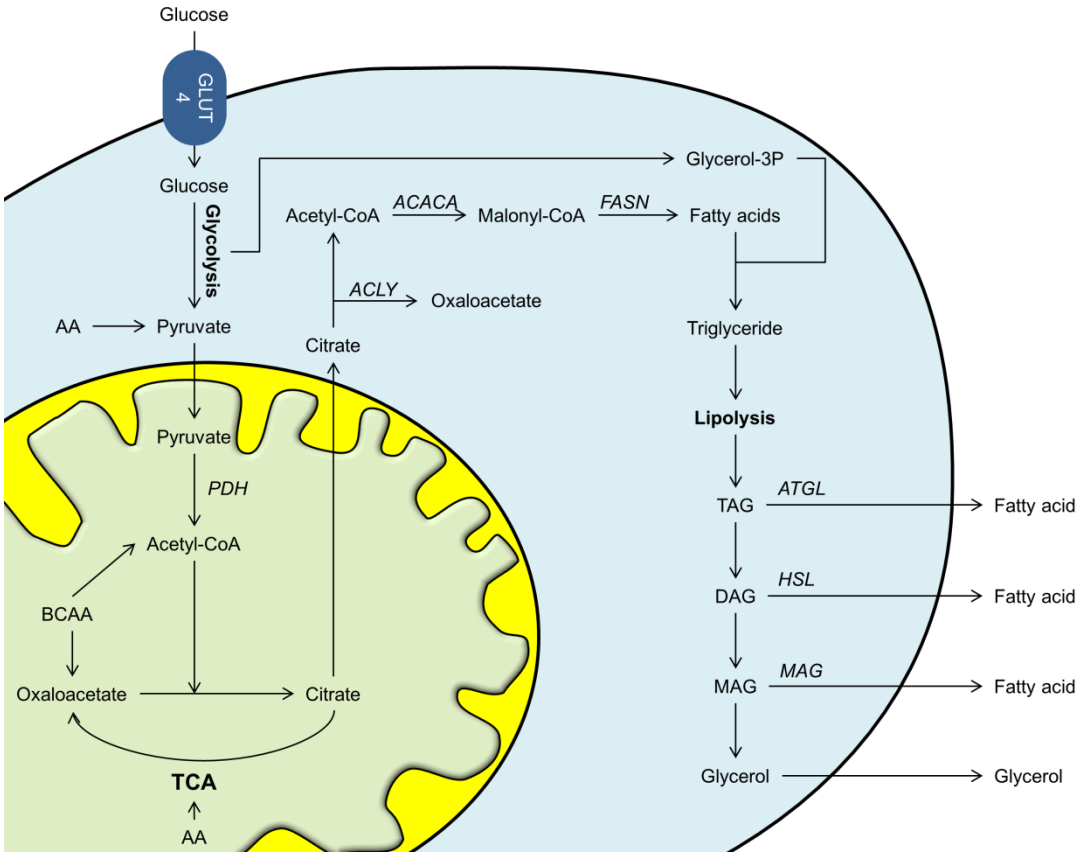

Figure 1.7 Lipolysis and lipogenesis in adipocytes

A schematic diagram of lipogenesis and lipolysis in adipocytes. In the post-prandial state insulin promotes the influx of glucose into an adipocyte via GLUT4, following glycolysis, pyruvate enters the mitochondria where it is converted to Acetyl-CoA via pyruvate dehydrogenase (PDH). This subsequently enters the tricarboxylic acid cycle forming citrate. Increased mitochondrial citrate enters the cytosol where citrate lyase liberates acetyl-CoA. The subsequent action of acetyl-CoA carboxylase forms malonyl-CoA which is acted upon by the fatty acid synthase complex forming fatty acids. Glycerol-3 phosphate and fatty acid are conjugated forming triglycerides. In the fasted state, lipolysis facilitated by lipases, liberates fatty acids and glycerol, which enter the circulation. Bold words represent processes, TCA= Tricarboxylic acid cycle, AA= amino acids, BCAA= branch chained amino acids, *ACLY*=ATP citrate lyase, *ACACA* acetyl-CoA carboxylase, *FASN*= fatty acid synthase, *ATGL*= Adipocyte triglyceride lipase, *HSL*= Hormone sensitive lipase and *MAG* = Monoacylglycerol lipase.

1.6 Adipose tissue as an endocrine organ

Since the 1990s adipose tissue has been shown to be more than a mere store of lipids, it has been shown to be an endocrine organ. The seminal discovery that adipose tissue produces the satiety hormone leptin opened up research into the hormones that adipose tissue produces. The discovery of a plethora of adipose generated hormones, or adipokines, allows adipose tissue to be described as an endocrine organ (Coelho et al., 2013).

1.6.1 Leptin

The cardinal adipokine is leptin. Identified in 1995, leptin has been demonstrated to induce satiety as previously described and is a modulator of energy homeostasis (section 1.3.6). Further evidence of leptin as a mediator of energy homeostasis and satiety can be demonstrated by patients who congenitally lack leptin. These patients develop florid obesity and present with hyperphagia which can be reversed following leptin administration (Farooqi et al., 1999; Montague et al., 1997). This phenotype was replicated in a classic rodent experiment (Pelleymounter et al., 1995). Secretion of leptin from adipocytes is tightly modulated in order to facilitate appropriate energy homeostasis in an organism. Although the direct molecular mechanism facilitating leptin secretion is not entirely clear, both chronic and acute modulators of leptin secretion are well characterised. At its highest level, leptin secretion follows a circadian rhythm, whereby leptin secretion is minimal in the morning and reaches is peak during the hours of sleep, irrespective of BMI (Langendonk et al., 1998).

1.6.1.1 Positive acute regulation of leptin secretion

Adipocytes display a basal level of leptin secretion; however other factors modulate this secretion. Leptin secretion is regulated acutely to modulate satiety in the post-prandial state and following events requiring more dietary calories. Acute regulation of leptin secretion is modulated by several factors, relating to caloric status. This is demonstrated by a post-prandial increase in circulating leptin in lean individuals, highlighting that factors associated with the post-prandial state promote leptin secretion (Korek et al., 2013). This post-prandial increase in leptin is linked to the post-prandial increase in insulin, where insulin has been demonstrated to increase leptin secretion both *in vitro* and *in vivo* settings (Kolaczynski et al., 1996; Malmström et al., 1996). Glucose and other molecules that facilitate the production of pyruvate have been demonstrated to increase both basal and insulin stimulated leptin secretion in rodent adipocytes (Levy et al., 2000). This is likely linked to the ability of malonyl-CoA, the precursor molecule to fatty acids, to potentiate leptin secretion (Shirai et al., 2004) (Fig1.8).

1.6.1.2 Negative acute regulation of leptin secretion

In the fasted state, plasma leptin decreases, due to the reduction in serum insulin and glucose following resolution of the post-prandial insulin peak (Boden et al., 1996). Catecholamines, affecters of the sympathetic branch of the autonomic nervous system, are secreted during times of stress. Adrenoceptor activation has been demonstrated to inhibit leptin secretion, mediated through lipolysis, whereby liberated Acyl-CoA moiety's inhibit ACC preventing malonyl-CoA synthesis (Gettys et al., 1996; Haystead and Grahame, 1986; Shirai et al.,

2004). Interestingly, intracellular free fatty acids have been demonstrated to inhibit both basal and insulin stimulated leptin secretion in rodent adipocytes, where shorter carbon back bone lipids exhibit stronger inhibition (Cammisotto et al., 2003). Lipolysis independent of catecholamines in the fasted state also inhibits leptin secretion via the mechanism described (Fig1.8).

1.6.2.3 Chronic regulation of leptin secretion

The most substantial contributor to long term leptin secretion is adipocyte volume, where increased adipocyte cross-sectional area is positively correlated with both leptin mRNA, adipocyte leptin secretion and unsurprisingly BMI (Lönnqvist et al., 1997). Furthermore, chronic glucocorticoid administration has been demonstrated to increase leptin secretion from adipocytes and increase serum leptin as demonstrated in Cushingoid and healthy individuals (Dagogo-Jack et al., 1997; Masuzaki et al., 1997). Insulin is also a chronic affector of leptin, where adipocytes secrete more leptin after chronic incubation with insulin (Kolaczynski et al., 1996).

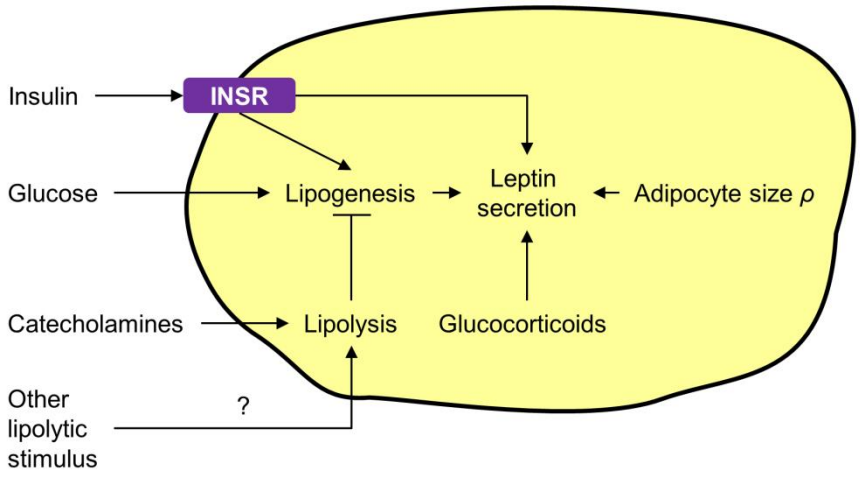

Figure 1.8 Effectors of leptin secretion

Adipose tissue secretes leptin at basal levels as determined by adipocyte size. However several processes promote leptin secretion. Insulin in the postprandial state increases leptin secretion directly and through promoting *de novo* lipogenesis. However lipolysis, mediated through catecholamines and other lipogenic stimulus, inhibits lipogenesis. Glucocorticoids also increase leptin secretion. Flat arrow head= inhibits, pointed arrow head = promotes, INSR= insulin receptor, ρ= correlation.

1.6.2 Adiponectin

Adiponectin is another peptide hormone secreted from adipose tissue and acts as a regulator of metabolism, whereby it stimulates β-oxidation and inhibits gluconeogenesis. Adiponectin secretion from adipose tissue and corresponding serum adiponectin levels are inversely correlated with BMI in both males and females (Kern et al., 2003). This demonstrates that adipose tissue regulates whole body metabolism.

1.6.2 Androgens and adipose tissue

Adipose tissue is a major organ for peripheral androgen metabolism, where adipose tissue expresses androgen activating enzymes (O'Reilly et al., 2014). Depot specific androgen metabolism has been demonstrated, where SC

adipose preferentially generates testosterone, OM adipose preferentially inactivates testosterone to androstenedione, although the precise enzyme involved remains controversial (Blouin et al., 2009; Quinkler et al., 2004). Consequently SC adipose can be described as a peripheral activator of androgens whereas OM adipose can be described as an androgen inactivation tissue. Androgens exert several effects on adipose tissue, these include increasing lipolysis, reducing lipogenesis and inhibition of pre-adipocyte differentiation (O'Reilly et al., 2014). Adipose tissue also expresses aromatase and possesses the ability to generate oestrogens (Killinger et al., 1987).

1.6.3 Glucocorticoids and adipose tissue

Adipose tissue is a peripheral tissue of GC activation, where depot specific 11β-HSD1 activity exists, OM adipose has a greater capacity to activate GCs than SC adipose (Bujalska et al., 2007). Furthermore, GCs promote depot specific effects on adipocyte maturation; CGs promote maturation in SC adipocytes and inhibit maturation in OM adipocytes, perhaps explaining why OM adipocytes are smaller than SC adipocytes (Bader et al., 2002; Bujalska et al., 2007; Tomlinson et al., 2002). Interestingly adipose tissue specific overexpression of 11β-HSD1 promotes obesity and metabolic syndrome in rodents in a similar manner to exogenous GC overdose, where 11β-HSD1 knockout prevents the development of metabolic syndrome (Masuzaki et al., 2001; Morgan et al., 2014). As such, GCs have been demonstrated to promote both lipolysis and lipogenesis in adipose tissue, increasing lipid turnover but favouring triglyceride formation and adipocyte hypertrophy (Masuzaki et al., 2001). Furthermore, patients with GC excess also develop florid abdominal obesity and metabolic disease,

highlighting the obesogenic effects of GCs. GCs also promote androgen inactivation in adipose tissue (Blouin et al., 2009).

1.7 Obesity

Obesity is a disease on pandemic proportions, affecting 650 million individuals as of 2016, where prevalence is highest in the developed world and is associated with low socio-economic status (McLaren, 2007). Being defined as having a BMI over 30 kg/m^2 by the World Health Organisation, obesity increases the chances of an individual developing serious morbidities including type 2 diabetes, cancer, musculoskeletal diseases, cardiovascular events, hypertension, metabolic syndrome, mental health issues and premature death (Flegal et al., 2013). Obesity is, however, a modifiable disease, where the reduction in BMI confers a reduction in comorbid symptoms and even amelioration of the comorbid conditions.

Obesity has a strong genetic component. This was demonstrated by an elegant study observing body composition in twins, where monozygotic twins had similar body compositions, lean or obese, whereas dizygotic twins often had differing body compositions (Börjeson, 1976). Recently, a genome wide association study identified that polymorphisms in genes associated with the nervous system are strongly associated with the development of raised BMI in European men and women (Locke et al., 2015). More recently it was demonstrated that polymorphisms associated with a lean phenotype also exist (Riveros-McKay et al., 2019). Together, these data highlight that genetics play strong role in obesogenisis and the environment is a modifiable component.

1.7.1 Obesity and adipose distribution

Obesity sees expansion of both visceral and subcutaneous adipose depots. The volume of the visceral adipose depot, including OM adipose is associated with heightened adverse metabolic outcomes including dyslipidaemia, insulin resistance and increased risk of metabolic syndrome (Smith et al., 2001; Taksali et al., 2008). This highlights that visceral adiposity is particularly damaging to health.

1.7.2 Biochemical phenotype of obesity

Obese women have a distinct biochemical profile, whereby they exhibit relative androgen excess and impaired systemic GC activation mediated via reduced hepatic 11β-HSD1 activity (Rask et al., 2002; Stewart et al., 1999; Taponen et al., 2003). Obese women also have increased circulating leptin (Lönnqvist et al., 1997). Obesity can be described as a state of leptin resistance, whereby despite increased serum and CSF leptin compared to lean individuals, obese patients remain obese (Nam et al., 2001). This is clearly demonstrated in leptin receptor knockout mice who develop a similar metabolic phenotype (Cohen et al., 2001).

Furthermore, it is well established that obese patients have increased levels of circulating pro-inflammatory cytokines and adipokines such as tumour necrosis factor alpha (TNFα) and interleukin (IL) 6 as well as decreased levels of anti-inflammatory cytokines such as adiponectin (Kern et al., 2003). Consequently obesity can be described as a chronic pro-inflammatory disease. Further evidence for obesity being a pro-inflammatory state is raised serum C-reactive protein (CRP), a protein involved in the acute phase inflammatory response and

is a risk factor for hypertension, independently of obesity (Chul Sung et al., 2003; Visser et al., 1999).

Furthermore, obesity has a differential biochemical phenotype compared to other diseases of chronic inflammation at the hormonal level. Whereas obese patients have raised circulating pro-inflammatory cytokines and reduced systemic 11β-HSD1 activity, other diseases of chronic inflammation such as rheumatoid arthritis and inflammatory bowel diseases display increased systemic 11β-HSD1 activity mediated by tissue level pro-inflammatory cytokines (Cooper et al., 2011; Hardy et al., 2008). This difference is perhaps mediated, in part, by reduced hepatic 11β-HSD1 activity in obesity (Rask et al., 2002).

Additionally, obese individuals display insulin resistance, hyperinsulinemia and are at a heightened risk of developing type 2 diabetes, which comes with its own distinct set of side effects (Dandona et al., 2004; Mokdad et al., 2003). Obese patients also exhibit dyslipidaemia, contributing to peripheral insulin resistance through inhibiting insulin stimulated hepatic and skeletal muscle glucose absorption (Huang and Czech, 2007).

1.7.3 Obesity and adipose tissue

At the cellular level, obesity sees adipocyte hypertrophy through enlargement of the central lipid droplet due to triglyceride accumulation, a direct consequence of prolonged positive caloric balance due to an imbalance in caloric intake and energy expenditure.

Adipocyte hypertrophy is not intrinsically pathological and is required for physiological energy storage. However, hypertrophy becomes pathological in

adipocytes due to reduced oxygen tension causing hypoxia, facilitated by insufficient angiogenesis (Sun et al., 2011). This hypoxia accompanied by adipocyte hypertrophy and adipocyte death creates an intra-adipose pro-inflammatory environment that promotes macrophage recruitment to adipose tissue depots (Rosen and Spiegelman, 2014; Sun et al., 2011). These recruited macrophages promote clearance of dead adipocytes through the formation of crown-like structures, forming a differentiation niche for pre-adipocytes. It has been hypothesised that these recruited macrophages promote the adverse metabolic consequences of obesity (Sun et al., 2011). Functional ablation of macrophages in obese mice improves insulin sensitivity and metabolic phenotype despite no alteration in adipocyte volume (Patsouris et al., 2008). This lends credit to the hypothesis that macrophages, in part, drive the obesity related metabolic phenotype.

One hormone derived from infiltrating macrophages is TNFα, whose secretion and expression is increased in obese adipose tissue (Hotamisligil et al., 1995). TNFα paracrine signalling contributes to adipocyte insulin resistance through inhibiting insulin receptor signal transduction (Hotamisligil et al., 1996, 1995). Furthermore, TNFα increases both the expression and activity of 11β-HSD1 in pre-adipocyte cultures, likely contributing to increased 11-βHSD1 expression and activity in whole SC and OM adipose tissue in obesity (Handoko et al., 2000; Rask et al., 2002; Tomlinson et al., 2001).

Increased local 11β-HSD1 activity, coupled with increased adipocyte volume contributes to the raised leptin secretion from adipose derived from obese individuals (Lönnqvist et al., 1997; Masuzaki et al., 1997). Furthermore

glucocorticoid mediated effects such as increased lipogenesis and increased pre-adipocyte differentiation contribute to the expansion of the adipose depots, exacerbating the remodelling and inflammation, generating the reciprocal conditions for further tissue expansion (Masuzaki et al., 2001). The increased GC exposure promotes lipolysis, contributing to hyperlipidaemia (Arnaldi et al., 2010). The increased circulating active androgens in obese women may be explained by the increased expression and activity of AKR1C3 in obese women, which appears to be regulated by increased circulating insulin acting upon the adipose tissue (O'Reilly et al., 2017; Quinkler et al., 2004; Taponen et al., 2003).

1.8 Adipose tissue, obesity and IIH

Adipose tissue is hypothesised to contribute to the pathology of IIH due to a striking association between obesity and IIH and the improvement of symptoms with weight loss (Sinclair et al., 2010a). Despite this association between obesity and IIH, very little is known about the underlying adipose phenotype in IIH. However, being as IIH patients are obese, their adipose tissue is by definition dysfunctional (Attie and Scherer, 2009). It is clear that IIH patients have a similar basal inflammatory response to obese individuals as they demonstrate BMI dependent CRP levels and have raised CRP compared to lean controls, however CRP has not compared between IIH patients and matched obese controls (Hannerz et al., 2011).

1.8.1 Adipose distribution in IIH

The investigation of adipose tissue distribution in IIH has been characterised by conflicting results, perhaps exacerbated by inadequate methodologies to

measure adipose distribution. Previous studies have highlighted that IIH patients have a more gynaecoid adipose distribution, however these studies utilised small patient numbers and used the subjective waist-to-hip ratio measurement (Kesler et al., 2010; Klein et al., 2013). More recent unpublished work utilising dual x-ray absorptiometry (DEXA), which provides a high resolution objective measure of adipose distribution, has highlighted that IIH patients have a similar adipose distribution to matched controls (Botfield et al unpublished). Furthermore, two studies assessing independent IIH cohorts, one of which is currently unpublished, have identified that truncal fat mass positively correlates with LP Opp (Hornby et al., 2018a). Congruent with this, a reduction in truncal adiposity reduces LP Opp, highlighting truncal adiposity as a putative pathogenic determinant in IIH (Hornby et al., 2018a). Although these DEXA studies highlight truncal adipose mass as a potential determinate of LP Opp, they fail to differentiate between SC and visceral adipose. Additionally it is unknown how adipose tissue could contribute to ICP dynamics.

1.8.2 Endocrinology of IIH adipose tissue

As previously stated, IIH patients are thought to have raised serum and CSF leptin (Ball et al., 2009). This suggests hypothalamic leptin resistance and dysfunctional leptin secretion, and it is assumed that this is derived from adipocytes but has yet to be demonstrated. Furthermore it is unknown what factors in IIH adipose could be facilitating this proposed leptin phenotype.

It has been demonstrated that weight loss in IIH patients reduces adrenal GC output and peripheral GC activation, suggesting that IIH adipose could be contributing to GC activation. However this study did not include a control

cohort, consequently an IIH specific GC phenotype has yet to be described (Sinclair et al., 2010b). This study also highlights that weight loss in IIH patients reduces total androgen output and decreases androgen activation (Sinclair et al., 2010b). This however, does not identify whether adipose tissue is the source of the unique androgen signature in IIH. Several studies have screened serum cytokines in IIH patients in order to determine a serum IIH specific profile of cytokines. These demonstrate homology with obese patients with the exception of reduced serum IL-8 (Ball et al., 2009; Samancl et al., 2017). These data suggest that IIH adipose tissue will secrete cytokines similarly to obese patients, however direct secretion of adipokines from IIH adipose tissue has yet to be described.

As the above detail alludes to, a significant amount of IIH adipose biology is currently presumed and therefore undetermined. The transcriptome, the expression of RNA, is undetermined. Furthermore the secretome, the hormones that IIH adipose secretes is unknown. Similarly the metabolome, the sum total of metabolic processes in IIH adipose tissue is unknown. Together investigating these factors in both SC and visceral adipose tissue, the two adipose depots contributing to truncal adipose, would provide a comprehensive phenotype of the proposed pathogenic adipose depots in IIH and facilitate future investigation as to their potential role in driving the pathogenesis of IIH.

1.9 Aims and Hypothesises

1.9.1 Hypothesis

Given that weight loss reduces the symptoms of IIH and that truncal obesity correlates with LP Opp, a marker of disease severity in IIH, it is hypothesised that truncal adipose tissue in IIH is phenotypically deranged and that this derangement drives the pathogenic phenotype in IIH (Hornby et al., 2018a; Sinclair et al., 2010a).

There is controversy in the leptin phenotype in IIH due to non-standard study designs and inappropriate controls. As such, this needs to be addressed in a large IIH cohort with appropriate controls. It is hypothesised that leptin dynamics are perturbed in IIH.

Given that IIH patients have an androgen excess phenotype and that therapeutic testosterone is thought to cause intracranial hypertension in female-to-male gender reassignment patients, it is hypothesised that testosterone can modulate the Na^+/K^+ ATPase, thus modulating ICP (Hornby et al., 2017; O'Reilly et al., 2019).

1.9.2 Aims

1. Comprehensively phenotype adipose tissue in IIH
2. Investigate leptin biology in IIH
3. Develop a novel *in vitro* Na^+/K^+ ATPase activity assay and validate against drugs and *in vivo* experiments
4. Evaluate the effects of testosterone on Na^+/K^+ ATPase activity in choroid plexus epithelial cells

Chapter 2 General methods

Unless otherwise stated, all chemicals and reagents come from Sigma, Poole, UK.

2.1Tissue culture

All tissue culture was carried out in a microbiological safely cabinet using aseptic technique.

2.1.1 Z310 cells

Z310 cells, a validated immortalised choroid plexus epithelial cell line derived from mixed sex Sprague-Dawley rats, express serval phenotypic markers of choroid plexus epithelial cells, such as transthyretin, tight junction markers and grow in a cobble-stone-like morphology (Fig2.1) (Zheng and Zhao, 2002).

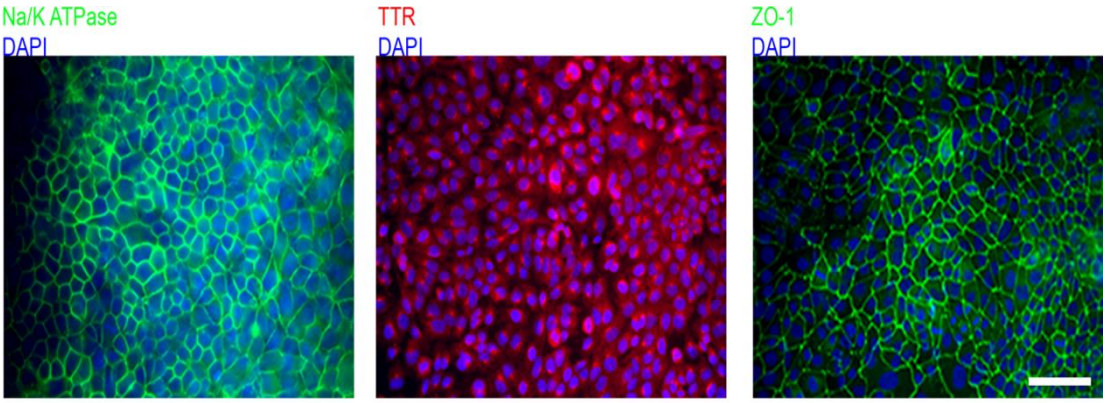

Figure 2.1 Z310 cells express phenotypic markers of choroid plexus epithelial cells

Z310 cells express Na^+/K^+ ATPase, Transthyretin (TTR) and zona-occluden 1 (ZO-1) Scale bar 100 microns. Based on previous unpublished work.

2.1.2 Z310 cell culture

Z310 cells were cultured in high glucose (25 mM) Dulbecco's modified eagle medium (DMEM) with 10% foetal bovine serum, 1% penicillin/streptomycin (Thermofisher, Paisley, UK) and 1 ng/ml epidermal growth factor (EGF) (PeproTech, London, UK) in T75 flasks and incubated at 37°C in a humidified atmosphere at 5% CO_2. For maintenance of the cells, Z310 cells were passaged at 80% confluence. Cells were washed in warm phosphate buffered saline (PBS) and dissociated with TrypLE express (Thermofisher) until cells had lifted from the flask and dissociated. Subsequent cell suspensions diluted 2:1 with DMEM and cell suspension was pelleted at 450 g. Cells were then re-suspended in culture medium and plated.

2.2 Plate based Na^+/K^+ ATPase activity assay

To determine the Na^+/K^+ ATPase activity of cultured Z310 cells, Z310 cells were cultured in 12 well plates to confluence. When confluent, Z310 cells were incubated in artificial cerebrospinal fluid (aCSF) (in mM: 118 NaCl, 22 $NaHCO_3$, 1.45 K_2HPO_4, 1 $MgSO_4$, 1 $CaCl_2$ and 10 glucose) at 37°C. Following this, aCSF was removed and Z310 cells were incubated in either vehicle (aCSF) or 1 mM ouabain (Na^+/K^+ ATPase inhibitor) in aCSF at 37°C. Subsequently, Z310 cells were incubated for 5 minutes with ice cold lysis buffer (in mM: 20 Tris-HCl pH 7.4, 150 NaCl, 1 EDTA, 0.5 EGTA, 1% NP-40 and 5 µg/ml protease inhibitor cocktail) and were centrifuged at 13,000g at 4ºC to remove cellular debris. Times of aCSF and ouabain incubation are assessed in chapter 5. Total inorganic phosphate was assayed (see section 2.3) and normalised to protein (see section 2.4). The difference between inorganic phosphate levels between

cells treated with aCSF and ouabain in a particular condition was deemed to be the contribution of Na^+/K^+ ATPase to total cellular phosphate, thus Na^+/K^+ ATPase activity.

2.3 Inorganic phosphate assay

Total cell lysate (section 2.2) inorganic phosphate concentration was determined via a colorimetric phosphate assay (ab65622, Abcam, Cambridge, UK) carried out according to manufacturer's instructions, where optical density (OD) was measured on a Wallac victor3 1420 plate reader (Perkin Elmer, London, UK) at 690nm. Samples were ran in triplicate. Sample values were interpolated from a standard curve generated from known quantities of inorganic phosphate (Fig2.2).

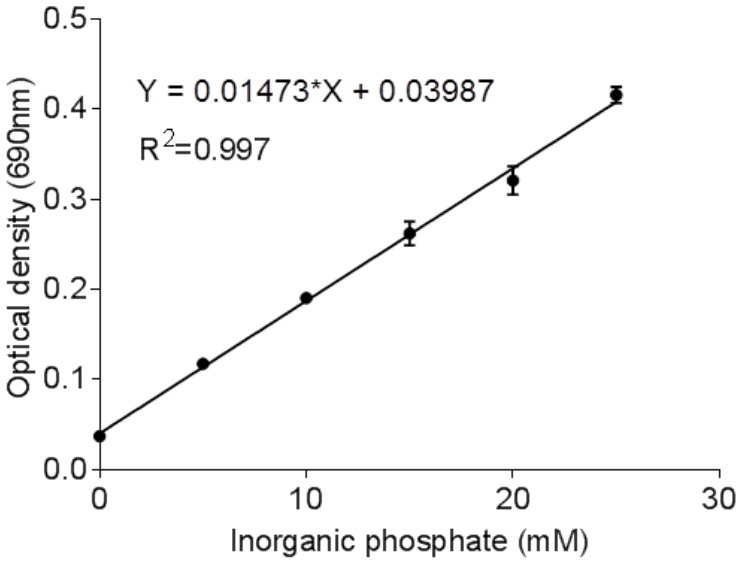

Figure 2.2 Exemplar phosphate assay standard curve

Following phosphate assay, a standard curve was generated using known concentrations of inorganic phosphate, samples were the interpolated using the straight line equation y=mx+c.

2.4 Protein assay

A protein assay (DC protein assay, BIO-RAD, Hemel Hempstead, UK) was used to quantify lysate protein (2.2) and carried out according to manufacturer's instructions, where samples were ran in triplicate on the Wallac victor3 1420 plate reader at 690nm. Sample values were interpolated from a standard curve generated from known quantities of bovine serum albumin (BSA) (Fig2.3).

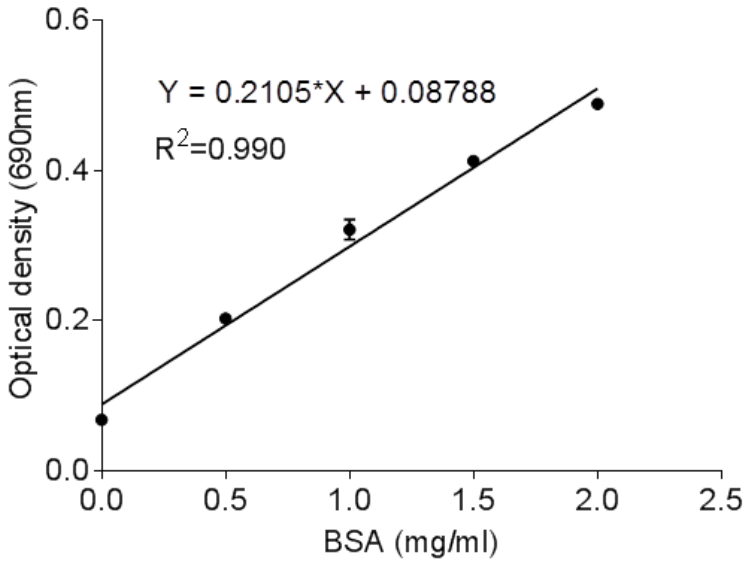

Figure 2.3 Exemplar protein assay standard curve

Following protein assay, a standard curve was generated using known concentrations of BSA, samples were the interpolated using the straight line equation y=mx+c.

2.5 Rat tissue collection

Female Sprague-Dawley rats (Charles-river, UK) weighing between 175-200 g were used at the University of Birmingham in accordance with the Animals and Scientific Procedures Act 1986, licensed by the UK Home Office and approved by the University of Birmingham Ethics Committee. Rats were housed in cages

under a 12 hour light/dark cycle with *ad libitum* access to food and water. Rats were sacrificed via rising CO_2 concentration and lateral and 4th ventricle choroid plexus, whole adrenal gland and whole ovary were dissected out and snap frozen in liquid nitrogen and transferred to a -80°C prior to RNA extraction.

2.6 Human choroid plexus

Human choroid plexus was obtained from the Parkinson Brain bank at Imperial Collage London, covered under ethics granted by the Wales research ethical committee (REC) (08/MRE09/31+5). Choroid plexus was retrieved within 24 hours post-mortem, where immediately after dissection tissue was placed into RNA later (Thermofisher). Upon arrival to University of Birmingham labs tissue in RNA later was placed into a -80°C prior to experimentation.

2.7 Ribonucleic acid extraction and analysis

2.7.1 Principle

Messenger ribose nucleic acid (mRNA) abundance and identity partially determines the protein quantity within a cell and determines cellular function and phenotype. Consequently assessing mRNA transcript abundance provides an assessment of the potential cellular phenotype.

2.7.2 Gene Elute RNA extraction kit

Total cell and tissue RNA was extracted in a nuclease free environment. For cultured cells and non-adipose tissue the Gene Elute kit was used according to manufacturer's instructions. Cultured cells were lysed in culture plates using lysis reagent supplemented with β-mercaptoethanol prior to going through the kits spin columns, whereas tissue was mechanically homogenised utilising a

rotational homogeniser in lysis reagent. Lysates were passed though spin column washes prior to elution utilising nuclease free H_2O.

2.7.3 Adipose tissue RNA extraction

The lipid rich nature of adipose tissue necessitates the use of the RNeasy Plus Universal kit (Qiagen, Manchester, UK) which separates lipids from polar molecules such as RNA. Adipose tissue was mechanically homogenised utilising a rotational homogeniser in QIAzol lysis reagent, incubated with a genomic DNA eliminator and incubated with molecular grade chloroform prior to column washes and elution in nuclease free H_2O.

2.7.4 RNA quantification

RNA purity and quantity was determined via a Nanodrop ND-1000 Spectrophotometer (Thermofisher), where 260/230 and 260/280 ratios provided information about sample purity and DNA contamination respectively. A ratio of around 2 for each represents good purity and DNA free extraction. RNA was stored at -80°C.

2.7.5 RNA reverse transcription

RNA is an inherently unstable molecule due to being single stranded, as such converting to the more stable double stranded DNA provides longevity for the transcript. RNA is converted to copy DNA (cDNA) utilising the high-capacity cDNA Reverse Transcription Kit (Thermofisher) in a 20µl reaction (See table 2.1 for components of reaction). A Gene Amp PCR system 2700 (Thermofisher) thermal cycler was ran in the following settings, 25°C (10mins), 37°C (120 mins), 85°C (5 mins) and at 4°C to cool the samples until storage at -20°C.

Component	Volume (µl)
10X RT buffer	2.0
25X dNTP Mix (100mM)	0.8
10X RT Random Primers	2.0
MultiScribe Reverse Transcriptase	1.0
RNA diluted in nuclease free H_2O	14.2

Table 2.1 Components of High capacity cDNA kit

Quantity of each reagent required for one cDNA generation reaction.

2.7.6 Quantitative real-time PCR

2.7.6.1 Quantitative real-time PCR principle

Quantitative real time PCR (RT-qPCR) is a sensitive technique that determines the quantity of a transcript through the use of fluorescent primers. These primers are specific to a particular nucleotide sequence, with primers specific for the 3'-prime and 5'-prime ends of the sequence of interest; as such they will bind to the cDNA molecule of interest and facilitate its amplification. Taqman gene expression assays also contain a probe that binds to a complementary portion of DNA between the 3'-prime and 5'-prime primers. The 5-prime end of the probe contains a fluorophore that is liberated when DNA-polymerase reaches it, this removes the dye from the proximity of a quencher on the 3-prime end of the probe allowing it to fluoresce and be quantified. Amplification runs in heat cycles, each cycle doubles the quantity of the cDNA, as such there is an exponential increase in cDNA and therefore fluorescence as cycles

progress. Consequently, 100 times difference in cDNA quantity is represented by a 6.64 difference in cycles. Amplification is measured in logarithmic portion of the graph, where it provides a cycle threshold value (Ct) (Fig2.4). This Ct value is the basis of quantification measurements.

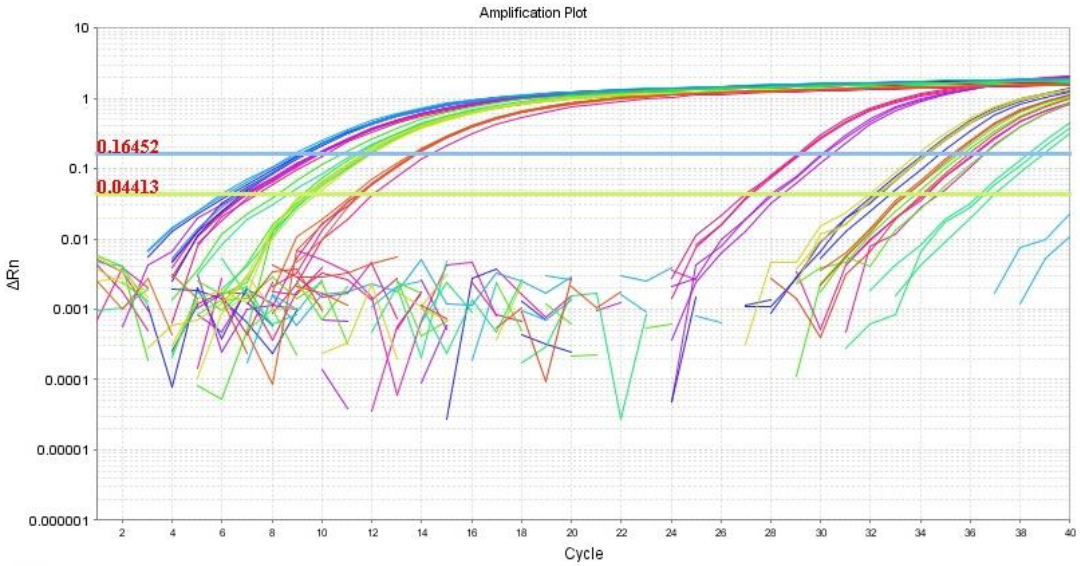

Figure 2.4 Exemplar RT-qPCR plot

Y-axis represents relative fluorescence compared to baseline. X-axis represents cycle. The horizontal lines represent threshold for amplified genes, whereby the threshold fall into the linier part of the graph. Coloured lines represent an individual gene's amplification.

2.7.6.2 Quantitative real-time PCR protocol

RT-qPCR was carried out with single-plex, 10ng cDNA, 10µl assays using an ABI 7500 PCR machine (Thermofisher). Assay mix comprises of 0.5 µl of primer/probe set, 5 µl of master mix (Thermofisher) and the remainder comprised of cDNA diluted in nuclease free H_2O. Genes of interest were ran in triplicate. Primer probe sets utilised the reporter fluorescein (FAM). VIC is the reporter for specific ribosomal subunit 18s, utilised as a reference gene. For a

full list of primer probe sets see appendix 2. The thermocycler conditions were 95°C for 10 minutes followed by 40 cycles of 95°C for 15 seconds and 60°C for 1 minute.

Expression was expressed relative to the housekeeper genes 18s or GAPDH as ΔCt, where ΔCt = [Ct gene of interest – Ct reference gene]. Arbitrary units (AU) were derived as follows: 1000*(2^-ΔCt). Fold change in expression was derived as follows 2^-((ΔCt of subject) - (mean ΔCt of control)).

2.8 Immunocytochemistry

2.8.1 Principle

Immunocytochemistry is a semi-quantitative technique that determines the presence and localisation of a target protein (epitope) in a cell utilising antibodies specific to the epitope (primary antibody). This primary antibody is detected by a secondary antibody that is conjugated to a fluorophore that emits a known spectrum of light under stimulation of a specific wavelength.

2.8.2 Method

Z310 cells were seeded onto 8-well culture slides (VWR, Lutterworth, UK) primed with poly-d-lysine (0.1 mg/ml in sterile H_20) and coated with laminin (20 µg/ml) (Thermofisher) for 1 hour each prior to seeding of cells. Following two days of culture, Z310 cells were fixed in fixative (2% PFA, 2 % glucose in PBS) for 20 minutes at room temperature before a single 3 minute wash in PBS. Z310 cells were permiabilised with methanol for 6 minutes before washing in PBS. Z310 cells were then blocked with blocking solution (10% normal goat serum (Vector Laboratories, Peterborough, UK), 2 % BSA in PBS) for 30 minutes and

incubated overnight at 4^{o}C with the primary antibody (diluted in 2% BSA in PBS) in a humidified chamber. Subsequently, the cells were washed with PBS before the addition of the secondary antibody (2% BSA, 1.5% normal goat serum in PBS) for 1 hour in the dark. Finally, Z310 cells were washed in PBS and a coverslip mounted using mounting media containing 4',6-diamidino-2-phenylindole (DAPI) to counterstain nuclei (Vector Laboratories). Slides were stored in the dark prior to microscopy. No primary antibody staining was used as control.

2.8.3 Microscopy

Z310 cell images were taken on a Zeiss Axioplan 2 imaging epifluorescent microscope (Carl Zeiss, Jena, Germany) and a AxioCam Hrc (Carl Zeiss) were used to view and capture images.

2.9 Serum, plasma and CSF

Plasma, serum and CSF were collected from IIH patients in both the IIH drug trial (IIH:DT) (NCT02017444) and IIH weight trial (IIH:WT) (NCT02124486) as well as controls in IIH:WT according to the published protocols, where CSF contained a DPP4 inhibitor (Millipore) and plasma contained both a protease inhibitor cocktail and a DPP4 inhibitor (Markey et al., 2017; Ottridge et al., 2017). Material from IIH:DT was covered under ethics granted by the York-Humber REC (13/YH/0366) and material from IIH:WT was covered under ethics granted by the Black Country REC (14/WM/0011).

Procedures and sample processing were carried out by staff at the Birmingham Wellcome trust clinical research facility (CRF) (IIH:WT and IIH:DT), Department of Eye Research Manchester Royal Eye Hospital (IIH:WT), Diabetes and

Vascular Research Royal Devon and Exeter Hospital (IIH:WT) and the Walton Centre for Neurology and Neurosurgery Liverpool (IIH:DT).

CSF was collected via a lumbar puncture (LP), were CSF was placed immediately on ice and centrifuged to pellet any cellular material. Acellular CSF was aliquoted and stored at -80°C. Sites of LPs received local anaesthetic. Serum was derived from clotted venous blood that was centrifuged prior to storage at -80°C. Plasma was derived from unclotted venous blood in EDTA tubes, centrifuged prior to aliqoting and storage at -80°C.

2.10 Adipose tissue acquisition

Adipose tissue was derived from two clinical trials, IIH:DT and IIH:WT. Adipose tissue collection from the IIH:DT were covered under ethical approval (13/YH/0366) and was biopsied, following written informed consent, by clinical staff at the CRF. Local anaesthetic applied to biopsy area and subcutaneous adipose tissue biopsied, where adipose tissue was placed directly into RNA later (Thermofisher) and placed into a -80°C freezer. Paired omental and subcutaneous adipose tissue was acquired as part of the IIH:WT (14/WM/0011) at Heartlands hospital (Heart of England NHS Foundation Trust Birmingham). Control patients, undergoing elective bariatric surgery, provided written informed consent and tissue was biopsied by the operating surgeon. Adipose tissue from IIH patients was taken from patients who were randomised to the surgical arm of the IIH:WT. Patients provided written informed consent for the tissue biopsies. Subcutaneous tissue was removed from an area containing local anaesthetic and adipose tissue was biopsied by the lead surgeon. Adipose

was either immediately placed into RNA later (Thermofisher), placed into phenol free DMEM/F12 containing no serum or antibiotics, or placed into 4% formaldehyde and kept for further analysis as described by figure 2.5.

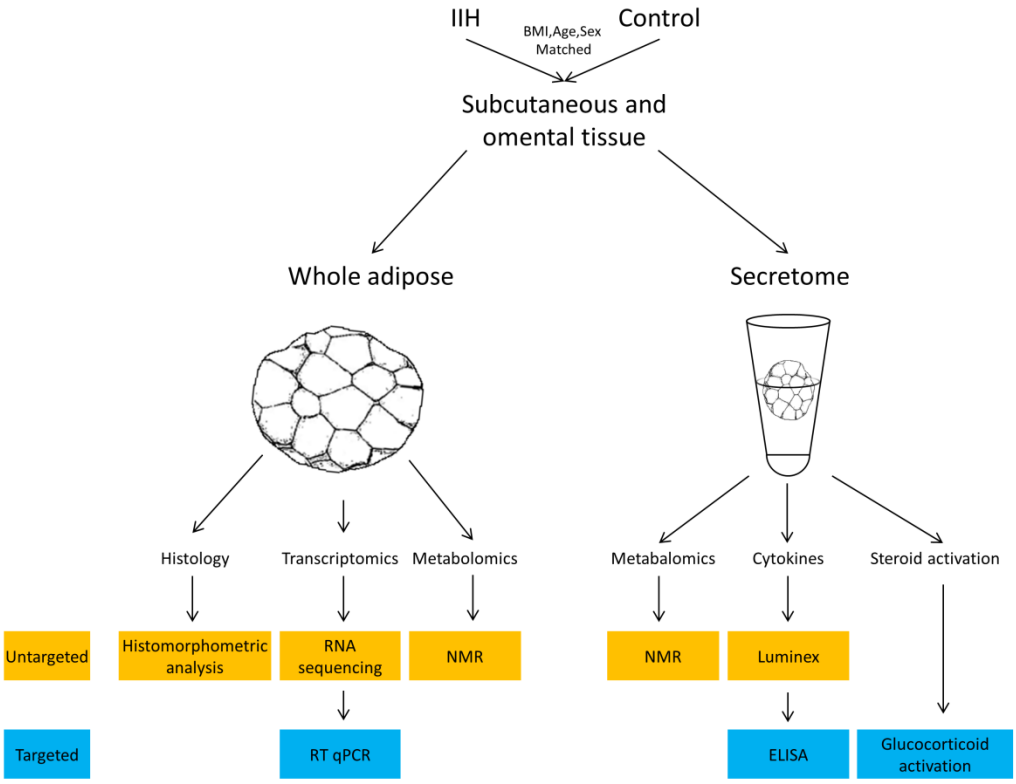

Figure 2.5 Adipose tissue analysis schematic

Schematic of the utilisation of biopsied adipose tissue.

2.11 Histology

2.11.1 Tissue processing

Human subcutaneous adipose and omental adipose were fixed in 4% PFA prior to processing. Tissue was dehydrated in serial increasing concentrations of industrial methylated spirit for 1 hour at 40%, 70% and twice at 100%. Tissue was subsequently cleared in xylene three times for 1 hour each. Tissue then incubated in paraffin wax twice for 1 hour each prior to an overnight incubation in wax. Tissue was then embedded in paraffin wax.

2.11.2 Haematoxylin and eosin staining

Embedded tissue was cut into 5 μm sections. Sections were initially dewaxed and rehydrated (immersion in xylene, 3 x 5 minutes, and then in 100% ethanol, 2 x 5 minutes). Staining was then carried out using Meyer's haematoxylin for approximately 30 seconds. Excess haematoxylin was removed by washing in running tap water for 5 minutes and then blued, through immersion in 1% acid alcohol for 30 seconds. Counter straining was carried out with eosin and again irrigated for 5 minutes in tap water. Sections were dehydrated in 100% ethanol (2 x 5 minutes) and cleared in xylene (2 x 5 minutes) prior to mounting with VectaMount Permanent Mounting Medium (Vector).

2.11.3 Histomorphometric analysis

Images were acquired using Leica DM ILM inverted microscope (Leica Microsystems UK Ltd, Milton Keynes, UK) though a Leica DFC290 camera (Leica) utilising the Leica application suite (V2.8.1, Leica). The Image J (National Institutes of Health, Bethesda, MD) plugin Adiposoft (Galarraga et al.,

2012), a semi-automated segmentation software, was utilised to segment, count and determine the area of adipocytes. Samples were manually segmented where adipocytes were not sampled, furthermore erroneous segmentations were removed. Where tissue quantity allowed, 3 images from three slides per patient were analysed. To determine the frequency of adipocyte areas, adipocyte areas for each patient were placed into GraphPad prism (V 7.1, GraphPad software, La Jolla, CA) and frequency distribution function was used, where the mean frequency for each area bin was calculated.

2.12 RNA sequencing

RNA was extracted commercially by AROS (Aarhus, Denmark), Library preparation and RNA sequencing was carried out commercially by Eurofins in Germany. Bioinformatics were carried out in collaboration with Mark Walsh and Daniel Hebenstreit at the University of Warwick and Ildem Akerman at the University of Birmingham.

2.12.1 RNA sequencing method

RNA was extracted using the RNeasy Lipid tissue mini kit by staff at Aros (Copenhagen, Denmark). RNA quality and quantity was analysed using a fragment analyser, where there was no difference in RNA quality (7.5±0.82 vs. 7.7±0.50, P=0.6) between IIH and control patients, indicating acceptable quality RNA. cDNA libraries were prepared using Illumina's Stranded mRNA kit (Illumina Inc. San Diego, CA) and sequencing was ran on the Illumina HiSeq 2500 platform (Illumina Inc), with 2X100pb paired end reads across two flow cells. RNA sequencing data presented as fragments per kilobase million

(FPKM), where this is derived as follows, number of mapped gene fragments normalised to both the length of the gene and depth of sequencing achieved in the sample.

2.12.2 Bioinformatic analysis

Quality control on the RNA sequencing was performed with FastQC v0.11.4. Read and adapter trimming was carried out using TrimGalore! v0.4.4 with Cutadept v1.13 with default settings (Martin, 2011). RNA-seq reads were mapped to the human genome (hg19, UCSC annotation) utilising STAR software v2.5.3a with default parameters (Dobin et al., 2013). Counts per gene were calculated using custom scripts acting in a HTSeqcount compatible mode with the following parameters: --format=bam --minaqual=10 --stranded=reverse –mode=union (Anders et al., 2015). Differentially expressed genes were identified using the DESeq2 (v1.14.1) from Bioconductor release 3.3 (Love et al., 2014). Differentially expressed genes were called at a false discovery rate of 5%. Normalised FPKM values for each gene were calculated using DESeq2 and GenomicFeatures v1.26.4 package (Lawrence et al., 2013). GSEA analysis was utilised to interrogate specific gene sets in the RNA-seq expression data (Mootha et al., 2003; Subramanian et al., 2005). GSEA calculates an Enrichment Score (ES) through scanning a ranked-ordered list of genes (according to significance of differential expression (-log10 p-value x the sign of fold enrichment), increasing a running-sum statistic when a gene is in the gene set and decreasing it when it is not. The top of this list (red) contains genes upregulated in IIH patients while the bottom of the list (blue) represents downregulated genes in IIH. Each time a gene from the gene set is found along

the list, a vertical black bar is plotted (hit). If the 'hits' accumulate at the bottom of the list, then this gene set is enriched in upregulated or downregulated genes, dependent where it is on the list. If the genes are distributed homogenously across the rank ordered list of genes, then that gene set is not enriched in any of the gene expression profiles (IIH vs Control subjects).

2.13 Adipose tissue incubation

Incubations were carried out in an aseptic manner in a microbiological safety cabinet. Tissue was weighed as wet weights prior to incubation. Paired omental and subcutaneous adipose tissue had large blood vessels dissected out prior to incubation of ~100 mg chunks in phenol free DMEM/F12 (Thermofisher) with no serum antibiotics in glass tubes (VWR) covered in cling film for 24 hours in a humidified incubator at 5% CO_2 at 37^0C without agitation. Media and adipose tissue explants were removed and immediately placed in a -80°C freezer. Tissue incubation time was optimised through assessing lactate concentrations, via NMR (2.14), in explants incubated for either 24 or 48 hours. Although all explants generated lactate in the millimolar range the 48 hour incubation generated significantly more lactate in both the OM (24h; 2.3±2.0 vs 45h; 9.7±1.7 ΔmM; P<0.0001) and SC adipose (1.7±0.8 vs 8.0±2.4 ΔmM; P<0.0001) indicating major hypoxia and likely cell death at the 48 hour time point. Consequently the 24 hour time point was selected (Fig 2.6).

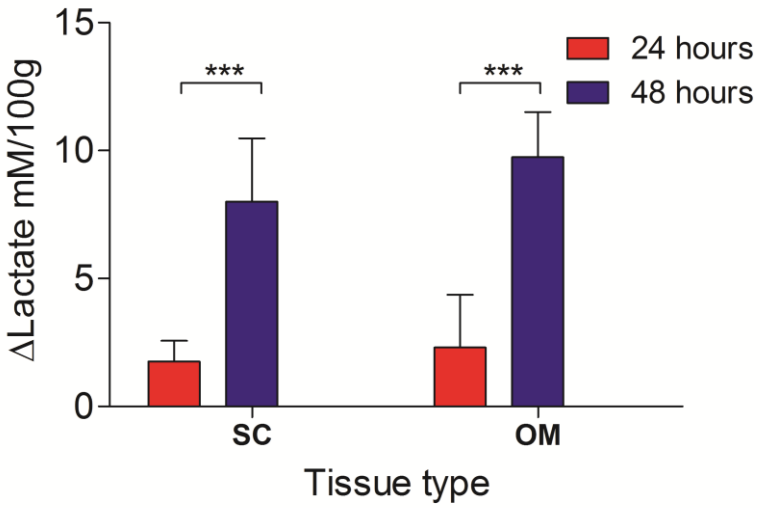

Figure 2.6 Adipose tissue time incubation optimisation

Adipose tissue from control subcutaneous and omental adipose underwent a time course experiment where NMR was ran on the conditioned media and lactate was assessed. N=5 for each group, data presented as mean±SD, ***=P<0.0001.

2.14 Nuclear Magnetic resonance spectroscopy

Thanks to Christian Ludwig who ran the samples on the NMR spectrometer at the Henry Wellcome NMR building at University of Birmingham.

2.14.1 NMR Principle

Atomic nuclei have a spin, this confers a magnetic property on the nucleus, similar to that of a bar magnet. This spin is determined the local nuclear environment of the nucleus. This can be manipulated by a magnet to pull all the nuclei in the same polarity. The removal of the magnetic force allows atomic nuclei to return to their original polarity. This return to polarity causes the nuclei to emit electromagnetic radiation which can be detected by a receiver. The pattern of the electromagnetic radiation relates to the orientation of molecules around the molecule of interest, in the case of this work, it is hydrogen atoms.

As such the local nuclear environment of a hydrogen atom will provide a unique wave form thus unique spectral footprint (Fig 2.7)

2.14.2 Sample preparation

Adipose tissue conditioned media from section 2.13 were thawed and placed into NMR buffer with a final concentration of 100 mM sodium phosphate buffer containing 500 µM 4,4-dimethyl-4-silapentane-1-sulfonic acid (DSS), 2 mM imidazole and 10% deuterium (D_2O).

Corresponding adipose tissue explants were homogenised in ice cold HPLC grade methanol (500 µl) prior to the addition of HPLC water (500 µl) and 10 minute sonication followed by 10 minute incubation on ice prior to the addition of ice cold HPLC grade chloroform (500 µl) and 10 minute agitation at 4°C. Samples were then centrifuged for 15 minutes at 1300 g. The procedure allows separation of lipids, protein and polar metabolites into distinct layers. The top clear layer containing polar metabolites was aliquoted into new tubes prior to evaporation of fluid under a vacuum. Dried samples reconstituted in 60 µl of 100 mM sodium phosphate buffer containing 100% D_2O and 500 µM DSS, where samples were sonicated for 10 minutes prior to a brief centrifugation. All samples were transferred into 1.7 mm Bruker Sample Jet NMR tubes (Cortecnet, Voisins-Le-Bretonneux , France) via an automatic Gilson.

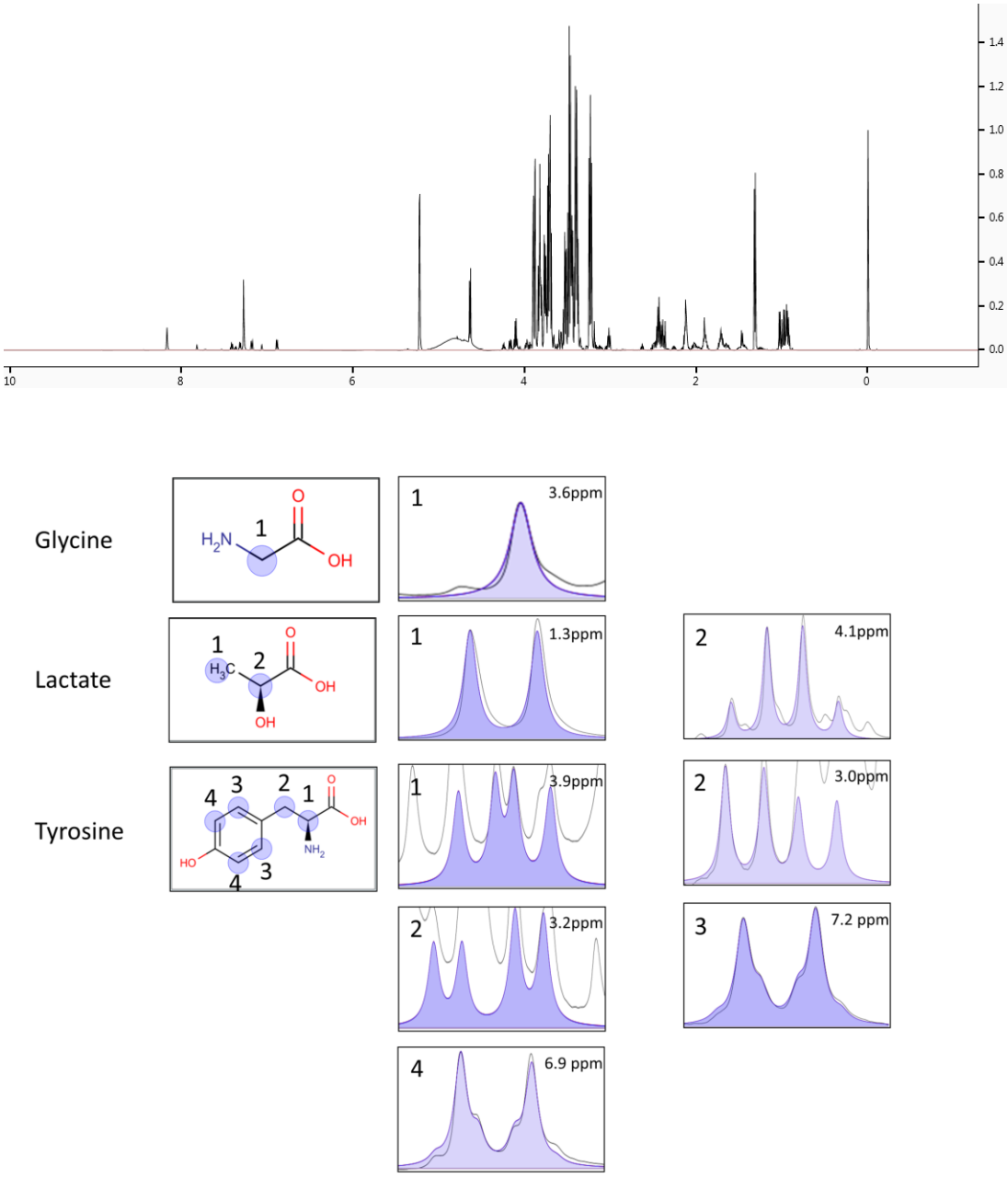

Figure 2.7 NMR peaks and corresponding hydrogen atoms

Exemplar NMR spectra from conditioned media. Blue dots and adjacent numbers correspond with numbered peaks.

2.14.3 NMR Spectroscopy

Samples were ran on a Bruker 600 MHz Bruker Avance III spectrometer (Bruker Biospin) with a TCI 1.7 mm z-PGF cryogenic probe set at 300K. 1D ^{1}H-NMR spectra were obtained, where spectral width was set to 7,812.5.

2.14.4 Data analysis

1D-^{1}H-NMR spectra were processed using MetaboLab software (Ludwig and Gunther, 2011). All 1D data sets were zero-filled to 131,072 data points prior to Fourier Transformation. The chemical shift was calibrated by referencing the DSS signal to 0 p.p.m. 1D-spectra were manually phase corrected. Batch baseline correction was achieved using a spline function. 1D ^{1}H-NMR spectra were exported into Bruker format for metabolite identification and concentration determination using Chenomx 7.0 (Chenomx INC, Edmonton, Canada). All values obtained were normalised to the mass of the appropriate adipose tissue explant. Conditioned media values were made relative to a media blank reference.

2.15 Luminex

2.15.1 Principle

Luminex is an immunoassay based technology that allows the identification of multiple analytes, multiplexing, through the use of antibody covered beads. A set of beads is coated with antibodies specific to one peptide; furthermore this set of beads has a specific colour allowing its identification. Secondary antibodies specific for the analyte of interest conjugated to phycoerythrin, a

fluorophore, allows for quantification of the analyte. An initial laser identifies the bead, thus antibody species and another allows quantification of the analyte.

2.15.2 Method

Conditioned media were ran using custom ProcartaPlex luminex kits (Thermofisher) used neat and manufacturer's instructions were followed with regards to the protocol. Samples were ran on the Luminex 200 system (Luminex Corp.'s-Hertogenbosch, Netherlands) according to manufacturer's instructions using supplied software.

2.15.3 Analysis

Operating software automatically constructs the standard curve and interpolates the concentrations of analytes. Data was then exported into Microsoft Excel spreadsheets to allow for further analysis. Concentrations were normalised to the mass of tissue. Assays ran can be seen in the table 2.2

	Peptide	Abbreviation	Bead region	Detection range (pg/ml)
3-plex	Interleukin-8	IL-8	27	9850-2.4
	Leptin	LEP	45	49200-12.01
	Monocyte chemotactic protein 1	MCP-1	51	14800-3.61
4-plex High-sensitivity	Interleukin-1β	IL-1β	18	825-0.2
	Interleukin 10	IL-10	28	925-0.23
	Interleukin 6	IL-6	25	3780-0.92
	Tumour necrosis factor-α	TNF-α	45	2950-0.72

Table 2.2 Analytes for Luminex assay

2.16 Enzyme-linked immunosorbent assay

2.16.1 Principle

Enzyme-linked immunosorbent assay (ELISA) is an immuno-assay that allows the quantification of a peptide in a fluid through a chromogenic change. Sandwich ELISAs utilise several antibodies to detect and quantify a peptide of interest (see figure 2.8). In brief a capture antibody binds the peptide of interest, immobilising it. A detection antibody, conjugated to biotin, then binds the peptide. The addition of streptavidin-HRP provides the enzyme that develops the chromogenic change following the addition of a chromogenic substrate.

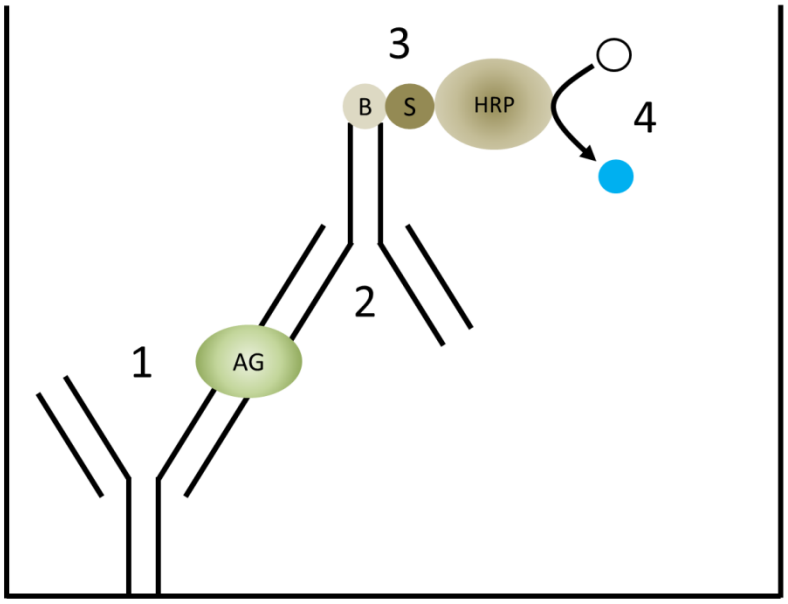

Figure 2.8 Sandwich ELISA Principle

Sandwich ELISAs utilise a capture antibody (1) that coats the well to capture and immobilise the antigen (AG). The AG is subsequently bound by a detection antibody (2) that has a conjugated biotin moiety. The addition of streptavidin (S) conjugated to the horseradish peroxidase (HRP) (3) allows for colour change flowing the addition of a chromogen (4). In this situation, the higher the optical density, the higher the concentration of the peptide of interest.

2.16.2 Protocol

Human leptin DuoSet ELISA (DY-398,Bio-techne, Abingdon, UK) was utilised, used according to manufacturer's instructions using recommended ancillary kit (Bio-techne, DY008). Dilution factor was optimised, where adipose conditioned media was diluted 1:50, serum was diluted 1:100, plasma was diluted 1:200 and CSF was diluted 1:5. All samples were diluted in supplied regent diluent. A standard curve was generated using known concentrations of recombinant human leptin, providing a detection range of 2000-31.3 pg/ml. OD was read at 450 nm, data were exported in Excel spreadsheet (Microsoft, WA) format and the standard curve was generated from the log_{10} OD in Graph-pad Prism using the sigmoidal 5PL function, prior to interpolation of samples (Fig2.9).

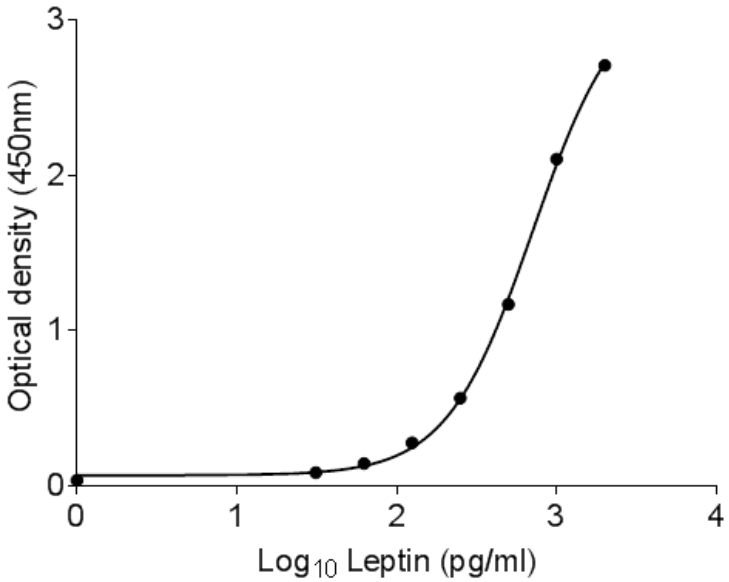

Figure 2.9 Exemplar leptin ELISA standard curve

Following an ELISA, a standard curve was generated using known log_{10} transformed concentrations of leptin, samples were then interpolated.

2.17 11β-HSD1 activity assay

Subcutaneous adipose tissue was cut into roughly 100 mg explants and were placed into glass tubes (VWR) in phenol free DMEM/F12 with a supraphysiological concentration of cortisone (200 nM) for 24 hours; samples were ran in triplicate. A glass tube with phenol free DMEM/F12 and 200 nM of cortisone without adipose tissue served as a no conversion control. The quantity of cortisol was measured via liquid chromatography-mass spectrometry (LCMS) (section 2.17.1). Values were normalised to the mass of the adipose tissue explants. Following the 24 hour experiment, samples were aliquoted and stored at -20°C prior LCMS.

2.17.1 LCMS

Tissue culture media (1ml) had the lipid portion, including steroid hormones, extracted via a liquid-liquid extraction with 3 ml of tert-butyl-methyl-ether (MTBE) in sylinised glass tubes. 20 µl of internal standard was added to facilitate quantitative analysis. Samples were vortexed, and frozen at -20°C for a minimum of 1 hour. The subsequent upper clear layer was transferred to a 96-well plate using glass Pasteur pipettes. Repeated cycles of evaporation at 55°C under nitrogen and further liquid transfer were carried out until samples had evaporated completely. Following evaporation, samples were reconstituted with 125 µl of methanol:H_2O (50:50) and frozen at -20°C until LCMS analysis. LCMS was ran at the University of Birmingham Steroid Metabolome Analysis Core.

2.18 Live cell Imaging

2.18.1 Plating and infection of Z310 cells

Z310 cells were plated on ethanol cleaned 25 mm diameter glass coverslips (VWR, Leighton Buzzard, UK) primed with poly-d-lysine (0.1 mg/ml in sterile H20) and sequentially coated with laminin (20 µg/ml in PBS) for 1 hour each. Z310 cells were then seeded and allowed to adhere for 30 minutes prior to the addition of culture media and an adenovirus containing the biosensor Perceval provided as a kind gift from Professor David Hodson (Berg et al., 2009; Hodson et al., 2014). Viral titre was sufficient to allow for experimentation 48h after infection.

2.18.2 Imaging protocol

In brief, ATP/ADP ratio was imaged using a Crest X-Light spinning disk head (Crestoptics S.p.A, Rome, Italy) coupled to a Nikon Ti-E automated base (Nikon Instruments Europe BV, Amsterdam, Netherlands) and 10x/0.4 NA objective. Excitation was delivered by a Lumencor Spectra X Light Engine (Lumencor, Beaverton, OR) at 458–482 nm (0.2 Hz), emitted signals were detected with a Photometrics Evolve Delta 512 EMCCD (Photometrics, Tucson, AZ) at 500–550 nm. The ATP/ADP traces were normalised as F/F_{min}, where F is the fluorescence at a given time point, F_{min} is the minimum measured fluorescence. A CO_2 saturated HEPES-bicarbonate buffer was used, containing in mM: 120 NaCl, 4.8 KCl, 24 NaHCO3, 0.5 Na2HPO4, 5 HEPES, 2.5 CaCl2, 1.2 MgCl2, 25 glucose. Cells were imaged to gain a stable 15 minute baseline prior to treatment with ouabain (1 mM) to resolve Na^+/K^+ ATPase activity. Concentrations for test reagents can be found in relevant chapters.

2.18.3 Analysis of live cell data

Images were acquired with MetaMorph (Molecular devices, CA). An image sequence was initially analysed on ImageJ, where individual random cells are selected as a region of interest, motile cells are excluded from the analysis. Following this, the multimeasure function was selected with the mean grey function to determine the intensity of individual cells at each frame. Subsequent to this the F/F_{min} is determined for each frame, where F is the intensity for the cell in that particular frame and F_{min} is the lowest fluorescence intensity in the baseline period. This normalises the intensity change to baseline, taking into account any quantitative difference in ATP/ADP ratio between cells or differences in Perceval protein expression. Ouabain administration was utilised to initiate a change ATP/ADP ratio. This change in ratio or 'Δ' is the maximum value F/F_{min} following ouabain administration minus the maximum F/F_{min} in the pre ouabain administration (baseline). Area under the curve is generated for each cell using the area under the curve function in GraphPad prism. Assessor was blinded to the treatment of the cells during evaluation of cell fluorescence intensity.

2.19 *In vivo* intracranial pressure experiments

2.19.1 Experimental animals

The study utilised female Sprague-Dawley rats (Taconic, Ejby, Denmark) weighing 150-250 g. The rats were housed in cages under an inverted 12 hour light/dark cycle with ad libitum access to food and water. All experimental procedures were approved by the Danish Animal Experiments Inspectorate

(license number 2014-15-0201-00256). After treatments and surgical procedures, the rats were monitored daily for any adverse effects.

2.19.2 Epidural intracranial pressure probe implantation

Surgical procedure was carried out as previously described (Uldall et al., 2014). In brief rats were anesthetised with a subcutaneous injection (1.25 mg/kg midazolam, fluanisone 2.5 mg/kg and 0.079 mg/kg fentanyl citrate made in sterile saline) and placed in a stereotaxic frame (David Kopf Instruments, Tujunga, CA). Body temperature was maintained via a thermostatic heat pad, controlled by a rectal probe. A lidocaine and adrenaline solution was injected subcutaneously over the skull to prevent haemorrhage and provide local analgesia. Subsequently a 2 cm midline incision was made, tissue retracted exposing bregma and lambda. Fascia covering the skull was scraped away, including sutural fascia. A transcranial hole to fit an epidural probe was burred utilising a dental drill, keeping the dura intact. Three smaller holes for anchoring were made and screws inserted into the holes. Epidural probe (PlasticsOne) fit was tested, if the probe balanced on the dura and pulsed, fit was good. Dental cement (Clearfil SA Cement, RH Dental, Gentofte, Denmark) was used to affix the probe to the skull using the three small screws to anchor the cement (Fig 2.10a). Intracranial pressure (ICP) probe and transducer (DTX-Plus, Argon Medical Devices, Frisco, TX) were then connected via a polyethylene tube filled with sterile water and signal tested (Fig 2.10b). Where a good ICP trace is observed, the breathing pattern of the animal is apparent on the trace, a jugular vein compression confirms correct monitoring of ICP (Fig 2.10c). Skin was then sutured together and the wound covered in petroleum jelly. Rats received post-

operative antibiotics and analgesia. ICP probes were covered with a bite proof cap (PlasticsOne). ICP was recorded and visualised using Perisoft v2.5.5 (Perimed AB, Jarfalla, Sweden).

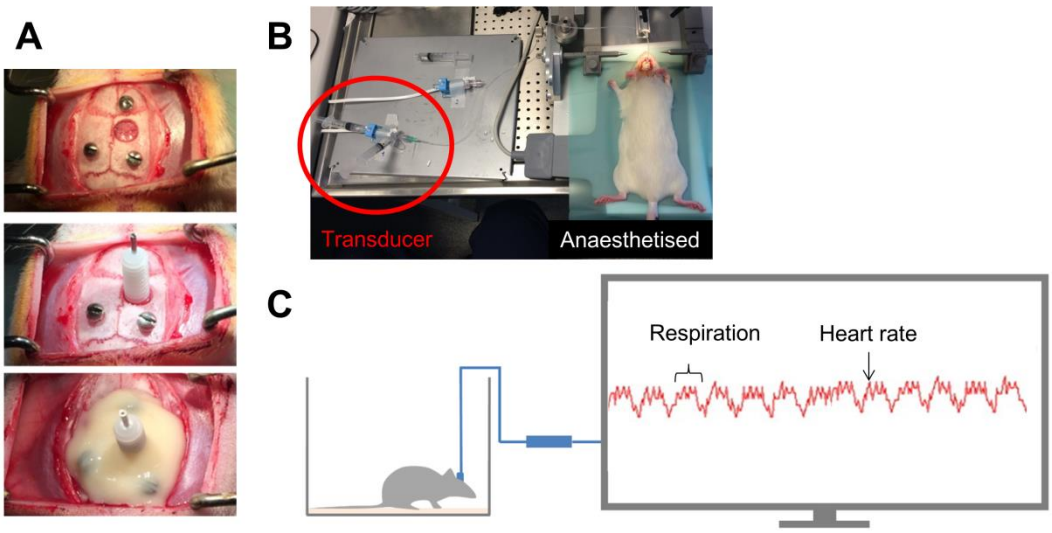

Figure 2.10 ICP surgery

Details of surgical procedure and experimental setup. A) Photographs of craniotomy with the insertion of anchoring screws, placement of ICP probe and application of dental cement. B) A rat attached to the fluid telemetric system. C) Schematic of experimental setup with a Perimed ICP trace detailing features of a resting ICP waveform.

2.19.3 Drugs

Acetazolamide (A6011, Sigma-Aldrich), furosemide (F4381, Sigma-Aldrich) powders were reconstituted in NaOH and then the pH lowered to 8.7 and 7.7 respectively. Furosemide was then diluted to working concentration in 0.9% saline. For acetazolamide, the osmolarity was equivalent to 2% NaCl for the clinical dose and high dose was equivalent to 4% NaCl.

Acetazolamide doses were 103.3 mg/kg (clinical) and 413.4 mg/kg (high) and Furosemide was used at 4.1 mg/kg (clinical) and 24.8 mg/kg (high), where

clinical dose represents a single human dose and high dose represents 1 day total dose. Dosage was work out via the following FDA derived equation [Rat drug] (mg/kg) = 6.2 X [human] (mg/kg based on 60kg human)(FDA, 2005). See table 2.3 for full dosage details.

Drug	Human single dose (Clinical)	Human daily dose (high)	Rat clinical dose	Rat high dose
Acetazolamide	1g	4g	103.3 mg/kg	413.4 mg/kg
Furosemide	40mg	240mg	4.1mg/kg	24.8 mg/kg

Table 2.3 Drug dosage equivalences

Drug dose equivalences based on assumed human mass of 60kg. Human dose based on the doses in the IIH:TT (Wall et al., 2014).

2.19.4 ICP monitoring and drug administration

Rats were sedated with 2.5 mg/kg midazolam (subcutaneous injection) and placed in an infusion cage (Instech Laboratories, Plymouth meeting, PA), which had a levered arm connected to the tube to provide unhindered movement. A stable baseline ICP reading was recorded for around 30 minutes, prior to a subcutaneous injection of the drug. ICP was recorded for a further 120 minutes after which the rat was returned to its normal cage. Animals received treatment in a randomised crossover study, where drugs were administered 3 days apart allowing for total elimination of the drug from circulation.

2.19.5 Power calculation

Power calculation was carried out based on a previous study (Uldall et al., 2017), where the minimum effect size was assessed. Where saline reduced ICP to 95 %, SD 10, power 0.8, alpha 0.05 for a 18% reduction in pressure yields N=5 rats per experimental group, minimising the use of animals.

2.19.6 Analysis of ICP

ICP was analysed using the Perisoft software. All ICP traces had the on the day atmospheric pressure subtracted to zero the pressure reading. Baseline ICP was determined through averaging the ICP 30 minutes prior to the injection of solution being investigated. After injection ICP was measured every 15 minutes whereby the average ICP 5 minutes prior to the 15 minute mark is averaged, this was repeated every 15 minutes for 120 minutes.

2.19 Statistics

The statistics package Graph-pad Prism (V7.1) was used to carry out statistical analysis and graph data. Normality of data was assessed using a Shapiro-Wilk normality test, where data was N<7, data was assumed to be normally distributed. Data were reported as mean ± standard deviation (SD) unless otherwise stated. Data variance assessed via F-test of equality variances. A P-value of 0.05 or less was considered significant. Inter-assay variability was identified by calculating the coefficient of variation (CV) via the following equation %CV = (standard deviation (SD) of plate means/mean of plate means) X 100. Intra-assay variability was calculated via the following equation %CV= (SD of sample/ mean of sample) X 100.

Chapter 3 The Adipose Phenotype in Idiopathic Intracranial Hypertension

3.1 Introduction

Idiopathic Intracranial Hypertension (IIH) is a condition that primarily affects obese women of reproductive age, where weight loss has been demonstrated to ameliorate the symptoms of IIH (Sinclair et al., 2010a). This suggests that IIH adipose tissue, which will be dysfunctional by definition due to concomitant obesity, may be functionally different from adipose tissue from the majority of obese women, who do not have IIH (Attie and Scherer, 2009; Sinclair et al., 2010a). Consequently it is proposed that adipose tissue in IIH is functionally distinct to non IIH obesity, such that mechanisms exist in IIH adipose to influence ICP, as suggested by the positive association between central adipose mass and ICP in IIH (Hornby et al., 2018a).

Evidence for adipose dysfunction in IIH comes from the observation that IIH patients have raised serum and CSF leptin, where this is presumed to come from increased adipose leptin secretion (Ball et al., 2009; Lampl et al., 2002). In addition, CSF leptin levels positivity correlate with lumbar puncture opening pressure (LP Opp)(Ball et al., 2009). Furthermore, it has been demonstrated in two independent IIH cohorts, utilising DEXA scans, that truncal adipose mass positivity correlates with LP Opp in IIH patients highlighting the potential for adipose tissue to contribute to the raised ICP in IIH (Hornby et al. 2018, Botfield et al. in preparation). These studies however, do not identify whether subcutaneous (SC) or omental (OM) adipose tissue mass is specifically associated with LP Opp and thus remains to be determined.

The association between both CSF leptin, truncal adipose mass and LP Opp suggests that factors associated with SC or OM adipose could directly

contribute to IIH disease activity and account for some level of differential phenotype. However beyond these associations there has been minimal assessment of the adipose phenotype in IIH patients. This chapter details the phenotyping of IIH adipose tissue.

3.1.1 Hypothesis

Given that weight loss improves IIH symptoms and that central adiposity is associated with LP Opp, a measure of IIH disease intensity, it is hypothesised that adipose tissue from IIH SC and OM adipose tissue is functionally distinct from simple obese adipose tissue, and contributes to disease activity in IIH.

3.1.2 Aims

1. Complete a histological survey of IIH adipose tissue
2. Determine the transcriptome of IIH adipose tissue
3. Investigate the metabolome in IIH adipose tissue
4. Investigate secreted peptides from IIH adipose tissue

3.2 Methods

3.2.1 Adipose tissue collection

Adipose tissue from the IIH weight (IIH:WT) and IIH drug (IIH:DT) trials were utilised in the current study, collected as described in section 2.10, under the following ethics codes: 13/YH/0366 for IIH:DT and 14/WM/0011 for IIH:WT as described in section 2.9. Control patients were selected from elective bariatric lists on the NHS at Heartlands hospital. Control patients were free from endocrinopathies, not on hormonal treatment, and BMI and age was collected as anthropomorphic measures. All patients were fasted overnight prior to adipose tissue biopsy. In brief adipose tissue was biopsied following written consent and was either placed immediately in RNA later, into phenol free DMEM/F12 with no antibiotics, or 4% formaldehyde. Tissue analysis was carried out according to figure 2.5, where a mixture of untargeted hypothesis generating experiments and targeted hypothesis driven experiments were carried out.

3.2.2 Histomorphometric analysis

Adipose tissue was treated as described in section 2.11. In brief, adipose tissue was fixed in 4% formaldehyde prior to dehydration and clearing and being embedded in paraffin wax. Embedded tissue was cut in 5 µm sections prior to a haematoxylin and eosin (H&E) stain. Sections were then imaged and adipocyte area assessed via the Image J plugin Adiposoft. Evaluator was blinded to tissue type and patient disease state during analysis.

3.2.3 RNA sequencing

Stranded mRNA was sequenced at 2X100 paired end reads on the Illumina HiSeq 2500 platform. Control and IIH RNA had comparable RNA integrity numbers quality (7.5±0.82 vs. 7.7±0.50, P=0.6), indicating acceptable quality RNA. Bioinformatic analysis was carried out according to section 2.12.2. In brief, raw RNA sequencing data had adapter sequences cut, mapped to the human genome (hg19, UCSC annotation). Gene counts were calculated and differentially expressed genes identified using DESeq2. Gene set enrichment analysis was carried out.

3.2.4 Conditioned media protocol

Adipose tissue had large blood vessels dissected out and was cut into ~100 mg chunks prior to a 24 hour incubation in phenol free DMEM/F12 with no antibiotics. Following incubation media was aliquoted and corresponding explant were stored at -80°C.

3.2.5 Metabolomics

NMR metabolomics was carried out according to section 2.14. In brief, conditioned media generated in section 3.2.4 was diluted in 1 in 4 in NMR buffer, yielding a final concentration of 100 µM sodium phosphate buffer. Corresponding OM and SC adipose explants underwent a methanol/water/chloroform extraction prior to evaporation of the polar layer. Dried metabolites were then reconstituted in NMR buffer containing 100% D_2O prior to being ran on a 600 MHz spectrometer. Spectra were phase and baseline corrected in MetaboLab prior to metabolite identification and quantification in Chenomx (Chenomx INC)(Ludwig and Gunther, 2011). Analyte

concentration was normalised to explant mass. Full details for this section can be found in section 2.14.

3.2.6 Luminex

Conditioned media generated in section 3.2.4 underwent a luminex experiment according to section 2.15. Total secreted adipokine was normalised to corresponding explant mass.

3.2.7 ELISA

Leptin was measured in conditioned media generated in section 3.2.4 using the human leptin DuoSet ELISA (DY-398,Bio-techne, Abingdon, UK). ELISA was carried out according to manufacturer's instructions using recommended ancillary kit (Bio-techne, DY008). Conditioned media was diluted 1:50 in reagent diluent. Samples were ran in duplicate. Total secreted leptin was normalised to corresponding explant mass. Intra-assay variability CV 7.28 %, inter-assay variability CV 8.2%.

3.2.8 RT-qPCR

Adipose tissue had RNA extracted via the RNeasy Plus Universal kit (Qiagen). RNA quantity was assessed via Nano drop prior to the generation of cDNA via the high capacity cDNA kit (Thermofisher). RT-qPCR was carried out according to section 2.7, where genes were run in triplicate for each sample where GAPDH was utilised as a housekeeper. QPCR data expressed as fold change, fold change= $2^{-\Delta\Delta Ct}$. Statistics were conducted on ΔCt values. See appendix 2 for a list of primer/probe sets. Due to 18s being differentially expressed between IIH and control adipose tissue (data not shown), GAPDH was selected as the

housekeeper where there is no difference in expression is GAPDH between IIH and control OM and SC adipose tissue (Fig 3.1).

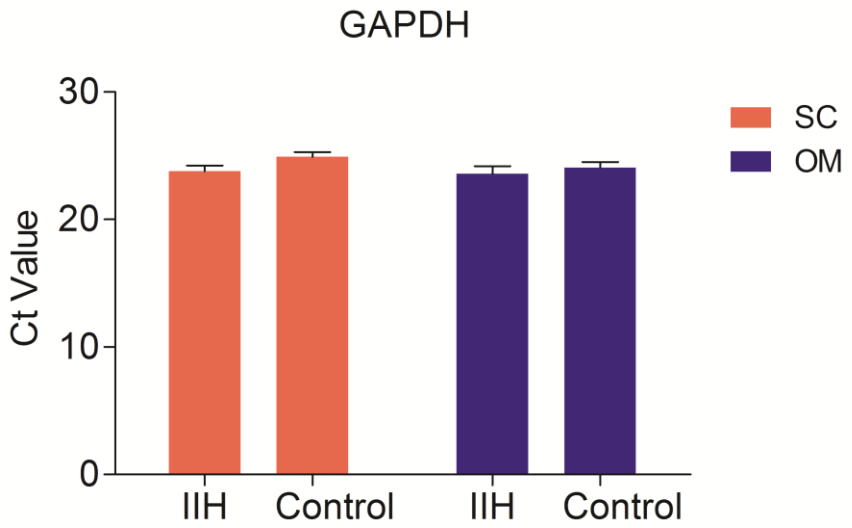

Figure 3.1 *GAPDH* expression comparison

GAPDH expression assessed via QPCR in control and IIH SC and OM adipose tissue, t-tests within each tissue. Data presented as mean±SEM.

3.2.9 11β-HSD1 activity assay

Adipose explants were prepared according to section 3.2.4 and incubated in 200 nM cortisone for 24 hours in triplicate. Samples underwent liquid/liquid extraction prior to liquid-chromatography/mass-spectrometry, according to section 2.17. Cortisol generation was normalised to explant mass.

3.2.10 Statistics

GraphPad prism (V7.1) was utilised to graph and carryout statistical analysis on data, where data is presented as mean±SD unless otherwise stated. Appropriate statistical tests utilised following a Shapiro-Wilk normality test. Inter-assay variability was calculated via the following equation %CV = (SD of plate

means /mean of plate means) X 100. Intra-assay variability was calculated via the following equation %CV= (SD of sample/ mean of sample) X 100. The data generated in multiplex assays, luminex and NMR, was not subjected to multiple comparison correction to prevent type II statistical error, due to the exploratory nature of the experiments.

3.3 Results

3.3.1 Sample matching

Paired OM and SC adipose tissue were taken from IIH and control patients, where group matching and experiments were carried out as per tissue availability due to the small quantities of biopsy tissue available. See figure 3.2 for the experimental matching.

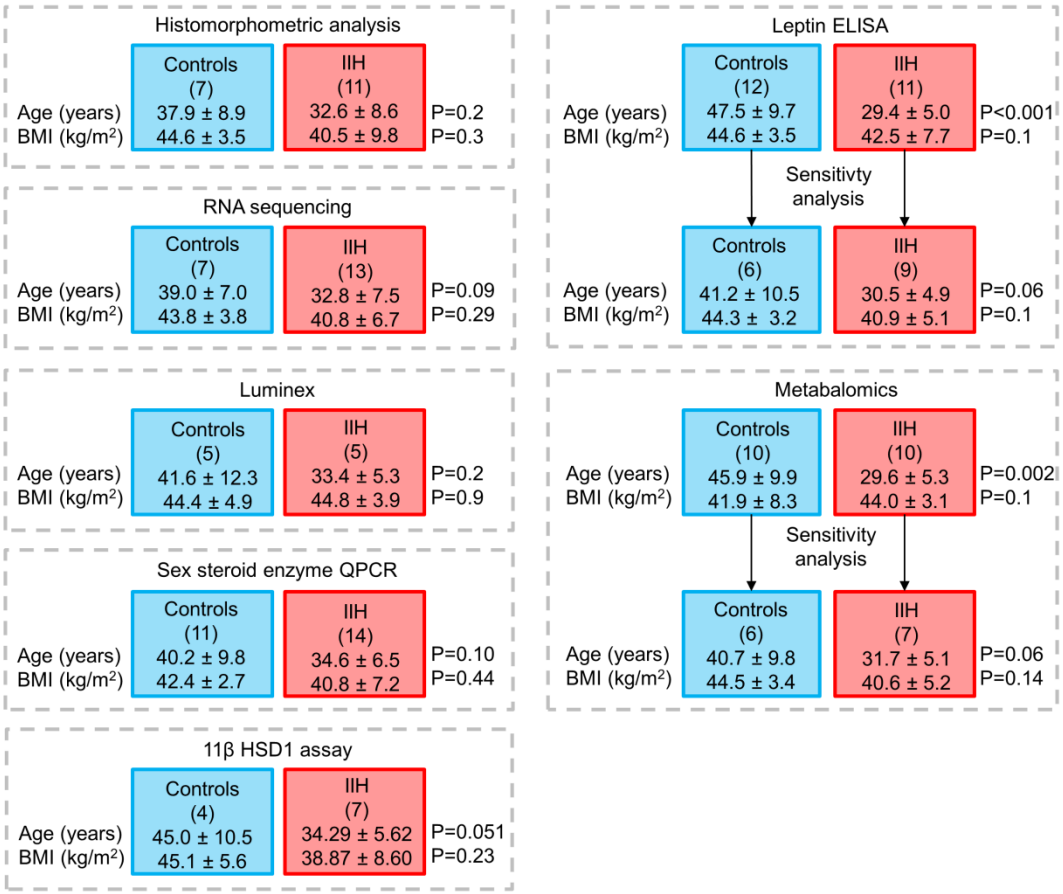

Figure 3.2 Sample matching

A diagram detailing the matching of experiments in the present chapter. Data presented as mean±SD. Unpaired T-tests, (N) in brackets.

3.3.2 Histomorphometric analysis

Changes in adipose histomorphometry are a good indicator for adipose dysfunction, therefore histomorphometric analysis was carried out on paired OM and SC adipose from IIH patients and controls from age, sex and BMI matched control cohort (Fig3.2).

3.3.2.1 Subcutaneous adipose

H&E staining of SC adipose tissue shows no change in adipocyte cross-sectional area of adipocytes between control and IIH (5041±488 Vs (5459±440 μm^2; P=0.5) (Fig3.3c).This was coupled with no changes in the distribution of adipocyte size (Fig3.3d).

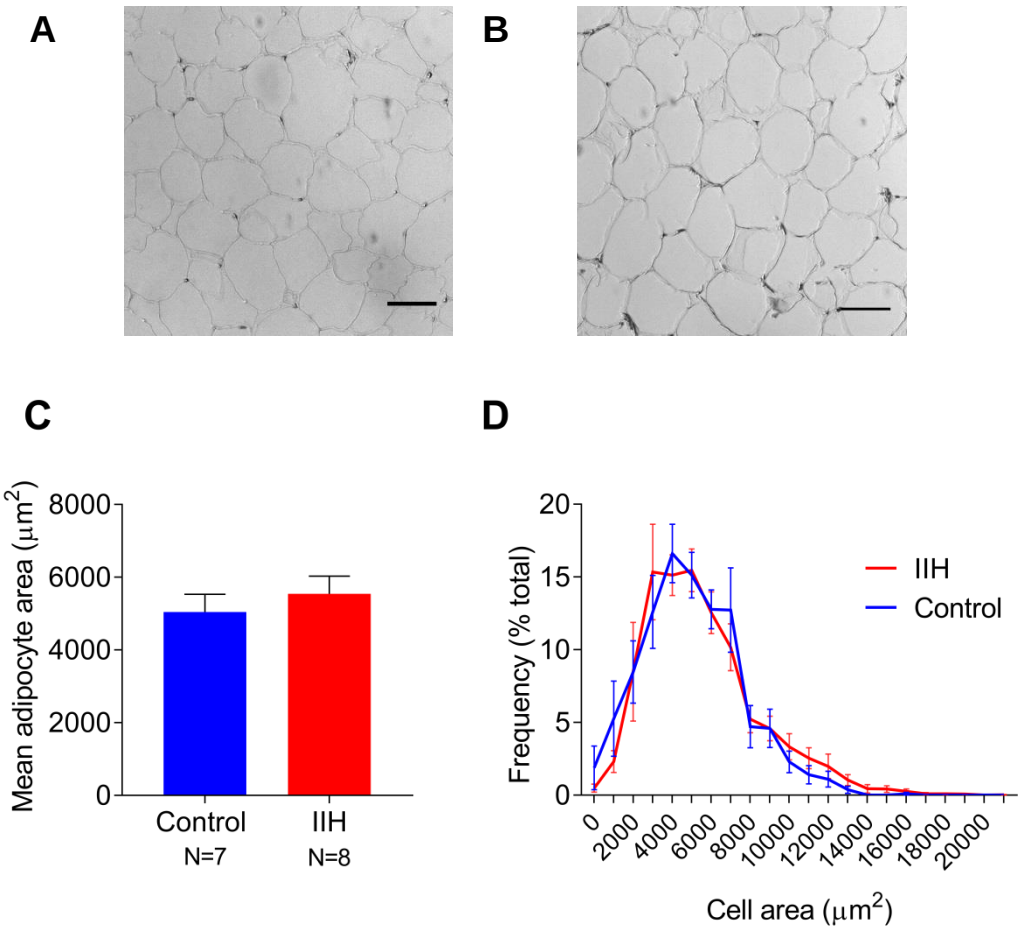

Figure 3.3 Morphology of IIH subcutaneous adipose tissue

H&E stain of IIH subcutaneous (SC) adipose tissue compared to age, sex and BMI matched controls. (A) Representative micrographs of control adipose tissue and (B) IIH SC adipose tissue. (C) Mean adipocyte area (D) Adipocyte area frequency. Data presented as mean±SEM. Where tissue quantity allowed, 3 sections per patient were analysed. Controls N=7, IIH N=8. Scale bar = 100 μm

3.3.2.2 Omental adipose

In contrast to SC adipose, H&E staining of OM adipose tissue shows that IIH OM adipocytes have a smaller cross-sectional area than control adipocytes (3273±117.1Vs 4056±342.8 μm^2; P=0.03) (Fig3.4c). This reduction in adipocyte area is due to an increase in the frequency of cells at 1000 μm^2 (8.8±1.7% vs 2.7±1.15%; P=0.01) and at 2000 μm^2 (27.9±2.6% vs 17.2±3.9%; P<0.0001). OM adipose in IIH is thus comparatively hypotrophic (Fig3.4d).

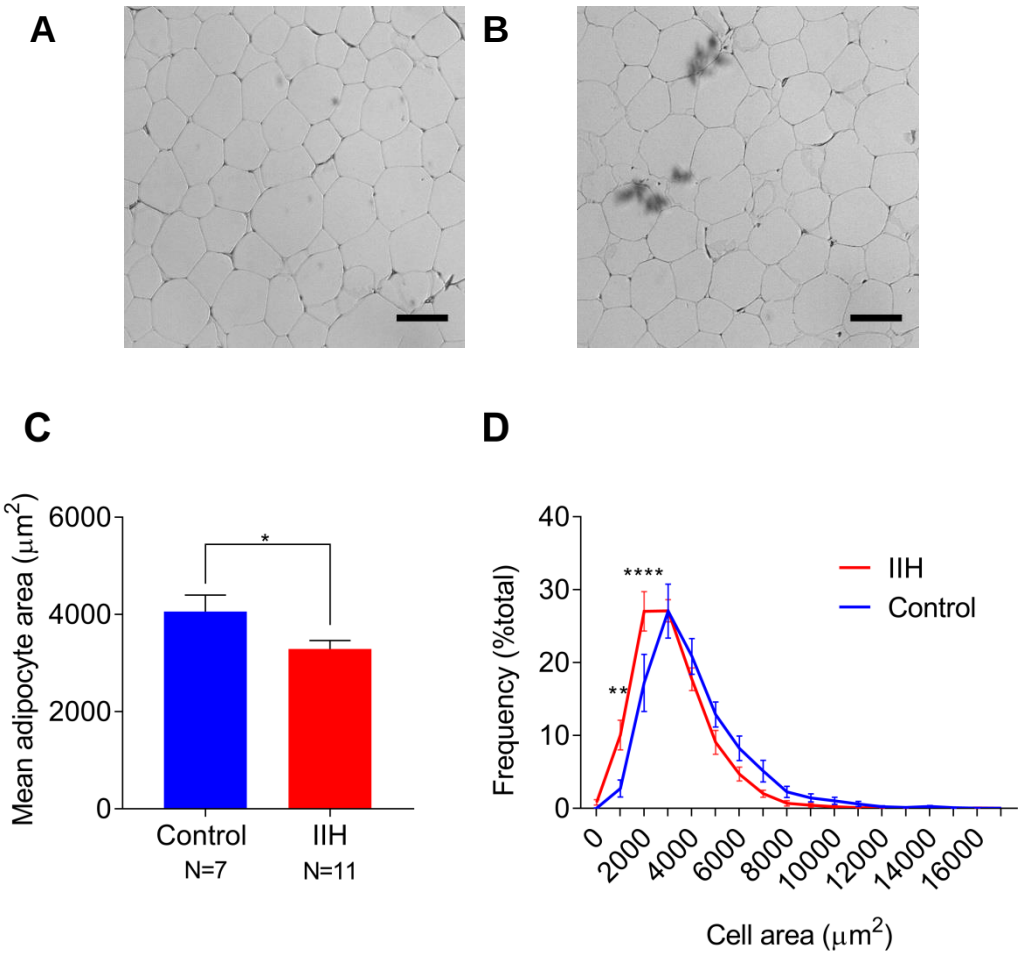

Figure 3.4 IIH omental adipocytes are smaller than controls

H&E stain of IIH omental (OM) adipose tissue compared to age, sex and BMI matched controls. Representative micrographs of (A) control and (B) IIH OM adipose tissue. (C) Mean adipocyte area in omental adipose (D) Adipocyte area frequency in omental adipose. Unpaired T-test for C, D Two-way ANOVA with Sidaks multiple comparison tests. Data presented as mean±SEM .Controls N=7, IIH N=11. Scale bar = 100 μm. *=P<0.05,**=P<0.01,****=P<0.0001.

3.3.2.3 Adipocyte area correlations

The association between adipocyte cross-sectional area and BMI was assessed in OM and SC adipose. In control patients, OM adipocyte area was correlates with BMI (P=0.017, R^2=0.74) whereas SC adipocyte area does not correlate with BMI (P=0.1, R^2=0.43), although the graph is comparatively linear (Fig3.5a). (Fig3.5b) Conversely in IIH patients, neither OM adipocyte (P=0.9, R^2=0.007) or SC adipocyte (P=0.7, R^2=0.05) correlate with BMI, with little indication of linearity.

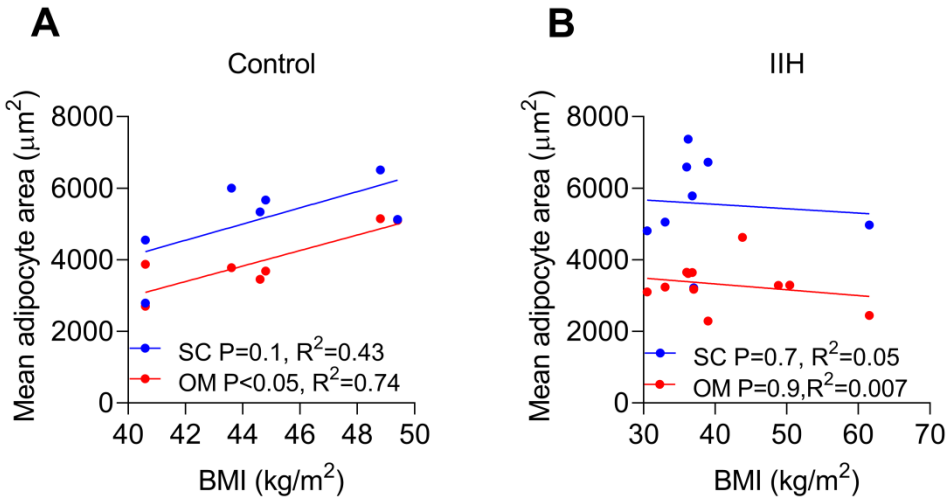

Figure 3.5 BMI correlations

Scatter graphs detailing average SC and OM adipocyte cross-sectional area versus BMI in (A) control and (B) IIH patients. Pearson's correlation for A, Spearman's correlation for B.

3.3.3 IIH adipose transcriptome

Transcriptomic analysis provides a global, unbiased assessment of mRNA transcription in a sample of interest, where differences in mRNA expression can be indicative of an altered phenotype. Consequently, to gain further insight into the IIH adipose phenotype, it was aimed to characterise the transcriptome of IIH adipose tissue, comparing IIH SC adipose tissue to a sex, BMI and age matched control cohort (fig3.2). SC adipose was selected for RNA sequencing due to the hypothesis that SC adipose in IIH could be specifically contributing to the pathology of the IIH, similar to SC adipose in PCOS. I.e. generating excess androgens and lipogenesis, contributing to systemic metabolic dysfunction (O'Reilly et al., 2017). Data highlights that IIH SC adipose tissue has 693 upregulated and 400 downregulated University of California Santa Crus (UCSC) genes based on unadjusted P-values (Fig3.6c).

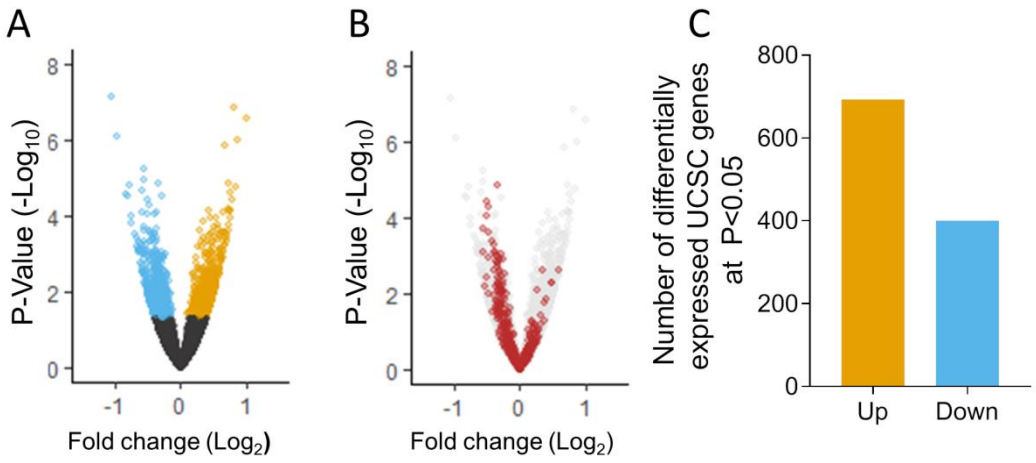

Figure 3.6 IIH SC adipose has a distinct transcriptome

Differential gene expression analysis of SC adipose tissue from control vs IIH patients. (A) Volcano plots of differential gene expression between adipose tissue from control vs IIH subjects. Fold change (Log2, x-axis) of gene expression is plotted against p-value for differential gene expression (-Log10, y-axis). Coloured dots represent UCSC genes that are either upregulated (in orange) or downregulated (in blue) in IIH patients at P<0.05. (B) Volcano plot detailing the top most highly expressed genes based on FPKM. (C) Bar plot displaying the number of differentially expressed UCSC genes at P<0.05. Control, N=7 ; IIH, N=13.

3.3.3.1 Differentially expressed genes

Following identification of gene expression levels, the most differentially expressed genes in IIH were evaluated within the same RNA sequencing cohort (Fig 3.2). This highlights 31 genes that are highly significantly differentially expressed. A description of these genes including expression levels can be found in appendix 3.

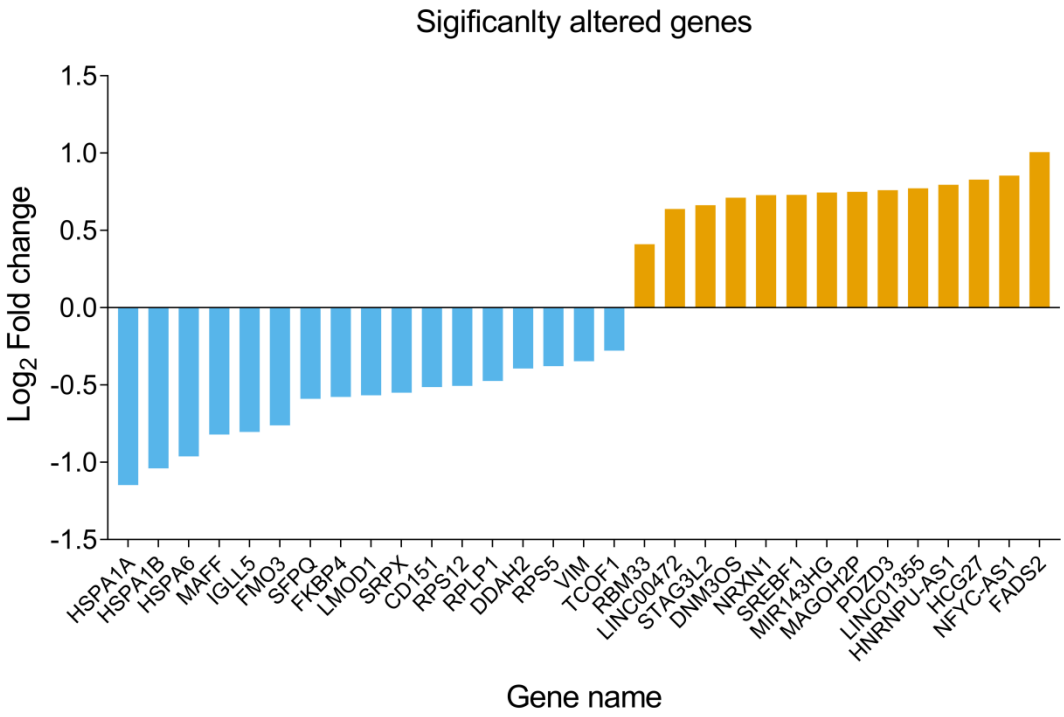

Figure 3.7 Top differentially expressed genes

Most differentially expressed genes as determined by DESeq2 RNA sequencing output following multiple comparison correction. Control, N=7; IIH N=13

3.3.3.2 Gene set enrichment analysis

To identify whether genes associated with specific functions are altered in IIH adipose, gene set enrichment analysis (GSEA) was carried out. GSEA highlights a depletion of ribosomal protein genes in IIH, with a net enrichment score (NES) of -3.059 and false discovery rate (FDR) of <0.00001. Conversely an enrichment of genes associated with lipid biosynthesis (NES= 1.263, FDR=0.01) was demonstrated. There is also an enrichment/depletion pattern in gene sets associated with positive caloric intake in IIH patients, in spite of the patients being fasted. Gene lists for these gene sets are in appendix 4.

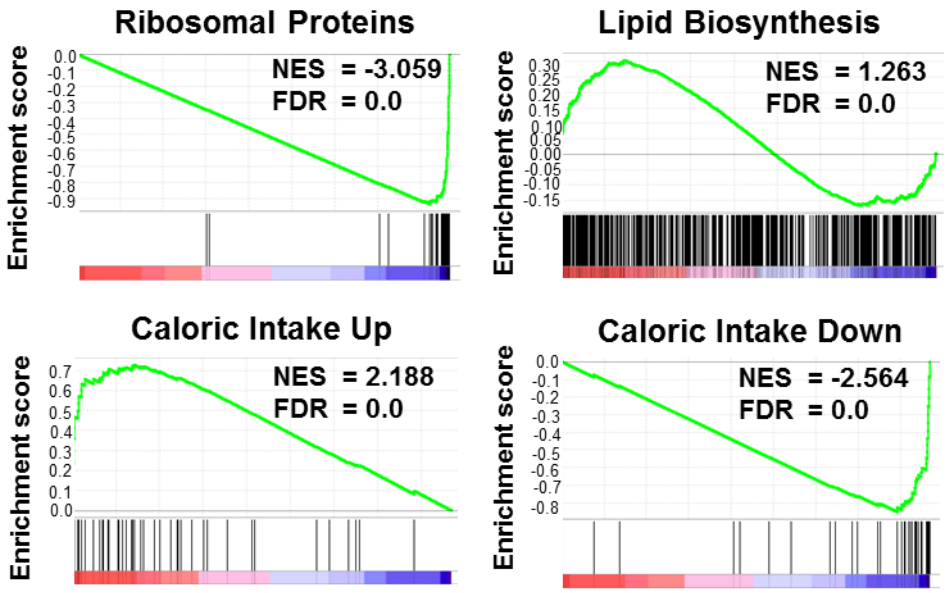

Figure 3.8 IIH adipose is transcriptomic ally primed for lipid production

Gene set enrichment analysis of four selected gene sets against differential expression data from adipose tissue of control vs IIH patients. NES= Net enrichment score, FDR= False Discovery Rate. A black line represents a gene, the colour gradient represents genes most expressed (red) to genes most lowly expression (blue) compared to controls. N=7 Control, N=13 IIH.

3.3.4 IIH adipose metabolism

Metabolomic analysis provides an assessment of the sum total metabolic processes in a tissue, where alterations in the metabolism denote altered cellular metabolism. Both tissue and conditioned media from *ex vivo* explants were assessed via NMR, providing an unbiased, semi-selective, quantitative assessment of metabolites. Analysis of the NMR spectra allowed profiling of 36 metabolites in the tissue and 34 metabolites in the media, see appendix 5 for table of metabolites in extracted tissue and conditioned media.

3.3.4.1 Glycolysis and energy metabolism

RNA sequencing data highlighted that IIH SC adipose tissue had an enrichment of genes associated with lipogenesis. Consequently glycolytic metabolites were assessed as glycolytic processes contribute to *de novo* lipogenesis. IIH OM adipose has unaltered glucose exchange (-1.74±4.7 vs -0.36±1.2 ΔmM/100 mg; P=0.84) (Fig3.10a), intracellular glucose (3.61±1.59 vs 4.10±1.13 mM/100 mg; P=0.44) (Fig3.10b) and intracellular lactate (1.598±1.98 vs 0.85±0.33 mM/100 mg; P=0.48) (Fig3.10d) compared to controls. However IIH OM adipose has increased intracellular pyruvate compared to controls (23.63±16.77 vs 4.58±7.18 mM/100 mg, P=0.0039) (Fig3.10c). Similarly to OM adipose, IIH SC adipose has no alteration in glucose exchange (-1.67±2.3 vs -0.62±0.37 ΔmM/100 mg; P=0.15) (Fig3.10e), intracellular glucose (3.55±1.23 vs 3.66±1.63 mM/100 mg; P=0.87) (Fig3.10f), intracellular lactate (0.66±0.33 vs 0.61±0.41 mM/100 mg; P=0.48) (Fig3.10h), and additionally unaltered pyruvate (21.33±29.47 vs 9.50±8.71 µM/100mg; P=0.48) (Fig3.10g).

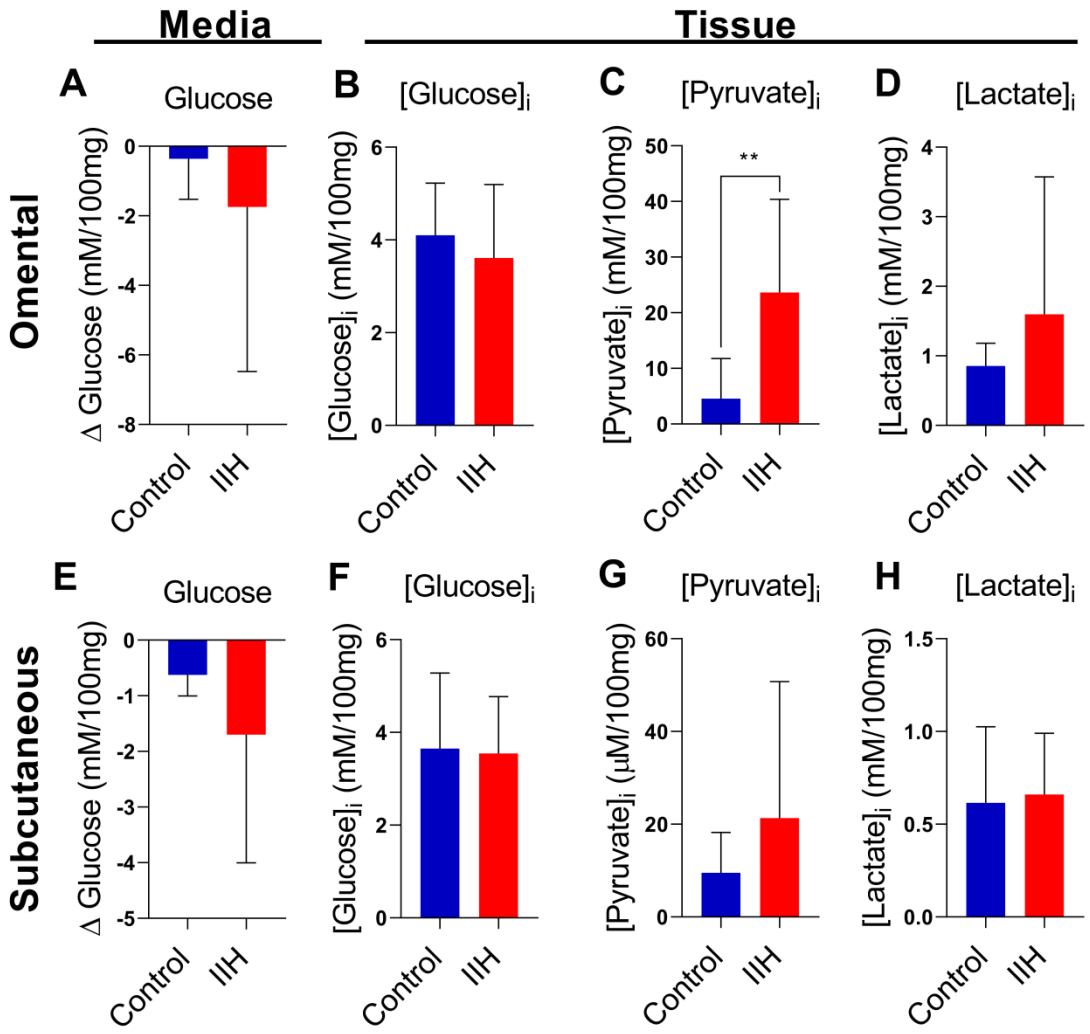

Figure 3.9 Glycolysis in adipose tissue

Glucose exchange (A,E), intracellular glucose (B,F), pyruvate (C,G) and lactase (D,H) as measured by NMR in OM (A,B,C,D) and SC (E,F,G,H) adipose tissue from control and IIH patients. Unpaired T-test for B and F, Mann-Whitney U-test for A,C,D,E,G and H. Data presented as mean±SD. N=10. **=P<0.01.

3.3.4.2 Lipogenesis surrogates

Metabolites known to contribute to *de novo* fatty acid synthesis, specifically the branch chained amino acids (BCAA) leucine and isoleucine, were assessed in the NMR data (Crown et al., 2015; Rosenthal et al., 1974). IIH OM adipose displays not difference in leucine (-9.85±78.57 vs 3.51±52.72 ΔμM/100 mg; P=0.66) (Fig3.11a) or isoleucine (-29.21±71.78 vs -9.73±41.67 ΔμM/100 mg; P=0.49) (Fig3.11b) uptake and not difference in intracellular isoleucine (124.4±25.00 vs 130.9±30.32 μM/100 mg; P=0.61) (Fig3.11c) and leucine (133.3±48.27 vs 139.8±53.75 μM/100 mg; P=0.78) (Fig3.11d).

Conversely, IIH SC adipose tissue displays preferential uptake of both leucine (-38.02±40.76 vs 22.62±54.25 ΔμM/100 mg; P=0.011) (Fig3.11e) and isoleucine (-30.22±25.21 vs 25.31±48.26 ΔμM/100 mg; P=0.002) (Fig3.11f) without changes in intracellular isoleucine (133.3±48.27 vs 139.8±53.75 μM/100 mg: P=0.81) (Fig3.11g) and leucine (133.3±48.27 vs 139.8±53.75 μM/100 mg; P=0.78) (Fig3.11h).

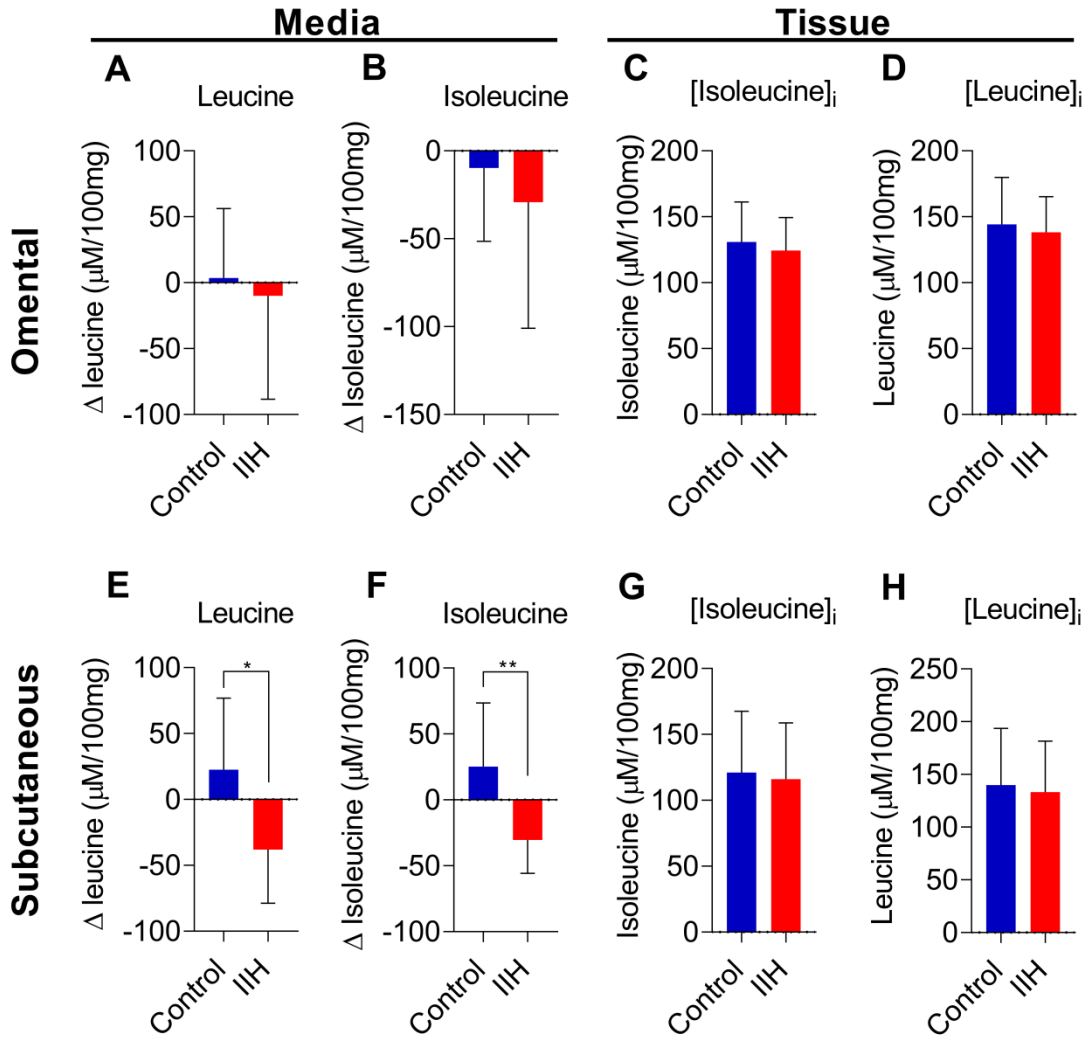

Fig 3.10 Flux of leucine and isoleucine

Exchange of leucine (A,E) and isoleucine (B,F) and tissue leucine (D,H) and isoleucine (C,G) as measured by NMR in OM (A,B,C,D) and SC (E,F,G,H) adipose from control and IIH patients. Unpaired t-test for A-E,G-H and Mann-Whitney U-test for F. Data presented as mean±SD, *=P<0.05, **=P<0.01. N=10.

3.3.4.3 IIH adipose tissue displays increased lipolysis

To determine the function of lipolysis, a major function of adipocytes, glycerol secretion and tissue glycerol was assessed on NMR spectra. IIH OM adipose tissue secretes more glycerol compared to controls (128.7±45.7 vs 79.4±33.6 ΔμM/100 mg; P=0.018) (Fig3.12a), without any alteration in intracellular glycerol (274.1±87.4 vs 296.1±38.6 μM/100 mg; P=0.16) (Fig3.12b). Furthermore IIH OM adipose has an increased secretion-to-intracellular glycerol ratio (0.50±0.18 vs 0.27±0.11; P=0.0045) (Fig3.12c). Similarly IIH SC adipose tissue secretes more glycerol than controls (157.3±62.6 vs 84.5±37.0; P=0.0053) (Fig3.12d), with no alteration in intracellular glycerol (305.7±90.8 vs 339.0±97.9 μM/100 mg; P=0.44) (Fig3.12e), and an increased secretion-to-intracellular glycerol ratio (0.58±0.43 vs 0.27±0.16; P=0.0052) (Fig3.12f). These data indicate IIH adipose tissue has increased lipolysis compared to controls. Age and BMI does not correlate with any of the parameters assessed here so sensitivity analysis is not required (see appendix 6).

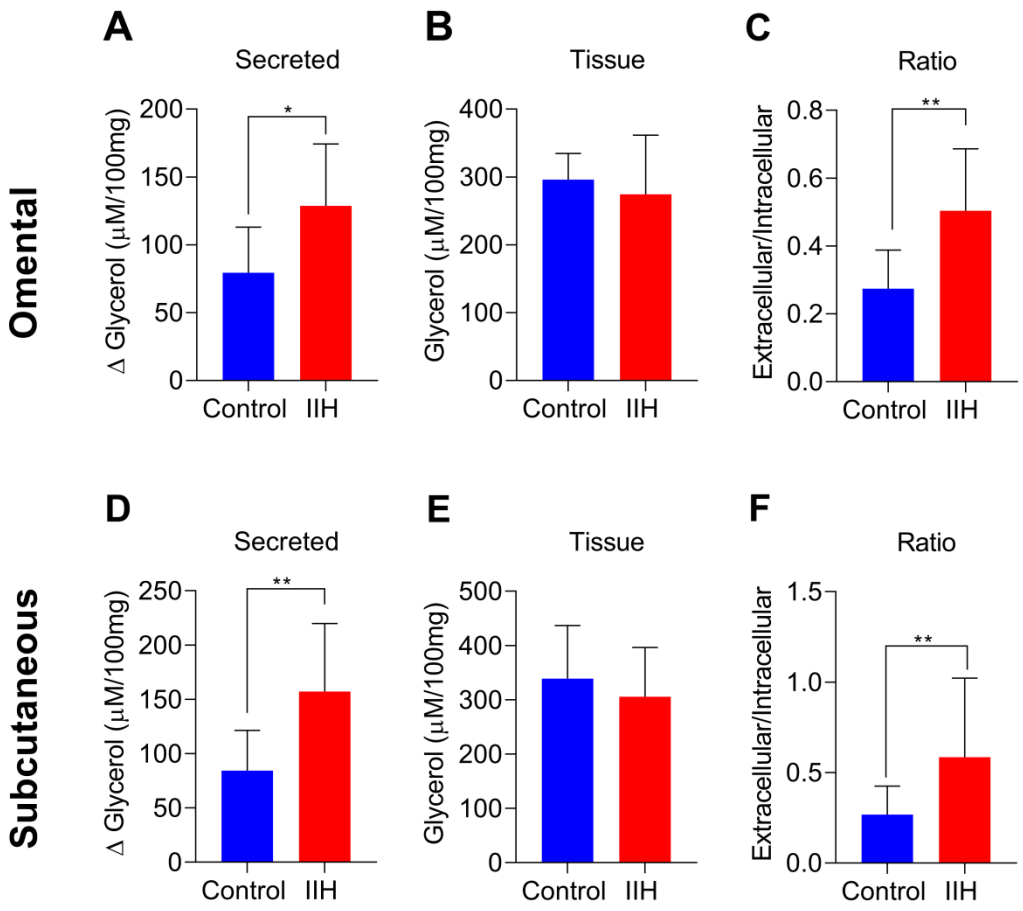

Figure 3.11 Glycerol secretion from adipose tissue

Glycerol secretion (A,D), tissue glycerol (B,E) and extracellular/tissue ratio (C,F) in OM (A,B,C) and SC (D,E,F) adipose tissue derived from IIH (red) and control (blue) patients following a 24 hour incubation, as measured via NMR. Data presented as mean±SD, Mann-Whitney-U tests for C and F, unpaired T-tests A,B,D,E. *=P<0.05, **=P<0.001. N=10.

To determine whether the increased lipolysis in IIH adipose tissue is associated with altered gene expression, genes associated with lipolysis and lipid storage were pulled from RNA sequencing data set, thus assessing expression in SC adipose only. There is no change in expression of the genes encoding for the lipases adipocyte triglyceride lipase (*PNPLA2*), hormones sensitive lipase (*LIPE*) and monacylglycerol lipase (*MGLL*) (Fig3.13a). Furthermore there is no difference in the expression of perilipin genes (Fig3.13b).

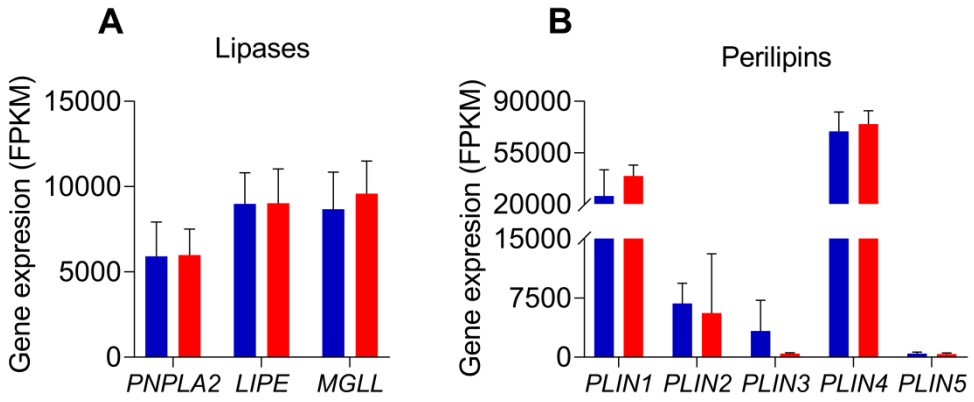

Fig 3.12 Lipolysis and lipid storage genes

DESeq2 output of RNA sequencing assessing the expression of (A) lipolysis genes and (B) perilipins. P-values based of DESeq2 following multiple comparison correction. Data presented as mean±SD.N=7 control N=13 IIH.

3.3.5 IIH adipose peptide secretion

Luminex panels were utilised to determine the secretion of a selection of peptide hormones from IIH adipose, where adipokines were selected based on adipokines previously assessed in IIH serum and CSF, as previously reviewed (Markey et al., 2016b). This experiment was utilised as a screening experiment to inform future experimentation.

3.3.5.1 SC adipose peptide secretion

In the SC adipose depot, no changes in secreted adipokines was demonstrated (Fig3.13). The expression of IL-1β (*IL1B*), IL-10 (*IL10*), IL-6 (*IL6*), TNFα (*TNF*), IL-8 (*CXCL8*), leptin (*LEP*) and MCP-1 (*CCL2*) was pulled from SC adipose RNA sequencing data, where no difference in gene expression was observed (Fig3.14).

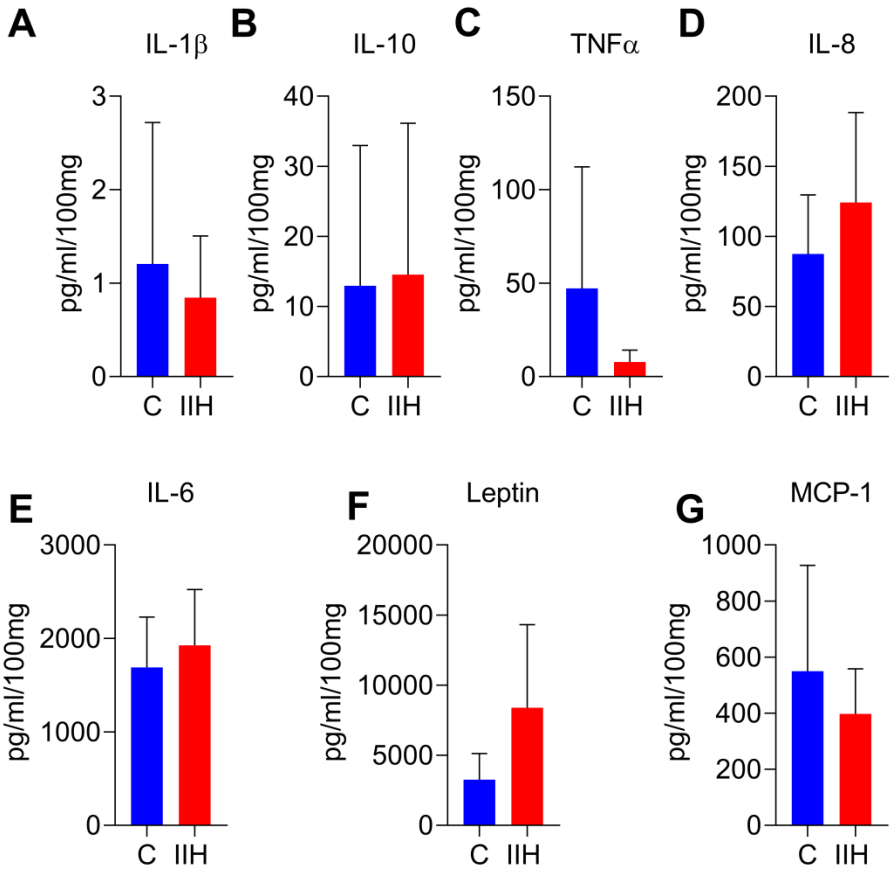

Figure 3.13 Secretion of adipokines from IIH SC adipose tissue

Luminex pannels ran on conditioned meida derived from SC adipose tissue from IIH patients and age,sex and BMI matched controls (C), where the secretion of (A) IL-β1, (B) IL-10, (C) TNFα , (D) IL-8, (E) IL-6 (F) Leptin and (G) MCP-1 was assessed. Unpaired T-tests. N=5. Data presented as mean±SD.

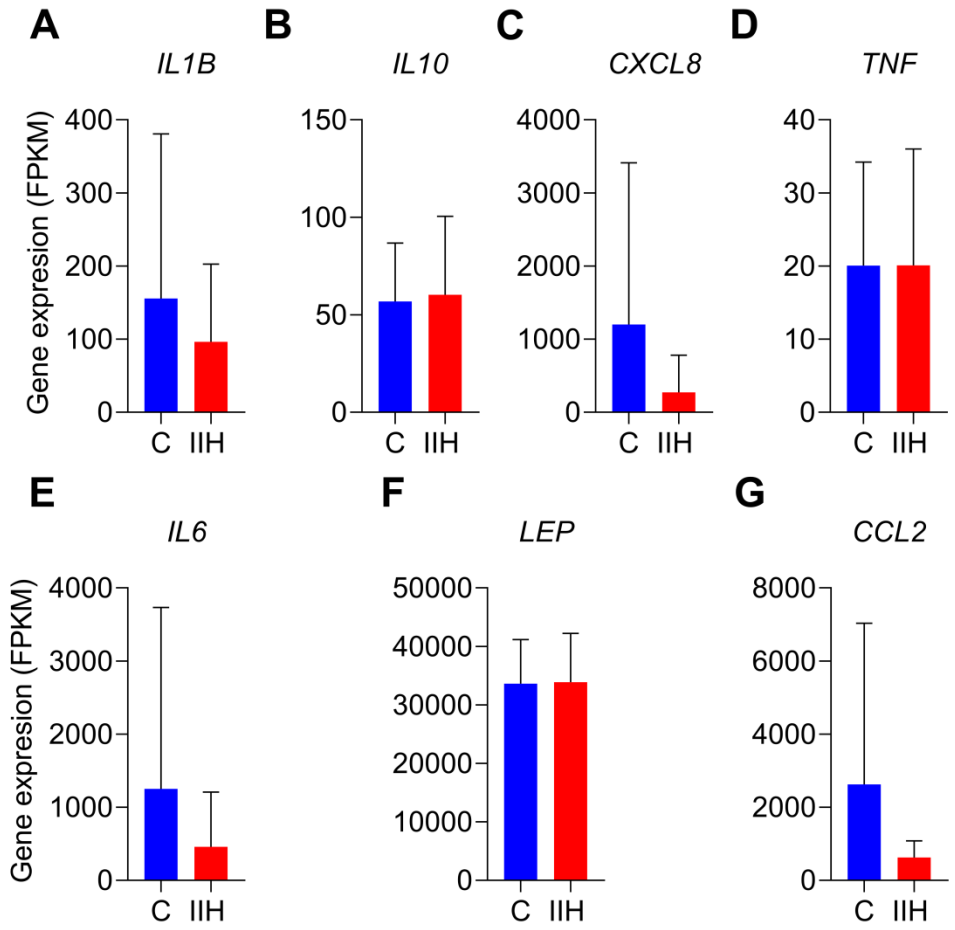

Figure 3.14 Evaluation of SC adipokine expression

The expression of (A) *ILB1,*(B) *IL10,*(C) *CXCL8* ,(D) *TNF,*(E) *IL6,*(F) *LEP* and (G) *CCL2* were called from DESeq2 output from SC adipose RNA-seq, controls vs IIH. P-values based on DESeq2 output following multiple comparison correction Data presented as mean±SD. N=7 for control, N=13 for IIH.

3.3.5.2 OM adipose peptide secretion

Investigation of OM adipose depot via luminex demonstrated, in similarity to the SC depot, general homology between IIH and control adipose tissue. However, monocyte chemoattractant protein 1 (MCP-1) had reduced secretion in IIH omental adipose tissue compared to controls (259.5±52.0 Vs 391.2±105.5 pg/ml/100mg; P=0.04) (Fig 3.15g).

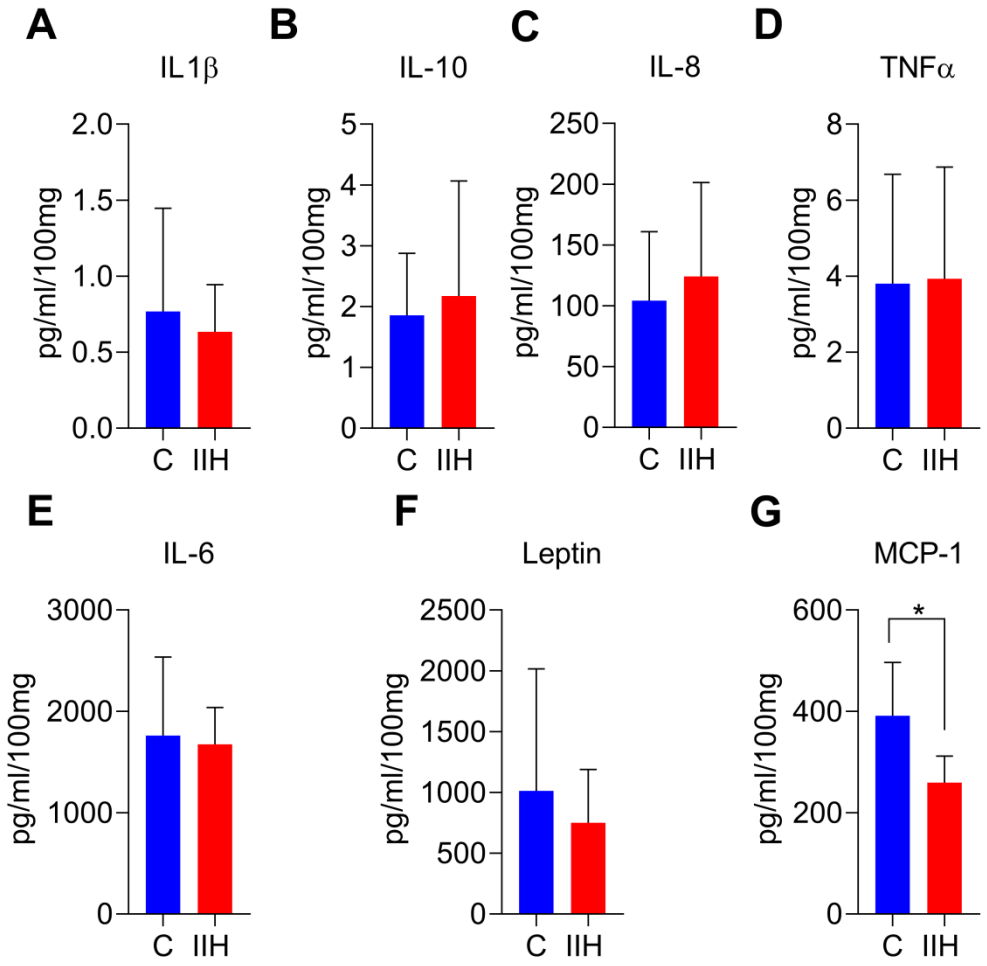

Figure 3.15 Secretion of adipokines from IIH OM adipose tissue

Luminex pannels ran on conditioned meida derived from OM adipose tissue incubatedfor 24hours, from IIH patients and age,sex and BMI matched controls (C), where the secretion of (A) IL-β1, (B) IL-10, (C) TNFα , (D) IL-8, (E) IL-6 (F) Leptin and (G) MCP-1 were assessed. Unpaired T-tests. N=5. Data presented as mean±SD. *=P<0.05.

3.3.5.3 Leptin secretion in IIH adipose tissue

IIH is a disease associated with a presumed circulating leptin excess, compared to obese individuals (Ball et al., 2009; Lampl et al., 2002). Being as adipose tissue is the predominant producer of leptin, leptin secretion from IIH adipose explant was compared to sex and BMI matched controls (Fig3.1) in paired SC and OM adipose explants in a hypothesis driven experiment. IIH SC adipose secretes more leptin compared to control SC adipose (8309±1593 Vs 2366±431 pg/ml/100mg; P=0.0039) (Fig3.16a), which is independent of gene expression as demonstrated in figure 3.14f. Similarly, IIH OM adipose secretes more leptin compared to control OM adipose (2994±824 Vs 571.9±102.2 pg/ml/100mg; P=0.016) (Fig3.16b). IIH adipose retains the function of SC adipose secreting more leptin compared to omental adipose tissue (Control P=0.0016, IIH p=0.0097, Fig3.16c and d respectively). No correlations were observed with clinical data. These data highlight increased leptin secretion from IIH adipose tissue.

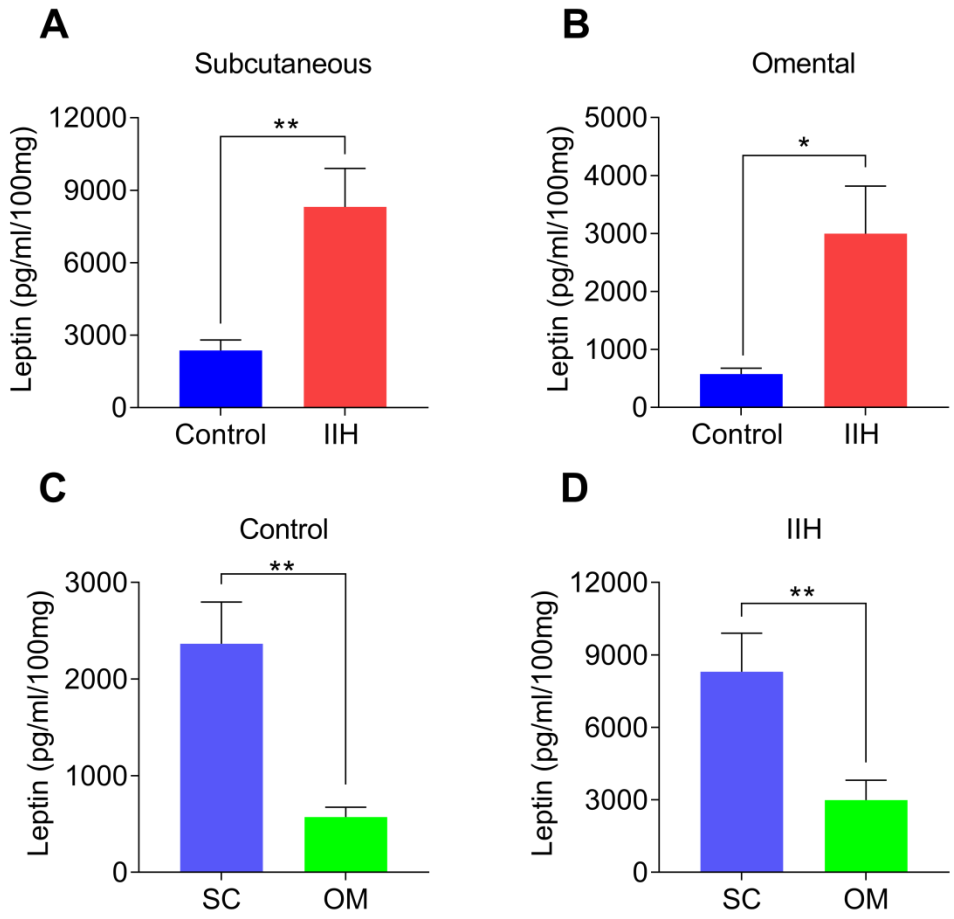

Figure 3.16 IIH adipose secretes more leptin

Leptin secretion from *ex vivo* (A) SC and (B) OM adipose tissue in sex and BMI matched control and IIH patients following a 24 hour incubation assessed via ELISA. Comparison of paired SC and OM leptin secretion in (C) controls and (D) IIH patients. **=P<0.01, *=P<0.05. Unequal variances T-test for A, B, C and D. Data presented as mean±SEM. N=12 for controls, N=11 for IIH.

The cohorts analysed for adipose leptin secretion were not matched for age, considering leptin secretion decreases with age a sensitivity analysis was carried out, matching the control and IIH groups additionally for age (Fig3.1). Here, IIH SC adipose retains increased leptin secretion compared to controls (8566±1954 vs 2620±1660; P=0.017) (Fig3.17a). Conversely, in OM adipose tissue, a trend to increase was demonstrated (2848±1034 vs 517±85; P=0.058) (Fig3.17b), indicating that age is a factor altering leptin secretion from OM adipose tissue.

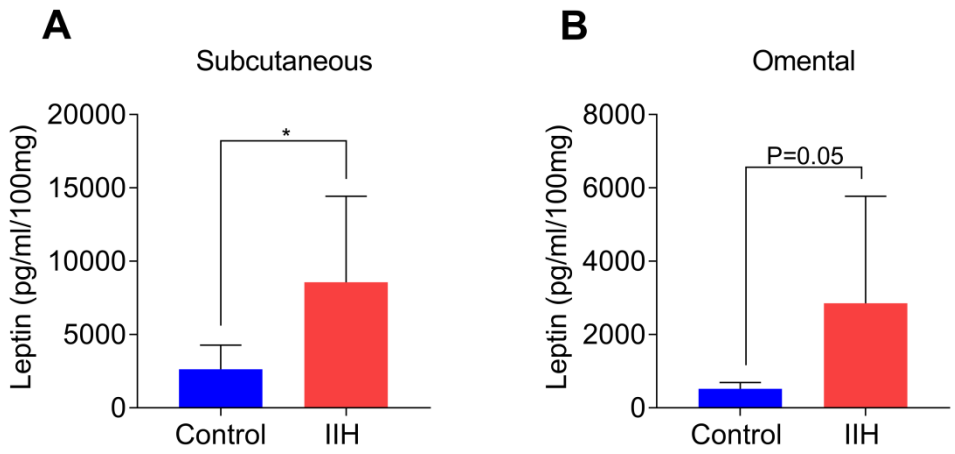

Figure 3.17 Leptin secretion sensitivity analysis

Sensitivity analysis on (A) SC and (B) OM adipose leptin ELISAs on age, sex and BMI matched IIH and control cohorts. Unequal variances t-test for A and B. *=P<0.05. Data presented as mean±SD.

3.3.6 IIH adipose has increased 11βHSD1 activity

Glucocorticoids are known to promote lipogenesis, lipolysis, leptin secretion and cause depletion of ribosomal subunits in human adipose tissue, all features identified in IIH adipose in the previous sections (Hochberg et al., 2015). Consequently a targeted assay assessing the activity of the enzyme that gates tissue specific GC activity, 11β-HSD1, was carried out on SC adipose from IIH and sex, BMI and age matched controls (Fig3.1). It is demonstrated that IIH SC adipose tissue produced more cortisol compared to controls (593.8±209.8 vs. 261.9±75.21 pg/h/100mg; P=0.015), indicating increased potential to produce cortisol (Fig3.18a). This increased activity is independent of gene expression: RNA sequencing data highlights those genes associated with pre-receptor glucocorticoid metabolism (*HSD11B1*, *HSD11B2* and *H6PD*) and the cognate receptors (*NR3C1* and *NR3C2*) have unaltered expression compared to controls, in a separate cohort to the 11β-HSD1 activity assay (Fig 3.18b).

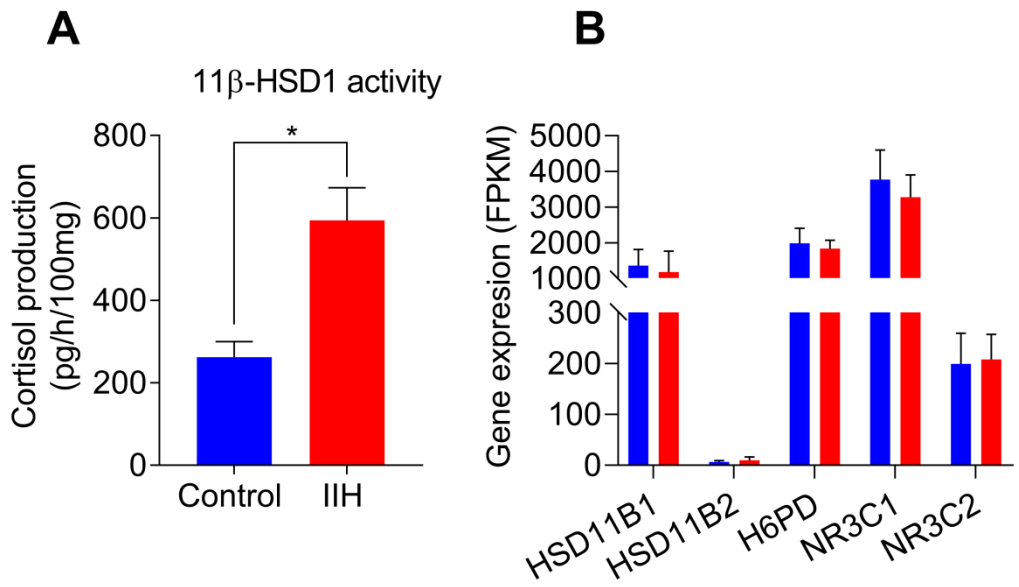

Figure 3.18 11β-HSD1 activity in IIH SC adipose tissue

Subcutaneous adipose tissue from IIH and control patients incubated with cortisone for 24 hours. (A) Cortisol generation in subcutaneous adipose explants measured via LCMS. (B) DESeq2 gene expression of glucocorticoid pre-receptor metabolism genes as measured by RNA sequencing, P-values based on DESeq output following multiple comparison correction. A, controls N=4, IIH N=7 where an N represents tissue ran in triplicate. B) Controls N=7, IIH N=13. Unpaired T-test for A. *=P<0.05. Data presented as mean±SD. Blue= control, Red=IIH.

3.3.7 IIH SC adipose tissue differentially expresses steroid metabolising enzymes

IIH patients have an androgen excess phenotype (appendix 1) and weight loss reduces circulating androgens (O'Reilly et al., 2019; Sinclair et al., 2010b). Given that adipose tissue is a well-defined site of peripheral androgens, it is hypothesised that IIH adipose tissue has altered expression of steroid metabolising enzymes that could increase circulating androgens (O'Reilly et al., 2014). A targeted RT-qPCR experiment was carried out on both SC and OM adipose tissue derived from IIH patients and age, BMI and sex matched controls to determine the expression of enzymes associated with sex steroid synthesis.

IIH SC adipose has decreased expression of *HSD3B1* (0.20±0.05, P=0.001), *HSD3B2* (0.49±0.20; P=0.007) and *SRD5A1* (0.42±0.08; P=0.007) with no alteration in the expression of *AKR1C3* (0.88±0.17; P=0.22) (Fig3.19a). Conversely IIH OM adipose has no alterations in the expression of *HSD3B1* (3.14±01.59; P=0.0504), *HSD3B2* (1.00±0.32; P=0.62), *AKR1C3* (1.62±0.27; P=0.62) and *SRD5A1* (0.84±0.07; P=0.69) (Fig3.19b).

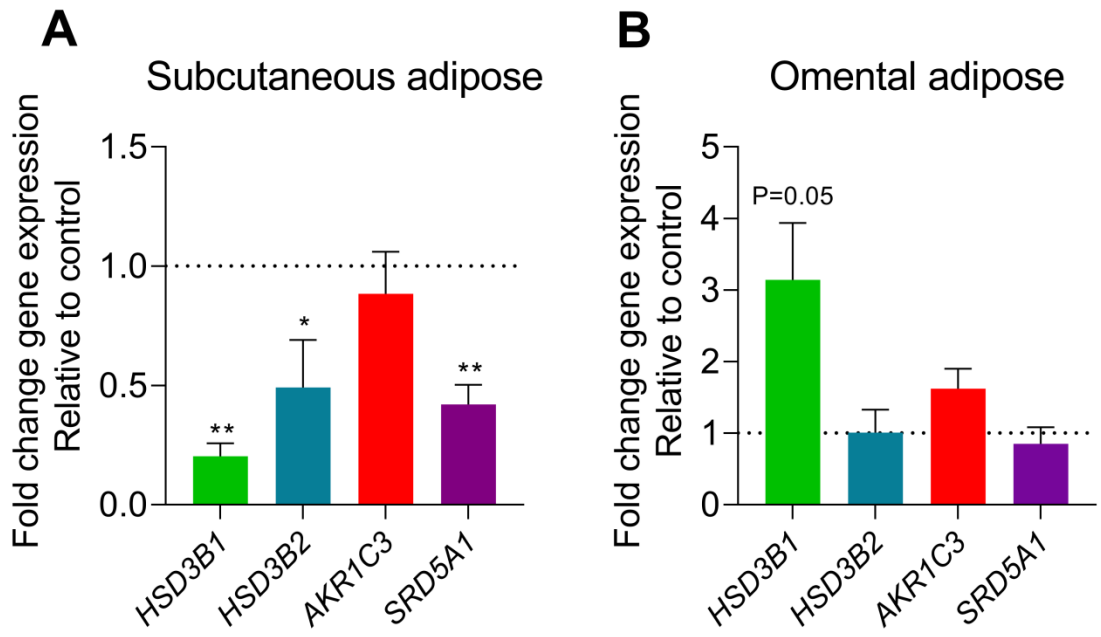

	Subcutaneous		Omental	
ΔCt	Control	IIH	Control	IIH
3BHSD1	10.00	11.77	10.01	8.48
S.E.M	0.31	0.68	0.53	0.33
3BHSD2	12.33	14.84	11.32	11.71
S.E.M	0.52	0.59	0.54	0.77
AKR1C3	5.93	6.55	6.24	5.76
S.E.M	0.31	0.35	0.83	1.08
SRD5A1	8.37	10.00	7.82	8.10
S.E.M	0.51	0.30	0.51	0.48

Figure 3.19 Expression of steroidogenic enzymes in IIH adipose tissue

Expression of *HSD3B1*, *HSD3B2*, *AKR1C3* and *SRD5A1* in (A) SC and (B) OM adipose tissue from IIH patients expressed as fold change relative to sex, age and BMI matched controls (dotted line), assessed via RT-qPCR. Table depicts ΔCt values for SC and OM adipose in controls and IIH patients, unpaired T-tests performed on ΔCt values of control vs IIH. Data presented as mean±SEM, all genes ran in triplicate. *=P<0.05, **=P<0.01. Control N=9, IIH N=14.

3.4 Discussion

IIH is a disease associated with obesity, where increased truncal mass is associated with increased LP Opp and weight loss improves the clinical phenotype in IIH patients (Hornby et al., 2018a; Sinclair et al., 2010a). Consequently IIH adipose is hypothesised to contribute the disease activity if IIH. As such, it was aimed to investigate the phenotype of IIH adipose tissue using a mixture of hypothesis free and hypothesis driven approaches.

3.4.1 IIH SC adipose displays a unique transcriptional and metabolic signature

IIH SC adipose tissue displays a distinct phenotype with transcriptomic differences, where ribosomal subunits are depleted and lipid biosynthetic genes are enriched. This phenotype is consistent with adipose tissue conserving energy, in favour of lipid synthesis (Oie et al., 2014). Furthermore, IIH adipose tissue has a transcriptome suggestive of recent caloric intake, despite being fasted, which could be interpreted as IIH patients being predisposed to weight gain (Franck et al., 2011). This is curious because it is established that IIH patients often experience an exacerbation or onset of symptoms following a period of rapid weight gain (Giuseffi et al., 1991).

This lipid synthetic phenotype is corroborated in part by the NMR metabolome; IIH SC adipose shows an increased propensity for uptake of branch chain amino acids (BCAA) leucine and isoleucine with no alteration in tissue BCAA levels. Although it is possible that IIH SC adipose was deficient in these essential amino acids *in vivo*, necessitating uptake from the media, it is also

plausible that they are preferentially catabolising leucine and isoleucine to promote *de novo* lipogenesis. Isoleucine and leucine catabolism contributes to a quarter of the lipogenic acetyl-CoA pool in rodent adipocytes (Crown et al., 2015). However this process has yet to be demonstrated in human adipocytes, as such this needs to be assessed. Future assessment utilising labelled BCAA and mass-spectrometry to facilitate metabolic tracing and an assessment of a greater range of metabolites would allow an understanding of the contribution of BCAA to *de novo* lipogenesis in IIH SC adipose.

This suggestion of increased *de novo* lipogenesis, with increased lipolysis, denoted by increased glycerol secretion, suggests that IIH SC adipose tissue has increased overall lipid turnover compared to controls. However, dynamic assessment of lipid turnover is required to evaluate this phenotype further.

The suggestion of increased fatty acid precursors from increased BCAA uptake could explain the increased leptin secretion from IIH adipose tissue; lipid precursors increase leptin secretion in adipocytes (Crown et al., 2015; Rosenthal et al., 1974; Shirai et al., 2004). This increased leptin secretion from IIH adipocytes suggests a cause for the presumed hyperleptinaemia in IIH patients (Ball et al., 2009; Lampl et al., 2002).

The depleted ribosomal subunits, increased lipid turnover and increased leptin secretion resemble the phenotype of SC adipose tissue from patients with Cushing's disease, thus resembles features of long term glucocorticoid excess (Hochberg et al., 2015). Indeed, IIH SC adipose tissue was demonstrated to generate more GC compared to controls, independently of genes associated

with GC pre-receptor metabolism. This increased cortisol generation might be explained by reduced *SRD5A1* expression as 5α-reductase is known to deactivate GCs (Miller and Auchus, 2011). This suggests that rather than generating more cortisol *per se*, IIH adipose is unable to generate 5α-dihydrocortisol at the same rate as control adipose tissue, leading to cortisol accumulation. Indeed global *srd5a1* knockout out leads to reduced corticosterone (active rodent GC) clearance in mice (Livingstone et al., 2014). The present study, however, does not fully assess the cause of the increased adipose cortisol generation. Systemic 5α-reductase activity is increased in IIH patients (appendix 1), although this does not contradict the present hypothesis, both hepatic and adipose 5 α-reductase activity need to be assessed, due to these being the major 5 α-reducing tissues (O'Reilly et al., 2019). As such, this hypothesis remains to be tested, with 5α-reductase activity, glucocorticoid clearance and intra-adipose 11β-HSD1 activity of IIH adipose tissue needing to be assessed. Furthermore other factors associated with 11β-HSD1 activity need to be assessed. For example the inability to quantify tissue levels of NADPH precluded the analysis of the NADPH/NADP+ ratio, thus potential activity of G6PDH activity, a key coenzyme for 11β-HSD1, highlighting this as an investigative avenue (Hewitt et al., 2005).

The reduced expression of androgen metabolising enzymes in IIH SC adipose is suggestive of a reduced capacity to activate androgens, contrary to the adipose phenotype in polycystic ovary syndrome (O'Reilly et al., 2017). However due to the unchanged expression of *AKR1C3*, it is plausible that IIH SC adipose tissue is capable of generating more testosterone compared to

control adipose, due to the reduced *SRD5A1* expression. 5α-reductase is required convert testosterone to dihydrotestosterone, thus the proposed catalytic block could cause increased testosterone due to reduced DHT generation, contributing to the systemic testosterone excess (Miller and Auchus, 2011; Schiffer et al., 2018). Indeed, global *srd5a1* knockout in female mice results in a mild oestrous cycle dependent testosterone excess, suggesting reduced metabolic testosterone clearance (Mahendroo et al., 1996). Assessing *in vivo* androgen generation following a DHEA bolus using adipose tissue microdialysis would address this hypothesis (O'Reilly et al., 2017).

Together, the data presented on IIH SC adipose allows the creation of a model formed of testable hypothesise. The proposed model suggests that the reduced *SRD5A1* expression and therefore reduced 5α-reductase activity is facilitating the reduced GC clearance in IIH SC adipose, allowing the development of a phenotype of glucocorticoid excess. Furthermore reduced *SRD5A1* expression is hypothesised to be contributing to the systemic androgen excess through reducing DHT generation, increasing testosterone (Fig 3.20). Systemic knockout of *srd5a1* in mice causes reduced glucocorticoid clearance and a moderate oestrus cycle dependent testosterone excess (Livingstone et al., 2014; Mahendroo et al., 1996). Assessing the phenotype of an adipose specific knockdown of 5α-reductase type 1 in female rodents would help to address this hypothesis further.

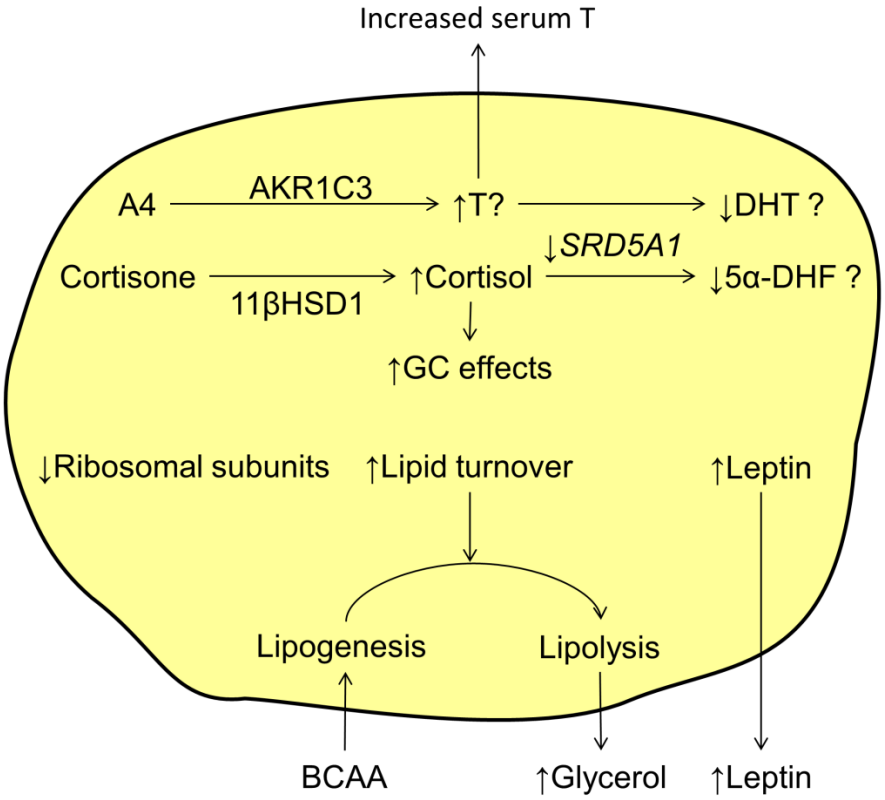

Figure 3.20 Model diagram IIH SC adipose tissue

Schematic diagram of the hypothesis model in IIH adipose tissue. Reduced 5α-reductase activity reduces the deactivation of cortisol, increasing the intracellular cortisol. Increased intra-adipose cortisol promotes classic glucocorticoid (GC) effects on adipose tissue such as reducing transcription, increasing lipogenesis and lipolysis and increasing leptin secretion. Furthermore, reduced *SRD5A1* expression would prevent further metabolism of testosterone (T), contributing to the peripheral T excess. A4= androstenedione, DHT=Dihydrotestosterone, 5α-DHF= dihydrocortisol,

3.4.2 IIH OM adipose displays differential features

IIH OM adipose displays a differential phenotype to control adipose, whereby OM adipocytes in IIH have a smaller cross-sectional area compared to matched controls, demonstrating relative cellular hypotrophy. This phenotype could be explained by the cellular metabolic processes contributing to a net loss in lipid mass. IIH OM adipose displays increased glycerol secretion, indicating increased lipolysis without any signs of increased *de novo* lipogenesis, this is suggestive of a net loss of lipid volume. The IIH androgen excess phenotype could be contributing to the reduced adipocyte cross-sectional area through promoting lipolysis (O'Reilly et al., 2014). The reduced cross-sectional area may explain the reduced MCP-1 secretion from IIH OM adipose, where smaller adipocytes are associated with reduced MCP-1 secretion (Skurk et al., 2007).

The reduced cross-sectional area of OM adipocytes could be contributing to the IIH androgen excess phenotype independently of the unchanged expression of androgen metabolising genes. Smaller omental adipocytes are associated with a reduced capacity of OM adipose to inactivate androgens (Blouin et al., 2003; Quinkler et al., 2004). Given that IIH OM adipose is of a smaller cross-sectional area, this allows the formation of the hypothesis that IIH OM adipose possesses a diminished ability to deactivate androgens, contributing to the androgen excess phenotype. As such, the capacity of IIH OM adipose to deactivate androgens should be assessed.

Other than the above changes, IIH OM adipose displays remarkable similarity with control OM adipose, where both the metabolomics and cytokine secretion

do not identify any changes. This suggests that IIH OM adipose has a general phenotype of obese OM adipose with the exception of the changes mentioned.

3.4.3 Limitations

The data in this chapter necessitates recruitment of larger cohorts that are more comprehensively phenotyped than the present cohort to confirm these preliminary findings. Adipose tissue from obese individuals are inherently metabolically deranged compared to lean individuals, consequently the IIH adipose features described are assumed to be in addition to obese phenotype (Attie and Scherer, 2009). Future studies incorporating adipose tissue from lean individuals would allow the comparison to IIH adipose to normal adipose tissue.

These preliminary data point toward the need to utilise a more integrated experimental approach utilising *in vivo* experimentation on IIH adipose tissue. Primarily, utilising microdialysis experiments would facilitate assessment of the metabolic phenotype of IIH SC adipose tissue *in situ* (O'Reilly et al., 2017). Moreover, this would facilitate the administration of precursor steroids, such as DHEA, facilitating the assessment of steroid activation IIH and control adipose. Utilising mass-spectrometry based metabolomics on adipose tissue microdialysate would provide a broader assessment of metabolites including lipids and allow a greater understanding of potential metabolic differences between IIH adipose and controls compared to NMR, which assessed a limited number of metabolites (O'Reilly et al., 2017).

This study assessed a small fraction of the peptide secretome from adipose tissue using a cytokine panel. In future, quantitative proteomics could be

deployed to assess a greater range of secreted peptides from adipose tissue within the adipose tissue microdialysate, facilitating the discovery of putative pathogenic molecules and biomarkers (Wasinger et al., 2013).

Although this study assessed the cross-sectional area of adipocytes in IIH adipose tissue, factors associated with adipocyte stress and inflammation were not assessed. Crown-like structures, the remnants of dead adipocytes and associated macrophages were not quantified, preventing an assessment of adipocyte stress and death, a feature of obese adipose tissue (Cinti et al., 2005). Furthermore, although a brief survey of the adipose tissue was completed, no formal assessment of inflammatory infiltrates was carried out. Future assessment of both crown-like structures, via macrophage staining, and inflammatory infiltrates would provide a greater insight into adipose tissue health in IIH adipose tissue.

This work presents the first assessment of the cellular phenotype of adipose tissue in IIH, where depot specific phenotypes exist. IIH SC adipose displays features of glucocorticoid excess and OM adipose displays a comparatively hypotrophic phenotype. However both SC and OM adipose tissue display general similarity in their metabolome and peptide secretion compared to controls. Being as adipose tissue has a strong role in the homeostasis of whole body metabolism; it is feasible that the metabolic disturbances in IIH patients are contributed to, in part, by the deranged metabolism of IIH adipose tissue.

Chapter 4 Leptin Phenotype of Patients with Idiopathic Intracranial Hypertension

4.1 Introduction

Idiopathic intracranial hypertension (IIH) is strongly associated with obesity. Consequently, several studies have evaluated inflammatory cytokines and adipokines, which are known to alter in obesity, to determine an IIH specific signature in an attempt to understand the pathogenesis of IIH (Markey et al., 2016b).

One adipokine that has garnered interest is the cardinal adipokine leptin. Studies of leptin in IIH have yielded conflicting results (see table 4.1). The original study of leptin in IIH conducted by Lampl et al demonstrated that IIH patients have raised serum leptin in a fasted state, compared to a well BMI matched control cohort, although there were low patient numbers (N=15 IIH, N=16 controls). This study has been corroborated and contradicted by subsequent studies. Leptin in cerebrospinal fluid (CSF) has also been measured in several studies; Ball et al demonstrated raised CSF leptin independent of BMI, however subsequent studies have not corroborated this, instead showing unaltered CSF leptin in IIH (Behbehani et al., 2010; Dhungana et al., 2009; Samancl et al., 2017). Interestingly it was shown that CSF leptin concentration correlates with lumbar puncture opening pressure, suggesting leptin could be pathogenic in IIH (Ball et al., 2009).

This conflicting nature of results can be explained by the varied study designs (table 4.1). The primary variable between studies is the fasting state of the patients, it is known that serum leptin increases in the post-prandial state (Korek et al., 2013). Furthermore the previous studies are often unmatched with regards to BMI and age. Control subjects comprised of mixed neurological

diseases have been utilised, whereby a disease specific leptin signature is likely being highlighted, rather than a true healthy control signature. Previous studies also have low numbers of IIH patients, reducing the power of the studies. Previous studies have had difficulty obtaining CSF from healthy individuals; lumbar punctures are painful procedures that are otherwise avoided unless clinically relevant. Consequently the studies utilising CSF have from patients with neurological diseases, thus are not true healthy controls. Of those studies with appropriate controls with fasted leptin measurements, only serum leptin was assessed.

There has not been an optimal study assessing leptin in IIH patients, namely a study assessing both serum and CSF levels in fasted IIH patients compared to sex, age and BMI matched controls that are otherwise medically healthy. Consequently a study fulfilling the aforementioned criteria is required. Furthermore, due to the disparity between fasted and non-fasted leptin measurements in IIH, assessing post-prandial leptin in IIH patients would be of interest. Previous studies have not assessed the effect of weight loss on leptin in IIH. In chapter 3, it was demonstrated that IIH adipose tissue secretes more leptin compared to control adipose tissue suggesting that serum leptin should be raised in IIH patients. This chapter details the leptin signature in IIH patients.

Study	Leptin in IIH	Numbers	Matching	Control	Fasted
(Lampl et al., 2002)	↑ Serum N/A CSF	IIH 15, Control 16	BMI: Yes Age: No	OMHO	Fasted
(Ball et al., 2009)	↑ Serum ↑ CSF	CSF 22 IIH, 56 control Serum :26 IIH, 53 Control	BMI: No Age: No	MND	Non-fasted
(Dhungana et al., 2009)	- Serum - CSF	8 IIH , 8 controls	BMI: Yes Age: Yes	MND	Non-fasted
(Behbehani et al., 2010)	↑Serum - CSF	IIH 10, Control 20	BMI: No Age: Yes	MNOD	Non-fasted
(Samancl et al., 2017)	-Serum N/A CSF	36 IIH, 40 Controls	BMI: Yes Age: Yes	OMHO	Fasted

Table 4.1 Previous papers characterising leptin in IIH

↑=Increased in IIH, - = Not altered in IIH, N/A = not analysed, MND= mixed neurological diseases, OMHO= Otherwise medically healthy obese, MNOD= Mixed neuro-ophthalmic disease.

4.1.2 Hypothesis

Given that IIH adipose tissue secretes more leptin than control adipose tissue, it is hypothesised that leptin levels are altered in IIH patients and contribute to the pathogenesis of IIH.

4.1.3 Aims

1. Assess fasting CSF and serum leptin levels in IIH patients
2. Assess the post-prandial response to leptin in IIH patients
3. Assess CSF and serum leptin in IIH patients following a weight loss intervention

4.2 Methods

4.2.1 IIH patients

IIH patients went through a trial visit at baseline in both the IIH:DT and IIH:WT and 12 months after baseline in IIH:WT only, according to the published protocols (Markey et al., 2017; Ottridge et al., 2017). IIH patients had active IIH confirmed and control patients had IIH ruled out via the modified Dandy criteria, as assessed by clinicians in the centres described in section 2.9. IIH patients in the IIH:WT trial were randomised 1:1 to either a community diet or bariatric surgery (gastric band, gastric sleeve or Roux-En-Y gastric bypass), baseline control patients had the same baseline visit as IIH patients. The clinical data presented is derived from locked trial data from the IIH:DT and unlocked trial data from the IIH:WT.

4.2.2 Meal stimulation test

After an overnight fast, control and IIH subjects in the IIH:WT received two bottles of Fortisip drinks (Nutricia, Trowbridge, UK). Each bottle contains a total of 300kcal, where each bottle comprises of 147kcal carbohydrates, 105 kcal fat and 48kcal protein. Plasma was taken prior to and two hours after administration of the meal.

4.2.3 Leptin ELISA

Human leptin DuoSet ELISA (DY-398,Bio-techne, Abingdon, UK) was utilised, used according to manufacturer's instructions using the recommended ancillary kit (Bio-techne, DY008). CSF was diluted 1:5, serum 1:100 and plasma 1:200 in

reagent diluent. The intra-assay coefficient of variation was 3.34% and inter-assay coefficient of variation was 7.9%.

4.2.4 Body fat assessment

Body fat percentage was assessed using bioimpedence via a Body Composition Analyser TANITA BC-418 MA. A 0.2kg correction was made for base layer clothing where a standard female body type pre-set was selected for all patients. The machine was used according to manufacturer's instructions.

4.2.5 Statistics

Statistical analysis was carried out using GraphPad prism (V7.1). Data normality was assessed using Shapiro-Wilk normality test. Data variance assessed via F-test of equality variances. Mann-Whitney U-test and Spearman's correlation were used for non-parametric data. Whereas a two-way repeated measured ANOVA, students T-test, unequal variances t-test (Welch's test) and Pearson's correlation was used for parametric data. $P<0.05$ was considered significant.

4.3 Results

4.3.1 Patient matching

IIH samples were sourced from the IIH:WT and IIH:DT. No serum samples were available from the IIH:DT, consequently serum analysis included only samples from the IIH:WT. As expected IIH patients have a higher LP Opp compared to control patients (Fig 4.1).

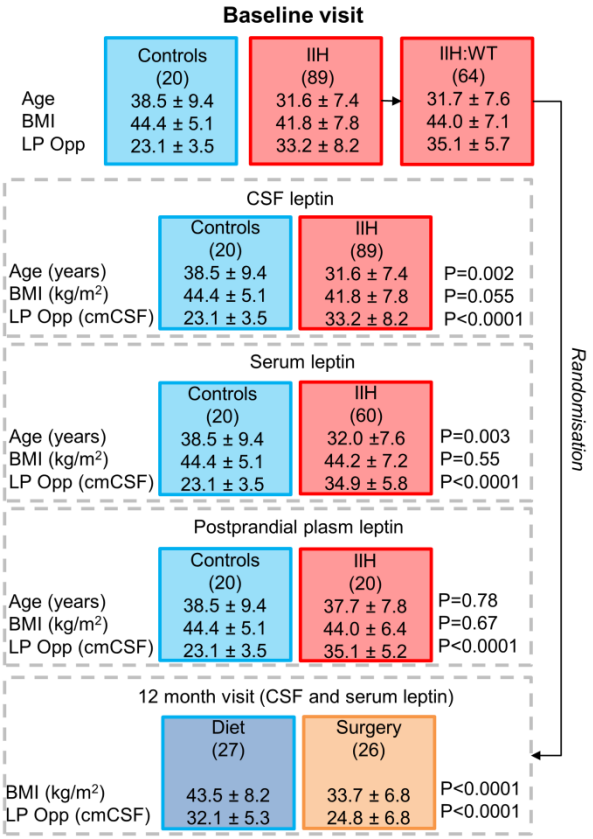

Figure 4.1 Consort diagram

Allocation of IIH and control patients to each of the analysis groups; CSF leptin measurement, serum leptin measurement, postprandial plasma leptin and 12 month leptin measurements.

4.3.2 IIH patients have raised serum leptin

Serum and CSF leptin was assessed in fasted IIH and control patients. Serum leptin was raised in IIH patients compared to control patients (71.5±29 vs. 56.3±14 ng/ml, P=0.0033) (Fig4.2a). CSF leptin was unaltered in IIH patients (504.8±197 vs. 493.8±152 pg/ml, P=0.99) (Fig4.2b). Serum and CSF correlate in both IIH (P<0.0001) and control (P=0.0041) patients where there is a plateau in the transport of leptin from the serum to the CSF, demonstrating saturatable transport of leptin from the serum to the CSF (Fig4.2c). This process in unaltered as demonstrated by the comparable serum/CSF ratio between IIH patients and control patients (154.5±56 vs. 137.8±33, P=0.44) (Fig4.2.d).

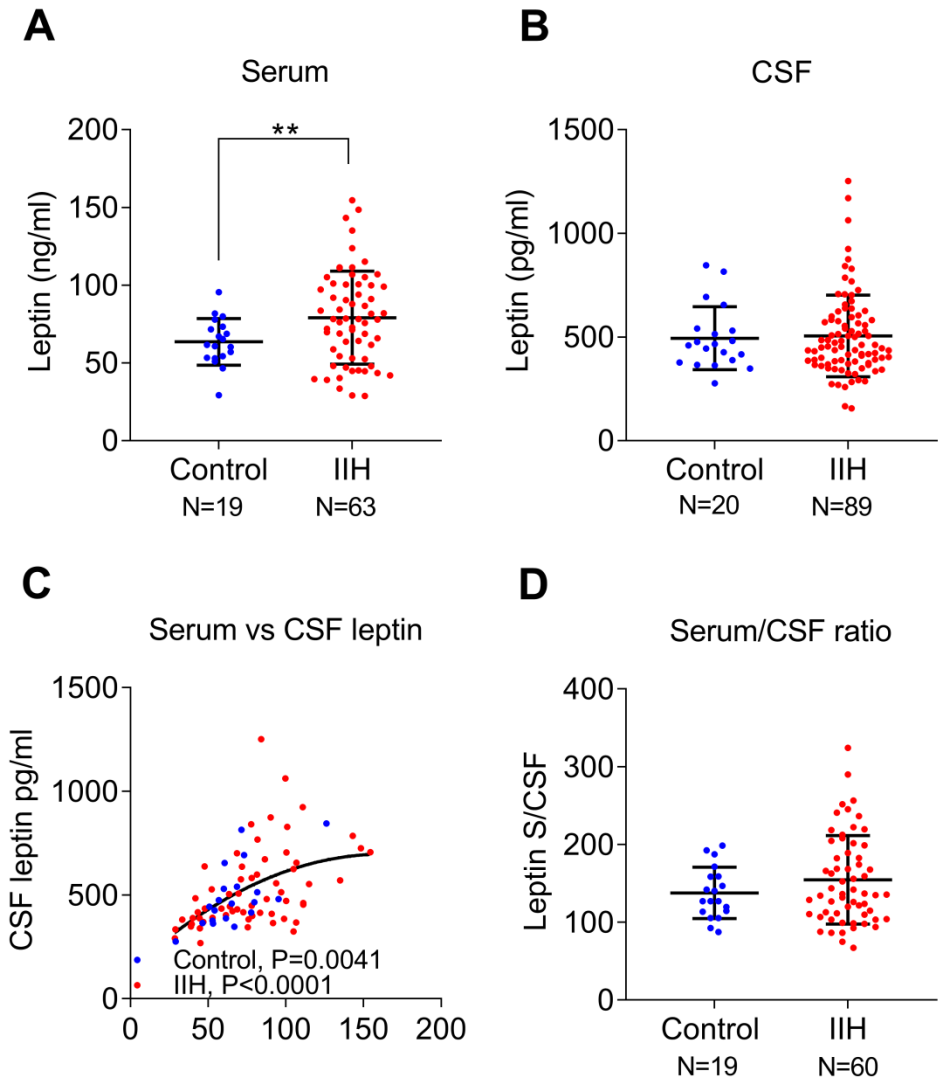

Figure 4.2 Baseline leptin characterisation

Leptin levels were evaluated in (A) serum, (B) cerebrospinal fluid (CSF) in control and IIH patients as measured by ELISA. (C) A correlation between serum and CSF leptin and (D) serum/CSF ratio were assessed in IIH patients and a sex and BMI matched cohort. Unequal variances t-test for A, Mann-Whitney test for B and C, Spearman correlation for C. **=P<0.01. Data presented as mean±SD.

The control and IIH cohorts were not matched for age, where age is a known determinant for serum leptin levels. Consequently a sensitivity analysis was carried out, matching the controls with a subgroup of IIH patients for age (control; 38.5±9.4 vs IIH; 34.9±6.9 years, P=0.061) and BMI (43.2±5.5 vs 44.6±6.6, P=0.6) (Fig4.3d). Serum leptin was raised in IIH (63.66±14.9 vs 75.57±30.41, P=0.04) (Fig4.3a). Furthermore, no difference in CSF (493.8±152.1 vs 516.8±208.4, P=0.96) (Fig4.3b) and serum/CSF ratio (137.8±33.1 vs 153.9±60.5, P=0.6) (Fig4.3c) was observed.

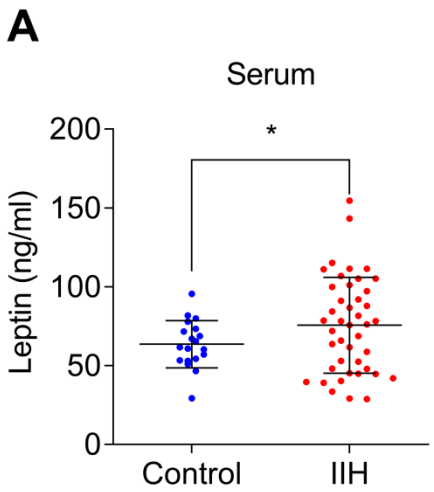

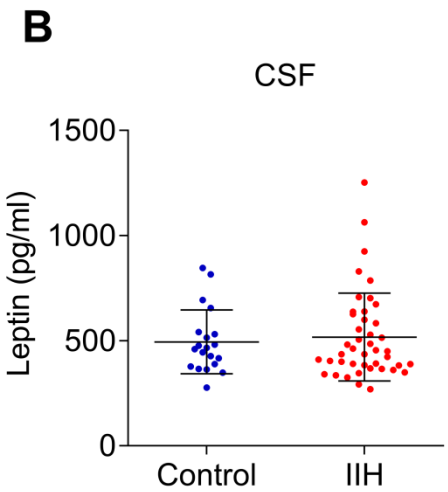

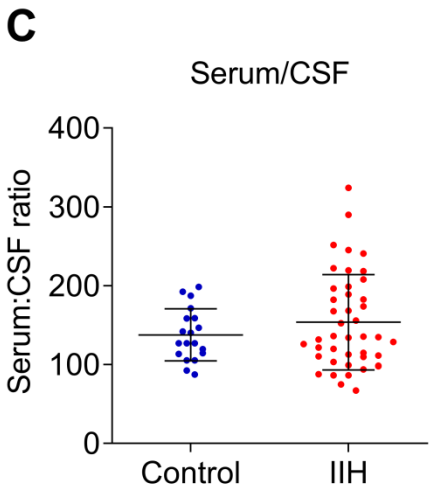

D

	Control	IIH	P-value
Age (Years)	38.5(9.4)	34.9(6.9)	P=0.06
BMI (kg/m^2)	43.2(5.5)	44.6(6.6)	P=0.6
LP Opp (cmCSF)	23.1(3.5)	34.7(5.5)	P<0.0001

Figure 4.3 Sensitivity analysis of leptin baseline characterisation

A sex, BMI and age matched cohort of control and IIH patients were sub analysed for (A) serum, (B) CSF leptin and (C) serum/CSF leptin ratio. Unequal variances t-test for A, Mann-Whitney test for B and C. N=19 for control, N=43 for IIH. Data presented as mean±SD or mean(SD), *=P<0.05.

4.3.3 Association between ICP and leptin

A previous study assessing CSF leptin levels noted that CSF leptin correlated with LP Opp in control patients whereas this was not evident in IIH patients, perhaps due to low numbers in the IIH cohort (IIH=22, Control, 52) (Ball et al., 2009). Consequently, serum and CSF leptin values were correlated against lumbar puncture opening pressure (LP Opp) to assess association, in a large IIH cohort. In control patients, serum leptin (Fig4.4a) was not found to correlate with ICP (P=0.053, R^2=0.15), however CSF leptin correlates with LP opening pressure (P=0.007, R^2=0.33) (Fig4.4b). In IIH patients neither serum (P=0.87, R^2=0.0001) (Fig4.4c) or CSF (P=0.14, R^2=0.01) (Fig4.4d) leptin levels correlate with LP Opp.

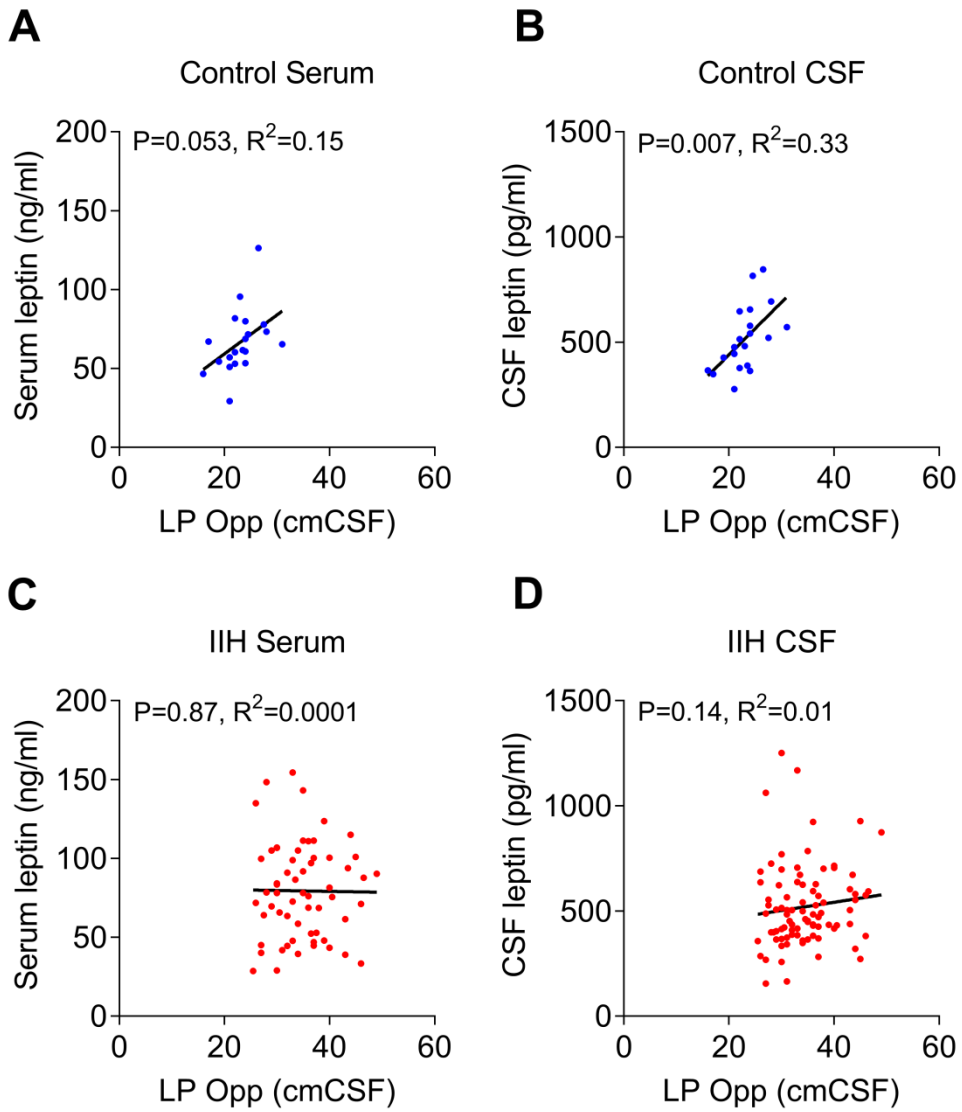

Figure 4.4 Association between leptin and lumbar puncture opening pressure

Scatter graphs detailing LP Opp vs (A,C) Serum and (B,D) CSF leptin in (A,B) control and (C,D) IIH patients. Pearson's correlation for A and B. Spearman's correlation for C and D. Significance was set at P<0.0125 following Bonferroni correction.

4.3.4 IIH patients have an altered post-prandial leptin response

The fasting status of subjects in studies assessing leptin in IIH patients has been mixed, where non-fasted studies have had a higher chance in finding raised serum leptin in IIH patients, suggesting that IIH leptin is altered in the post-prandial state (table 4.1). Consequently, the post-prandial leptin response was assessed in IIH patients and controls where the groups a well matched (Fig4.1). As part of their trial days, IIH patients and controls received a meal stimulation test. Here, post-prandial plasma leptin was assessed two hours after a meal. Control patients had reduced plasma leptin two hours after a meal compared to baseline (65.4±19 vs 58.0±17 ng/ml, P=0.002) (Fig4.5a). In contrast, IIH plasma leptin was unaltered (69.2±33 vs 68.4±34 ng/ml, P=0.92) (Fig4.5a). Furthermore the control cohort had a greater change in leptin compared to controls (89.75±15 vs 100.7±20 % of baseline, P=0.043) (Fig4.5b). These data highlight an altered postprandial leptin response in IIH patients compared to obese controls. Plasma leptin correlated strongly with paired serum leptin measurements (P<0.0001, R^2=0.85) (Fig4.5c), indicating that dilutions and experiments were carried out correctly.

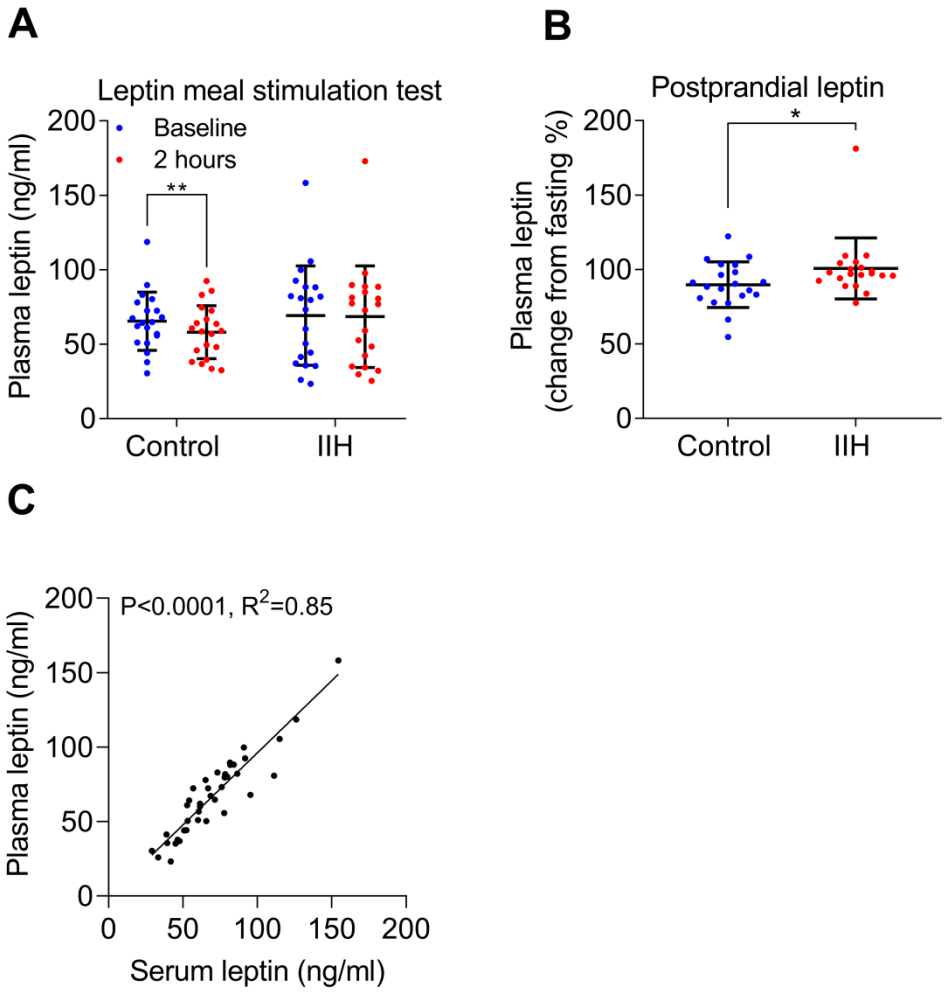

Figure 4.5 Postprandial leptin response in IIH patients

Fasting and post prandial leptin was assessed in control and IIH patients at their baseline visit. (A) Fasted and post prandial plasma leptin. (B) Post-prandial leptin as a percentage of fasted leptin. (C) Plasma vs serum leptin in both control and IIH. (A) Two-way repeated measures ANOVA with Sidak's multiple comparison test, (B) Mann-Whitney test, Pearson's correlation for C. Data presented as mean±SD. N=20, *=P<0.05, **=P<0.01.

4.3.5 Weight loss and leptin in IIH

Previous studies have not assessed the physiological response of weight loss to leptin in IIH patients, as such serum and CSF from IIH patients in the IIH:WT were taken from the 12 month visit where patients had been randomised to either community weight loss (diet) or bariatric surgery. Although the weight loss data from each group is locked clinical trial data, is apparent that patients in the surgical arm have a lower BMI compared to those in the diet arm at the 12 month visit (Fig4.1) .Serum leptin at 12 months was lower in the surgical arm compared to the diet arm (29.4±24 vs 75.9±32 ng/ml, P<0.0001) (Fig4.6a). Furthermore CSF leptin at 12 months was lower in the surgical arm compared to the diet arm (325.7±179.9 vs 504.7±180.1 pg/ml, P=0.001) (Fig4.6b). When compared to their respective baseline leptin values, the surgical patients display reduced CSF leptin (77.8±26 vs 29.4±24 ng/ml, P<0.0001) (Fig4.6c). Conversely the diet arm had no change in CSF leptin (79.2±35 vs 75.8±32 ng/ml, P=0.77) (Fig4.6c) at 12 months. Similarly, when compared to their respective baseline leptin values, the surgical patients have reduced CSF leptin (545.2±325.7 vs 325.7±179 pg/ml, P<0.0001) (Fig4.6d). Conversely the diet arm had no change in CSF leptin (524.2±175 vs 504.7±180.1 pg/ml, P=0.86) at 12 months (Fig4.6d).

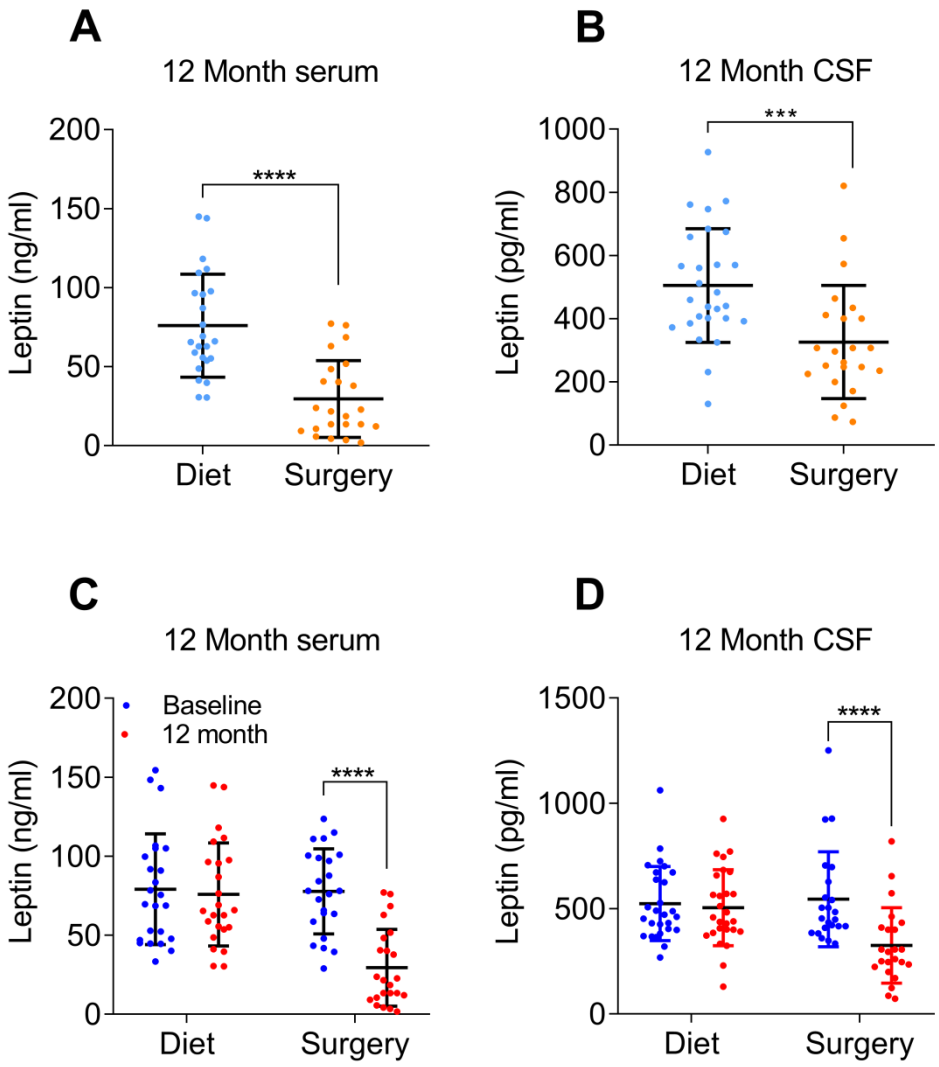

Figure 4.6 Bariatric surgery reduces leptin in IIH patients

Following a 12 month intervention, IIH patients randomised to diet and surgery had (A,C) serum and (B,D) CSF. Direct comparison between groups (A,B) and (C,D) comparison to baseline values. Mann-Whitney U-test for A and unpaired T-test for B, 2-way repeated measures ANOVA with Sidak's multiple comparison test for C and D. Data presented as mean±SD. Diet N=27, Surgery N=24. ***=P<0.0001, ****=P<0.00001.

At the baseline visit, CSF leptin was found to be correlated with LP Opp in control but not IIH patients. Consequently, at the 12 month visit, the association between serum and CSF leptin and LP Opp was assessed. At the 12 month visit, serum leptin in both the diet (P=0.62, R^2=0.008) and surgical arm (P=0.16, R^2=0.09) do not correlate with ICP. Conversely, in the surgical group, CSF leptin correlates with LP pressure (P=0.0097, R^2=0.32), akin to the control subjects, whereas diet arm has no correlation (P=0.8, R^2=0.006)

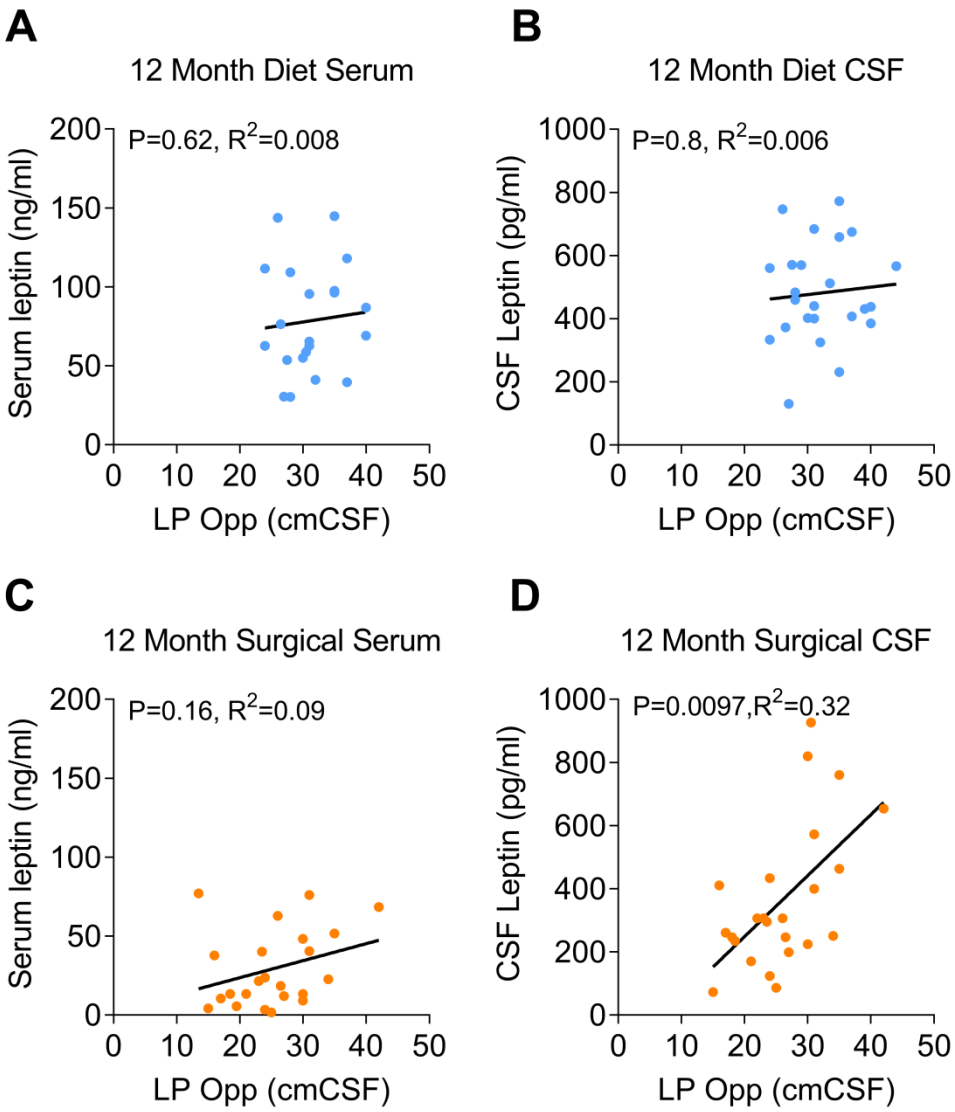

Figure 4.7 Association between leptin and lumbar puncture opening pressure following bariatric surgery

Scatter graphs detailing LP Opp vs (A,C) serum and (B,D) CSF leptin in (A,B) diet and (C,D) surgically randomised IIH patients at their 12 month visit. Spearman's correlations, where significance was set at P<0.0125 following Bonferroni correction.

4.3.7 Leptin reduction is weight loss dependent in IIH

Previous studies have identified that weight loss reduces serum and CSF leptin, this however has not been assessed in IIH patients. As such, the change in both serum and CSF leptin in all patients that completed a 12 month visit was assessed against change in BMI and fat mass, factors known to confer changes in leptin. Weight loss in IIH patients in the form of BMI reduction is associated with a reduction in (Fig4.8a) serum leptin ($P<0.0001$, $R^2=0.62$) and a reduction in (Fig4.8C) CSF leptin ($P=0.0002$, $R^2=0.27$). Similarly a reduction in fat mass is strongly associated with a reduction in serum leptin ($P<0.0001$, $R^2=0.45$) (Fig4.8b), however, fat mass reduction is not associated with a reduction of CSF leptin levels ($P=0.057$, $R^2=0.021$) (Fig4.8d).

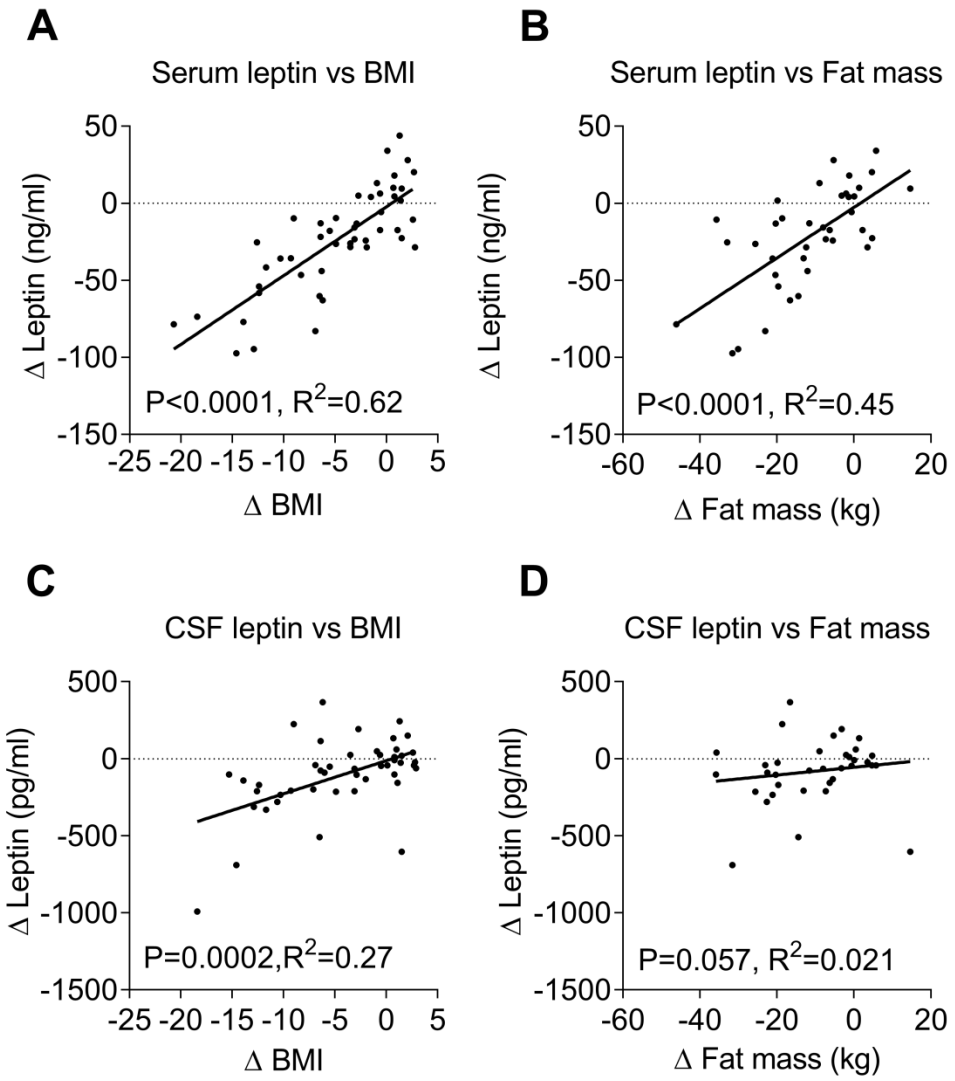

Figure 4.8 Weight loss reduces circulating leptin in IIH

Scatter graphs of combined 12 month IIH cohort where change in BMI (A,C) and fat mass (B,D) from baseline versus change in serum (A,B) and CSF (C,D) leptin from baseline. Following Bonferroni correction P<0.025 was considered significant. Pearson's correlation for A,B Spearman's correlation for C,D.

4.3.8 A reduction in fat mass reduces LP Opp in IIH

One pathogenesis hypothesis of IIH is that leptin could be driving the raised LP Opp. As such the correlation between change in LP Opp and change in leptin levels was assessed. At the 12 month time point, a reduction in BMI is strongly associated with a reduction in LP Opp (P=0.0001, R^2=0.48) (Fig4.9a). Similarly a reduction in fat mass is strongly associated with a reduction in LP Opp (P=0.0003, R^2=0.29) (Fig4.9b). Both reductions in CSF (P=0.003, R^2=0.13) (Fig4.9c) and serum (P=0.0003, R^2=0.342) (Fig4.9d) leptin are associated with a reduction in LP Opp.

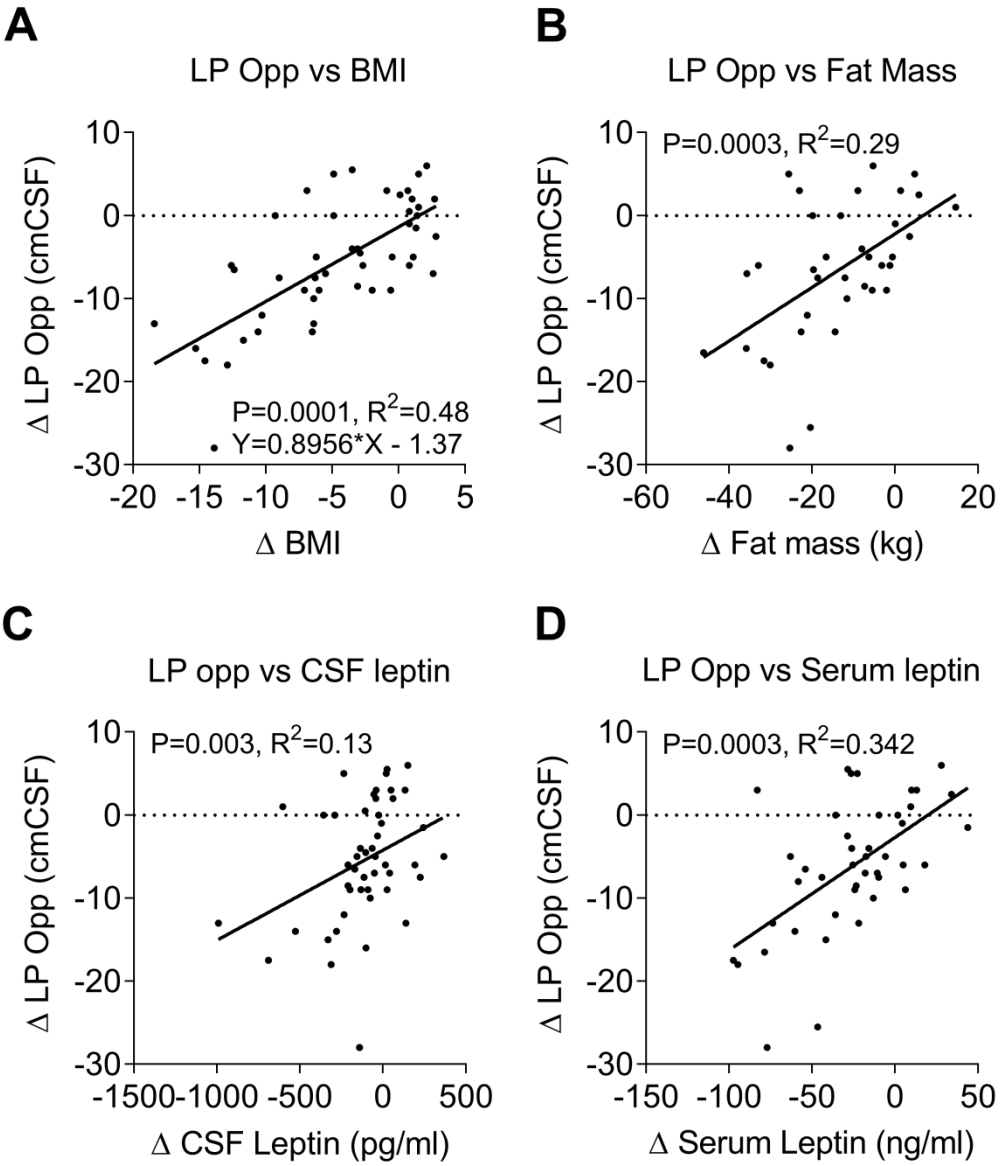

Figure 4.9 Association between weight loss and LP Opp reduction

Scatter graphs of combined 12 month IIH cohort change LP Opp from baseline versus change in (A) BMI, (B) fat mass, (C) CSF and (D) serum leptin from baseline. Spearman's correlation's where following Bonferroni correction, P<0.0125 was considered significant.

4.4 Discussion

4.4.1 Fasted-leptin in IIH

IIH in women is strongly associated with obesity, consequently leptin has been assessed in IIH patients in several studies (Markey et al., 2016b). However, the previous studies do not suggest a definitive leptin phenotype due to conflicting study designs and inappropriate controls. Furthermore work in chapter 3 highlights that IIH adipose secretes more leptin compared to matched controls. Consequently, the present study aimed to evaluate the fasting levels of leptin in IIH patients compared to a well matched control cohort.

This study demonstrates that IIH patients have raised serum leptin compared to controls, suggesting that increased subcutaneous adipose leptin secretion directly contributes to IIH hyperleptinaemia. In contrast, no difference in CSF leptin or the serum/CSF leptin ratio was observed, corroborating some studies and refuting others. These changes are retained when selecting for a better matched cohort. Moreover, the current data replicates previous studies demonstrating saturatable transport of leptin from the blood to the CSF, indicating that leptin transport into the CSF is not observably perturbed in IIH (Schwartz et al., 1996).

A strength of this study is that the control cohort is the first true healthy cohort to provide CSF leptin as a comparator for IIH patients; previous studies assessing CSF leptin used mixed neurological controls where a disease specific leptin signature could be measured. Furthermore, the current data corroborates a previous study highlighting that CSF leptin concentration positively correlated

with LP Opp in controls, whereas this is not demonstrated in patients with active IIH (Ball et al., 2009).

4.4.2 IIH patients have an altered post-prandial leptin response

A further aim of the study was to assess the post-prandial leptin response in IIH patients. The study highlights altered post-prandial leptin response in IIH patients whereby there is no post-prandial response to leptin, in contrast to controls who have reduced plasma leptin in response to a meal, replicating a previous study (Korek et al., 2013). Consequently the post-prandial leptin phenotype in IIH is intermediate between obese patients, whose leptin decreases post-prandialy, and non-obese patients whose leptin increases post-prandialy (Korek et al., 2013). The present data could suggest that IIH adipose is more responsive to insulin, the predominant leptin secretagogue in the post-prandial state, or to glucose stimulated leptin secretion compared to obese controls. These factors have yet to be fully assessed and should be followed up. This study has failed to investigate other hormones associated with satiety in the post-prandial state, such as ghrelin.

4.4.3 Weight loss, leptin and LP Opp in IIH patients

The final aim of the study was to assess the physiological response of leptin to weight loss in IIH patients. It is well established in obese patients that reducing BMI and fat mass reduces circulating serum and CSF leptin levels, however this has never been assessed in IIH patients (Maffei et al., 1995; Nam et al., 2001). The present study demonstrates a weight loss dependent serum and CSF leptin reduction in IIH patients, highlighting that obesity as a primary determinant of raised serum leptin in IIH, rather than inherent high leptin secretion.

Furthermore, a reduction in BMI through reduction in fat mass is strongly correlated with a reduction in LP Opp, and is coupled with a reduction in serum leptin.

The lack of correlation with CSF leptin and LP Opp at baseline coupled with unaltered CSF leptin levels in IIH patients suggests that leptin is not driving the raised LP Opp in IIH. Rather, this change in LP Opp is most likely linked to the change in fat mass, as such the raised serum leptin is probably a bystander to the metabolic perturbations of IIH adipose as discussed in chapter 3. This study highlights that adipose may be driving the pathology in IIH. Perhaps of clinical significance, the striking association between BMI reduction and reduction in LP Opp is almost prescriptive. Based on the current data, where a patient is required to reduce their LP Opp by a certain amount to achieve a normal LP Opp value, and appropriate method of weight loss could be prescribed. This needs further investigation to identify whether this is a true association.

4.4.4 Limitations

The present study has several limitations. Primarily the control cohort is not large, compared to the largest IIH cohort to have leptin assessed. Furthermore, the narrow eligibility criteria for both IIH:DT and IIH:WT limits applicability of the current results to the well-defined and characterised cohort of obese women of reproductive age with active IIH, excluding applicability to other IIH patient groups such as paediatric and male IIH, although these make a minority of IIH patients. Assessing serum and CSF leptin in male IIH patients would be a of future interest, due to the association of male IIH with obesity (Bruce et al., 2009). This study also did not directly assess leptins capacity to modulate ICP

or CSF secretary processes at the choroid plexus. However it is clear that rodent choroid plexus does not express the signalling splice variant of the leptin receptor, OB-Rb, and protein expression for this has not been observed in humans (Burguera et al., 2000; Couce et al., 1997; Mitchell et al., 2009). Rather the choroid plexus expresses the transporting splice variant, OB-Ra, in humans and rodents that has minimal signalling capacity and primarily transports leptin from the blood to the CSF (Burguera et al., 2000; Couce et al., 1997; Mitchell et al., 2009). This does not preclude leptins capacity to alter CSF drainage; however leptins effects on CSF drainage have yet to be assessed. Furthermore assessing leptins capacity to modulate ICP in an appropriate rodent model is nearly impossible. Ideally an obese female rodent will be infused with leptin and ICP assessed. However, leptin induces rapid robust weight loss in rodents, thus preventing a long term assessment of leptins capacity to alter ICP in obese rodents (Halaas et al., 1997).

The current study fails to assess the mechanisms that could underpin altered leptin dynamics in IIH. Although chapter 3 suggests that increased intra-adipose glucocorticoid accumulation could be influencing serum leptin levels, other factors could be altering leptin. Assessment of leptin secretagogoues such as insulin and catecholamine's in the basal state and post-prandial insulin state would inform on the potential causes of the altered leptin dynamics in IIH. Perhaps more interesting, the present study fails to investigate other factors that regulate energy intake, such as cholecystokinin, glucagon, glucagon-like peptide 1 and ghrelin in both the fasting and post-prandial state. Assessing these would give a stronger assessment on hormonal control of energy

homeostasis in IIH patients. Ghrelin has however been investigated in IIH, where no difference in fasting or post-prandial ghrelin was demonstrated, however the study had multiple IIH phenotypes and an unmatched cohort limiting the utility of the study (Subramanian et al., 2004). Further investigation into these factors would allow for an understanding of the role of gut neuropeptides in weight and energy homeostasis in IIH.

The present study highlights that IIH patients have increased fasting serum leptin but unaltered CSF leptin levels. Furthermore IIH patients have a distinct post-prandial leptin signature. The present data suggests that the leptin phenotype is most likely a consequence of other metabolic perturbations rather than a pathogenic moiety in IIH due to the strong association between weight loss and reduction in LP Opp.

Chapter 5 Developing and Validating an *in vitro* Na^+/K^+ ATPase Activity Assay

5.1 Introduction

Cerebrospinal fluid (CSF) bathes the brain, simultaneously delivering nutrients and flushing waste as well as providing buoyancy, allowing the brain to maintain its normal functionality and anatomy. CSF volume is a critical determinant of intracranial pressure (ICP). This dynamic is tightly regulated: therefore any aberration of ICP, as seen in hydrocephalus, idiopathic intracranial hypertension (IIH) or following traumatic brain injury can have life-altering consequences. Manipulation of CSF volume is used clinically to lower ICP, however, pharmacological manipulations of CSF secretion to date low efficacy and are poorly tolerated (Mollan et al., 2018b). Consequently there is a need to develop and screen for novel therapies that can lower ICP.

There are currently many methods available to determine ICP, CSF secretion or surrogate markers of these (see table 3.1). Current *in vivo* methods either directly measure ICP or measure CSF fluid volume. Such methods provide powerful physiological data about molecules that modulate ICP and CSF production. Furthermore, they provide temporal data on how ICP or CSF production changes following drug administration. Critically, ICP can be monitored chronically, providing an understanding of both acute and chronic administration drug action (Uldall et al., 2014). However, *in vivo* methods do not allow high-throughput screening of putative modulators of ICP due to the requirement of large numbers of animals: consequently animal models are more suited to targeted physiological experimentation and pre-clinical evaluation rather than high-throughput drug screening. Therefore, *in vitro* methods provide

the optimal method for high-throughput screening of molecules that could alter CSF secretion.

Author	Method	Direct or surrogate measure
(Uldall et al., 2014)	*In vivo* transcranial pressure monitor	Direct long term monitoring of ICP
(Oshio et al., 2004)	*In vivo* CSF production	Direct measure of CSF production
(de Rougemont et al., 1960)	*Ex vivo* oil covered choroid plexus	Direct measure of fluid secretion
(Klarr et al., 1997)	In vitro ^{86}Rb Uptake assay	Direct measure of Na^+/K^+ ATPase activity
(Botfield et al., 2017)	*In vitro* inorganic phosphate assay	Indirect measure of Na^+/K^+ ATPase activity
(Hakvoort et al., 1998)	*In vitro* FITC-dextran assay	Indirect measure of *In vitro* CSF production

Table 5.1 Non-exhaustive list of CSF secretion assay methods

One *in vitro* method involves the measurement of CSF secretion. Due to the choroid plexus forming a strong barrier between the blood and the CSF, any *in vitro* CSF secretion assay requires a competent barrier (Hakvoort et al., 1998). However, these require large quantities of tissue and are technically difficult to

produce. Consequently, using surrogates for CSF secretion is a more convenient option, specifically assaying the activity of the ubiquitously expressed membrane bound Na^+/K^+ ATPase.

The physiological rationale of utilising Na^+/K^+ ATPase activity as a surrogate for CSF secretion is clear. Inhibiting the Na^+/K^+ ATPase at the choroid plexus inhibits CSF secretion up to 80% *in vivo*, thus Na^+/K^+ ATPase activity is intrinsically linked to CSF secretion, however the exact link between Na^+/K^+ ATPase activity and CSF secretion has yet to be elucidated (Pollay et al., 1985; Vates et al., 1964). Furthermore, reducing Na^+/K^+ ATPase activity at the choroid plexus through indirect means such as inhibiting carbonic anhydrases is associated with reduced CSF secretion (Oshio et al., 2004; Uldall et al., 2017). Na^+/K^+ ATPase assays assess either ATP turnover or assess the movement of ions. Na^+/K^+ ATPase activity is elucidated with the cardiotonic steroid ouabain, a Na^+/K^+ ATPase specific inhibitor. Traditional *in vitro* Na^+/K^+ ATPase activity assays are unphysiological, requiring the lysis of the cells in order to assay ATP turnover. This uncouples the underlying biochemistry of the cell from the Na^+/K^+ ATPase and prevents instantaneous changes, such as phosphorylation, from being assessed. A further method to investigate Na^+/K^+ ATPase activity includes using a rubidium radio-isotope (^{86}Rb) (Klarr et al., 1997). This assay works on the principle that ^{86}Rb is transported through the Na^+/K^+ ATPase similarly to potassium cations. This assay, however useful, requires specialist equipment due to use of radioactive isotopes. Furthermore, the previously discussed *in vitro* Na^+/K^+ ATPase assays measure endpoints, preventing real-time recordings of activity and understanding of Na^+/K^+ ATPase dynamics. As

such, there is a need for a convenient and reproducible assay to assess therapeutic and putative pathogenic molecules that are suspected to alter ICP. This chapter details the development of a novel *in vitro* Na^+/K^+ ATPase activity assay.

5.1.2 Aims

1. Develop an *in vitro* surrogate assay for CSF secretion
2. Compare the developed assay to a validated *in vivo* model

5.2 Methods

5.2.1 Cell culture

Z310 cells (section 2.1) were cultured in DMEM supplemented with 10% foetal calf serum, 1% Penicillin/streptomycin and 1ng/ml epidermal growth factor (PeproTech, London, UK), at 37°C with 5% CO_2. For microscopy cells were cultured to confluence on 25mm diameter glass coverslips (VWR, Leighton Buzzard, UK) seeded with poly-D-lysine and incubated with laminin (20ng/ml).

5.2.2 Plate based Na^+/K^+ ATPase activity assay

Z310 cells were cultured in 12 well plates and phosphate and protein assays were ran on the same samples as outlined in sections 2.2, 2.3 and 2.4.

5.2.3 Live cell microscopy

Live cell microscopy was carried out as outlined in section 2.18. In brief, Z310 cells infected with an adenovirus containing the Perceval biosensor for 48h were imaged on a confocal microscope in real time. Cells were incubated with acetazolamide (100μM), furosemide (100μM) or an appropriate vehicle for two days and Na^+/K^+ ATPase activity elucidated by ouabain octahydrate (1mM). Data presented as F/F_{min} where F= fluorescence at a given time and F_{min} = minimum fluorescence during the recording. Assessor was blinded to the treatment of the cells during evaluation of cell fluorescence intensity.

5.2.4 Animals

The study utilised female Sprague-Dawley rats (Taconic, Denmark) weighing 150-250g. The rats were housed in cages under an inverted 12 hour light/dark cycle with ad libitum access to food and water. All experimental procedures were approved by the Danish Animal Experiments Inspectorate (license number 2014-15-0201-00256). Surgical procedures were carried out according to section 2.19.2. After treatments and surgical procedures, the rats were monitored daily for any adverse effects.

5.2.5 Drugs

Acetazolamide and furosemide were administered via subcutaneous injection where acetazolamide was used at 103.3 mg/kg and 413.4 mg/kg and furosemide was used at 4.1 mg/kg and 24.8 mg/kg. The smaller dose represents a clinically relevant dose, the large dose represents a daily maximal dose. Dosage was worked out via the following FDA derived equation [Rat drug] (mg/kg) = 6.2 X [human] (mg/kg based on 60kg human). Further details can be found in section 2.19.3.

5.2.6 ICP measurements

Rats were sedated with 2.5 mg/kg midazolam (subcutaneous injection) and placed in an infusion cage (Instech Laboratories, Plymouth meeting, PA), which had a levered arm to provide unhindered movement. A stable baseline ICP reading was recorded for 30 minutes. A subcutaneous injection of drug or vehicle was administered at time zero on ICP traces. ICP was recorded for a further 120 minutes and then the animal was allowed to recover in its normal

cage. ICP was analysed using the Perimed software as outlined in section 2.19.6. Monitoring period was selected to measure the maximal plasma concentration of the administered drugs.

The animals featured in this work will have had repeated treatments, including treatments of drugs otherwise not described here in a randomised fashion. However animals had a washout period sufficient to allow for full clearance of the drug in question, the equivalent of 5 half-lives of a drug.

5.2.7 Statistics

Data was analysed using GraphPad Prism (V7.1) software. Data are presented as either median (interquartile range) or mean± standard deviation (SD) unless otherwise stated, subject to a Shapiro-Wilk normality test to determine the normality of the data. $P<0.05$ was considered significant.

5.3 Results

5.3.1 Phosphate assay

The phosphate assay determines inorganic phosphate content of a cell. In the context of CSF secretion, the Na^+/K^+ ATPase liberates inorganic phosphate and ADP following the cleavage of ATP to facilitate its function. As such, where a cell has higher Na^+/K^+ ATPase activity there should be increased inorganic phosphate when ouabain is added to cells. Although the assay is functional in primary choroid plexus cells, the assay requires large quantities of cells that cannot be ethically justified in the cost of animal life for drug screening experimentation (Botfield et al., 2017). As such, the assay needed to be optimised in an immortalised cell line. The particular method used in this assay is unique as far as the cells remain complete during the course of the assay and only lysed once the assay is completed, keeping the internal biochemistry intact. A 1 hour aCSF incubation followed by a 30 minute ouabain incubation was selected according to a previous paper that utilised primary choroid plexus epithelial cells as a starting point for optimisation (Botfield et al., 2017).

5.3.2 Ouabain incubation time course

Initial optimisation involved optimisation of the ouabain incubation time on Z310 cells. (Fig5.1a) The present data highlights that only a 30 minute incubation with ouabain yields a small but significant reduction in inorganic phosphate (42.43±1.56) compared to control (52.4±4.56) (P=0.02). Of note, there is high variability in the levels of phosphate between the control conditions. (Fig5.1b) When comparing the ouabain reductions it is found that 30 minute ouabain

incubation (80.98±2.97) is significantly different only to a 60 minute incubation of ouabain (100.8±5.56)(P=0.005).

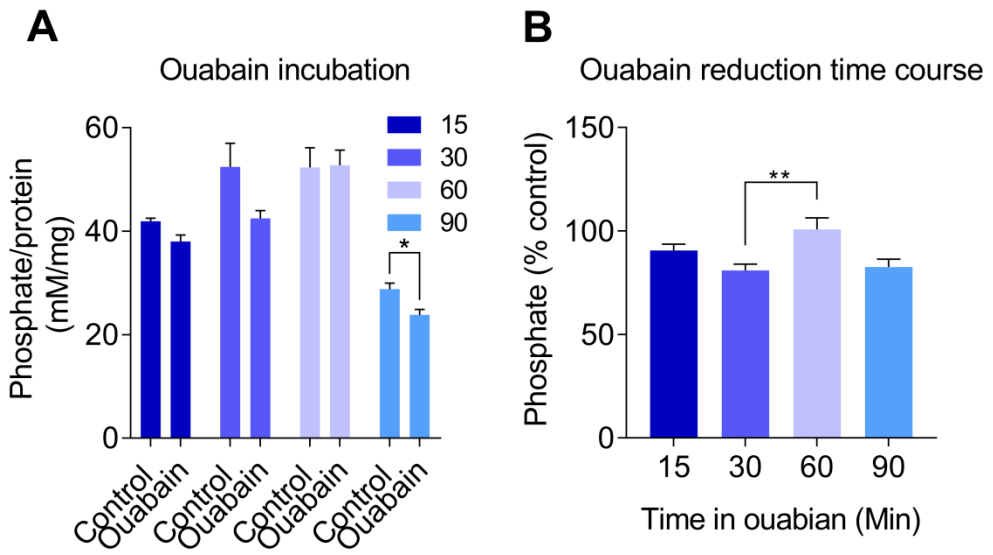

Figure 5.1 Ouabain incubation time course

Z310 cells incubated with ouabain for various times. (A) Bar graph of raw normalised phosphate values with and without ouabain over various times. (B) Bar graph representing the percentage reduction elicited by ouabain relative for control. Sidak's multiple comparisons test for A, one-way ANOVA with post-hoc Tukey's test for B. N=5 for all groups. *=P<0.05, **=P<0.01.

5.3.3 aCSF incubation time course

Following ouabain time optimisation, the aCSF preincubation time was assessed. (Fig5.2a) It was demonstrated that 1 hour aCSF incubation has higher levels of phosphate (54.99±9.1) compared to 3 hours (27.9±1.1, $P<0.01$), 6 hours (15.74±0.6, $P<0.0001$) and an overnight incubation of aCSF (37.20±1.20, $P=0.04$). (Fig5.2b) Only 1 hour incubation of aCSF yields a significant reduction in inorganic phosphate following ouabain administration (54.99±9.2 vs 39.47±2.1, $P=0.03$). (Fig5.2c) Furthermore 1 hour aCSF incubation allowed ouabain to deliver a more robust reduction (71.77±3.7%) compared to 3 hour (95.93±5.1%, $P=0.03$) and 6 hours (113.3±4.8%, $P=0.006$) aCSF incubations. The is no difference in reduction compared to an overnight aCSF incubation (90.89±7.9%, $P=0.09$).

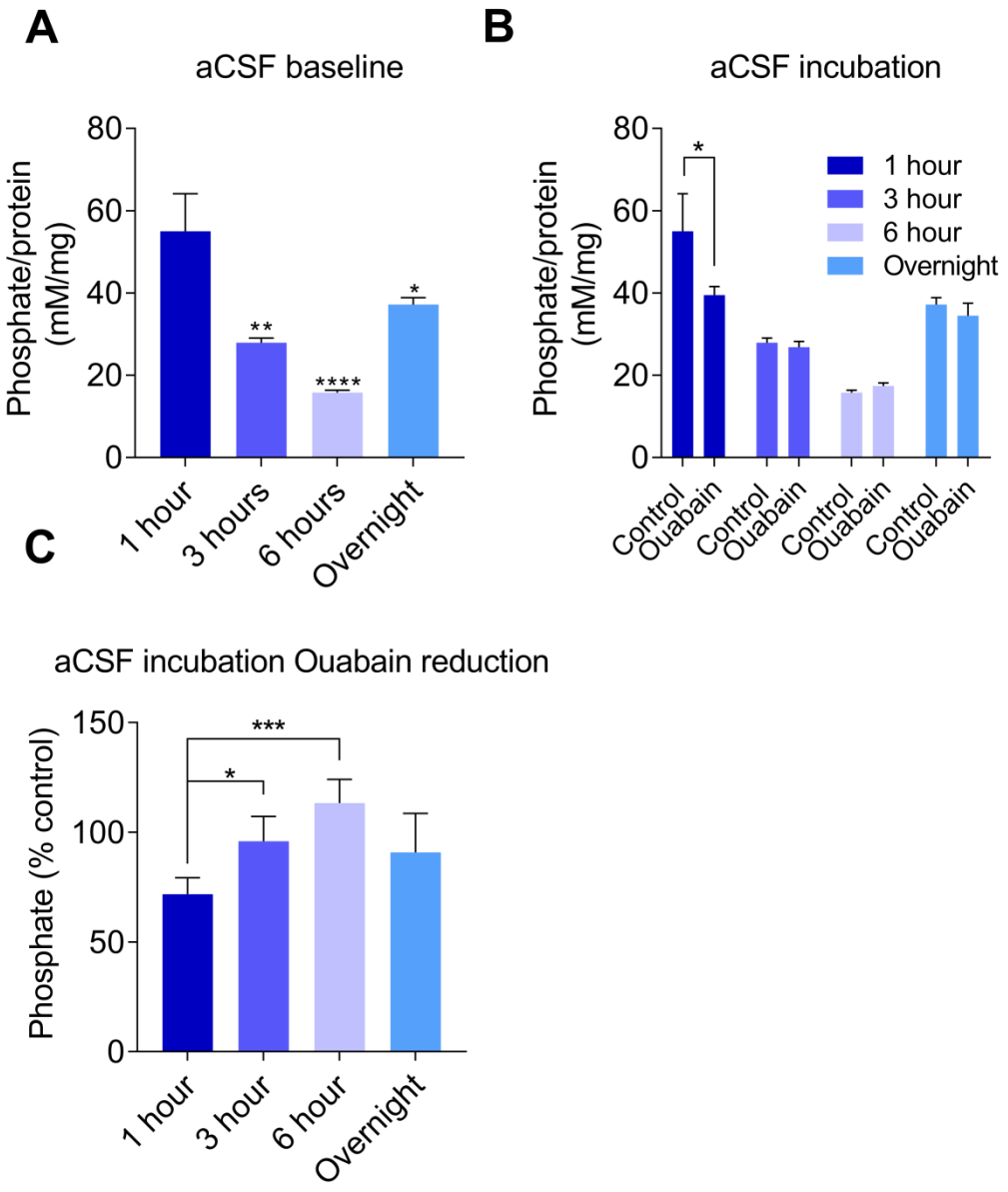

Figure 5.2 Artificial cerebrospinal fluid incubation optimisation

Z310 cells incubated for various times in artificial cerebrospinal fluid (aCSF) prior to inorganic phosphate measurement. A) Represents basal normalised phosphate over an aCSF timecourse. B) Represents phosphate following subsequent 30 minute incubations with ouabain. C) Ouabain reduction as a percentage of baseline. Data presented as mean±SEM. A and C one-way ANOVA with post-hoc Dunns test, B Two-way ANOVA with post-hoc Sidak's test's. *=P<0.05, **=P<0.001, ***=P<0.0001 and ****=P<0.00001. N=5 biological repeats

The optimised experimental setup of 1 hour aCSF pre-incubation followed by 30 minute ouabain administration, generated an intra-assay variability coefficient of 26.3% and an inter-assay variability coefficient of 39.7%. This indicates that the assay produces high variability in Z310 cells, reducing reproducibility. Furthermore, the reduction achieved through ouabain was not sufficient due to the aforementioned variability, preventing the analysis of drugs. As such, this assay was deemed unfit for purpose in Z310 cells.

5.3.4 Perceval and the ATP:ADP ratio

The failure of the previous assay facilitated the development of a novel *in vitro* Na^+/K^+ ATPase activity assay. The utilisation of genetically encoded biosensors enables a more physiological method to assess biological parameters. One candidate is the Perceval biosensor. Perceval is derived from bacterial GlnK1 protein and contains a circularly permuted GFP molecule and reports the ATP/ADP ratio in real time, where an increased ATP/ADP ratio increases emitted fluorescence (Berg et al., 2009). This property presents the possibility of Perceval acting as a reporter of Na^+/K^+ ATPase activity, due to the Na^+/K^+ ATPase deriving its energy from the hydrolysis of ATP to ADP (Fig5.3a). Theoretically the addition of ouabain should increase the ATP:ADP ratio (Fig5.3b) due to the reduction in ATP hydrolysis. In conditions where the Na^+/K^+ ATPase is less active thus consuming less ATP, it would be expected that there would be a smaller increase in ATP compared to basal conditions under ouabain addition (Fig5.3c). Conversely, in conditions where the Na^+/K^+ ATPase is more active, thus consuming more ATP, it would be expected that there would be a greater increase in ATP compared to basal conditions under

ouabain addition (Fig5.3d). These changes in ATP:ADP ratio under the previous conditions should be reported by the Perceval biosensor. It was aimed to determine whether Perceval is an appropriate biosensor to determine Na^+/K^+ ATPase activity.

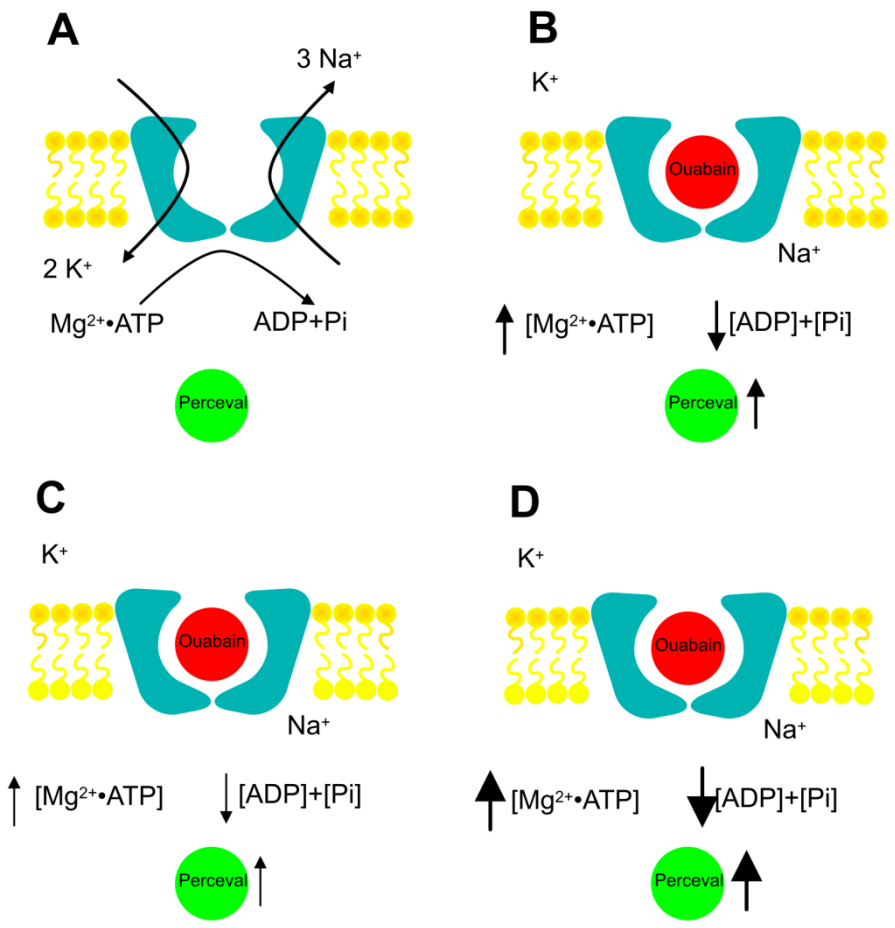

Figure 5.3 Perceval assay theory

(A) The Na^+/K^+ ATPase transduces energy via ATP lysis, transporting ions, where this can be inhibited via ouabain (B). Such an inhibition causes an increase in cellular ATP:ADP ratio, a change that could be detected by the Perceval biosensor though changes in fluorescence (B). In situations where Na^+/K^+ ATPase activity is decreased (C) or increase (D), ouabain administration is hypothesised to resolve either a smaller (C) or larger (D) change in ATP:ADP ratio compared to normal situations (B), which is detectable by the Perceval biosensor as changes in fluorescence. Arrows by Perceval represent change in fluorescence.

5.3.5 Z310 cells express Perceval

Following two days of infection with an adenovirus harbouring the Perceval biosensor, Z310 cells showed Perceval expression (Fig5.4). Z310 cells retained their cobblestone-like morphology. Furthermore there is heterogeneity in fluorescence emitted by the Z310 cells, indicating different levels of ATP turnover, or heterogeneity in expression of the biosensor.

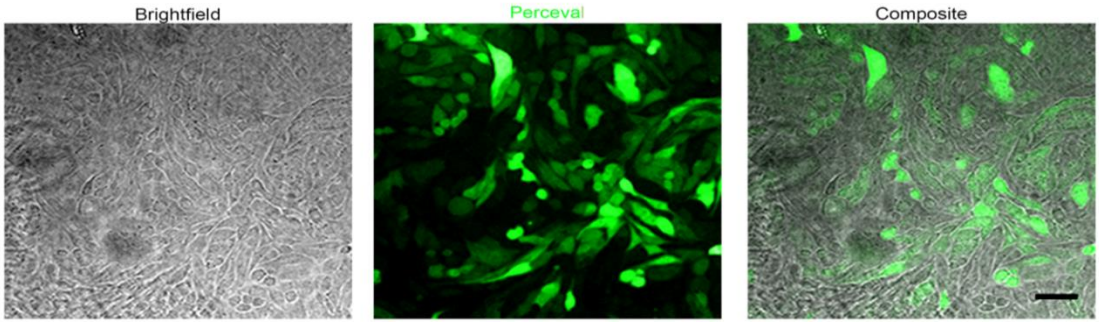

Figure 5.4 Z310 cells express Perceval

Confluent Z310 cells express Perceval two days post adenovirus infection, where fluorescence is variable between cells. Scale bar = 50 µm.

5.3.6 Heterogeneity in Z310 ATP:ADP ratio

Due to Z310 cells apparent fluorescence heterogeneity in Perceval infected Z310 cells, the size of the variability was assessed. This highlighted a 18.5% variability in baseline fluorescence, as shown by Fig5.5a, where the distribution of fluorescence is non-parametric. To address this, cellular fluorescence was normalised to its minimum fluorescence in the baseline period. This reduced the variability to 3.3%, as highlighted in Fig5.5b, where 50% of the cells fall in the 1.02 bin.

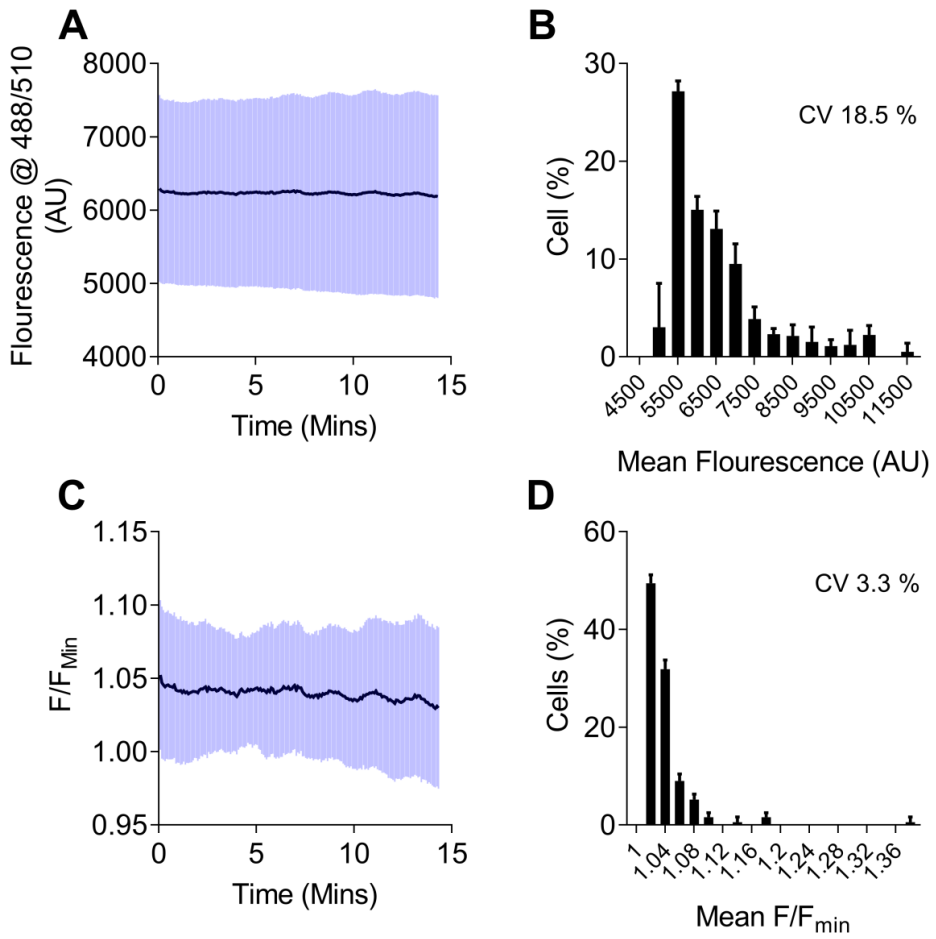

Figure 5.5 Fluorescence heterogeneity in Z310 cells

A) Traces of raw fluorescence of Z310 cells (B) Histogram representing the distribution of mean cell fluorescence in Z310 cells over 15 minutes, where the cell to cell variability in fluorescence is 18.5%. (C) Trace of normalised fluorescence of Z310 cells. (D) Histogram representing the normalised (F/F_{min}) fluorescence of the same cells in A, where variability in cellular fluorescence is 3.3%. N=167 cells from 3 pooled coverslips. A and C presented as mean±SD. F=fluorescence at a given time, F_{min} = minimum fluorescence in the trace.

5.3.7 Perceval reports changes in the ATP/ADP ratio elicited by ouabain

Following confirmation of Perceval expression and demonstration of a stable ATP:ADP ratio, it was aimed to determine whether ouabain could increase the ATP/ADP ratio. Consequently two treatment groups, vehicle (HEPES-bicarbonate buffer) and ouabain (1 mM) had fluorescence measured prior to and after treatment. The raw trace (Fig5.6a) indicates that F/F_{min} remains stable prior to the administration of the treatment. The addition of treatment creates an artefact (0 minutes on trace) perhaps due to disrupted light transit. Vehicle treated cells (Fig5.6b) showed a decrease in F/F_{min} from 1.043(0.027) to 1.034(0.03) (P=0.026) indicating that the volume of vehicle alters the transmission of light. Conversely, ouabain increases F/F_{min} from 1.045(0.23) to 1.072(0.039) (P<0.0001), indicating that ouabain is increasing the ATP/ADP ratio, as predicted. Following this the change in maximum F/F_{min} was assessed for both groups (Fig5.6c). It was observed that ouabain changes F/F_{min} more compared to the vehicle treated group (0.027(0.0269) Vs. -0.005(0.0129), P<0.0001). The area under the curve (AUC) of the traces (Fig5.6d), was larger in ouabain treated cells versus vehicle treated cells (0.93(0.517) Vs. 0.55(0.434); P=0.0003).

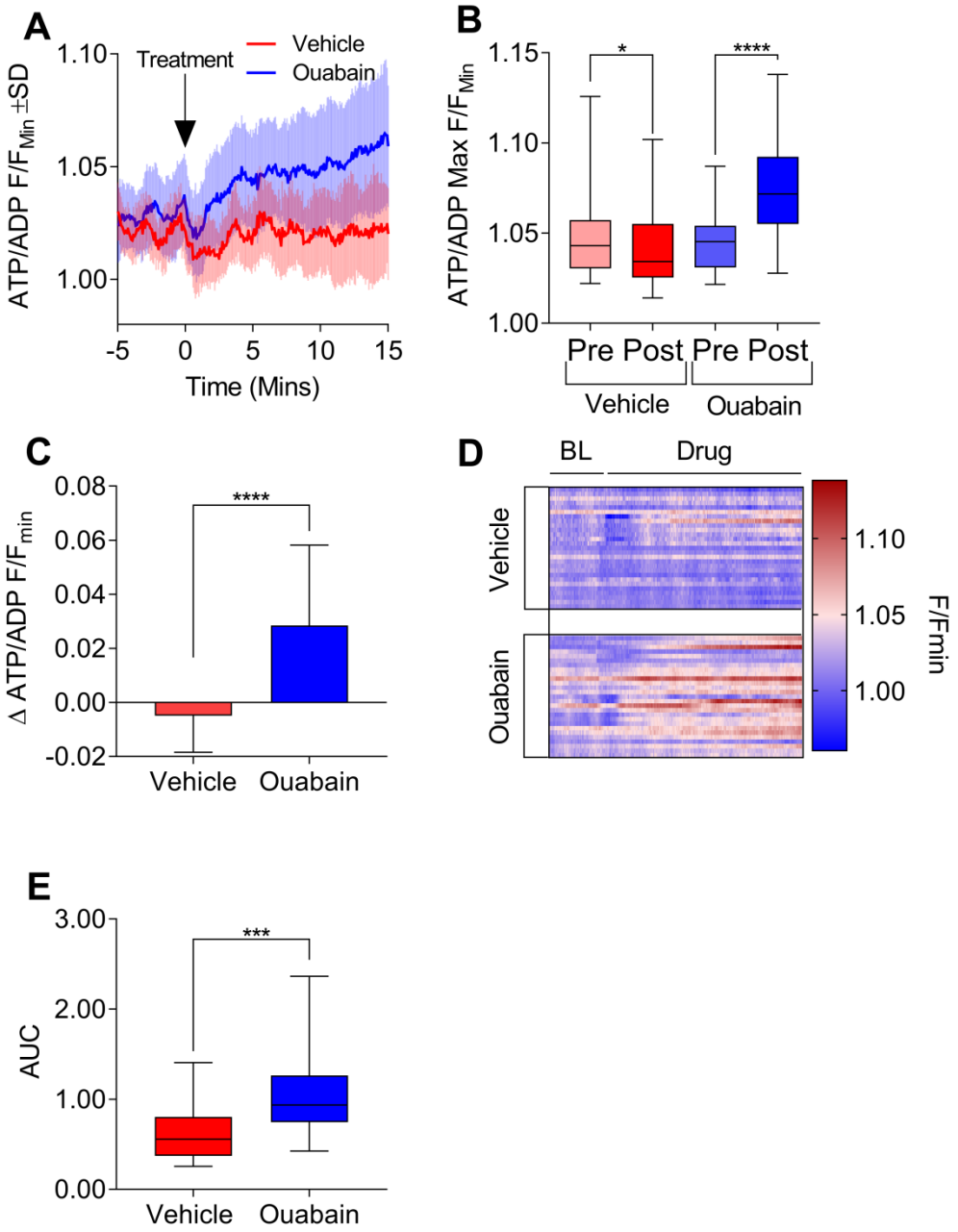

Figure 5.6 Ouabain elicits a change in ATP:ADP ratio in Z310 cells

Z310 cells live cell imaged following Perceval infection, with acute vehicle and ouabain (1mM) treatment. (A) A trace graph detailing the change in ATP/ADP ratio in vehicle treated (red) and ouabain treated (blue) Z310 cells. (B) Represents the F/F_{min} of cells with and without treatment. (C) Details the change in ATP:ADP ratio elicited by ouabain or control. (D) A heat map detailing the F/F_{min} in individual cells over the course of the experiment. (E) The area under curve (AUC) derived from both traces on A for the course of the experiment. A and C are presented as mean±SD. B and E presented as median (IQR). N = 27 for vehicle and ouabain treated cells, derived from 4 pooled

coverslips. B Wilcoxon test, C students t-test, E Mann-Whitney U test. ***=P<0.001, ****=P<0.0001. B presented at median(IQR).

5.3.8 Reversible action of ouabain

Washout experiments were carried out to determine if the effect of ouabain could be reversed. The maximal fluorescence elicited by ouabain peaks around 15 minutes after administration. It is demonstrated that a washout of media containing ouabain reduces F/F_{min} (1.16 Vs. 1.10; P=0.03) (Fig5.7b). Furthermore, subsequent addition of ouabain increases F/F_{min} (1.10 Vs. 1.23; P=0.004). Additionally, there is no difference between the changes in F/F_{min} ouabain elicits prior to or after the washout (Δ9.5±4.4% Vs. Δ11.4±3.8%; P=0.1) (Fig 6.7c). These data highlight that the effects of ouabain can be reversed.

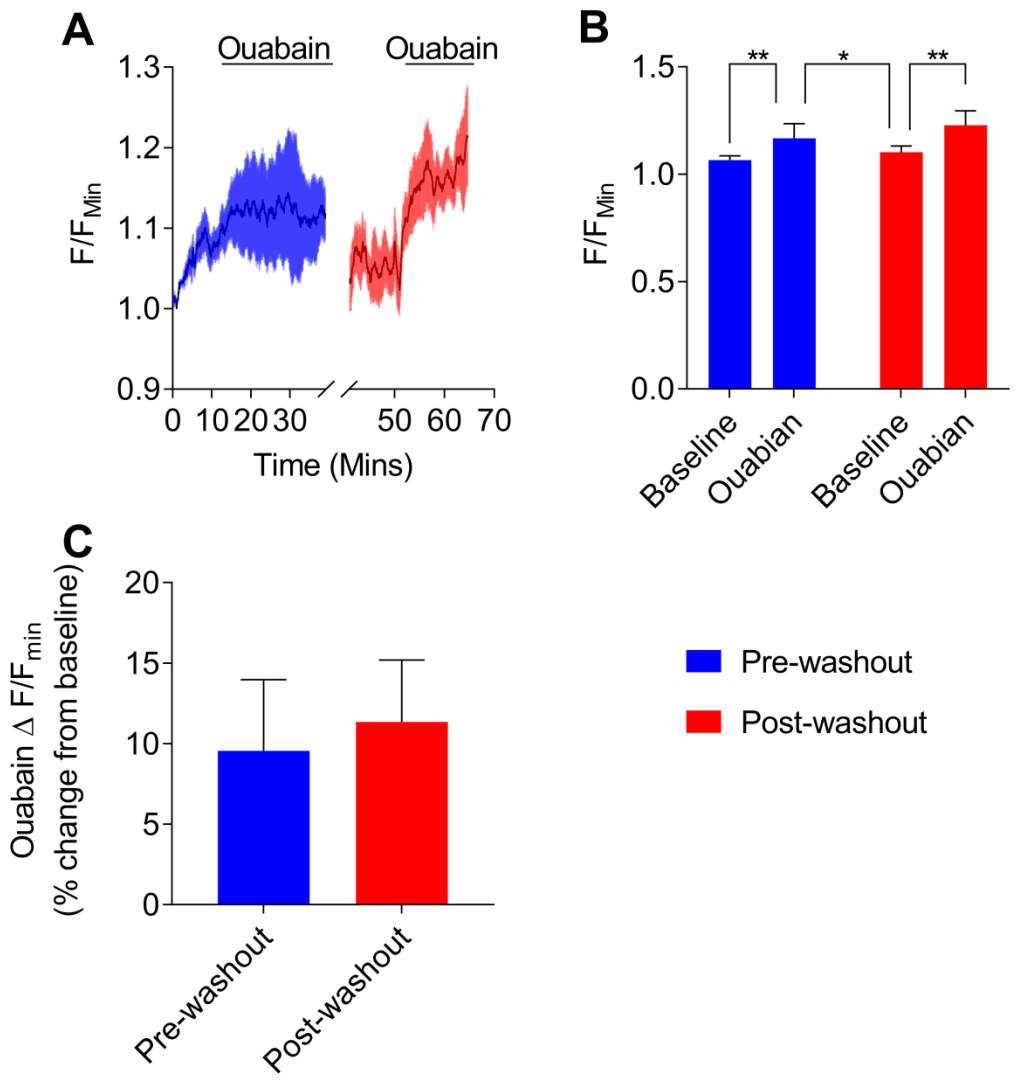

5.7 Reversible action of ouabain in Z310 cells

Live cell imaging of Z310 cells following Perceval introduction. (A) Trace detailing the F/F_{min}, whereby pre-washout is blue, post-washout is red. Break in axis represents washout period. (B) Highlights F/F_{min} of cells following subsequent treatment of cells. (C) Details ouabain mediated change in F/F_{min} pre- and post-washout. For B Two way repeated measures ANOVA with post-hoc Sidak's test. For C paired T-test. N=7 cells from one coverslip. *=P<0.05, **=P<0.01.

5.3.9 Acetazolamide manipulates the ATP/ADP ratio

Utilising the carbonic anhydrase inhibitor acetazolamide, which has previously been shown to reduce Na^+/K^+ ATPase activity choroid plexus and CSF secretion, it was aimed to determine if the current assay can replicate previous results (Oshio et al., 2004; Sterling et al., 2001; Uldall et al., 2017). Z310 cells were incubated for two days either with vehicle (DMEM) or 100μM acetazolamide prior to imaging. Ouabain administration elucidated a smaller change in F/F_{min} in acetazolamide treated cells compared to vehicle treated cells (0.007(0.0103) Vs. 0.024 (0.0318); P=0.029) (Fig5.8b). Furthermore, the AUC is smaller for acetazolamide treated Z310's compared to vehicle treated cells (0.0447 (0.3452) Vs. 0.61(0.378); P=0.044) (Fig5.8c). This data indicates that acetazolamide decreases Na^+/K^+ ATPase activity, in keeping with previous literature.

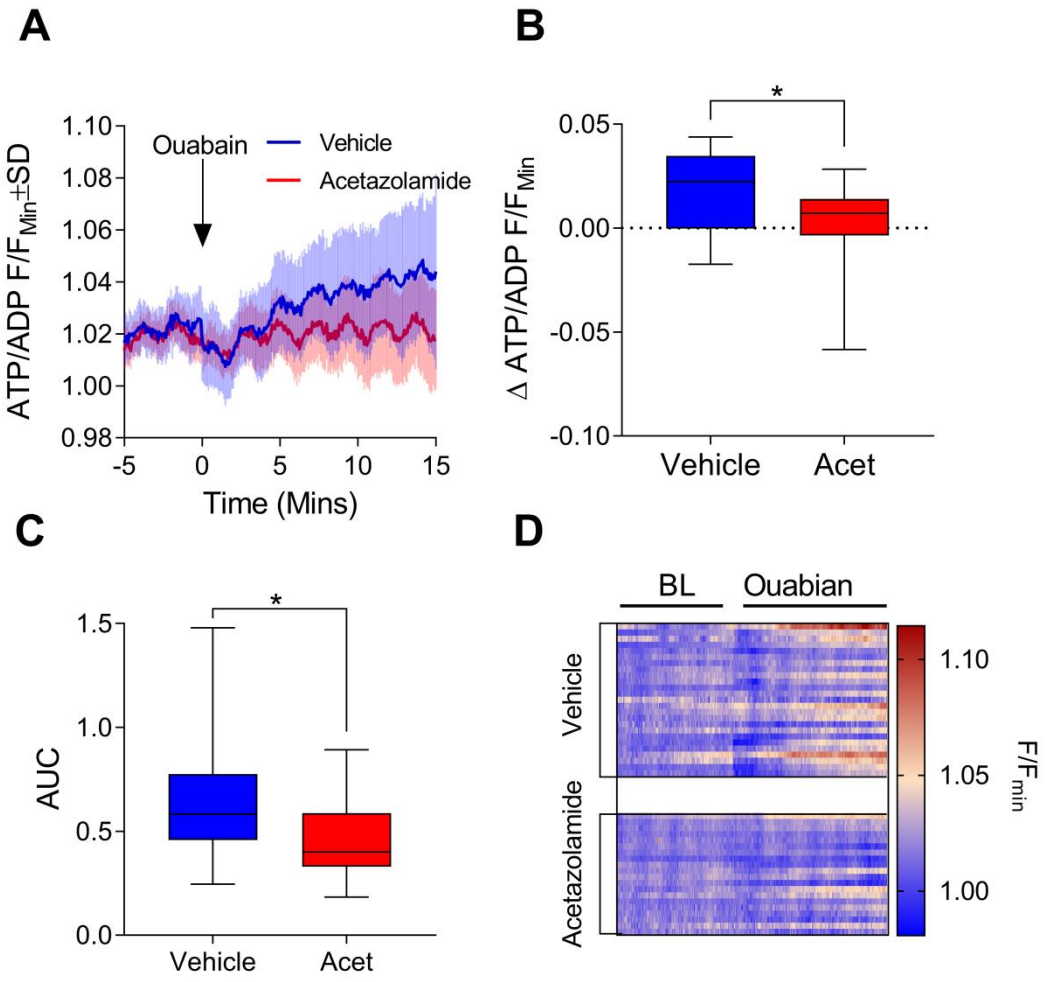

Figure 5.8 Acetazolamide decreases Na^+/K^+ ATPase activity in Z310 cells

Z310 cells infected with adenovirus harbouring adenovirus and were treated with acetazolamide (100μM) or vehicle for two days. (A) Perceval F/F_{min} trace of vehicle treated cells (blue) and acetazolamide treated cells (red). (B) The change in ATP/ADP maximum following ouabain. (C) The AUC of both treatments over the course of the recording. (D) Represents individual cell F/F_{min} over the course of the recording. Mann-Whitney U test. *=P<0.05. N=27 cells from 4 pooled coverslips. Data presented as median (IQR).

5.3.10 Furosemide

Furosemide, an inhibitor of the NKCC1 and KCC transporters, is utilised as a treatment to reduce ICP. However, it is not understood whether its activity is independent of the Na^+/K^+ ATPase, considering its outward facing nature in choroid plexus. Z310 cells were incubated with 100μM furosemide for two days prior to imaging. There is no difference between the change in F/F_{min} between vehicle and furosemide treated cells (0.014(0.017) Vs. 0.016(0.017), P=0.76) upon acute ouabain administration (Fig5.9b). AUC is indistinguishable between vehicle and furosemide treated groups (0.58(0.29) vs 0.54(0.24); P=0.46) (Fig5.9c). These data indicate that furosemide does not alter Na^+/K^+ ATPase activity in Z310 cells.

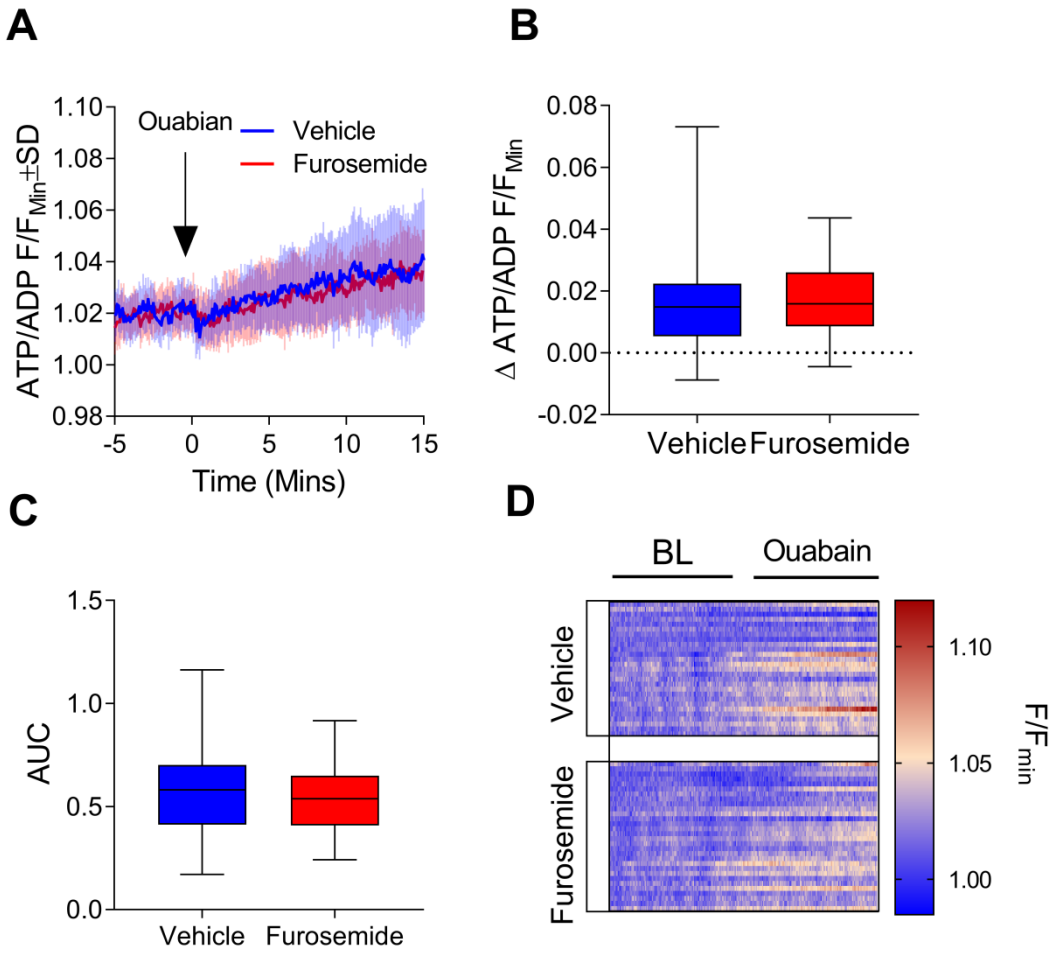

Figure 5.9 Furosemide does not alter Na^+/K^+ ATPase activity in Z310 cells

Z310 cells infected with adenovirus harbouring Perceval and were treated with Furosemide (100μM) or vehicle for two days. (A) Perceval F/F_{min} trace of vehicle treated cells (blue) or furosemide treated cells (red). (B) Represents change in ATP:ADP ratio following ouabain administration. (C) The AUC is indistinguishable between the treatment groups. (D) Represents individual cell F/F_{min} over the course of the recording. Mann-Whitney U test for B, students T-test for C. N=27 cells from 4 pooled coverslips. Data presented as median (IQR)

5.3.11 Perceval can distinguish between drugs

To assess whether this assay is suitable to compare between drugs the change in fluorescence was compared between acetazolamide and furosemide after the result was made relative to the appropriate control. We found that acetazolamide was more effective at reducing Na^+/K^+ ATPase activity compared to furosemide (41.1(122.6) Vs. 73.74(129.7)%; P=0.03) (Fig5.10). This highlights that Perceval in Z301 cells has the dynamic range to distinguish between the effectiveness of different drugs.

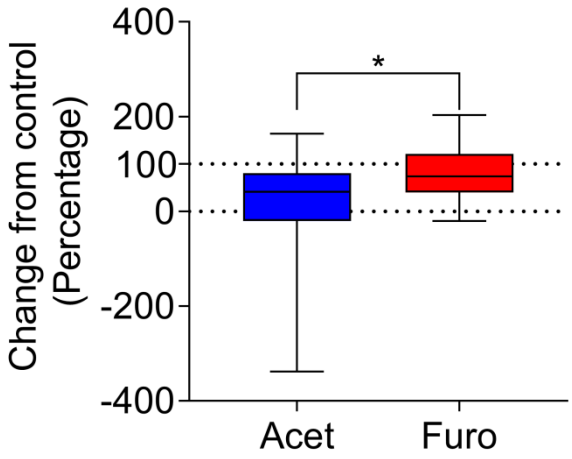

Figure 5.10 Acetazolamide is a more effective manipulator of Na^+/K^+ ATPase activity than Furosemide

Comparison of change in F/F_{min} between acetazolamide and furosemide treated Z310 cells relative to respective vehicle. Dotted line at 100% represents control. Mann-Whitney U test. N=27 cells from 4 pooled coverslips. *=P<0.05.

5.3.12 *In vivo* comparison

To determine whether the Na^+/K^+ ATPase inhibitor activity of the drugs assessed corresponds to an effect on ICP, and to assess their capability to modulate ICP at clinically relevant doses, acetazolamide and furosemide were evaluated in a validated *in vivo* ICP monitoring model.

5.3.13 Hypertonic Saline decreases ICP

Different salinities were required to dissolve the various quantities of acetazolamide, generating different vehicles. Consequently the 0.9% saline was compared to the 2% and 4% saline in the *in vivo* ICP monitoring model.

Compared to their respective baseline measurement, neither 0.9% or 2% saline reduced ICP. When comparing overall pressure change between all groups, 4% saline differs significantly ($P<0.0001$) compared to both 2% and 0.9% saline, whereas 0.9% and 2% saline have no difference in pressure ($P=0.28$) (Fig5.11a). AUC analysis highlights that 4% saline has a significantly smaller AUC (63.8±9.1) compared to 0.9% saline (100±2.4) ($P=0.007$) whereas 2% saline (92.2±8.9) is not different to 0.9% saline (Fig5.11b). However, 4% saline decreases ICP relative to baseline at 60 minutes, therefore ICP is significantly reduced (-1.1±0.3mmHg, $P=0.017$)(Fig5.11c). The pressure continues to decrease to the end of the recording at 120 minutes (-1.433±0.313mmHg, $P=0.0005$). These data highlight that 4% saline is effective at reducing ICP over the time period measured.

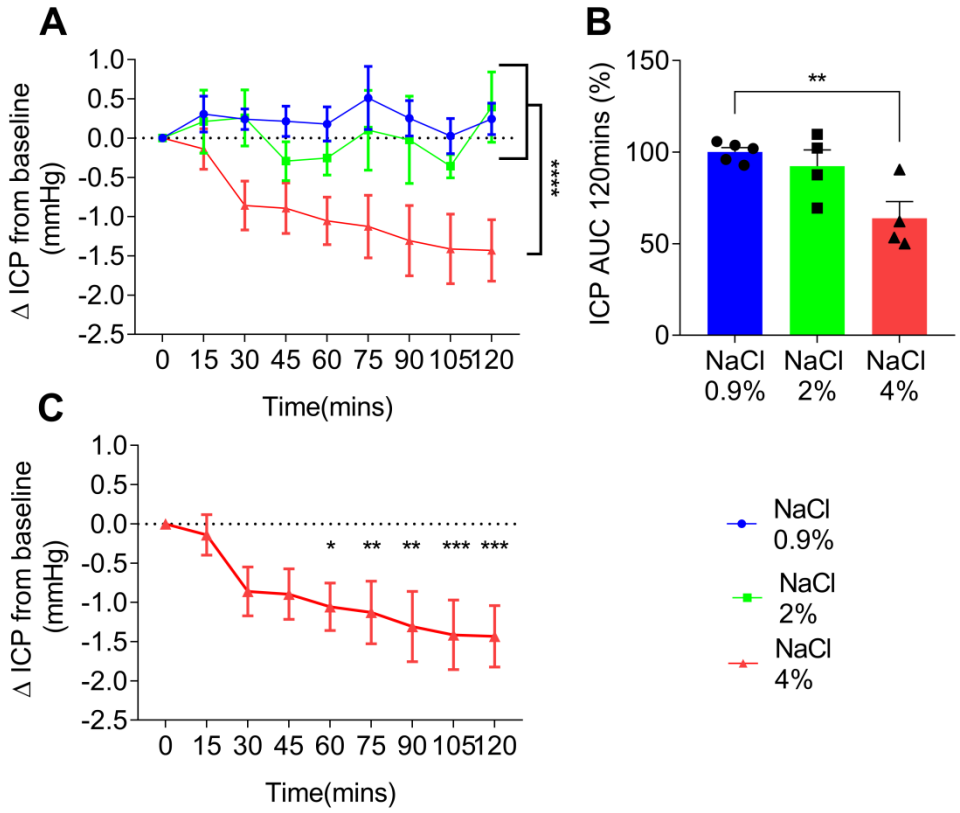

Figure 5.11 Hypertonic saline decreases ICP in normal pressure rats

Intracranial pressure measurements (ICP) in rats following subcutaneous (SC) injections of 0.9% (blue), 2% (green) and 4% (red) saline. (A) ICP traces over 120 minute recording, where 0 is time of injection. Dotted line represents no change in ICP. (B) AUC for the whole length of the recording in A. (C) graph detailing the pressure change in 4% saline relative to baseline. Two–way ANOVA with Tukey's post-hoc test comparing pressure in each group for A. One-way ANOVA with post-hoc Dunnett's test for B. Two-way repeated measures ANOVA with post-hoc Dunnett's test for C .N=5 for 0.9% saline, N=4 for 2% and 4% saline. *=P<0.05,**=P<0.01 and ***=P<0.001.

5.3.14 Acute acetazolamide administration does not alter ICP

Acetazolamide was tested at two doses, a clinically equivalent dose (103.3mg/kg) and a high (413.4mg/kg) dose, equivalent to a daily maximal dose in humans achieved in the IIH treatment trial (Wall et al, 2014). At the clinically equivalent dose, the acetazolamide trace does not alter ICP compared to 2% saline, where there is no difference in the AUC with low dose acetazolamide relative to 2 % saline (80.8±5.1 vs 100±9.7 %; P=0.1) (Fig5.12b).

However, high dose acetazolamide has a similar ability to reduce ICP compared to baseline as 4% saline, where a significant reduction on pressure is observed 45 minutes after injection (-0.895±0.322 mmHg; P<0.001) (Fig5.13c). The decrease in pressure is maintained for the remainder of the recording, where at 120 minutes pressure is reduced (-1.433±0.392 mmHg; P<0.0001) compared to baseline. This is probably a function of the vehicle due to no differences between vehicle and acetazolamide existing (see Fig5.11). At high dose, acetazolamide does not alter ICP compared to 4% saline, (Fig5.13b) where there is no difference in the AUC with high dose acetazolamide relative to 4 % saline (80.2±19.18 vs 100±10.03%; P=0.1). These data indicate that high dose acetazolamide does not have an acute pharmacological effect on ICP.

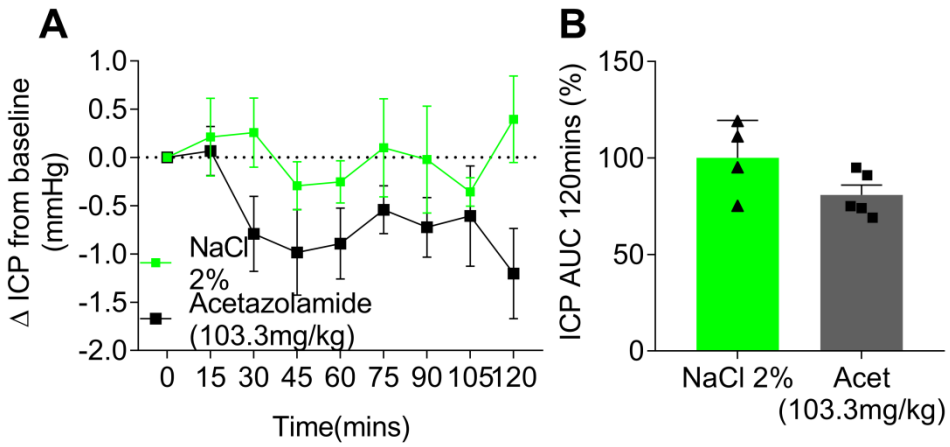

Figure 5.12 Clinically equivalent acetazolamide does not alter ICP in normal pressure rats

Intracranial pressure measurements in rats following subcutaneous (SC) injections of 2% saline (green) and acetazolamide (103.3 mg/kg) (grey). (A) ICP trace of both treatment over 120 minutes where 0 is time of injection. Dotted line represents no change in ICP. (B) AUC for the whole length of the recording in A. Two way repeated measures ANOVA for A, Students T-test for B. N=4 for saline, N=5 for acetazolamide.

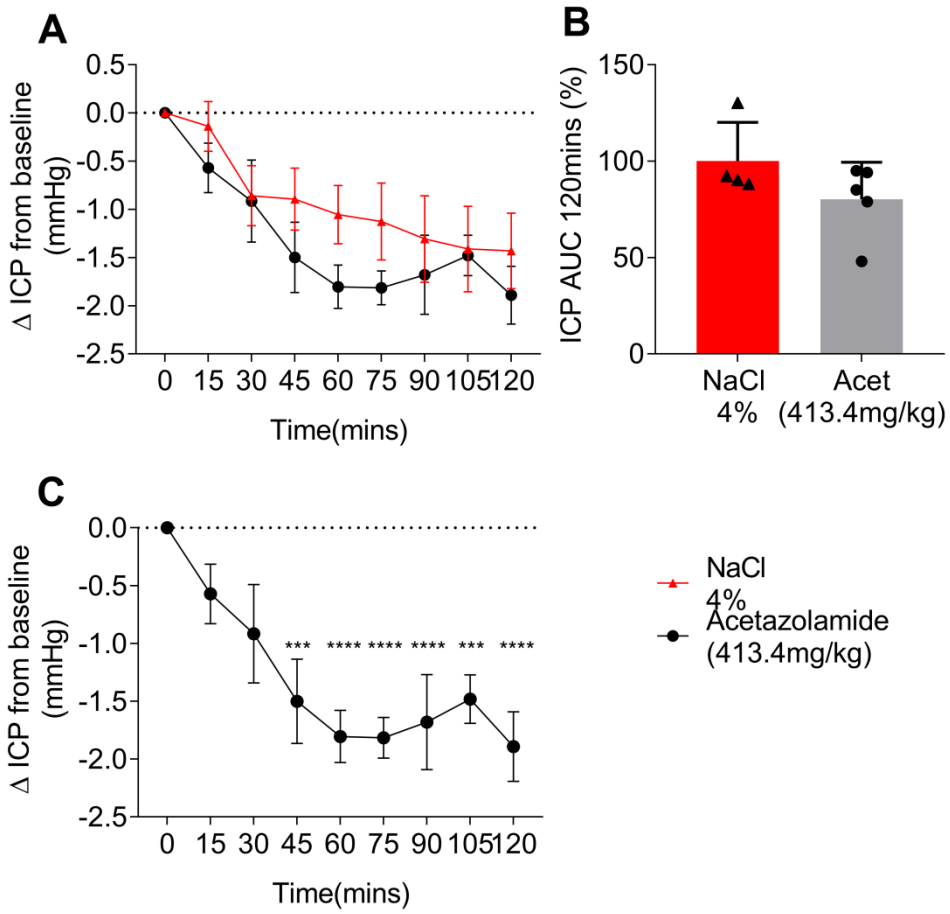

Figure 5.13 High dose acetazolamide has no pharmacological effect on ICP in normal pressure rats

Intracranial pressure measurements in rats following subcutaneous (SC) injections of 4% saline (red) and a high dose of acetazolamide (413.4 mg/kg) (grey). (A) ICP trace of both treatment over 120 minutes where 0 is time of injection. Dotted line represents no change in ICP. (B) AUC for the whole length of the recording in A. (C) Acetazolamide compared to baseline. Two-way repeated measures ANOVA with post-hoc Sidak's test for A. Students T-test for B. Two-way repeated measures ANOVA with post-hoc Dunnett's test for C. N=4 for saline, N=5 for high dose acetazolamide. ***=P<0.001, ****=P<0.0001.

5.3.15 Furosemide does not acutely alter ICP

The acute effects of the NKCC1 cotransporter inhibitor furosemide on ICP were assessed. The appropriate vehicle (0.9% saline) was compared to a clinically equivalent dose (4.1mg/kg) and high dose (24.8mg/kg) furosemide. ICP trace highlights that furosemide does not alter ICP when compared to the vehicle (Fig5.14a). AUC does not differ between saline (100±5.4) and high dose furosemide (86.8±17.6%; P=0.27) or clinically equivalent furosemide (101.2±16.68%; P=0.99) (Fig5.14b). Data highlights that furosemide does not alter ICP acutely in rats following a SC injection.

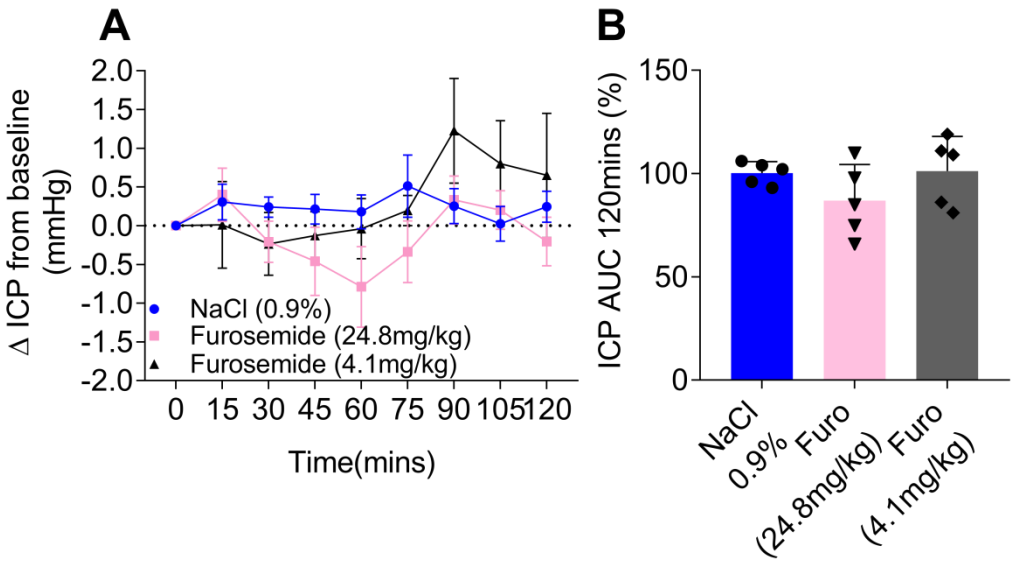

Figure 5.14 Furosemide does not alter ICP in normal pressure rats

Intracranial pressure measurements in rats following SC injections of vehicle (0.9% saline) (blue), high dose furosemide (24.8mg/kg) (pink) and low dose furosemide (4.1mg/kg) (grey). (A) ICP traces detailing no difference in pressure between saline and high dose furosemide and low dose furosemide. (B) AUC for the course of the recording in A. Two-way repeated measures ANOVA with post-hoc Dunnett's test for A. One-way ANOVA with post-hoc Dunnett's test for B. N=5 for all groups.

5.4 Discussion

5.4.1 Development of an in vitro Na^+/K^+ ATPase activity

In this work, a novel *in vitro* Na^+/K^+ ATPase activity was developed utilising the biosensor Perceval. It was successfully demonstrated that ouabain can elicit an increase in the ATP:ADP ratio, indicating that the ATP production relating to Na^+/K^+ ATPase ATP utilisation can be detected by the Perceval biosensor.

This novel assay has several advantages over previous assays. Primarily, the Perceval assay allows the underlying cellular biochemistry to be maintained with continuous recording, this facilitates temporal analysis pharmacological agents on Na^+/K^+ ATPase activity. Moreover, temporal analysis allows for an individual cell's baseline to be taken into account, removing cell-to-cell variability at baseline as a confounding factor in analysis.

The reversibility of ouabain mediated Na^+/K^+ ATPase inhibition demonstrates specific reversible inhibition that allows for complex experimental designs where multiple pharmacological agents could be assessed, including experiments assessing rapid changes in Na^+/K^+ ATPase activity. The fluorescent modality of the assay predisposes its use in high-throughput plate based assays, a potential route for future assay development.

There are however limitations with the current assay. Primarily, Perceval was introduced into Z310 cells via a functionally active adenovirus, consequently cellular metabolism is likely perturbed by intracellular virion assembly, meaning that the current results should be interpreted with caution. Furthermore the use

of the virus reduces the practicality of the assay due to the need to maintain viral stocks and infect cells for every assay. In the future, stable transfection of the Perceval biosensor into Z310 cells would allow for a more practical assay that enables Z310 cells to maintain a more physiological phenotype, in particular metabolism, unperturbed by viral load. Additionally, the current assay assumes that the Na^+/K^+ ATPase activity is the primary facilitator of CSF secretion at the choroid plexus, whereas other factors have been identified that contribute to CSF secretion. The present assay presents with a small change in fluorescence upon ouabain addition, roughly 4-5% in untreated conditions, this represents a small change relative to baseline. However the variant of Perceval utilised has a relatively small dynamic range and saturates at low ATP:ADP ratio, around 10, with low fluorescent resolution, whereas mammalian cells can have much larger ATP:ADP ratios, up to 100 (Berg et al., 2009; Tantama et al., 2013). Consequently the Perceval variant utilised is perhaps suboptimal for use in the present assay as the addition of ouabain is likely saturating the biosensor. Development of this assay with a higher range variant, PercevalHR, would facilitate experiments with better resolution and perhaps allow greater changes in the ATP:ADP ratio to be observed following ouabain administration (Tantama et al., 2013). Carrying out this assay in primary choroid plexus epithelial cells would facilitate further validation as other Na^+/K^+ ATPase activity assays could be utilised to confirm results (Botfield et al., 2017; Uldall et al., 2017). Assessment of the infection efficacy though assessing plaque forming units and Perceval expression via PCR would provide important information for experimental replication.

5.4.2 Pharmacological manipulation of *in vitro* Na^+/K^+ ATPase activity

Following establishment of the Na^+/K^+ ATPase activity assay, functional studies were carried out to validate the function of the assay. It was demonstrated that acetazolamide decreases Na^+/K^+ ATPase activity following a two day incubation, matching previous data using a different Na^+/K^+ ATPase activity assay in primary choroid plexus epithelial cells, thus validating the activity of the assay (Uldall et al., 2017). This highlights that carbonic anhydrase activity is fundamental in driving Na^+/K^+ ATPase activity and confirming the utility of the assay. However these data do not assess who acetazolamide elicits its action on the Na^+/K^+ ATPase, assessing bicarbonate transport and changes in intracellular pH will help elucidate this mechanism further (Sterling et al., 2001).

Conversely, it was demonstrated that furosemide does to supress Na^+/K^+ ATPase activity in Z310 cells, in contrast to the renal proximal tubule, where furosemide indirectly inhibits the Na^+/K^+ ATPase through a reduction in available sodium ions (Grossman and Hebert, 1988). This is perhaps unsurprising considering recent work has identified that the NKCC1 channel, the target for furosemide, functions as an efflux pump on the apical membrane of the choroid plexus. This functions to efflux sodium, potassium and chloride ions, rather than facilitating the influx the aforementioned ions as previously thought (Steffensen et al., 2018). In the context of Na^+/K^+ ATPase activity at the choroid plexus, this would suggest that the NKCC1 channel is not contributing to the ion gradient that the Na^+/K^+ ATPase requires for function. It has also been demonstrated that NKCC1 activity corresponds with CSF secretion *in vivo*: consequently experimental approaches combining both Na^+/K^+ ATPase activity

and NKCC1 activity assays would further elucidate the effect of drugs on CSF secretion (Steffensen et al., 2018). This highlights that the present assay can only assay drugs that either modulate the Na^+/K^+ ATPase or alter processes contributing to the ionic gradient facilitating Na^+/K^+ ATPase activity.

5.4.3 In vivo assessment of drugs on ICP

To determine the physiological relevance and validate the novel Na^+/K^+ ATPase activity assay, *in vitro* experiments were validated in a rodent ICP model. Prior to assessment of pharmacological agents, the vehicles were assessed due differing osmolalities. The current data highlights that hypertonic saline decreases ICP, which is in keeping with current clinical practice, most likely due to a reduced osmotic gradient in the CP blood vessels (Mortazavi et al., 2012).

The current data also demonstrates that at clinically relevant doses, acetazolamide has no pharmacological effect on ICP in rats: this is not congruent with previous data which suggests that acetazolamide reduces ICP in rats (Uldall et al., 2017). However, the previous study does not use a clinically relevant dose of acetazolamide, but instead uses a large dose of 769-869 mg/kg, double the current dose of this study. Furthermore, the previous study uses 0.9% saline as a control, which the current study identifies as an inappropriate vehicle for acetazolamide. Consequently, the current study provides physiologically relevant data on acetazolamide in rats, highlighting it has no pharmacological effect at the concentrations used.

The current study demonstrates that a subcutaneous dose of furosemide does not alter ICP. This could be due to the apical membrane position of the NKCC1

on choroid plexus epithelial cells (Steffensen et al., 2018). Previous studies indicate that furosemide and loop diuretics in its class only inhibit the NKCC1 channel when applied to the ventricular surface of the choroid plexus. This demonstrates that furosemide cannot penetrate the blood cerebrospinal fluid barrier at sufficient concentrations to elicit an acute response (Karimy et al., 2017; Vogh and Langham, 1981). Although furosemide can inhibit CSF secretion at supra-clinical doses (50mg/kg), this is most likely through weak carbonic anhydrase inhibition, rather than through directly inhibiting the NKCC1 channel (Vogh and Langham, 1981). These previous data and the current study highlight that acute furosemide administration does not reduce ICP through clinically relevant doses and delivery methods.

5.4.4 Disparity between Na^+/K^+ ATPase assay and *in vivo* ICP measurements

The *in vitro* acetazolamide data is not congruent with the *in vivo* data. It is possible that the acetazolamide concentration utilised in the *in vitro* assay exceeds the concentration that the clinically relevant dose of acetazolamide could achieve at the choroid plexus *in vivo*. Indeed, when administered intravenously, brain acetazolamide concentrations reach 30% of the plasma max, indicating relative lipophobicity (Ichikawa et al., 1998). Consequently, this indicates that acetazolamide may not exit the subcutaneous depot appropriately, suggesting that subcutaneous administration of acetazolamide is unsuitable for acetazolamide. However, when acetazolamide is administered orally, a clinically relevant route, it does not lower ICP when given at clinically relevant doses in rats (Scotton et al., 2018a). Together these suggest that

clinically relevant delivery routes are not suitable for acetazolamide at clinically relevant doses.

Furthermore, the effects of these drugs on other aspects of CSF dynamics are not fully understood; although drugs have the potential to reduce Na^+/K^+ ATPase activity in normal physiology, ICP is strongly regulated, through changes in cerebral blood flow or alterations in drainage. Furthermore, acetazolamide might not be effective at modulating ICP in healthy ranges. In a situation where ICP is pathologically raised, drugs observed to decrease Na^+/K^+ ATPase activity may decrease ICP. As such, further *in vivo* experimentation to investigate the role of drugs in a model of raised ICP, such as kaolin induced hydrocephalus, which has been used successfully to identify novel ICP reducing agents, could identify the role of acetazolamide and furosemide in modulating raised ICP (Botfield et al., 2017). Consequently, the current study is only applicable to normal pressure rats. Additionally, these studies are based on a single dose; future studies with chronic, multiple dosing of these drugs would be informative on their role in regulating ICP.

In summary, the Perceval assay is a novel *in vitro* assay that determines Na^+/K^+ ATPase activity in immortalised choroid plexus epithelial cells. However, this data cannot currently be generalised to ICP modulation because the drugs tested do not elicit an effect due to their pharmacological availability. This Perceval assay has the potential for drug screening studies to identify novel modulators of Na^+/K^+ ATPase activity.

Chapter 6 Evaluating the Role of Testosterone in CSF Secretion

6.1 Introduction

The pathogenesis of IIH remains unclear. The primary symptom of the pathogenesis is raised ICP which drives the common symptoms of IIH, headache and papilloedema. Consequently, studies investigating IIH attempt to understand the cause of the raised ICP. Several molecules have been hypothesised to be causative in the raised ICP in IIH, but there have been limited *in vitro* studies assessing these putative pathogenic molecules.

One putative pathogenic molecule in IIH is testosterone. Recent data highlights a distinct androgen profile in IIH patients, of reduced serum androstenedione, and raised serum testosterone, indicative of increased systemic 17β-hydroxysteroid dehydrogenase (17β-HSD) activity. Moreover, IIH patients have raised cerebrospinal fluid (CSF) testosterone and androstenedione (Appendix 1) (O'Reilly et al., 2019). Furthermore, several case reports highlight that female-to-male gender reassignment patients receiving therapeutic testosterone can develop IIH, where the IIH resolves temporally with testosterone withdrawal (Hornby et al., 2017). In line with this, androgen excess is associated with earlier onset of IIH (Klein et al., 2013). These data together highlight testosterone as a potential pathogenic molecule in IIH.

There is, however, no literature describing the effects of testosterone on CSF secretion or intracranial pressure. Interestingly, it has been demonstrated that testosterone increases intraocular pressure, whose fluid secretion system is analogous to secretion at choroid plexus epithelial cells (Kass and Sears, 1977; Toker et al., 2003). Similarly, oestrogen has been demonstrated to decrease intraocular pressure and Na^+/K^+ ATPase activity, a surrogate for CSF

secretion, suggesting that the effects of sex steroids on intraocular pressure is mirrored by proposed changes CSF secretion (Dewundara et al., 2016; Kass and Sears, 1977; Lindvall-Axelsson and Owman, 1989).

Furthermore, there is limited evidence describing the expression of the enzymes and receptors that metabolise and respond to sex hormones in the choroid plexus (CP). The presence of aromatase has been described in human CP but its activity has not been assessed (Ishunina et al., 2005). As such, the expression of sex steroid metabolising enzymes in CP needs to be evaluated prior to assessing whether testosterone could alter CSF secretion. This chapter details the characterisation of androgen metabolising enzymes in both human and rodent CP and an assessment of the effects of testosterone on Na^+/K^+ ATPase activity as a basis for future studies.

6.1.2 Hypothesis

Given that IIH patients have a unique androgen excess phenotype and that testosterone is potentially causative in intracranial hypertension in female-to-male gender reassignment patients, it is hypothesised that the choroid plexus expresses the enzymatic pathway capable of producing testosterone as a mechanism to modulate Na^+/K^+ ATPase activity.

6.1.3 Aims

1. Characterise the mRNA expression of sex steroid metabolising enzymes in the choroid plexus
2. Assess effects of testosterone on Na^+/K^+ ATPase activity

6.2 Methods

6.2.1 Z310 cell culture

Z310 cells (see section 2.1) were cultured in DMEM supplemented with 10% foetal calf serum, 1% Penicillin/streptomycin and 1ng/ml epidermal growth factor at 37ºC with 5% CO_2. For microscopy, Z310 cells were cultured to confluence on either 8-well culture slides or 25 mm diameter glass coverslips (VWR, Leighton Buzzard, UK) seeded with poly-D-lysine and incubated with laminin as described in section 2.8 and 2.19.

6.2.2 Human tissue and RNA

Human choroid plexus derived from the Parkinson's UK Brain Bank (Imperial Collage London) arrived in RNA later and stored immediately in -80ºC(section 2.6 for more detail). See table 6.1 for donor characteristics. Commercial human RNA, derived from non-diseased tissue were utilised as control tissue from both Agilent (Agilent biotechnologies, Craven Arms, UK) and AMS (AMS Biotechnology, Abingdon, UK), see table 6.2 for donor characteristics.

Patient ID	Disease	Sex	Age
CO87	No disease	F	84
CO88	No disease	M	94
MS620	Multiple sclerosis	F	88
PD847	Parkinson's disease	F	82
PD858	Parkinson's disease	M	90

Table 6.1 Characteristics of donor derived choroid plexus

Age in years, M=male, F=female.

Sample	Sex	Age
Liver 1	P	*43*
Liver 2	F	43
Liver 3	F	33
Adrenal 1	P	*25*
Adrenal 2	M	60
Adrenal 3	M	49
Ovary 1	F	47
Ovary 2	F	20
Ovary 3	F	37

Table 6.2 Characteristics of control tissue donors

Age in years, mix represents pooled donors, P=mixed pooled sample, M=male and F=female.

6.2.3 Rat tissue

Female Sprague-Dawley rats (Charles-river) weighing between 175g-200g were sacrificed via rising CO_2 concentration and the choroid plexus from the lateral and fourth ventricles as well as whole adrenal and ovary were dissected out. Tissue was snap frozen in liquid nitrogen and transferred to a -80ºC freezer prior to RNA extraction. Rats were housed in the Biomedical Service Unit (University of Birmingham) in accordance with the Animals and Scientific

Procedures Act 1986, licensed by the UK Home Office and approved by the University of Birmingham Ethics Committee in a 12 hour light/dark cycle with *ad libitum* access to food and water.

6.2.4 RNA extraction

RNA was extracted from human and rat choroid plexus using the Genelute total RNA kit, where tissue was mechanically homogenised prior to the column steps. Z310 cells had RNA extracted via five minute incubation in lysis buffer prior to column steps. RNA was then converted to cDNA using the high-capacity cDNA kit as described in section 2.7.5.

6.2.5 RT-qPCR

RT-qPCR was carried out as previously described in section 2.7.6 Details of primer/probe sets can be found in appendix 2.

6.2.6 Immunocytochemistry

Z310 cells were cultured and processed as described in section 2.8. In brief, Z310 cells were cultured on 8 well culture slides for two days. Z310 cells were sequentially fixed, permiabilised, blocked and incubated with primary and secondary antibody prior to mounting with media containing DAPI as a counterstain. Z310 cell images were taken on a Zeiss Axioplan 2 imaging epifluorescent microscope (Carl Zeiss) and a AxioCam Hrc (Carl Zeiss) was used to view and capture images. Antibody information including dilutions can be found in table 6.3.

Target	Reactivity	Working concentration	Species raised	Catalogue number
Androgen receptor	m,r,h	400 ng/ml	Mouse	Santa-Cruz biotechnology (sc-7305)
Anti-mouse Ig (Alexa 594)	m	2 µg/ml	Goat	Thermofisher (A11032)

Table 6.3 Antibody concentration table

Antibody reactivity, m=mouse, r=rat and h =human.

6.2.7 Live cell microscopy

Live cell microscopy was carried out according to the method in section 2.19. In brief Z310 cells infected with an adenovirus containing the biosensor Perceval were grown to confluence prior to imaging on a confocal microscope. Z310 cells were incubated with testosterone (100 nM) or vehicle for 48 hours prior to treatment with ouabain (1 mM) to resolve Na^+/K^+ ATPase activity. Assessor was blinded to the treatment of the cells during evaluation of cell fluorescence intensity.

6.2.8 ATP production rate

To determine the arbitrary cellular ATP production rate in Z310 cells, the slope on the trace was measured as the following for each cell ((F/F_{min} value at end of recording – F/F_{min} value at addition of ouabain) / length of time ouabain present), where F= fluorescence at a specific time point and F_{min}= minimal fluorescence in the trace.

6.2.9 Statistics

GraphPad prism (V7.1) was utilised for statistical analysis where $P<0.05$ was considered significant. Students T-test or Mann-Whitney U-Test subject so Shapiro-Wilk normality test. Data presented as mean±SEM unless otherwise stated.

6.3 Results

6.3.1 Human choroid plexus expresses steroidogenic enzymes

To determine whether human CP has the capacity metabolise androgens, CP from aged, mixed sex and diseased post-mortem donors were probed via RT-qPCR to determine the presence of sex steroidogenic enzymes (Fig6.1). Human CP expresses *3BHSD2* (Fig6.1a) at low levels compared to the other tissues assessed. Human CP expresses the 17βHSD enzymes 17β-HSD5 (*AKR1C3)* and *17BHSD3* (Fig6.1b and c) at levels comparable to the liver, suggesting the CP is an androgen activating tissue. Furthermore human CP expresses 5α-reductase (*SRD5A1, SRD5A2*) (Fig6.1d and e), suggesting the ability to generate the more potent androgen dihydrotestosterone. Aromatase (*CYP19A1*) (Fig6.1f) expression is negligible in human CP. The CP does not express *CYP11B1* (Fig6.1g) or *AKR1D1* (Fig6.1h) suggesting an inability to generate 11-oxygenated androgens or 5-β reduced steroid metabolites.

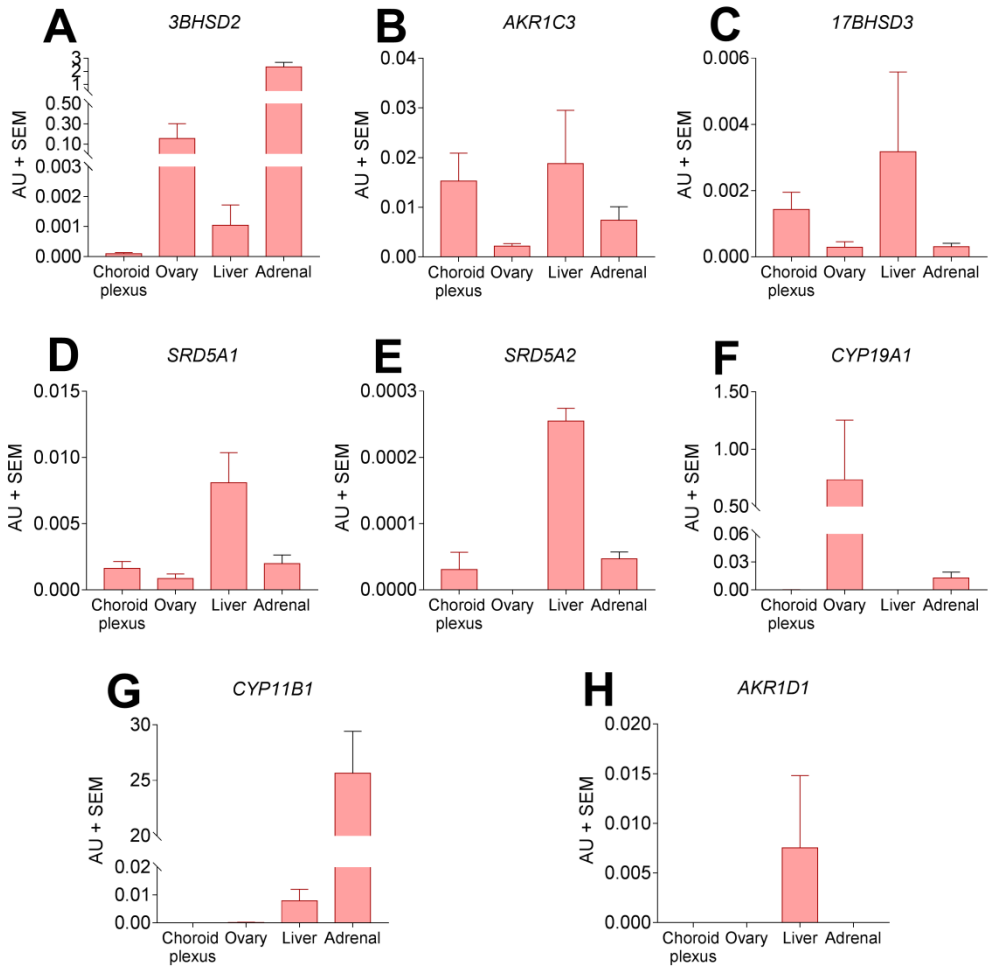

Figure 6.1 Human choroid plexus expresses androgen metabolising enzymes

RT-qPCR on human tissue to determine the expression of sex steroid metabolising enzymes in the choroid plexus (CP), (A) *3BHSD2*, (B) *AKR1C3*, (C) *17BHSD3*, (D) *SRD5A1*, (E) *SRD5A2*, (F) *CYP19A1*, (G) *CYP11B1* and (H) *AKR1D1*. Data presented as arbitrary units (AU) Mean+SEM N=5 for human CP, N=3 for other tissues.

6.3.2 Human choroid plexus expresses androgen receptor

To determine whether human CP has the potential to respond to sex steroids, the mRNA expression of cognate receptors for sex steroids was assessed. Human CP expresses androgen receptor (*AR*) (Fig6.2a) and oestrogen receptors *ESR1* and *ESR2* (Fig6.2b and c).

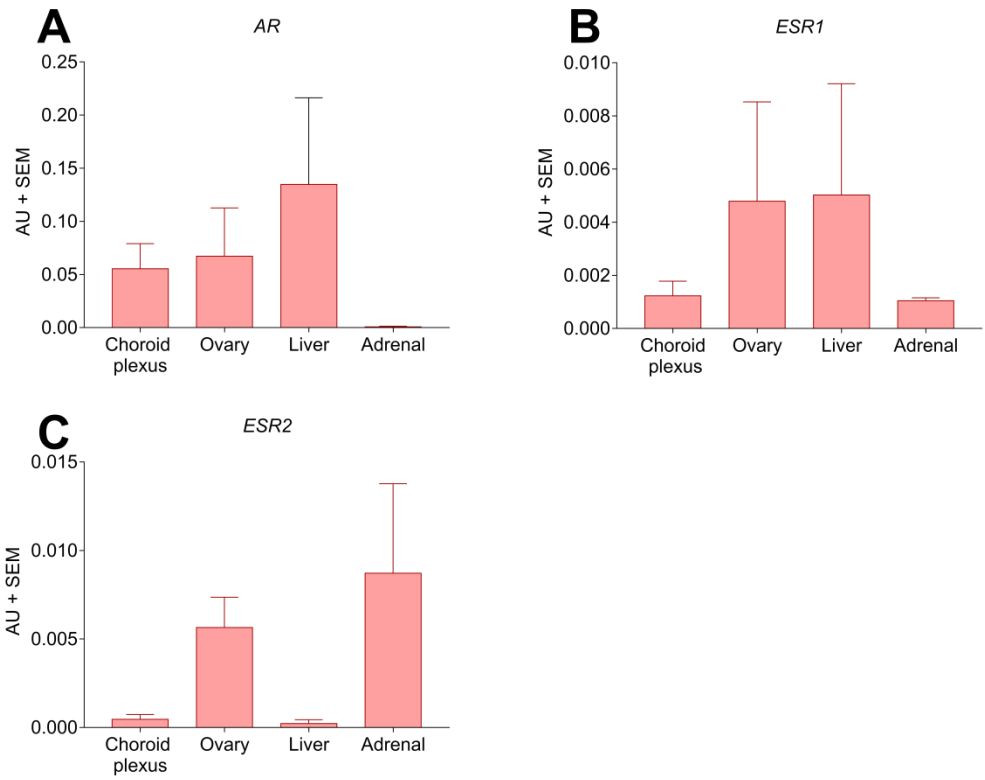

Figure 6.2 Human choroid plexus expresses cognate sex steroid receptors

RT-qPCR on human tissues to determine the expression of (A) *AR*, (B) *ESR1* and (C) *ESR2* in human CP**.** Data presented as arbitrary units (AU) Mean+SEM, N=5 for human CP, N=3 for other tissues.

6.3.3 Rat choroid plexus expresses steroidogenic enzymes

For comparative purposes, CP from female rats were probed via RT-qPCR for the expression of sex steroidogenic enzymes. Rat CP expresses 17βHSD enzymes *Akr1c3* and *17bhsd3,* Z310 cells also demonstrate amplification of the 17β-HSD genes (Fig6.3a and c). Rat CP and Z310 cells expresses both 5α-reductase (*Srd5a1*) and aromatase (*Cyp19a1*) (Fig6.3 b and c).

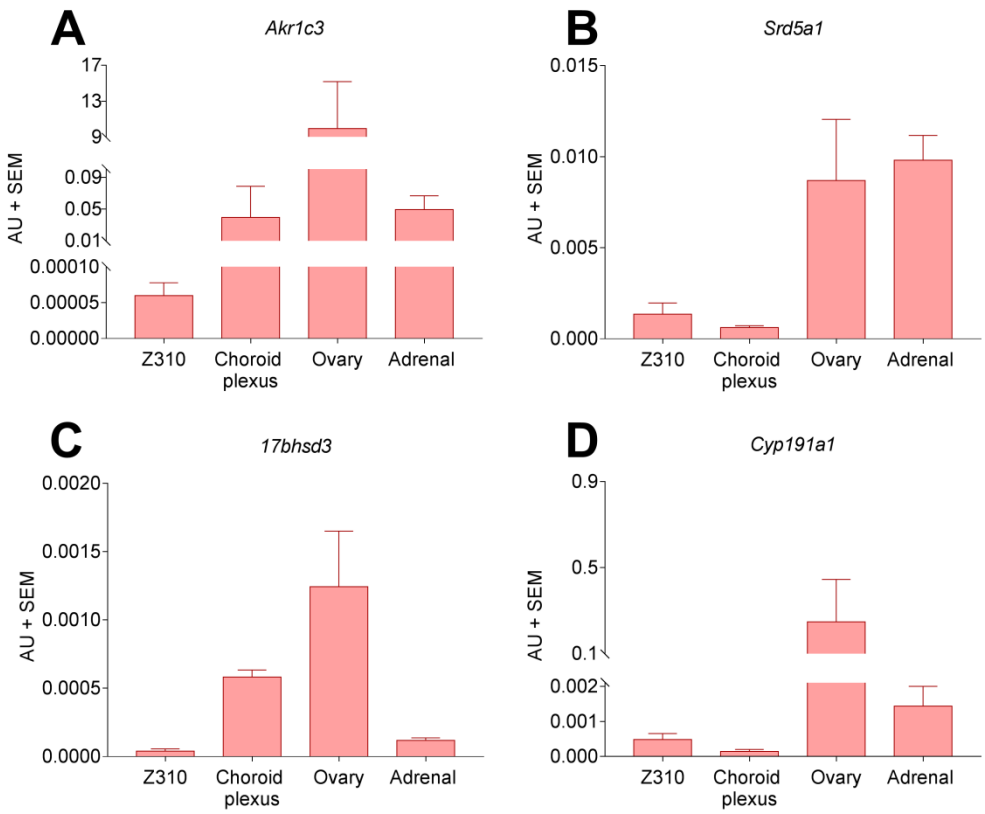

Figure 6.3 Rat choroid plexus expresses androgen metabolising enzymes

RT-qPCR on whole female rat tissues and Z310 cells to determine the expression of (A) Akr1c3, (B) Srd5a1, (C) *17bhsd3* and (D) *Cyp19a1* in CP and Z310 cells. Data presented as arbitrary units (AU) mean+SEM N=3 animals or 3 independent passages.

6.3.4 Rat choroid plexus expresses cognate sex steroid receptors

The expression of cognate sex steroid receptors was assessed in rat CP. Female rat CP expresses *Ar* and *Esr1* at comparable levels, with *Esr2* being the lowest expressed (Fig6.4 a-c). Z310 cells display minimal expression of sex steroid receptors, however, immunofluorescence highlights immune reactive androgen receptor present in discrete cytoplasmic loci (Fig6.4d). No IgG control can be found in appendix 7.

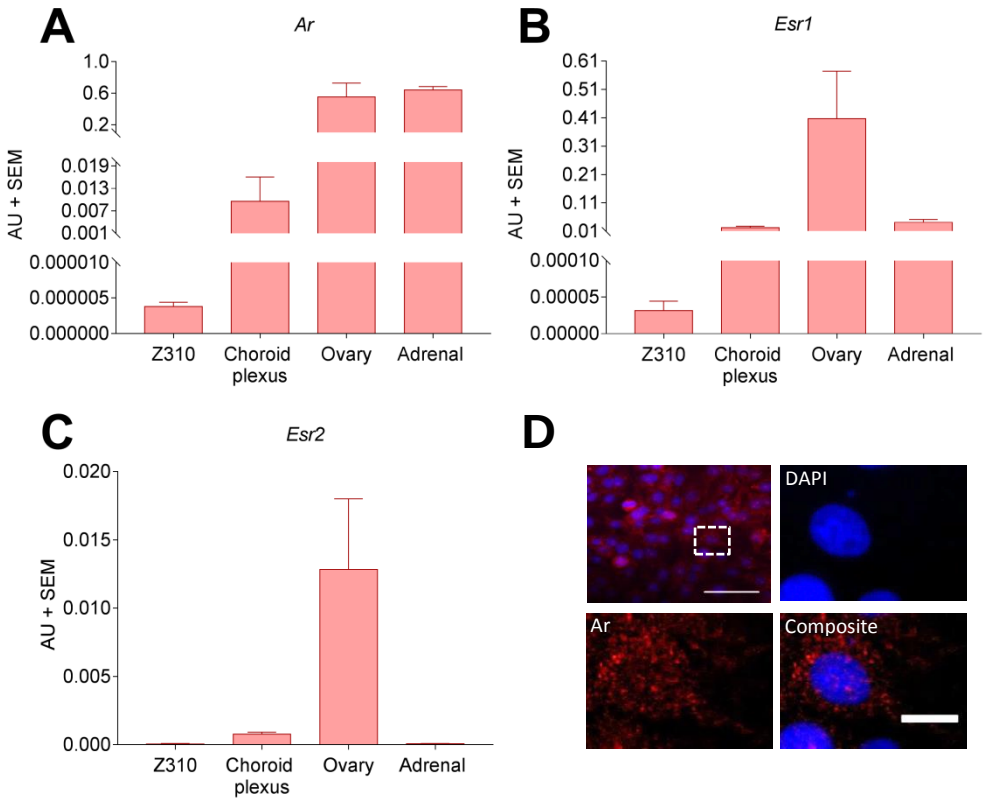

Figure 6.4 Rat choroid plexus expresses cognate sex steroid receptors

RT-qPCR on whole female rat tissues and Z310 cells to determine the expression of (A) Ar, (B) *Esr1* and (C) *Esr2* in CP and Z310 cells. (D) Immunofluorescence staining for androgen receptor (AR) where DAPI represents nuclei. Insert represents a single cell. Scale bars represent 50 µm and 10 µm in insert images. Data presented as arbitrary units (AU) Mean+SEM N=3 animals or 3 independent passages.

6.3.5 Testosterone increases Na/K ATPase activity

The effect of testosterone on Na^+/K^+ ATPase activity was assessed in Z310 cells (Fig6.5a). Following two days of testosterone (100 nM) incubation, there was an increase in the ATP/ADP ratio change compared to control (Δ0.042(0.07) Vs. Δ0.01(0.022); P<0.0001), following acute ouabain administration (Fig6.5b). Furthermore, area under the curve (AUC) analysis highlights that testosterone treated Z310 cells have a higher AUC compared to controls (0.81(0.53) Vs 0.58(0.27); P<0.01) (Fig6.5c). These data indicate that testosterone increases Na^+/K^+ ATPase activity in Z310 cells.

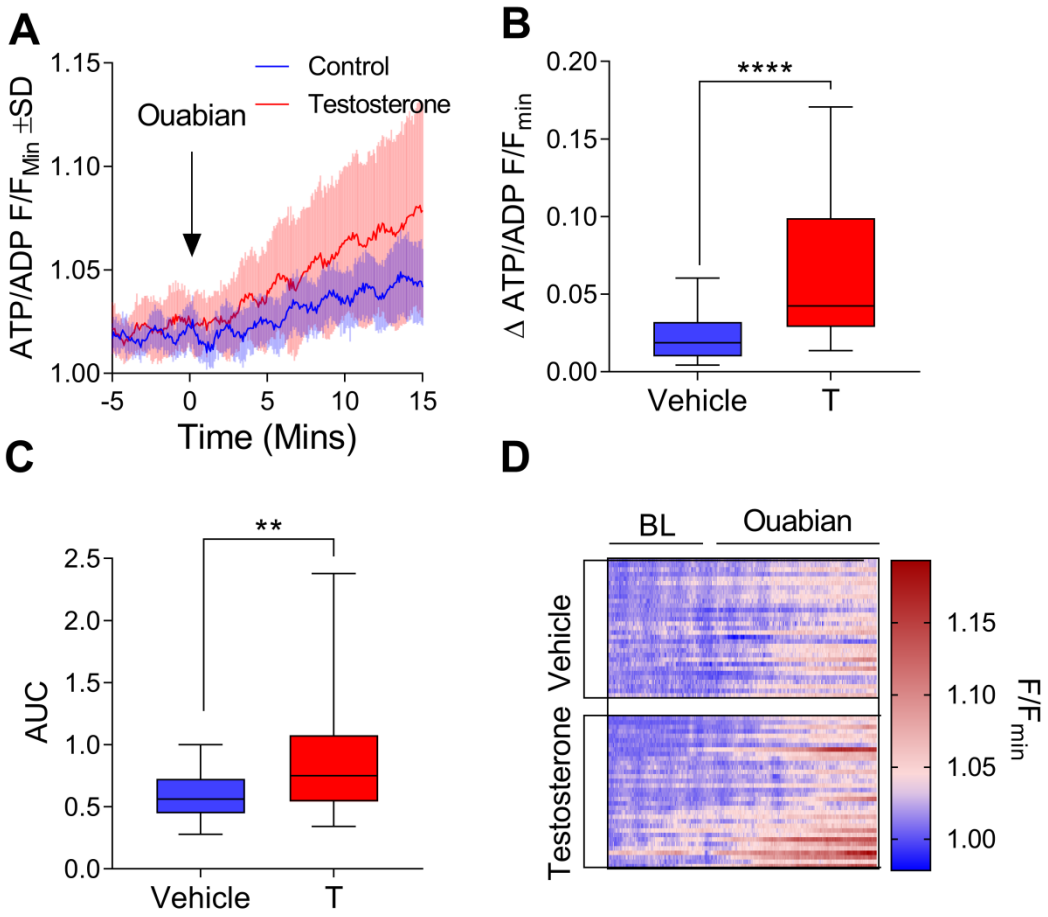

Figure 6.5 Testosterone increases Na^+/K^+ ATPase activity

Z310 cells infected with adenovirus harbouring adenovirus and were treated with testosterone (100 nM) or vehicle for two days. (A) Perceval F/F_{min} trace of vehicle treated cells (blue) or testosterone treated cells (red). (B) The change in ATP/ADP maximum following ouabain. (C) The area under the curve of both treatments over the course of the recording (20 minutes). (D) Individual cell F/F_{min} over the course of the recording. Mann-Whitney U-test for B and C. **=P<0.01, ****=P<0.0001. N=30-39 cells from 4 pooled independent coverslips. Data presented as median (IQR). T=testosterone.

6.3.6 Testosterone increases ATP production in Z310 cells

The ATP production rate was assessed in Z310 cells with and without testosterone treatment. Testosterone treated Z310 cells had a greater slope gradient compared to vehicle treated cells (0.24(0.41) vs. 0.12(0.19); P<0.001), indicating an increased rate of ATP production (Fig6.6).

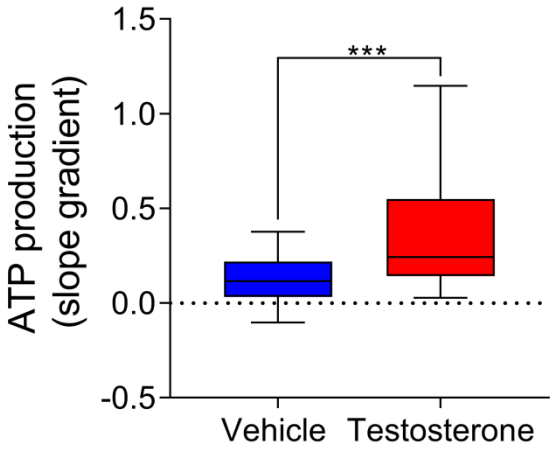

Figure 6.6 Testosterone increases ATP production in Z310 cells

Slope gradient of the ouabain incubation period on live cell trace. Mann-Whitney U-test. Data presented as median(IQR) N=30-39 cells from 4 pooled independent coverslips. ***=P<0.001.

6.3.7 Testosterone increases carbonic anhydrase expression

Proteins known to modulate Na^+/K^+ ATPase activity, *Atp1a1*, *Car2* and *Car3*, had gene expression assessed after a 48 hour incubation with testosterone, the time point that Na^+/K^+ ATPase activity was assessed. Expressed as fold change, no change in expression was observed for *Atp1a1* (1.6±0.2; P=0.06), whereas both *Car2* (2.36±0.32; P<0.025) and *Car3* (2.8±0.39; P<0.015) displayed increased expression (Fig6.7).

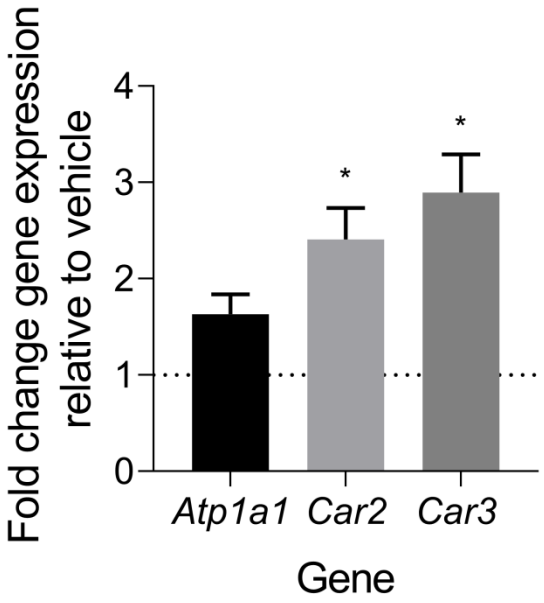

ΔCt	Control	Testosterone
Atp1a1	12.7	12.1
S.E.M	1.82	1.82
Car2	19.23	17.99
S.E.M	1.39	1.47
Car3	18.79	17.28
S.E.M	1.64	1.55

Figure 6.7 Testosterone increases carbonic anhydrase expression

RT-qPCR on Z310 cell treated with 100nM testosterone for 48 hours, where *Atp1a1*, *Car2* and *Car3* expression was interrogated. Dotted line represents vehicle. Data expressed as fold change±S.E.M, T-tests ran on ΔCt values. Table details ΔCt values. .N=3 biological replicates. *=P<0.05.

6.4 Discussion

6.4.1 The choroid plexus as peripheral organ of steroid activation

An aim of the present study was to characterise the expression of steroid metabolising enzymes within the CP. This work demonstrates both rodent and human CP expresses, at the mRNA level, the genes responsible for the peripheral activation of classical androgens. However, the lack of expression of CYP11B1 and 11β-HSD2 suggests the inability to generate and activate 11-oxygenated androgens (Sinclair et al., 2010b). Although the present data demonstrates negligible expression of aromatase in human CP, a previous study identified protein expression (Ishunina et al., 2005). Furthermore the presence of cognate sex steroid receptors suggests that the choroid plexus has the capacity to respond to androgens and oestrogens. However, this work fails to confirm the expression of the steroidogenic genes at both the protein level and at the enzyme activity level, as such these experiments need to be carried out. The exception is with androgen receptor in Z310 cells, where the demonstration of androgen receptor corroborates previous work (Costa et al., 2016). These data together, with the previous demonstration of active 11β-HSD1 in both human and rabbit choroid plexus, suggests that the choroid plexus is a peripheral organ of steroid hormone metabolism (Sinclair et al., 2010b, 2007).

The expression of 5α-reductase enzymes has further implications for the steroid environment of the central nervous system. 5α-reductase enzymes are able to metabolise not only testosterone to the more potent androgen dihydrotestosterone but also modify other steroid classes to their 5α-metabolites

(Reddy, 2010). It has been demonstrated that within the brain, 5α-reduced cortisone and progesterone undergo a subsequent 3α-reduction, generating potent modulators of GABAergic and glutamatergic receptors, which potentiate and inhibit receptors depending on the steroid species (Reddy, 2010). As such, it could be suggested that the choroid plexus has a role in modulating the excitability of neurons through supplying precursor 5α-reduced steroids, through the CSF to neocortical and circumventricular regions, where 3α-reductase expression has been demonstrated (Stoffel-Wagner et al., 2003). Further work to identify whether the choroid plexus generates 5α-reduced steroids and assess the choroid plexus' contribution to steroid mediated neuro-modulation would be worthwhile.

The human CP RT-qPCR data should be interpreted with caution, due to the tissue originating from post-mortem samples from elderly donors with a mixture of disease states and mixed sex. Obtaining fresh tissue from younger and healthier individuals would provide a more comprehensive understanding of the expression of these genes in normal physiology. Furthermore, expression of steroidogenic enzymes was not directly assessed in choroid plexus epithelial cells, highlighting a requirement to assess this in future experimentation, particularly because of the differences seen in gene expression between Z310 cells and whole choroid plexus.

6.4.2 Androgens and Na^+/K^+ ATPase activity

A further objective of the present study was to assess the effects of testosterone on Na^+/K^+ ATPase activity in Z310 cells. The novel Na^+/K^+ ATPase activity assay determined that testosterone increases Na^+/K^+ ATPase activity in

Z310 cells, suggesting that testosterone could increase CSF secretion and ICP, thus be pathogenic in IIH as previously proposed (Hornby et al., 2017). Gene expression analysis suggests that testosterone treatment increases carbonic anhydrase expression, providing a potential mechanism for a testosterone mediated increase in Na^+/K^+ ATPase activity: increased carbonic anhydrase expression generates a higher proton gradient, allowing for greater movement of sodium across the CP epithelial cell driving osmosis and CSF secretion. This corroborates previous work suggesting expression of carbonic anhydrases is under control of androgens (Jeffery et al., 1984). Assessing carbonic anhydrase activity in Z310 cells following testosterone incubation utilising an oxeograph to measure extracellular acidification rate would confirm this mechanism, through indirectly assessing extracellular carbonic acid accumulation and confirm the ATP production rate through assessing oxygen consumption.

Increased ATP production, facilitated by the anabolic action of testosterone, could also be potentiating the increased Na^+/K^+ ATPase activity independently of gene expression changes, through providing more substrate for the Na^+/K^+ ATPase. The current data does not assess the ability of testosterone to modulate ICP in rodents or the effects of testosterone on Na^+/K^+ ATPase activity in both human or in the more physiologically relevant primary rodent choroid plexus epithelial cells, highlighting avenues for future study.

6.4.3 Testosterone and ICP in IIH patients

The choroid plexus lies at the interface of both the blood and the CSF compartments. In IIH where there is raised serum and CSF testosterone, it is plausible that testosterone is acting to increase CSF secretion. Furthermore, the

increased CSF androstenedione (Appendix 1) in IIH patients and the presence of AKR1C3 in human choroid plexus suggests that androstenedione could be activated in to testosterone, further increasing CSF secretion (Fig6.8). This data, however, presents a paradox: if high levels of testosterone increase ICP, males should have pathologically raised ICP. However, studies suggest males that develop IIH have hypoandrogenism rather than hyperandrogenism (Fraser et al., 2010). Indeed, it has been hypothesised that androgen concentrations that constitute male hypoandrogenism and female hyperandrogenism pose heightened metabolic risk, where IIH and raised ICP could fall within this bracket of raised metabolic risk (Schiffer et al., 2017).

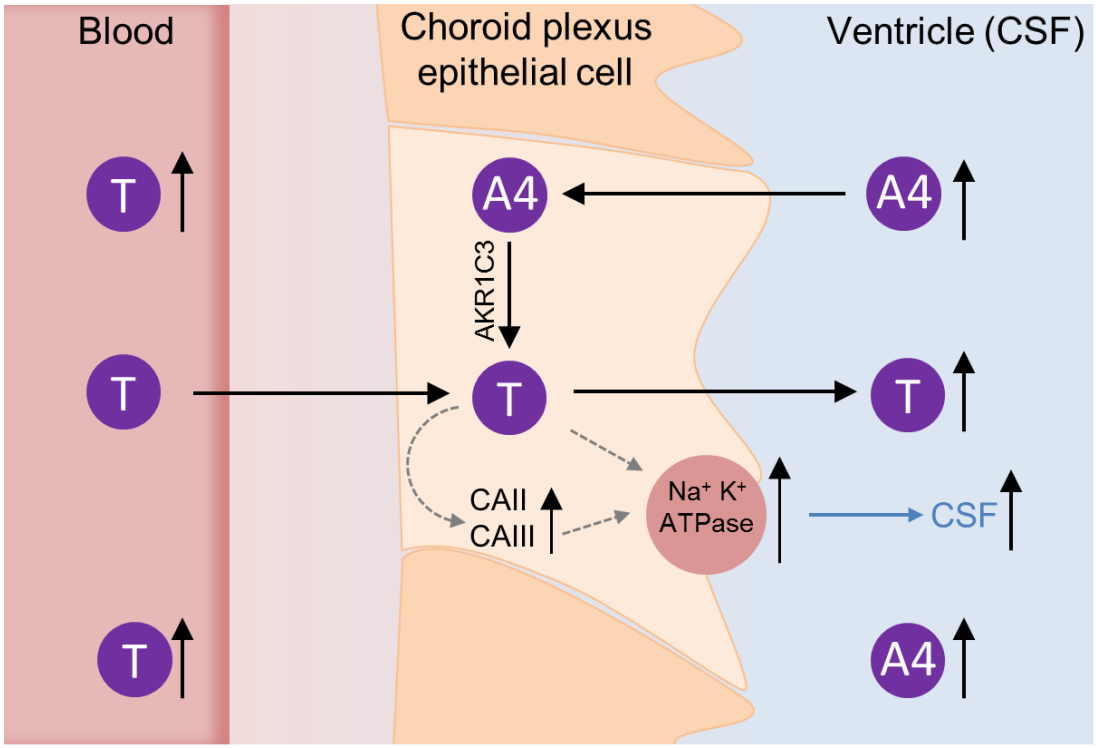

Figure 6.8 Suggested action of testosterone at the choroid plexus in IIH
In IIH patients, where there is raised serum testosterone, it is hypothesised that the testosterone (T) diffuses into the CP, acting to increase the expression of carbonic anhydrases 2 and 3 (CAII and CAIII) where the increase in ionic gradients drives the activity of the Na^+/K^+ ATPase, increasing CSF secretion. Furthermore, it is hypothesised that the raised CSF androstenedione (A4) in converted to T in CP epithelial cells, increasing T exposure, further increasing CSF secretion.

This data does not exclude other effects of testosterone on ICP dynamics or claim that testosterone is the only pathogenic molecule in IIH. It was recently demonstrated that IIH patients have astrogliosis, suggesting a reactive inflammatory state within their cerebral parenchyma (Eide et al., 2016). Interestingly, increased astrogliosis was negatively correlated with aquaporin 4 expression at astrocyte end feet, suggesting that glymphatic drainage could be impaired in IIH patients. Furthermore, it was demonstrated in female rats that

testosterone excess can induce astrocyte expansion (Chowen et al., 1995). This data suggests that raised testosterone could play a role in the astrogliosis in IIH patients. This has the potential to alter CSF dynamics due to astrocytes being a principle component in forming perivascular spaces (Iliff et al., 2013). This highlights the need to research the effects of testosterone on glymphatic drainage of CSF and the modulation of cerebral compliance.

These data highlight that the CP expresses, at mRNA level, genes that can metabolise and activate androgens. Furthermore, these data indicate that testosterone can increase Na^+/K^+ ATPase activity in Z310 cells. Consequently, these data are the first *in vitro* demonstration that a putative pathogenic biomarker in IIH, testosterone, has the potential to raise ICP. This highlights the need for further *in vivo* research to ascertain the role of testosterone in ICP regulation.

Chapter 7 General Discussion

7.1 General conclusions

IIH is a rare disease primarily affecting obese women of reproductive age, where patients present with debilitating headache and papilloedema causing significant morbidity. However, the pathogenic mechanism underlying IIH is poorly understood. Reducing abdominal obesity confers improvements in disease morbidity in IIH, allowing the formation of the hypothesis that adipose tissue in IIH is pathogenic (Hornby et al., 2018b; Sinclair et al., 2010a). Consequently, this thesis explored the adipose phenotype of IIH patients and evaluated putative pathogenic mechanisms hypothesised to be derived from the adipose tissue.

The adipose phenotype in IIH was assessed utilising targeted and non-targeted approaches which demonstrate that IIH adipose tissue presents with a distinctive phenotype. This IIH SC adipose phenotype presents with features of glucocorticoid excess which appear to be driven by reduced intra-adipose glucocorticoid (GC) clearance, potentially mediated by reduced *SRD5A1* expression. This phenotype of adipose glucocorticoid excess appears to be driving the raised serum leptin. Reduced *SRD5A1* expression could also be driving the increased serum testosterone through reducing the generation of dihydrotestosterone, this would highlight that *AKR1C3* inhibitors could be a potential therapeutic intervention in IIH to reduce circulating testosterone levels. These data highlight that IIH adipose tissue is metabolically deranged.

Furthermore, it was demonstrated that although IIH patients have raised fasting and post-prandial leptin, it is likely that this raised leptin is not pathogenic in IIH

and is merely a bystander of the metabolic consequences of SC adipose glucocorticoid excess, causing hypersecretion of leptin from adipocytes.

It was also aimed to develop and evaluate a novel *in vitro* Na^+/K^+ ATPase activity assay to assess a CSF secretion surrogate in a more physiological setting for high-throughput assessment. Here it is demonstrated that the Perceval biosensor can detect specific reversible inhibition of the Na^+/K^+ ATPase by ouabain. Furthermore pharmacological manipulation of Na^+/K^+ ATPase activity can be assessed, where the reduction in Na^+/K^+ ATPase activity observed with acetazolamide is congruent with previous data (Uldall et al., 2017). This assay was utilised to demonstrate that testosterone can modulate Na^+/K^+ ATPase activity in Z310 cells. Given this modulation, it is possible that the raised serum and CSF testosterone in IIH could drive the raised ICP in IIH. This demonstrates the need to assess androgen receptor modulation therapy as potential treatment for IIH in the future, as this could target both the ICP and the generic androgen excess phenotype. The novel demonstration that the choroid plexus has the potential to be a peripheral organ of androgen activation is of interest due to its implications on cerebral homeostasis, highlighting the need for this property to be further explored in the future.

The data in this thesis allows the formation of the following testable hypothesis: reduced SC adipose *SRD5A1* expression is, in part, driving the pathogenic phenotype of IIH (Figure 7.1). It can be hypothesised that this is driving the increased serum testosterone though reducing intra-adipose androgen clearance, where this raised serum testosterone is increasing ICP (chapter 6).

Similarly the reduced *SRD5A1* expression is hypothesised to cause glucocorticoid accumulation in SC adipose, through reducing GC clearance, (chapter 3). This adipose dysfunction is hypothesised to be driving the phenotype of raised serum leptin (chapter 4), suggesting that raised serum leptin is a biomarker adipose dysfunction in IIH. This hypothesis is however not fully encompassing as it does not address the cause of the reduced SC *SRD5A1* expression, and neither does it address other organ systems that could be contributing to the disease state such as the adrenal glands and the liver.

Of note, IIH patients within this thesis display high levels of variance while following a Gaussian distribution, compared to control groups, despite the tight inclusion criteria intended to make the IIH patients as homogenous as possible. This is indicative that the IIH syndrome associated with obese women of reproductive age could be a disease of several biochemical phenotypes presenting with a similar clinical phenotype. This heterogeneity in IIH patients should be subject to further investigation.

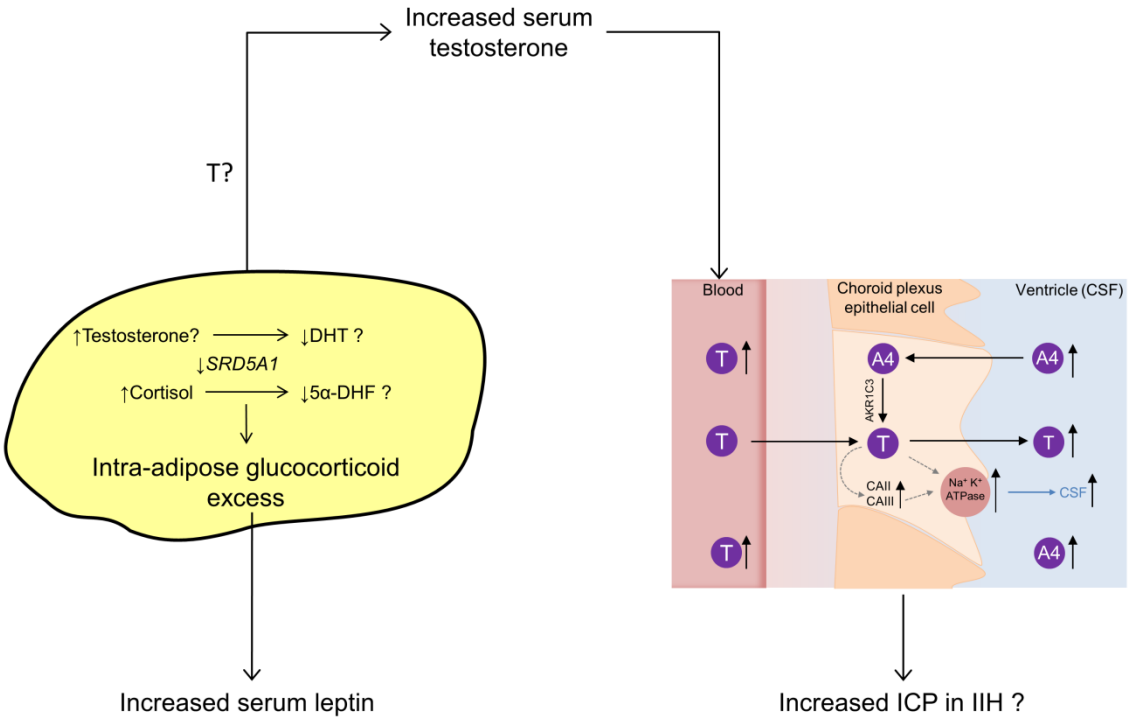

Figure 7.1 IIH pathogenesis model diagram

A schematic model for proposed pathogenesis in IIH. Reduced *SRD5A1* expression in IIH SC adipose serves as a molecular road block, reducing the deactivation of both testosterone (T) and cortisol. The increased intra-adipose F facilitates the generation of a glucocorticoid excess phenotype that is contributing to increased serum leptin. Reduced T deactivation promotes increased serum testosterone in IIH, driving the increased ICP in IIH. CAII= carbonic anhydrase 2, CAIII= carbonic anhydrase3, A4= androstenedione, DHT= dihydrotestosterone, 5α-DHF= 5α-dihydrocortisol.

7.2 Future experimentation

Future experimentation is required to further elucidate the phenotype and pathogenesis of IIH. On the basis of the work presented in this thesis, future work should be focused on the following areas.

7.2.1 *In vivo* assessment of the IIH adipose phenotype

The current adipose data represents the first molecular phenotyping of IIH adipose tissue, it is limited by the *ex vivo* nature of the metabolomic and secretomic experimentation due to being in an artificial environment which will alter the properties of the tissue. Utilising the microdialysate method in adipose tissue, the comparative metabolome could be assessed *in vivo* via mass spectrometry, assessing whether the changes observed *ex vivo* are congruent with the *in vivo* phenotype in IIH patients (O'Reilly et al., 2017). Moreover, the microdialysate method would facilitate the assessment of the *in vivo* adipose steroid metabolism, where further data could be garnered through providing test subjects with a DHEA bolus, assessing the capability of IIH adipose tissue to activate androgens (O'Reilly et al., 2017). Furthermore, explicit assessment of factors associated with intra-adipose glucocorticoid metabolism, specifically G6PDH activity, adipose tissue NADPH/$NADP^+$ ratio, 5 α-cortisol/cortisol ratio is required, especially in lieu of IIH patients having increased systemic 5 α-reductase activity (O'Reilly et al., 2019).

7.2.2 *In vivo* assessment of testosterone on intracranial pressure

The current data suggests that testosterone can increase Na^+/K^+ ATPase activity, they however do not identify whether this alters ICP *in vivo*, or even if

testosterone increases Na^+/K^+ ATPase activity in primary choroid plexus cells. Assessment of the effects of testosterone on whole rodent and human choroid plexus Na^+/K^+ ATPase activity would be prudent to validate the current data. Furthermore, assessing the effects of chronic testosterone exposure on ICP in obese female rodents is vital in order to ascertain whether testosterone could be truly pathogenic in IIH.

7.2.3 *In vivo* adipose specific knockdown of 5α-reductase type 1

The model presented in figure 7.1 is underpinned by the reduced expression of *SRD5A1* in IIH SC adipose tissue and the proposed metabolic consequences. Although a global knockout of *srd5a1* in mice causes reduced glucocorticoid clearance and a moderate oestrus cycle dependent testosterone excess, the global knockout does not assess adipose tissue specific contributions to the steroid phenotype (Livingstone et al., 2014; Mahendroo et al., 1996). Consequently knocking down 5α-reductase specifically in adipose tissue, either through genetic knockdown or pharmacologically in female rodents, would be required in order test if the proposed mechanism could modulate ICP.

7.2.4 Developing a high through-put Na^+/K^+ ATPase screening assay

The novel *in vitro* Na^+/K^+ ATPase activity assay has utility, however, the inability to simultaneously assay multiple pharmaceuticals is the rate limiting factor in the acquisition of data. Furthermore, the necessity to infect cells with viruses will cause metabolic disturbances that could confound any results. Several steps could be utilised in order improve the assay. Firstly, developing a stable line of Z310 cells with the Perceval biosensor present would negate viral transcription

mediated metabolic disturbances. Developing a plate based assay to generate a high throughput assay would increase the rate of data acquisition, through facilitating the assessment of multiple pharmaceuticals at once in a fraction of the time it takes to complete one experiment on a microscope, allowing the rapid identification of potential therapeutics that could modulate ICP. Furthermore the present assay is limited through the use of a low resolution Perceval biosensor that may be saturated in the experiments, limiting its current utility (Berg et al., 2009). Utilisation of a higher resolution variant, PercevalHR, could allow experiments to observe changes in ATP:ADP ratio over a much larger dynamic range (Berg et al., 2009; Tantama et al., 2013)

7.3 Closing remarks

The field of IIH research is currently maturing, where old hypotheses of IIH pathogenesis are being addressed and novel pathogenic hypothesise are being developed, although the pathogenic mechanism for IIH remains undiscovered (Hornby et al., 2018b; Libien et al., 2017). Furthermore, recent work has moved IIH away from being neuro-ophthalmic disease to being a disease with unique metabolic derangement where neuro-ophthalmic symptoms form part of a greater disease. The work in this thesis demonstrates that adipose tissue, a fundamental tissue in determining whole body metabolism, has a deranged phenotype that has the potential to influence the deranged whole body metabolism in IIH. Furthermore, the demonstration of an androgen excess phenotype with data highlighting the potential for testosterone to increase ICP highlights a novel hypothesis for the pathogenesis of IIH.

Chapter 8 Appendices

Appendix 1 – Steroid profile of IIH patients

The following table present the androgen phenotype in IIH patients, the data is for reference purposes only as I had no participation in the analysis of the data. I however extracted the CSF prior samples to LCMS.

	Controls (n=40)	**PCOS (n=60)**	**IIH (n=70)**
Age (years)	34 (28-38)	30 (27-35)	34 (28-38)
BMI (kg/m^2)	37.3 (35.0-41.1)	38.5 (35.5-43.1)	37.9 (34.9-42.3)
Serum androgen concentrations (nmol/L)			
T	1.0 (0.5-1.4)	1.2 (0.5-1.5)	1.7 (1.0-2.4) [c, f]
A4	3.6 (2.7-7.5)	5.7 (4.3-9.1) [b]	2.4 (1.4-4.4) [a, f]
DHEA	17.9 (9.7-25.1)	13.3 (8.5-22.6)	9.5 (4.9-18.9) [d]
DHEAS(μmol/L)	4.1 (3.0-6.4)	6.2 (4.3-8.5)	4.5 (2.5-8.4)
11OHA4	3.4 (2.1-7.4)	30.0 (10.6-42.1) [c]	2.5 (1.6-3.4) [f]
11KA4	0.7 (0.3-1.0)	12.1 (6.6-21.2) [c]	0.4 (0.2-0.7) [f]
11OHT	0.3 (0.1-0.5)	0.3 (0.2-0.5)	0.2 (0.1-0.45)
11KT	1.7 (0.8-2.2)	2.3 (1.5-3.6) [a]	2.3 (1.9-3.1)
24-h urine androgen metabolite profiling			
5α-THF/THF	0.9 (0.5-1.3)	0.9 (0.7-1.3)	1.2 (0.8-1.80) [a, d]
An/Et ratio	1.3 (0.9-1.8)	1.3 (0.9-1.8)	1.4 (0.9-2.2)
Total androgen metabolites (An+Et, μg/24h)	2575 (1864-4436)	4341 (2508-5497)	3332 (1914-5847)

Table 8.1 Serum and urine androgen characterization of IIH patients

Baseline characteristics and biochemical data in healthy controls, women with PCOS and women with IIH as measured by LCMS for serum data and GCMS for 24 hour urine data. Data are presented as median and interquartile range. Statistical comparison was carried out by analysis of variance with *post hoc* Tukey testing. Significance levels were indicated as follows: a, $p<0.05$, b, $p<0.01$, c, $p<0.001$ for the comparison of PCOS *or* IIH v healthy controls; d, $p<0.05$; e, $p<0.01$; f, $p<0.001$ for the comparison PCOS v IIH. Abbreviations: 5α-THF, 5alpha-tetrahydrocortisol; 11OHA4, 11β-hydroxyandrostenedione; 11KA4, 11-ketoandrostenedione; 11OHT, 11β-hydroxytestosterone; 11KT, 11-ketotestosterone; A4, androstenedione; An, urinary androsterone; BMI, body mass index; DHEA, dehydroepiandrosterone; DHEAS, dehydroepiandrosterone sulfate; Et, urinary etiocholanolone; T, testosterone; THF, tetrahydrocortisol.

	Lean controls (n=31)	**Obese controls (n=19)**	**IIH (n=55)**
Age (years)	46 (38-57)[a]	37 (32-46)	30 (27-35)
BMI (kg/m^2)	27 (22.7-32.3)[a]	44.8 (39.7-47.3)[a]	37.9 (34.9-42.3)
LP pressure (cm H_20)	16.5 (13.5-20.8)[a]	23.5 (21-25.5)[a]	36.0 (29.5-40.0)
CSF androgen concentration (nmol/l)			
T	0 (0-0)	0 (0-0)	0.10 (0.06-0.13)[c,e]
A4	0.28 (0-1.83)	0.70 (0.21-0.98)	8.25 (3.43-12.19)[b,e]
DHEA	2.23 (0.14-8.49)	0.81 (0.54-1.44)[c]	1.09 (0.33-2.59)
DHEAS (µmol/l)	0.16 (0.15-0.18)	0.70 (0.29-0.93)[d]	0.07 (0.05-0.17) [b,e]

Table 8.2 Androgen characterisation of CSF in IIH patients

Baseline characteristics of CSF study patients. Data are presented as median and interquartile range. Statistical comparison was carried out by analysis of variance with *post hoc* Tukey testing. Significance levels were indicated as follows: a, $p<0.001$, b, $p<0.0001$ for the comparison of lean controls v IIH; c, $p<0.05$, d, $p<0.0001$ for comparison between lean vs obese controls; e, $p<0.0001$ for obese controls vs IIH. Abbreviations: BMI, body mass index; IIH, idiopathic intracranial hypertension; LP, lumbar puncture; DHEA, dehydroepiandrosterone; DHEAS, dehydroepiandrosterone sulfate; A4, androstendione; T, testosterone.

Appendix 2 – Primer probe sets

This appendix contains a list of Taqman primer-probe sets used in this work.

Gene	Species specificity	Manufacturer	codes	Reporter
18s	Mammalian	Thermofisher	431941E	VIC
Esr1	*Rattus norvegicus*	Thermofisher	Rn01640372_m1	FAM
Esr2	*Rattus norvegicus*	Thermofisher	Rn00562610_m1	FAM
Cyp19a1	*Rattus norvegicus*	Thermofisher	Rn00567222_m1	FAM
Hsd17b3	*Rattus norvegicus*	Thermofisher	Rn00588942_m1	FAM
Srd5a1	*Rattus norvegicus*	Thermofisher	Rn00567064_m1	FAM
Akr1c3	*Rattus norvegicus*	Thermofisher	Rn00684527_m1	FAM
Ar	*Rattus norvegicus*	Thermofisher	Rn00560747_m1	FAM
Car2	*Rattus norvegicus*	Thermofisher	Rn01462065_M1	FAM
Car3	*Rattus norvegicus*	Thermofisher	Rn01461970_M1	FAM
AR	*Homo sapien*	Thermofisher	Hs00171172_m1	FAM
AKR1C3	*Homo sapien*	Thermofisher	Hs00366267_m1	FAM
CYP19A1	*Homo sapien*	Thermofisher	Hs00903411_m1	FAM
GAPDH	*Homo sapien*	Thermofisher	Hs99999005_m1	FAM
HSD3B1	*Homo sapien*	Thermofisher	Hs04194787_g1	FAM
HSD3B2	*Homo sapien*	Thermofisher	Hs00605123_m1	FAM
SDR5A1	*Homo sapien*	Thermofisher	Hs00602694_m1	FAM
17BHSD3	*Homo sapien*	Thermofisher	Hs00970004_m1	FAM
CYP11B1	*Homo sapien*	Thermofisher	Hs01596404_m1	FAM
ESR1	*Homo sapien*	Thermofisher	Hs01100353_m1	FAM
ESR2	*Homo sapien*	Thermofisher	Hs01046816_m1	FAM
SRD5A2	*Homo sapien*	Thermofisher	Hs00165843_m1	FAM
AKR1D1	*Homo sapien*	Thermofisher	Hs00818881_m1	FAM

Table 8.3 List of QPCR primers

Appendix 3 – Most differentially expressed genes

This appendix highlights the most differentially expressed genes in IIH, DESeq2 output as referred to in section 3.3.3.1

Gene	Expression	Fold Change	Padj	name
HSPA1A	816	-1.15	7.94E-05	Heat shock protein family A (Hsp70) member 1A
HSPA1B	448	-1.04	0.000619	Heat shock protein family A (Hsp70) member 1B
HNRNPU-AS1	809	0.80	0.000768	NA
FADS2	649	1.01	0.001117	Fatty acid desaturase 2
HSPA6	121	-0.96	0.002605	Heat shock protein family A (Hsp70) member 6
NFYC-AS1	37	0.85	0.002667	NFYC antisense RNA 1
STAG3L2	219	0.66	0.003288	Stromal antigen 3-like 2 (pseudogene)
SRPX	1163	-0.55	0.011518	Sushi repeat containing protein, X-linked
LMOD1	1417	-0.57	0.020383	Leiomodin 1
DNM3OS	474	0.71	0.021029	DNM3 opposite strand/antisense RNA
FMO3	320	-0.76	0.021029	Flavin containing monooxygenase 3
HCG27	42	0.83	0.021029	HLA complex group 27 (non-protein coding)
VIM	48131	-0.35	0.021029	Vimentin
FKBP4	509	-0.58	0.025744	FK506 binding protein 4
MIR143HG	162	0.75	0.025744	NA
MAFF	373	-0.82	0.027337	MAF bZIP transcription factor F
IGLL5	77	-0.80	0.028142	Immunoglobulin lambda like polypeptide 5
TCOF1	342	-0.28	0.028142	Treacle ribosome biogenesis factor 1
LINC01355	155	0.77	0.031745	Long intergenic non-protein coding RNA 1355
RPS12	6522	-0.50	0.031931	Ribosomal protein S12
RPLP1	7347	-0.47	0.040782	Ribosomal protein lateral stalk subunit P1
MAGOH2P	23	0.75	0.046975	Mago homolog 2, pseudogene
PDZD3	25	0.76	0.046975	PDZ domain containing 3
RBM33	1176	0.41	0.046975	RNA binding motif protein 33
SREBF1	800	0.73	0.046975	Sterol regulatory element binding transcription factor 1
NRXN1	9	0.73	0.047343	Neurexin 1
LINC00472	137	0.64	0.04767	Long intergenic non-protein coding RNA 472
RPS5	2975	-0.38	0.04767	Ribosomal protein S5
SFPQ	1595	-0.59	0.04767	Splicing factor proline and glutamine rich
CD151	5624	-0.51	0.049961	CD151 molecule (Raph blood group)
DDAH2	1498	-0.39	0.049961	Dimethylarginine dimethylaminohydrolase 2

Table 8.4 List of differentially expressed genes in IIH SC adipose

List of most differentially expressed UCSC genes in IIH SC adipose tissue compared to age, sex and BMI matched controls based on DESeq2 output following multiple comparison correction. Expression = Mean combined expression of both groups. Fold change = Log_2 fold change in expression from control. Padj= adjusted P-value.

Appendix 4 – Gene set enrichment analysis gene lists

Gene set enrichment analysis gene lists as referred to in section 3.3.3.2

Ribosomal Proteins		Caloric Intake UP		Caloric Intake DOWN	
RPSA	*RPL7*	*AACS*	*FLJ10357*	*ACSM5*	*MATN2*
RPS2	*RPL7A*	*ABCC6*	*GCSH*	*ANGPTL4*	*NAP1L1*
RPS3	*RPL8*	*ABCC6P2*	*GLYAT*	*C1NH*	*NFE2L1*
RPS3A	*RPL9*	*ACACA*	*GPX1*	*C6*	*PCK2*
RPS4X	*RPL10*	*ACLY*	*HSPA12A*	*CCNI*	*PRDX6*
RPS4Y	*RPL10A*	*ACSL1*	*INSIG1*	*CDKN1C*	*RPL13*
RPS5	*RPL12*	*AGTRL1*	*LAMB3*	*CIDEA*	*RPL13A*
RPS6	*RPL13A*	*ALDH9A1*	*LOC55908*	*CLIPR-59*	*RPL14*
RPS7	*RPL14*	*ALDOC*	*LOX*	*CPT1B*	*TD26*
RPS8	*RPL15*	*AQP1*	*LOXL2*	*EIF3E*	*RPL30*
RPS9	*RPL17*	*ATP2B4*	*MGC4172*	*EIF3F*	*RPL36AL*
RPS10	*RPL18*	*ATR*	*MGLL*	*EIF4B*	*RPL37*
RPS11	*RPL18A*	*C1orf54*	*MME*	*EIF4EBP1*	*RPL5*
RPS12	*RPL19*	*COL3A1*	*MXRA5*	*EIF4EBP2*	*RPL9*
RPS13	*RPL21*	*COL5A1*	*NMB*	*FAU*	*RPLP1*
RPS14	*RPL22*	*COL5A2*	*PEDF*	*FXYD1*	*RPS15A*
RPS15	*RPL23*	*COL5A3*	*PRDX2*	*GPD1L*	*RPS16*
RPS15A	*RPL23A*	*CYP46A1*	*PTPLB*	*GPR153*	*RPS24*
RPS16	*RPL24*	*DBI*	*SCD*	*GPX3*	*RPS25*
RPS17	*RPL26*	*DLAT*	*SEMA3C*	*GSDML*	*RPS4X*
RPS18	*RPL27*	*DOCK6*	*SPARC*	*HNRPA1*	*RANGNRF*
RPS19	*RPL27A*	*ECHDC1*	*TCTA*	*IGBP1*	*SEMA3G*
RPS20	*RPL30*	*ELOVL5*	*TF*	*IMPA2*	*SIK2*
RPS21	*RPL31*	*FADS1*	*THBS4*	*ITSN1*	*SRPX*
RPS23	*RPL32*	*FADS2*	*TP53I3*	*MAOB*	*TINP1*
RPS24	*RPL34*	*FASN*	*TSPO*		
RPS25	*RPL35*				
RPS26	*RPL36*				
RPS27	*RPL36A*				
RPS27A	*RPL37*				
RPS28	*RPL39*				
RPS29	*RPL40*				
RPS30	*RPL41*				
RPL3	*RPP0*				
RPL4	*RPP1*				
RPL5	*RPP2*				
RPL6					

Lipid Biosynthesis						
A4GALT	*ALDH1A2*	*CDS2*	*CYP46A1*	*FAM57B*	*GBGT1*	*IDI2*
ABCB11	*ALDH1A3*	*CECR5*	*CYP51A1*	*FAR1*	*GGPS1*	*IMPA1*
ABCD3	*ALDH3A2*	*CEPT1*	*CYP7A1*	*FASN*	*GGT1*	*INPP4A*
ABHD3	*ALDH3B1*	*CERS1*	*CYP7B1*	*FCER1A*	*GGT2*	*INPP4B*
ABHD5	*ALDH3B2*	*CERS2*	*CYP8B1*	*FDFT1*	*GGT3P*	*INPP5D*
ACAA2	*ALDH8A1*	*CERS3*	*DDHD1*	*FDPS*	*GGT5*	*INPP5E*
ACACA	*ALG1*	*CERS4*	*DDHD2*	*FDX1*	*GGT6*	*INPP5F*
ACACB	*ALG5*	*CERS5*	*DECR2*	*FDX1L*	*GGT7*	*INPP5J*
ACBD3	*ALOX12*	*CERS6*	*DEGS1*	*FDXR*	*GGTA1P*	*INPP5K*
ACER1	*ALOX12B*	*CFTR*	*DEGS2*	*FGF1*	*GGTLC1*	*INPPL1*
ACER2	*ALOX15*	*CH25H*	*DGAT1*	*FGF10*	*GGTLC2*	*INSIG1*
ACER3	*ALOX15B*	*CHAT*	*DGAT2*	*FGF16*	*GGTLC3*	*INSIG2*
ACHE	*ALOX5*	*CHKA*	*DGKE*	*FGF17*	*GK*	*IRS1*
ACLY	*ALOX5AP*	*CHKB*	*DHCR24*	*FGF18*	*GNPAT*	*IRS2*
ACOT7	*ALOXE3*	*CHPT1*	*DHCR7*	*FGF19*	*GPAA1*	*ISPD*
ACOT8	*AMACR*	*CLN8*	*DHDDS*	*FGF2*	*GPAM*	*ISYNA1*
ACOX2	*ANG*	*CNBP*	*DHRS9*	*FGF20*	*GPAT2*	*JUB*
ACSF3	*APOA1*	*COL4A3BP*	*DOLK*	*FGF22*	*GPD1*	*KDSR*
ACSL1	*APOA2*	*COQ2*	*DOLPP1*	*FGF23*	*GPD1L*	*KL*
ACSL3	*APOA4*	*CPNE1*	*DPAGT1*	*FGF3*	*GRB2*	*KLB*
ACSL4	*APOA5*	*CPNE3*	*DPM1*	*FGF4*	*HEXB*	*LARGE*
ACSM1	*ARF1*	*CPNE6*	*DPM2*	*FGF5*	*HINT2*	*LBR*
ACSM3	*ARF3*	*CPNE7*	*DPM3*	*FGF6*	*HMGCR*	*LCAT*
ACSS1	*ARV1*	*CRH*	*EBP*	*FGF7*	*HMGCS1*	*LCLAT1*
ACSS2	*ATM*	*CRLS1*	*EDN1*	*FGF8*	*HMGCS2*	*LHB*
ADM	*B3GNT5*	*CSNK1G2*	*EDN2*	*FGF9*	*HPGDS*	*LIAS*
AGK	*B4GALNT1*	*CWH43*	*ELOVL1*	*FGFR1*	*HSD11B1*	*LIPC*
AGMO	*BAAT*	*CYB5R1*	*ELOVL2*	*FGFR2*	*HSD11B2*	*LIPT2*
AGPAT1	*BCMO1*	*CYB5R2*	*ELOVL3*	*FGFR3*	*HSD17B1*	*LOC100288072*
AGPAT2	*BRCA1*	*CYB5R3*	*ELOVL4*	*FGFR4*	*HSD17B11*	*LOC643181*
AGPAT3	*C14orf1*	*CYP11A1*	*ELOVL5*	*FIG4*	*HSD17B12*	*LPCAT1*
AGPAT4	*C1orf93*	*CYP11B1*	*ELOVL6*	*FITM1*	*HSD17B14*	*LPCAT2*
AGPAT5	*C20orf173*	*CYP11B2*	*ELOVL7*	*FITM2*	*HSD17B2*	*LPCAT3*
AGPAT6	*C20orf79*	*CYP17A1*	*EPT1*	*FRS2*	*HSD17B3*	*LPCAT4*
AGPAT9	*C5orf4*	*CYP19A1*	*ETNK1*	*FSHB*	*HSD17B4*	*LPGAT1*
AGPS	*C9orf3*	*CYP1A1*	*ETNK2*	*G6PD*	*HSD17B6*	*LPIN1*
AGXT2L1	*CACNA1H*	*CYP21A2*	*FA2H*	*GAB1*	*HSD17B7*	*LPIN2*
AKR1B1	*CBR1*	*CYP27A1*	*FABP5*	*GAL3ST1*	*HSD17B8*	*LPIN3*
AKR1B15	*CBR4*	*CYP27B1*	*FADS1*	*GAL3ST2*	*HSD3B1*	*LPL*
AKR1C3	*CD74*	*CYP2R1*	*FADS2*	*GAL3ST3*	*HSD3B2*	*LSS*
AKR1C4	*CDIPT*	*CYP39A1*	*FADS3*	*GAL3ST4*	*HSD3B7*	*LTA4H*
AKR1D1	*CDS1*	*CYP3A4*	*FADS6*	*GBA*	*IDI1*	*LTC4S*

Gene list continued on next page.

Lipid biosynthesis (continued)					
MBOAT1	*PDSS1*	*PIK3CG*	*PPAP2C*	*SCP2*	*ST6GALNAC2*
MBOAT2	*PDSS2*	*PIK3R1*	*PPARD*	*SDR42E1*	*ST6GALNAC3*
MBOAT7	*PECR*	*PIK3R2*	*PPM1L*	*SERAC1*	*ST6GALNAC4*
MCAT	*PEMT*	*PIK3R3*	*PRG3*	*SERINC1*	*ST6GALNAC5*
MECR	*PEX7*	*PIK3R4*	*PRKAA1*	*SERINC4*	*ST6GALNAC6*
MED1	*PGAP1*	*PIK3R5*	*PRKAA2*	*SERINC5*	*ST8SIA1*
MGLL	*PGAP2*	*PIK3R6*	*PRKAB1*	*SGMS1*	*ST8SIA2*
MGST2	*PGAP3*	*PIKFYVE*	*PRKAB2*	*SGMS2*	*ST8SIA3*
MIF	*PGS1*	*PIP4K2A*	*PRKAG1*	*SGPL1*	*ST8SIA4*
MLYCD	*PHOSPHO1*	*PIP4K2B*	*PRKAG2*	*SGPP1*	*ST8SIA5*
MOGAT1	*PI4K2A*	*PIP4K2C*	*PRKAG3*	*SGPP2*	*ST8SIA6*
MOGAT2	*PI4K2B*	*PIP5K1A*	*PRKD1*	*SH3YL1*	*STAR*
MOGAT3	*PI4KA*	*PIP5K1B*	*PRLR*	*SLC27A1*	*STARD3*
MPPE1	*PI4KB*	*PIP5K1C*	*PRPF19*	*SLC27A2*	*STARD5*
MSMO1	*PIGA*	*PISD*	*PTDSS1*	*SLC27A5*	*SYK*
MTM1	*PIGB*	*PLA2G10*	*PTDSS2*	*SLC44A1*	*SYNJ1*
MTMR1	*PIGC*	*PLA2G12A*	*PTEN*	*SLC44A2*	*SYNJ2*
MTMR14	*PIGF*	*PLA2G16*	*PTGDS*	*SLC44A3*	*TAMM41*
MTMR2	*PIGG*	*PLA2G1B*	*PTGES*	*SLC44A4*	*TAZ*
MTMR3	*PIGH*	*PLA2G2A*	*PTGES2*	*SLC44A5*	*TBXAS1*
MTMR4	*PIGK*	*PLA2G2D*	*PTGES3*	*SMPD1*	*TECR*
MTMR6	*PIGL*	*PLA2G2E*	*PTGIS*	*SMPD2*	*TFCP2L1*
MTMR7	*PIGM*	*PLA2G2F*	*PTGS1*	*SMPD4*	*THNSL2*
MVD	*PIGN*	*PLA2G4A*	*PTGS2*	*SPHK1*	*TLR9*
MVK	*PIGO*	*PLA2G4B*	*PTPLA*	*SPHK2*	*TM7SF2*
MYO5A	*PIGP*	*PLA2G4D*	*PTPLAD1*	*SPTLC1*	*TPTE2*
NANS	*PIGQ*	*PLA2G4F*	*PTPLAD2*	*SPTLC2*	*TRERF1*
NDUFAB1	*PIGS*	*PLA2G5*	*PTPLB*	*SPTLC3*	*TSPO*
NPC1L1	*PIGT*	*PLA2G6*	*PTPMT1*	*SPTSSA*	*UGCG*
NR0B1	*PIGU*	*PLAUR*	*PTPN11*	*SPTSSB*	*UGT8*
NSDHL	*PIGV*	*PLCE1*	*QKI*	*SQLE*	*VAC14*
NUS1	*PIGW*	*PLCG2*	*RBP1*	*SRD5A1*	*VAPA*
OCRL	*PIGX*	*PLD1*	*RDH10*	*SRD5A2*	*VAPB*
OLAH	*PIGY*	*PLD2*	*RDH8*	*SRD5A3*	*WNT4*
OXSM	*PIGZ*	*PLD6*	*RNPEP*	*SREBF1*	*XBP1*
P2RX1	*PIK3C2A*	*PLP1*	*RNPEPL1*	*ST3GAL1*	
P2RX7	*PIK3C2B*	*PLSCR1*	*SACM1L*	*ST3GAL2*	
PBX1	*PIK3C2G*	*PMVK*	*SAMD8*	*ST3GAL3*	
PCK1	*PIK3C3*	*PNPLA3*	*SC5DL*	*ST3GAL4*	
PCYT1A	*PIK3CA*	*PNPLA8*	*SCARB1*	*ST3GAL5*	
PCYT1B	*PIK3CB*	*PPAP2A*	*SCD*	*ST3GAL6*	
PCYT2	*PIK3CD*	*PPAP2B*	*SCD5*	*ST6GALNAC1*	

Appendix 5 – NMR Metabolite tables

	Subcutaneous			Omental		
µM/100mg	Control	IIH	P	Control	IIH	P
Acetate	232.7(176.8)	215.4(145.5)	0.81	286.8 (64.8)	166.5 (75.2)	0.0012
Alanine	51.1 (20.8)	82.1 (43.0)	0.06	62.6 (28.7)	109.0 (73.4)	0.052[$]
Arginine	202.8 (62.4)	215.8(117.7)	0.76	246.9 (72.2)	238.3 (88.4)	0.81
Formate	57.6 (47.9)	72.5 (52.9)	0.35[$]	56.1 (28.5)	53.9 (34.7)	0.73[$]
Glucose (mM)	3.7 (1.6)	3.6 (1.2)	0.86	4.1 (1.1)	3.6 (1.5)	0.43
Glutamate	N/A			146.5 (63.0)	150.6 (69.0)	0.79[$]
Glutamine	551.5(287.2)	509.7(253.5)	0.73	679.6(241.7)	719.6(233.7)	0.71
Glutathione	13.2 (6.6)	22.9 (17.6)	0.12[$]	20.9 (13.3)	16.7 (5.6)	0.57[$]
Glycerol	339.0 (97.9)	305.7 (90.8)	0.44	296.1 (38.5)	274.1 (87.4)	0.16[$]
Glycine	105.5 (44.6)	117.3 (47.7)	0.57	132.8 (36.3)	148.5 (68.2)	0.53
Histidine	41.9 (21.3)	36.4 (13.1)	0.49	38.9 (10.3)	43.5 (10.0)	0.32
Isoleucine	121.0 (46.6)	116.1 (42.8)	0.81	130.9 (30.3)	124.4 (25.0)	0.6
Lactate (mM)	616.2(409.3)	660.5(330.1)	0.48[$]	0.85 (0.33)	1.59 (1.97)	0.48[$]
Leucine	139.8 (53.8)	133.3 (48.3)	0.78	144.3 (35.6)	138.3 (26.9)	0.67
Lysine	134.1 (60.4)	151.1 (55.8)	0.52	162.1 (51.10	172.1 (43.0)	0.64
Methionine	34.1 (17.5)	29.7 (17.6)	0.58	34.1 (9.4)	41.3 (11.2)	0.13
Methylsuccinate	5.1 (3.7)	4.3 (2.4)	0.85[$]	4.9 (2.8)	7.1 (5.1)	0.49[$]
NAD+	5.3 (2.4)	5.4 (2.5)	0.96	6.2 (2.9)	8.1 (4.7)	0.31
NADH	N/A			8.2 (4.0)	13.1 (9.1)	0.16[$]
HAD+NADH	N/A			14.4 (6.0)	21.2 (12.9)	0.1[$]
NADP+	1.4 (0.7)	2.1 (0.9)	0.07[$]	2.7 (0.8)	2.7 (1.1)	0.93
NADPH	N/A			11.5 (7.9)	18.5 (12.2)	0.14
NADP+NADPH	N/A			14.3 (8.6)	21.3 (12.9)	0.16[$]
Niacinamide	6.8 (1.3)	6.4 (3.2)	0.77	5.8 (2.2)	6.2 (1.7)	0.36[$]
Phenylalanine	60.0 (27.4)	58.5 (19.7)	0.89	65.1 (18.7)	72.5 (15.7)	0.34
Proline	56.1 (38.2)	60.1 (30.7)	0.39	74.5 (24.9)	83.1 (23.4)	0.43
Pyroglutamate	191.6 (89.3)	184.2(132.1)	0.88	190.0 (84.4)	181.9 (86.3)	0.83
Pyruvate	9.5 (8.7)	21.3 (29.4)	0.79[$]	4.5 (7.1)	23.6 (16.7)	0.003[$]
Sarcosine	6.7 (2.6)	6.4 (2.9)	0.81	5.4 (1.4)	6.7 (2.6)	0.22
Succinate	N/A			13.5 (4.6)	18.2 (8.4)	0.14
Threonine	149.4 (57.7)	166.9 (70.0)	0.48[$]	188.3 (44.5)	196.1 (60.4)	0.74
Tryptophan	10.6 (4.6)	11.3 (2.9)	0.66	12.3 (3.5)	13.8 (3.4)	0.34
Tyrosine	71.4 (30.4)	75.9 (28.7)	0.74	87.4 (23.4)	95.0 (21.4)	0.46
Valine	144.6 (52.5)	142.3 (50.9)	0.92	159.3 (38.3)	157.1 (31.1)	0.89
myo-Inositol	162.0 (74.1)	171.4 (86.7)	0.79	130.7 (59.0)	147.2 (86.7)	0.91[$]
Sn-glycero-3-PC	94.0 (26.9)	95.9 (54.8)	0.79	83.9 (27.5)	77.3 (22.6)	0.56

Ratios	Control	IIH	P	Control	IIH	P
NADP/NADPH	N/A			0.87 (0.41)	0.73 (0.41)	0.47
NAD/NADH	N/A			0.32 (0.18)	0.14 (0.07)	0.02
Lactate/Pyruvate	140.6(154.9)	155.2(160.3)	0.85[$]	544.9(380.7)	145.0(199.9)	0.015[$]

Table 8.5 Adipose tissue metabolite concentration

Concentration of tissue explant metabolite concentration in adipose explants from paired OM and SC adipose tissue from IIH and control patients as determined by NMR. [$]= Mann-Whitney U-test, unmarked = unpaired T-test. Data presented as mean±SD.

	Subcutaneous			Omental		
ΔμM/100mg	Control	IIH	P	Control	IIH	P
Acetate	596.6 (336.8)	532.5 (250.5)	0.63	800.9(414.6)	335.4(176.4)	0.004
Adenosine	-2.8 (0.4)	-1.9 (0.8)	0.012	N/A		
Alanine	87.1 (84.8)	141.6 (84.3)	0.16	67.9 (43.9)	102.8(53.4)	0.14
Arabinose	-32.2 (5.2)	-23.1 (22.9)	0.23$	N/A		
Arginine	-70.9 (90.9)	-90.4 (90.6)	0.31$	-227.0 (274.7)	-58.4 (265.9)	0.18$
Asparagine	2.8 (18.3)	-1.5 (19.0)	0.60	0.1 (6.3)	8.3 (10.8)	0.31$
Aspartate	-23.9 (15.7)	-29.2 (15.6)	0.45	-23.6 (14.0)	-24.7 (5.3)	0.82
Choline	-5.2 (13.4)	-7.4 (14.3)	0.27$	-6.5 (17.0)	0.3 (3.4)	0.76
Cysteine	19.6 (27.3)	30.1 (52.9)	0.58	12.9 (23.6)	10.0 (21.1)	0.18
Cystine	0.9 (37.5)	5.2 (61.7)	0.78	-42.6 (31.9)	-2.8 (21.5)	0.005
Formate	34.6 (21.1)	53.5 (41.0)	0.31$	40.5 (18.2)	40.3 (21.5)	0.98
Glucose (ΔmM)	-0.625 (376.8)	-1.015 (0.840)	0.22	-0.35 (1.2)	-0.27 (0.91)	0.85
Glutamate	1.7 (72.6)	-2.4 (35.5)	0.54	1.3 (64.0)	-10.2 (45.8)	0.85$
Glutamine	-8.1 (467.9)	34.9 (28.6)	0.94	-86.8 (380.4)	105.3 (203)	0.18
Glycerol	84.5 (37.0)	157.3 (62.6)	0.005	79.4 (33.5)	128.7 (45.6)	0.016
Glycine	56.2 (40.3)	41.7 (52.5)	0.19$	39.6 (34.1)	47.2 (28.5)	0.6
Histidine	39.8 (16.1)	33.8 (10.1)	0.33	28.9 (9.9)	33.9 (14.9)	0.40
Hypoxanthine	0.3 (10.4)	3.8 (9.6)	0.45	3.5 (7.2)	-2.9 (6.5)	0.055
Inosine	1.1 (2.8)	-0.2 (1.1)	0.59$	N/A		
Isoleucine	25.3 (48.3)	-30.5 (25.2)	0.002$	-9.7 (41.6)	-29.2 (71.8)	0.48
Lactate (ΔmM)	1.4 (0.6)	1.5 (0.5)	0.35	1.8 (1.5)	1.8 (0.9)	0.29$
Leucine	22.6 (54.3)	-38.0 (40.8)	0.011	3.8 (55.9)	-9.8 (78.6)	0.66
Lysine	29.4 (139.1)	-8.4 (64.5)	0.97	17.6(159.7)	9.7 (50.5)	0.24$
Methionine	-0.5 (15.1)	-8.9 (8.3)	0.16$	-3.2 (12.4)	-1.7 (10.2)	0.54$
Niacinamide	15.8 (4.1)	12.9 (3.5)	0.12	16.3 (6.9)	11.9 (2.4)	0.08
Phenylalanine	26.5 (19.6)	21.5 (17.9)	0.56	22.8 (10.6)	19.7 (13.5)	0.57
Proline	-11.2 (44.1)	38.8 (178.2)	0.73$	-54.1 (56.8)	13.9 (36.4)	0.007
Pyroglutamate	-123.3 (300.2)	-242.3 (244.0)	0.34	-160.9 (196.3)	-172.2 (252.3)	0.91
Pyruvate	-332.5 (128.2)	-188.9 (329.2)	0.24$	-344.0 (107)	-226.1 (100)	0.02
Serine	-129.8 (42.0)	-102.4 (79.5)	0.34	-120.7 (82.5)	-90.5 (91.5)	0.46
Threonine	119.6 (56.3)	77.6 (58.6)	0.19$	106.1(82.2)	69.1 (51.6)	0.25
Tryptophan	0.5 (4.0)	-1.5 (2.8)	0.63$	-4.5 (4.6)	-1.4 (1.9)	0.07
Tyrosine	54.9 (34.3)	39.0 (23.7)	0.43$	48.2 (17.5)	52.0 (10.9)	0.18$
Valine	103.2 (63.9)	52.8 (49.3)	0.04$	83.6 (52.8)	66.0 (43.7)	0.43

Table 8.6 Conditioned media metabolite flux

Conditioned media metabolites as assessed by NMR In paired omental and subcutaneous adipose tissue explants from IIH and control patients.$= Mann-Whitney U-test, unmarked = unpaired T-test. Data presented as mean±SD.

Appendix 6 – Correlation matrices

Glycolysis

	Age	BMI	G influx OM	G influx SC	$[G]_i$ OM	[G]i SC	$[Pyr]_i$ OM	$[Pyr]_i$ SC	$[Lac]_i$ OM	$[Lac]_i$ SC
Age		0.29	0.77	0.69	0.49	0.70	0.01	0.70	0.87	0.65
BMI	0.29		0.31	0.23	0.61	0.49	0.39	0.39	0.75	0.20
G influx OM	0.77	0.31		0.82	0.20	0.14	0.24	0.11	0.68	0.49
G influx SC	0.69	0.23	0.82		0.88	0.59	0.76	0.44	0.89	0.53
$[G]_i$ OM	0.49	0.61	0.20	0.88		0.20	0.53	0.68	0.53	0.20
[G]i SC	0.70	0.49	0.14	0.59	0.20		0.75	0.70	0.16	0.00
$[Pyr]_i$ OM	0.01	0.39	0.24	0.76	0.53	0.75		0.31	0.52	0.84
$[Pyr]_i$ SC	0.70	0.39	0.11	0.44	0.68	0.70	0.31		0.77	0.49
$[Lac]_i$ OM	0.87	0.75	0.68	0.89	0.53	0.16	0.52	0.77		0.07
$[Lac]_i$ SC	0.65	0.20	0.49	0.53	0.20	0.00	0.84	0.49	0.07	

Table 8.7 Glycolysis correlation matrix

P-values for correlation matrix for glycolysis metabolites compared to BMI and age. Spearman's correlation. Abbreviations: G=glucose, Pyr =pyruvate, Lac=lactate, SC=subcutaneous, OM=omental. $[\ ]_i$ = Intracellular concentration.

Branch chain amino acids

	Age	BMI	Leu Flux OM	Leu Flux SC	Iso Flux OM	Iso Flux SC	$[Leu]_i$ OM	$[Leu]_i$ SC	$[Iso]_i$ OM	$[Iso]_i$ SC
Age		0.71	0.41	0.15	0.35	0.06	0.56	0.88	0.63	0.82
BMI	0.71		0.74	0.95	0.49	0.67	0.52	0.84	0.43	0.71
Leu Flux OM	0.41	0.74		0.37	0.00	0.96	0.57	0.54	0.51	0.49
Leu Flux SC	0.15	0.95	0.37		0.76	0.00	0.56	0.54	0.69	0.80
Iso Flux OM	0.35	0.49	0.00	0.76		0.96	0.93	0.38	0.92	0.34
Iso Flux SC	0.06	0.67	0.96	0.00	0.96		0.87	0.85	0.92	0.61
$[Leu]_i$ OM	0.56	0.52	0.57	0.56	0.93	0.87		0.03	0.00	0.03
$[Leu]_i$ SC	0.88	0.84	0.54	0.54	0.38	0.85	0.03		0.04	0.00
$[Iso]_i$ OM	0.63	0.43	0.51	0.69	0.92	0.92	0.00	0.04		0.04
$[Iso]_i$ SC	0.82	0.71	0.49	0.80	0.34	0.61	0.03	0.00	0.04	

Table 8.8 Branch chain amino acids correlation matrix

P-values for correlation matrix for branch chain amino acid metabolites compared to BMI and age. Spearman's correlation. Abbreviations: Leu=leucine, Iso =isoleucine, SC=subcutaneous, OM=omental. $[\ ]_I$ = Intracellular concentration.

Lipolysis

	Age	BMI	$[OM]_{Ex}$	$[SC]_{Ex}$	$[OM]_{i}$	$[SC]_{i}$	OM R	SC R
Age		0.386	0.009	0.250	0.461	0.970	0.023	0.347
BMI	0.288		0.551	0.386	0.003	0.975	0.086	0.262
$[OM]_{Ex}$	0.009	0.551		0.367	0.495	0.808	<0.001	0.758
$[SC]_{Ex}$	0.25	0.386	0.367		0.184	0.531	0.079	<0.001
$[OM]_{i}$	0.461	0.184	0.495	0.184		0.920	0.016	0.112
$[SC]_{i}$	0.347	0.975	0.808	0.531	0.920		0.994	0.014
OM R	0.023	0.086	<0.001	0.079	0.016	0.994		0.235
SC R	0.347	0.262	0.748	<0.001	0.112	0.014	0.235	

Table 8.9 Glycerol correlation matrix

P-values for correlation matrix for glycerol secretion in subcutaneous (SC) and omental (OM) adipose for secreted (Ex), intracellular (i) and ratio (R) tissue compared to BMI and age. Spearman's correlation.

Appendix 7 – No IgG control AR staining

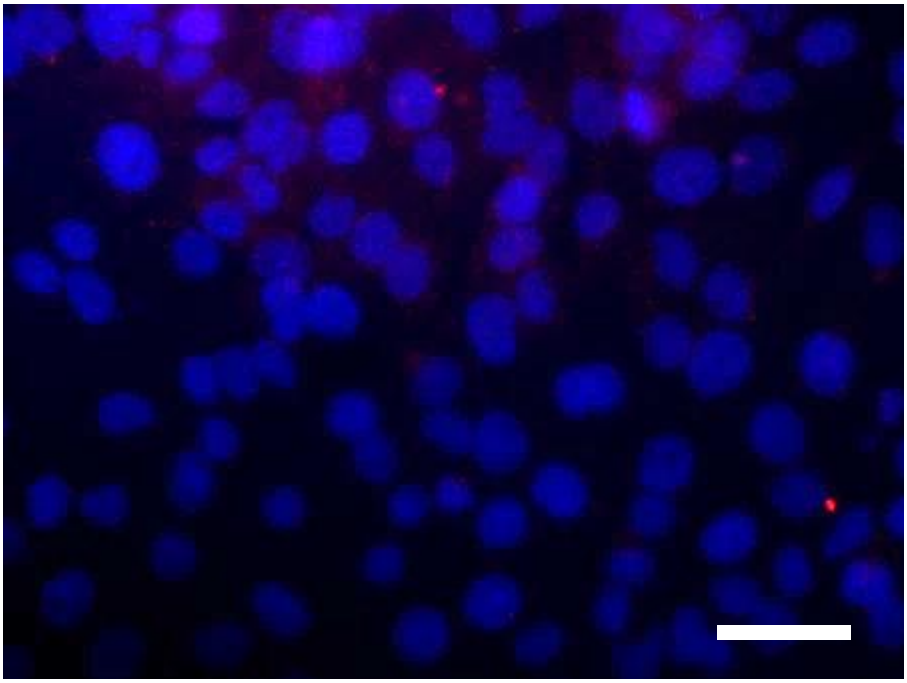

Figure 8.1 No IgG control for androgen receptor

No IgG staining control for androgen receptor staining in figure 6.4 on Z310 cells containg both blue and red channels. Note some non-specific staining. Scale bar = 50 µm.

Chapter 9 Bibliography

Akay, R., Kamisli, O., Kahraman, A., Oner, S., Tecellioglu, M., 2015. Evaluation of aqueductal CSF flow dynamics with phase contrast cine MR imaging in idiopathic intracranial hypertension patients: Preliminary results. Eur. Rev. Med. Pharmacol. Sci. 19, 3475–3479.

Alimajstorovic, Z., 2016. Investigation into the Molecular Mechanisms Underlying Idiopathic Intracranial Hypertension. Open University.

Ameer, F., Scandiuzzi, L., Hasnain, S., Kalbacher, H., Zaidi, N., 2014. De novo lipogenesis in health and disease. Metabolism 63, 895–902. DOI:10.1016/J.METABOL.2014.04.003

Anders, S., Pyl, P.T., Huber, W., 2015. HTSeq--a Python framework to work with high-throughput sequencing data. Bioinformatics 31, 166–169. DOI:10.1093/bioinformatics/btu638

Anoop, T.M., Jain, N., Nair, S.G., Narayanan, G., 2014. All-trans-retinoic acid-induced pseudotumor cerebri in acute promyelocytic leukemia. J. Neurosci. Rural Pract. 5, 273–5. DOI:10.4103/0976-3147.133595

Arnaldi, G., Scandali, V.M., Trementino, L., Cardinaletti, M., Appolloni, G., Boscaro, M., 2010. Pathophysiology of dyslipidemia in Cushing's syndrome. Neuroendocrinology 92 Suppl 1, 86–90. DOI:10.1159/000314213

Aspelund, A., Antila, S., Proulx, S.T., Karlsen, T.V., Karaman, S., Detmar, M., Wiig, H., et al., 2015. A dural lymphatic vascular system that drains brain interstitial fluid and macromolecules. J. Exp. Med. 212, 991–999. DOI:10.1084/jem.20142290

Attie, A.D., Scherer, P.E., 2009. Adipocyte metabolism and obesity. J. Lipid Res. 50 Suppl, S395-9. DOI:10.1194/jlr.R800057-JLR200

Avisar, I., Gaton, D.D., Dania, H., Stiebel-Kalish, H., 2012. The Prevalence of Polycystic Ovary Syndrome in Women with Idiopathic Intracranial Hypertension. Scientifica (Cairo). 2012, 1–4. DOI:10.6064/2012/708042

Bader, T., Zoumakis, E., Friedberg, M., Chrousos, G.P., Hochberg, Z., Hochberg, Z., 2002. Human Adipose Tissue under *in Vitro* Inhibition of 11β-Hydroxysteroid Dehydrogenase Type 1: Differentiation and Metabolism Changes. Horm. Metab. Res. 34, 752–757. DOI:10.1055/s-2002-38255

Ball, A.K., Howman, A., Wheatley, K., Burdon, M.A., Matthews, T., Jacks, A.S., Lawden, M., et al., 2011. A randomised controlled trial of treatment for idiopathic intracranial hypertension. J. Neurol. 258, 874–881.

DOI:10.1007/s00415-010-5861-4

Ball, A.K., Sinclair, A.J., Curnow, S.J., Tomlinson, J.W., Burdon, M.A., Walker, E.A., Stewart, P.M., et al., 2009. Elevated cerebrospinal fluid (CSF) leptin in idiopathic intracranial hypertension (IIH): evidence for hypothalamic leptin resistance? Clin. Endocrinol. (Oxf). 70, 863–869. DOI:10.1111/j.1365-2265.2008.03401.x

Baxter, J.D., Forsham, P.H., 1972. Tissue effects of glucocorticoids. Am. J. Med. 53, 573–589. DOI:10.1016/0002-9343(72)90154-4

Behbehani, R., Mabrook, A., Abbas, J.M.K., Al-Rammah, T., Mojiminiyi, O., Doi, S.A.R., 2010. Is cerebrospinal fluid leptin altered in idiopathic intracranial hypertension? Clin. Endocrinol. (Oxf). 72, 851–852. DOI:10.1111/j.1365-2265.2009.03722.x

Bełtowski, J., Jamroz-Wiśniewska, A., Borkowska, E., Wójcicka, G., 2004. Up-regulation of renal Na+, K+-ATPase: the possible novel mechanism of leptin-induced hypertension. Pol. J. Pharmacol. 56, 213–22.

Berg, J., Hung, Y.P., Yellen, G., 2009. A genetically encoded fluorescent reporter of ATP:ADP ratio. Nat. Methods 6, 161–166. DOI:10.1038/nmeth.1288

Blouin, K., Nadeau, M., Mailloux, J., Daris, M., Lebel, S., Luu-The, V., Tchernof, A., 2009. Pathways of adipose tissue androgen metabolism in women: depot differences and modulation by adipogenesis. Am. J. Physiol. Metab. 296, E244–E255. DOI:10.1152/ajpendo.00039.2008

Blouin, K., Richard, C., Bélanger, C., Dupont, P., Daris, M., Laberge, P., Luu-The, V., et al., 2003. Local Androgen Inactivation in Abdominal Visceral Adipose Tissue. J. Clin. Endocrinol. Metab. 88, 5944–5950. DOI:10.1210/jc.2003-030535

Boden, G., Chen, X., Mozzoli, M., Ryan, I., 1996. Effect of fasting on serum leptin in normal human subjects. J. Clin. Endocrinol. Metab. 81, 3419–3423. DOI:10.1210/jcem.81.9.8784108

Börjeson, M., 1976. THE AETIOLOGY OF OBESITY IN CHILDREN A Study of 101 Twin Pairs. Acta Paediatr. 65, 279–287. DOI:10.1111/j.1651-2227.1976.tb04887.x

Botfield, H.F., Uldall, M.S., Westgate, C.S.J., Mitchell, J.L., Hagen, S.M., Gonzalez, A.M., Hodson, D.J., et al., 2017. A glucagon-like peptide-1 receptor agonist reduces intracranial pressure in a rat model of hydrocephalus. Sci. Transl. Med. 9, eaan0972. DOI:10.1126/scitranslmed.aan0972

Brasaemle, D.L., Subramanian, V., Garcia, A., Marcinkiewicz, A., Rothenberg, A., 2009. Perilipin A and the control of triacylglycerol metabolism. Mol. Cell. Biochem. 326, 15–21. DOI:10.1007/s11010-008-9998-8

Brinker, T., Stopa, E., Morrison, J., Klinge, P., 2014. A new look at cerebrospinal fluid circulation. Fluids Barriers CNS 11, 10. DOI:10.1186/2045-8118-11-10

Brown, P.D., Davies, S.L., Speake, T., Millar, I.D., 2004. Molecular mechanisms of cerebrospinal fluid production. Neuroscience 129, 955–968. DOI:10.1016/j.neuroscience.2004.07.003

Bruce, B.B., Kedar, S., Van Stavern, G.P., Monaghan, D., Acierno, M.D., Braswell, R.A., Preechawat, P., et al., 2009. Idiopathic intracranial hypertension in men. Neurology 72, 304–9. DOI:10.1212/01.wnl.0000333254.84120.f5

Bujalska, I.J., Durrani, O.M., Abbott, J., Onyimba, C.U., Khosla, P., Moosavi, A.H., Reuser, T.T.Q., et al., 2007. Characterisation of 11β-hydroxysteroid dehydrogenase 1 in human orbital adipose tissue: A comparison with subcutaneous and omental fat. J. Endocrinol. 192, 279–288. DOI:10.1677/JOE-06-0042

Burguera, B., Couce, M.E., Long, J., Lamsam, J., Laakso, K., Jensen, M.D., Parisi, J.E., et al., 2000. The Long Form of the Leptin Receptor (OB-Rb) Is Widely Expressed in the Human Brain. Neuroendocrinology 71, 187–195. DOI:10.1159/000054536

Cammisotto, P.G., Gélinas, Y., Deshaies, Y., Bukowiecki, L.J., 2003. Regulation of leptin secretion from white adipocytes by free fatty acids. Am. J. Physiol. Metab. 285, E521–E526. DOI:10.1152/ajpendo.00052.2003

Çelebisoy, N., Gökçay, F., Şirin, H., Akyürekli, Ö., 2007. Treatment of idiopathic intracranial hypertension: topiramate vs acetazolamide, an open-label study. Acta Neurol. Scand. 116, 322–327. DOI:10.1111/j.1600-0404.2007.00905.x

Chowen, J.A., Busiguina, S., García-Segura, L.M., 1995. Sexual dimorphism and sex steroid modulation of glial fibrillary acidic protein messenger RNA and immunoreactivity levels in the rat hypothalamus. Neuroscience 69, 519–532. DOI:10.1016/0306-4522(95)00250-M

Chul Sung, K., Suh, J.Y., Kim, B.S., Kang, J.H., Kim, H., Lee, M.H., Park, J.R., et al., 2003. High sensitivity c-reactive protein as an independent risk factor for essential hypertension. Am. J. Hypertens. 16, 429–433. DOI:10.1016/S0895-7061(03)00566-1

Cinti, S., Mitchell, G., Barbatelli, G., Murano, I., Ceresi, E., Faloia, E., Wang, S., et al., 2005. Adipocyte death defines macrophage localization and function in adipose tissue of obese mice and humans. J. Lipid Res. 46, 2347–55. DOI:10.1194/jlr.M500294-JLR200

Coelho, M., Oliveira, T., Fernandes, R., 2013. Biochemistry of adipose tissue: an endocrine organ. Arch. Med. Sci. 9, 191–200. DOI:10.5114/aoms.2013.33181

Cohen, P., Zhao, C., Cai, X., Montez, J.M., Rohani, S.C., Feinstein, P., Mombaerts, P., et al., 2001. Selective deletion of leptin receptor in neurons leads to obesity. J. Clin. Invest. 108, 1113–21. DOI:10.1172/JCI13914

Conn, P.J., Sanders-Bush, E., Hoffman, B.J., Hartig, P.R., 1986. A unique serotonin receptor in choroid plexus is linked to phosphatidylinositol turnover. Proc. Natl. Acad. Sci. U. S. A. 83, 4086–8. DOI:10.1073/PNAS.83.11.4086

Cooper, M.S., Kriel, H., Sayers, A., Fraser, W.D., Williams, A.M., Stewart, P.M., Probert, C.S., et al., 2011. Can 11β-Hydroxysteroid Dehydrogenase Activity Predict the Sensitivity of Bone to Therapeutic Glucocorticoids in Inflammatory Bowel Disease? Calcif. Tissue Int. 89, 246–251. DOI:10.1007/s00223-011-9512-2

Corbett, J.J., 1983. Problems in the Diagnosis and Treatment of Pseudotumor Cerebri. Can. J. Neurol. Sci. / J. Can. des Sci. Neurol. 10, 221–229. DOI:10.1017/S0317167100045042

Corbett, J.J., Savino, P.J., Thompson, H.S., Kansu, T., Schatz, N.J., Orr, L.S., Hopson, D., 1982. Visual Loss in Pseudotumor Cerebri: Follow-up of 57 Patients From Five to 41 Years and a Profile of 14 Patients With Permanent Severe Visual Loss. Arch. Neurol. 39, 461–474. DOI:10.1001/archneur.1982.00510200003001

Cornford, E.M., Varesi, J.B., Hyman, S., Damian, R.T., Raleigh, M.J., 1997. Mitochondrial content of choroid plexus epithelium. Exp. Brain Res. 116, 399–405. DOI:10.1007/PL00005768

Costa, A.R., Marcelino, H., Gonçalves, I., Quintela, T., Tomás, J., Duarte, A.C., Fonseca, A.M., et al., 2016. Sex Hormones Protect Against Amyloid-β Induced Oxidative Stress in the Choroid Plexus Cell Line Z310. J. Neuroendocrinol. 28. DOI:10.1111/jne.12404

Couce, M.E., Burguera, B., Parisi, J.E., Jensen, M.D., Lloyd, R. V., 1997. Localization of Leptin Receptor in the Human Brain. Neuroendocrinology 66, 145–150. DOI:10.1159/000127232

Crown, S.B., Marze, N., Antoniewicz, M.R., 2015. Catabolism of Branched Chain Amino Acids Contributes Significantly to Synthesis of Odd-Chain and Even-Chain Fatty Acids in 3T3-L1 Adipocytes. PLoS One 10, e0145850. DOI:10.1371/journal.pone.0145850

Cushing, H., 1925. The third circulation and its channels. Lancet 206, 851–857. DOI:10.1016/S0140-6736(01)17422-2

Da Mesquita, S., Louveau, A., Vaccari, A., Smirnov, I., Cornelison, R.C., Kingsmore, K.M., Contarino, C., et al., 2018. Functional aspects of meningeal lymphatics in ageing and Alzheimer's disease. Nature 1. DOI:10.1038/s41586-018-0368-8

Dagogo-Jack, S., Selke, G., Melson, A.K., Newcomer, J.W., 1997. Robust Leptin Secretory Responses to Dexamethasone in Obese Subjects 1. J. Clin. Endocrinol. Metab. 82, 3230–3233. DOI:10.1210/jcem.82.10.4154

Damkier, H.H., Prasad, V., Hübner, C.A., Praetorius, J., 2009. Nhe1 is a luminal Na^+/H^+ exchanger in mouse choroid plexus and is targeted to the basolateral membrane in Ncbe/Nbcn2-null mice. Am. J. Physiol. Physiol. 296, C1291–C1300. DOI:10.1152/ajpcell.00062.2009

Dandona, P., Aljada, A., Bandyopadhyay, A., 2004. Inflammation: the link between insulin resistance, obesity and diabetes. Trends Immunol. 25, 4–7. DOI:10.1016/J.IT.2003.10.013

Dandy, W.E., 1937. Intracranial Pressure Without Brain Tumor: Diagnosis and Treatment. Ann. Surg. 106, 492–513.

de Rougemont, J., Ames, A., Nesbett, F.B., Hofmann, H.F., 1960. Fluid formed by choroid plexus; a technique for its collection and a comparison of its electrolyte composition with serum and cisternal fluids. J. Neurophysiol. 23, 485–95. DOI:10.1152/jn.1960.23.5.485

Dewundara, S.S., Wiggs, J.L., Sullivan, D.A., Pasquale, L.R., 2016. Is Estrogen a Therapeutic Target for Glaucoma? Semin. Ophthalmol. 31, 140–6. DOI:10.3109/08820538.2015.1114845

Dhungana, S., Sharrack, B., Woodroofe, N., 2009. Cytokines and chemokines in idiopathic intracranial hypertension. Headache 49, 282–285. DOI:10.1111/j.1526-4610.2008.001329.x

Dobin, A., Davis, C.A., Schlesinger, F., Drenkow, J., Zaleski, C., Jha, S., Batut, P., et al., 2013. STAR: ultrafast universal RNA-seq aligner. Bioinformatics 29, 15–21. DOI:10.1093/bioinformatics/bts635

Donaldson, J.O., 1979. Cerebrospinal fluid hypersecretion in pseudotumor cerebri. Trans. Am. Neurol. Assoc. 104, 196–8.

Donaldson, J.O., Horak, E., 1982. Cerebrospinal fluid oestrone in pseudotumour cerebri. J. Neurol. Neurosurg. Psychiatry 45, 734–6. DOI:10.1136/JNNP.45.8.734

Dunn, L.T., 2002. Raised intracranial pressure. J. Neurol. Neurosurg. Psychiatry 73 Suppl 1, i23-7. DOI:10.1136/JNNP.73.SUPPL_1.I23

Eide, P.K., Eidsvaag, V.A., Nagelhus, E.A., Hansson, H.A., 2016. Cortical astrogliosis and increased perivascular aquaporin-4 in idiopathic intracranial hypertension. Brain Res. 1644, 161–175. DOI:10.1016/j.brainres.2016.05.024

Eide, P.K., Kerty, E., 2011. Static and pulsatile intracranial pressure in idiopathic intracranial hypertension. Clin. Neurol. Neurosurg. 113, 123–128. DOI:10.1016/J.CLINEURO.2010.10.008

Faraci, F.M., Mayhan, W.G., Heistad, D.D., 1990. Effect of vasopressin on production of cerebrospinal fluid: possible role of vasopressin (V1)-receptors. Am. J. Physiol. 258, R94-8. DOI:10.1152/ajpregu.1990.258.1.R94

Farooqi, I.S., Jebb, S.A., Langmack, G., Lawrence, E., Cheetham, C.H., Prentice, A.M., Hughes, I.A., et al., 1999. Effects of Recombinant Leptin Therapy in a Child with Congenital Leptin Deficiency. N. Engl. J. Med. 341, 879–884. DOI:10.1056/NEJM199909163411204

FDA, 2005. Guidance for Industry Estimating the Maximum Safe Starting Dose in Initial Clinical Trials for Therapeutics in Adult Healthy Volunteers Pharmacology and Toxicology Guidance for Industry Estimating the Maximum Safe Starting Dose in Initial Clinical Trials [WWW Document]. URL http://www.fda.gov/cder/guidance/index.htm (accessed 11.16.18).

Fei, H., Okano, H.J., Li, C., Lee, G.-H., Zhao, C., Darnell, R., Friedman, J.M., 1997. Anatomic localization of alternatively spliced leptin receptors (Ob-R) in mouse brain and other tissues. Proc. Natl. Acad. Sci. 94, 7001–7005. DOI:10.1073/pnas.94.13.7001

Finsterer, J., Kues, E.W., Brunner, S., 2006. Pseudotumour cerebri in a young obese woman on oral contraceptives. Eur. J. Contracept. Reprod. Heal. Care 11, 237–240. DOI:10.1080/13625180600766396

Flegal, K.M., Kit, B.K., Orpana, H., Graubard, B.I., 2013. Association of all-cause mortality with overweight and obesity using standard body mass index categories: a systematic review and meta-analysis. JAMA 309, 71–82. DOI:10.1001/jama.2012.113905

Franck, N., Gummesson, A., Jernås, M., Glad, C., Svensson, P.A., Guillot, G., Rudemo, M., et al., 2011. Identification of adipocyte genes regulated by caloric intake. J. Clin. Endocrinol. Metab. 96, E413–E418. DOI:10.1210/jc.2009-2534

Fraser, J.A., Bruce, B.B., Rucker, J., Fraser, L.-A., Atkins, E.J., Newman, N.J., Biousse, V., 2010. Risk factors for idiopathic intracranial hypertension in men: a case-control study. J. Neurol. Sci. 290, 86–9. DOI:10.1016/j.jns.2009.11.001

Friesner, D., Rosenman, R., Lobb, B.M., Tanne, E., 2011. Idiopathic intracranial hypertension in the USA: The role of obesity in establishing prevalence and healthcare costs. Obes. Rev. 12, e372–e380. DOI:10.1111/j.1467-789X.2010.00799.x

Galarraga, M., Campión, J., Muñoz-Barrutia, A., Boqué, N., Moreno, H., Martínez, J.A., Milagro, F., et al., 2012. Adiposoft: automated software for the analysis of white adipose tissue cellularity in histological sections. J. Lipid Res. 53, 2791–2796. DOI:10.1194/jlr.D023788

Gettys, T.W., Harkness, P.J., Watson, P.M., 1996. The beta 3-adrenergic

receptor inhibits insulin-stimulated leptin secretion from isolated rat adipocytes. Endocrinology 137, 4054–4057. DOI:10.1210/endo.137.9.8756584

Gideon, P., Sørensen, P.S., Thomsen, C., Ståhlberg, F., Gjerris, F., Henriksen, O., 1994. Assessment of CSF dynamics and venous flow in the superior sagittal sinus by MRI in idiopathic intracranial hypertension: a preliminary study. Neuroradiology 36, 350–4.

Giuseffi, V., Wall, M., Siegel, P.Z., Rojas, P.B., 1991. Symptoms and disease associations in idiopathic intracranial hypertension (pseudotumor cerebri): a case-control study. Neurology 41, 239–44. DOI:10.1212/WNL.41.2_PART_1.239

Glueck, C.J., Aregawi, D., Goldenberg, N., Golnik, K.C., Sieve, L., Wang, P., 2005. Idiopathic intracranial hypertension, polycystic-ovary syndrome, and thrombophilia. J. Lab. Clin. Med. 145, 72–82. DOI:10.1016/j.lab.2004.09.011

Glueck, C.J., Iyengar, S., Goldenberg, N., Smith, L.-S., Wang, P., 2003. Idiopathic intracranial hypertension: associations with coagulation disorders and polycystic-ovary syndrome. J. Lab. Clin. Med. 142, 35–45. DOI:10.1016/S0022-2143(03)00069-6

Gonçalves, I., Hubbard, P.C., Tomás, J., Quintela, T., Tavares, G., Caria, S., Barreiros, D., et al., 2016. 'Smelling' the cerebrospinal fluid: olfactory signaling molecules are expressed in and mediate chemosensory signaling from the choroid plexus. FEBS J. 283, 1748–1766. DOI:10.1111/febs.13700

Griekspoor, A., Zwart, W., Neefjes, J., Michalides, R., 2007. Visualizing the action of steroid hormone receptors in living cells. Nucl. Recept. Signal. 5, e003. DOI:10.1621/nrs.05003

Grossman, E.B., Hebert, S.C., 1988. Modulation of Na-K-ATPase activity in the mouse medullary thick ascending limb of Henle. Effects of mineralocorticoids and sodium. J. Clin. Invest. 81, 885–892. DOI:10.1172/JCI113399

Haas, M., Forbush III, B., 2000. The Na-K-Cl Cotransporter of Secretory Epithelia. Annu. Rev. Physiol. 62, 515–534. DOI:10.1146/annurev.physiol.62.1.515

Hakvoort, A., Haselbach, M., Galla, H.J., 1998. Active transport properties of porcine choroid plexus cells in culture. Brain Res. 795, 247–256. DOI:10.1016/S0006-8993(98)00284-4

Halaas, J.L., Boozer, C., Blair-West, J., Fidahusein, N., Denton, D.A., Friedman, J.M., 1997. Physiological response to long-term peripheral and central leptin infusion in lean and obese mice. Proc. Natl. Acad. Sci. U. S. A. 94, 8878–83. DOI:10.1073/PNAS.94.16.8878

Hamann, S., Herrera-Perez, J.J., Zeuthen, T., Alvarez-Leefmans, F.J., 2010. Cotransport of water by the Na+-K+-2Cl cotransporter NKCC1 in mammalian epithelial cells. J. Physiol. 588, 4089–4101. DOI:10.1113/jphysiol.2010.194738

Hammarström, L., 1966. AUTORADIOGRAPHIC STUDIES ON THE DISTRIBUTION OF C 14 -LABELLED ASCORBIC ACID AND DEHYDROASCORBIC ACID. Acta Physiol. Scand. 70, 1–83. DOI:10.1111/j.1748-1716.1966.tb03661.x

Handoko, K., Yang, K., Strutt, B., Khalil, W., Killinger, D., 2000. Insulin attenuates the stimulatory effects of tumor necrosis factor α on 11β-hydroxysteroid dehydrogenase 1 in human adipose stromal cells. J. Steroid Biochem. Mol. Biol. 72, 163–168. DOI:10.1016/S0960-0760(00)00029-7

Hannerz, J., Antovic, J.P., Blombäck, M., Edman, G., Khademi, M., Piehl, F., 2011. Inflammatory and haemostatic markers in idiopathic intracranial hypertension. J. Intern. Med. 270, 496–499. DOI:10.1111/j.1365-2796.2011.02446.x

Hardy, R., Rabbitt, E.H., Filer, A., Emery, P., Hewison, M., Stewart, P.M., Gittoes, N.J., et al., 2008. Local and systemic glucocorticoid metabolism in inflammatory arthritis. Ann. Rheum. Dis. 67, 1204–10. DOI:10.1136/ard.2008.090662

Hatem, C.F., Yri, H.M., Sørensen, A.L., Wegener, M., Jensen, R.H., Hamann, S., 2018. Long-term visual outcome in a Danish population of patients with idiopathic intracranial hypertension. Acta Ophthalmol. 96, 1–5. DOI:10.1111/aos.13664

Haystead, T.A.J., Grahame, D., 1986. Evidence that activation of acetyl-CoA carboxylase by insulin in adipocytes is mediated by a low-Mr effector and not by increased phosphorylation, Biochem. J.

Hayw, J.R., Vogh, B.P., 1979. Some Measurements of Autonomic Nervous System Influence on Production of Cerebrospinal Fluid in the Cat. J. Pharmacol. Exp. Ther. 208, 341–346.

Heisey, S.R., Held, D., Pappenheimer, J.R., 1962. Bulk flow and diffusion in the cerebrospinal fluid system of the goat. Am. J. Physiol. Content 203, 775–781. DOI:10.1152/ajplegacy.1962.203.5.775

Hewitt, K.N., Walker, E.A., Stewart, P.M., 2005. Minireview: Hexose-6-Phosphate Dehydrogenase and Redox Control of 11β-Hydroxysteroid Dehydrogenase Type 1 Activity. Endocrinology 146, 2539–2543. DOI:10.1210/en.2005-0117

Hibuse, T., Maeda, N., Nagasawa, A., Funahashi, T., 2006. Aquaporins and glycerol metabolism. Biochim. Biophys. Acta - Biomembr. 1758, 1004–1011. DOI:10.1016/J.BBAMEM.2006.01.008

Hochberg, I., Harvey, I., Tran, Q.T., Stephenson, E.J., Barkan, A.L., Saltiel, A.R., Chandler, W.F., et al., 2015. Gene expression changes in subcutaneous adipose tissue due to cushing's disease. J. Mol. Endocrinol. 55, 81–94. DOI:10.1530/JME-15-0119

Hodson, D.J., Tarasov, A.I., Gimeno Brias, S., Mitchell, R.K., Johnston, N.R., Haghollahi, S., Cane, M.C., et al., 2014. Incretin-Modulated Beta Cell Energetics in Intact Islets of Langerhans. Mol. Endocrinol. 28, 860–871. DOI:10.1210/me.2014-1038

Hornby, C., Botfield, H.F., O'Reilly, M.W., Westgate, C., Mitchell, J., Mollan, S.P., Manolopoulos, K., et al., 2018a. Evaluating the Fat Distribution in Idiopathic Intracranial Hypertension Using Dual-Energy X-ray Absorptiometry Scanning. Neuro-Ophthalmology 42, 99–104. DOI:10.1080/01658107.2017.1334218

Hornby, C., Mollan, S.P., Botfield, H.F., O'Reilly, M.W., Sinclair, A.J., 2018b. Metabolic Concepts in Idiopathic Intracranial Hypertension and Their Potential for Therapeutic Intervention. J. Neuro-Ophthalmology 1. DOI:10.1097/WNO.0000000000000684

Hornby, C., Mollan, S.P., Mitchell, J., Markey, K.A., Yiangou, A., Wright, B.L.C., O'Reilly, M.W., et al., 2017. What Do Transgender Patients Teach Us About Idiopathic Intracranial Hypertension? Neuro-Ophthalmology 41, 326–329. DOI:10.1080/01658107.2017.1316744

Hotamisligil, G.S., Arner, P., Caro, J.F., Atkinson, R.L., Spiegelman, B.M., 1995. Increased adipose tissue expression of tumor necrosis factor-alpha in human obesity and insulin resistance. J. Clin. Invest. 95, 2409–2415. DOI:10.1172/JCI117936

Hotamisligil, G.S., Peraldi, P., Budavari, A., Ellis, R., White, M.F., Spiegelman, B.M., 1996. IRS-1-mediated inhibition of insulin receptor tyrosine kinase activity in TNF-alpha- and obesity-induced insulin resistance. Science 271, 665–8. DOI:10.1126/SCIENCE.271.5249.665

Huang, S., Czech, M.P., 2007. The GLUT4 Glucose Transporter. Cell Metab. 5, 237–252. DOI:10.1016/J.CMET.2007.03.006

Ibañez-Tallon, I., Pagenstecher, A., Fliegauf, M., Olbrich, H., Kispert, A., Ketelsen, U.-P., North, A., et al., 2004. Dysfunction of axonemal dynein heavy chain Mdnah5 inhibits ependymal flow and reveals a novel mechanism for hydrocephalus formation. Hum. Mol. Genet. 13, 2133–2141. DOI:10.1093/hmg/ddh219

Ichikawa, N., Naora, K., Hirano, H., Iwamoto, K., 1998. Quantitation of acetazolamide in rat plasma, brain tissue and cerebrospinal fluid by high-performance liquid chromatography. J. Pharm. Biomed. Anal. 17, 1415–1421. DOI:10.1016/S0731-7085(98)00024-7

Iliff, J.J., Wang, M., Liao, Y., Plogg, B.A., Peng, W., Gundersen, G.A.,

Benveniste, H., et al., 2012. A paravascular pathway facilitates CSF flow through the brain parenchyma and the clearance of interstitial solutes, including amyloid β. Sci. Transl. Med. 4, 147ra111. DOI:10.1126/scitranslmed.3003748

Iliff, J.J., Wang, M., Zeppenfeld, D.M., Venkataraman, A., Plog, B.A., Liao, Y., Deane, R., et al., 2013. Cerebral Arterial Pulsation Drives Paravascular CSF-Interstitial Fluid Exchange in the Murine Brain. J. Neurosci. 33, 18190–18199. DOI:10.1523/JNEUROSCI.1592-13.2013

Ishunina, T.A., Van Beurden, D., Van Der Meulen, G., Unmehopa, U.A., Hol, E.M., Huitinga, I., Swaab, D.F., 2005. Diminished aromatase immunoreactivity in the hypothalamus, but not in the basal forebrain nuclei in Alzheimer's disease. Neurobiol. Aging 26, 173–194. DOI:10.1016/j.neurobiolaging.2004.03.010

Janny, P., Chazal, J., Colnet, G., Irthum, B., Georget, A.-M., 1981. Benign intracranial hypertension and disorders of CSF absorption. Surg. Neurol. 15, 168–174. DOI:10.1016/0090-3019(81)90131-2

Jeffery, S., Carter, N.D., Wilsont, C., 1984. Carbonic anhydrase II isoenzyme in rat liver is under hormonal control. Biochem. J 221, 927–929.

Jensen, R.H., Radojicic, A., Yri, H.M., 2016. The diagnosis and management of idiopathic intracranial hypertension and the associated headache. Ther. Adv. Neurol. Disord. 9, 317–326. DOI:10.1177/1756285616635987

Johnston, M., Zakharov, A., Papaiconomou, C., Salmasi, G., Armstrong, D., 2004. Evidence of connections between cerebrospinal fluid and nasal lymphatic vessels in humans, non-human primates and other mammalian species. Cerebrospinal Fluid Res. 1, 2. DOI:10.1186/1743-8454-1-2

Jones, H.C., Deane, R., Bucknall, R.M., 1987. Developmental changes in cerebrospinal fluid pressure and resistance to absorption in rats. Brain Res. 430, 23–30.

Kapoor, K.G., 2015. Regarding Secondary Intracranial Hypertension from Testostereone Therapy in a Transgender Patient. Semin. Ophthalmol. 30, 241–242. DOI:10.3109/08820538.2013.847111

Karimy, J.K., Zhang, J., Kurland, D.B., Theriault, B.C., Duran, D., Stokum, J.A., Furey, C.G., et al., 2017. Inflammation-dependent cerebrospinal fluid hypersecretion by the choroid plexus epithelium in posthemorrhagic hydrocephalus. Nat. Med. 23, 997–1003. DOI:10.1038/nm.4361

Kass, M.A., Sears, M.L., 1977. Hormonal regulation of intraocular pressure. Surv. Ophthalmol. 22, 153–176. DOI:10.1016/0039-6257(77)90053-4

Katz, S.E., Klisovic, D.D., O'Dorisio, M.S., Lynch, R., Lubow, M., 2002. Expression of Somatostatin Receptors 1 and 2 in Human Choroid Plexus and Arachnoid Granulations. Arch. Ophthalmol. 120, 1540.

DOI:10.1001/archopht.120.11.1540

Keep, R.F., Jones, H.C., 1990. A morphometric study on the development of the lateral ventricle choroid plexus, choroid plexus capillaries and ventricular ependyma in the rat. Dev. Brain Res. 56, 47–53. DOI:10.1016/0165-3806(90)90163-S

Kelesidis, T., Kelesidis, I., Chou, S., Mantzoros, C.S., 2010. Narrative review: the role of leptin in human physiology: emerging clinical applications. Ann. Intern. Med. 152, 93–100. DOI:10.7326/0003-4819-152-2-201001190-00008

Kern, P.A., Di Gregorio, G.B., Lu, T., Rassouli, N., Ranganathan, G., 2003. Adiponectin expression from human adipose tissue: relation to obesity, insulin resistance, and tumor necrosis factor-alpha expression. Diabetes 52, 1779–85. DOI:10.2337/DIABETES.52.7.1779

Kersten, S., 2001. Mechanisms of nutritional and hormonal regulation of lipogenesis. EMBO Rep. 2, 282–6. DOI:10.1093/embo-reports/kve071

Kesler, A., Kliper, E., Shenkerman, G., Stern, N., 2010. Idiopathic Intracranial Hypertension Is Associated with Lower Body Adiposity. Ophthalmology 117, 169–174. DOI:10.1016/J.OPHTHA.2009.06.030

Kilgore, K.P., Lee, M.S., Leavitt, J.A., Frank, R.D., McClelland, C.M., Chen, J.J., 2018. A Population-Based, Case-Control Evaluation of the Association between Hormonal Contraceptives and Idiopathic Intracranial Hypertension. Am. J. Ophthalmol. 197, 74–79. DOI:10.1016/j.ajo.2018.09.014

Killinger, D.W., Perel, E., Daniilescu, D., Kharlip, L., Lindsay, W.R.N., 1987. The relationship between aromatase activity and body fat distribution. Steroids 50, 61–72. DOI:10.1016/0039-128X(83)90062-4

Kim, D.-J., Czosnyka, Z., Kasprowicz, M., Smieleweski, P., Baledent, O., Guerguerian, A.-M., Pickard, J.D., et al., 2012. Continuous Monitoring of the Monro-Kellie Doctrine: Is It Possible? J. Neurotrauma 29, 1354–1363. DOI:10.1089/neu.2011.2018

Kiser, P.D., Palczewski, K., 2016. Retinoids and Retinal Diseases. Annu. Rev. Vis. Sci. 2, 197–234. DOI:10.1146/annurev-vision-111815-114407

Klarr, S.A., Ulanski, L.J., Stummer, W., Xiang, J., Betz, A.L., Keep, R.F., 1997. The effects of hypo- and hyperkalemia on choroid plexus potassium transport. Brain Res. 758, 39–44. DOI:10.1016/S0006-8993(96)01440-0

Klein, A., Stern, N., Osher, E., Kliper, E., Kesler, A., 2013. Hyperandrogenism is associated with earlier age of onset of idiopathic intracranial hypertension in women. Curr. Eye Res. 38, 972–976. DOI:10.3109/02713683.2013.799214

Kolaczynski, J.W., Nyce, M.R., Considine, R. V, Boden, G., Nolan, J.J., Henry, R., Mudaliar, S.R., et al., 1996. Acute and chronic effects of insulin on leptin production in humans: Studies in vivo and in vitro. Diabetes 45, 699–701. DOI:10.2337/DIAB.45.5.699

Korek, E., Krauss, H., Gibas-Dorna, M., Kupsz, J., Piątek, M., Piątek, J., 2013. Fasting and postprandial levels of ghrelin, leptin and insulin in lean, obese and anorexic subjects. Prz. Gastroenterol. 8, 383–9. DOI:10.5114/pg.2013.39922

Kuehn, M.H., Mishra, R., Deonovic, B.E., Miller, K.N., McCormack, S.E., Liu, G.T., Kupersmith, M.J., et al., 2018. Genetic Survey of Adult-Onset Idiopathic Intracranial Hypertension. J. Neuroophthalmol. 1. DOI:10.1097/WNO.0000000000000648

Lampl, Y., Eshel, Y., Kessler, A., Fux, A., Gilad, R., Boaz, M., Matas, Z., et al., 2002. Serum leptin level in women with idiopathic intracranial hypertension. J. Neurol. Neurosurg. Psychiatry 72, 642–643. DOI:10.1136/jnnp.72.5.642

Langendonk, J.G., Pijl, H., Toornvliet, A.C., Burggraaf, J., Frölich, M., Schoemaker, R.C., Doornbos, J., et al., 1998. Circadian Rhythm of Plasma Leptin Levels in Upper and Lower Body Obese Women: Influence of Body Fat Distribution and Weight Loss. J. Clin. Endocrinol. Metab. 83, 1706–1712. DOI:10.1210/jcem.83.5.4717

Lawrence, M., Huber, W., Pagès, H., Aboyoun, P., Carlson, M., Gentleman, R., Morgan, M.T., et al., 2013. Software for Computing and Annotating Genomic Ranges. PLoS Comput. Biol. 9, e1003118. DOI:10.1371/journal.pcbi.1003118

Levy, J.R., Gyarmati, J., Lesko, J.M., Adler, R.A., Stevens, W., 2000. Dual regulation of leptin secretion: intracellular energy and calcium dependence of regulated pathway. Am. J. Physiol. Metab. 278, E892–E901. DOI:10.1152/ajpendo.2000.278.5.E892

Libien, J., Kupersmith, M.J., Blaner, W., McDermott, M.P., Gao, S., Liu, Y., Corbett, J., et al., 2017. Role of vitamin A metabolism in IIH: Results from the idiopathic intracranial hypertension treatment trial. J. Neurol. Sci. 372, 78–84. DOI:10.1016/j.jns.2016.11.014

Lindvall-Axelsson, M., Owman, C., 1989. Changes in transport functions of isolated rabbit choroid plexus under the influence of oestrogen and progesterone. Acta Physiol. Scand. 136, 107–111. DOI:10.1111/j.1748-1716.1989.tb08635.x

Livingstone, D.E.W., Di Rollo, E.M., Yang, C., Codrington, L.E., Mathews, J.A., Kara, M., Hughes, K.A., et al., 2014. Relative adrenal insufficiency in mice deficient in 5α-reductase 1. J. Endocrinol. 222, 257–266. DOI:10.1530/JOE-13-0563

Locke, A.E., Kahali, B., Berndt, S.I., Justice, A.E., Pers, T.H., Day, F.R., Powell,

C., et al., 2015. Genetic studies of body mass index yield new insights for obesity biology. Nature 518, 197–206. DOI:10.1038/nature14177

Lönnqvist, F., Nordfors, L., Jansson, M., Thörne, A., Schalling, M., Arner, P., 1997. Leptin secretion from adipose tissue in women. Relationship to plasma levels and gene expression. J. Clin. Invest. 99, 2398–404. DOI:10.1172/JCI119422

Louveau, A., Smirnov, I., Keyes, T.J., Eccles, J.D., Rouhani, S.J., Peske, J.D., Derecki, N.C., et al., 2015. Structural and functional features of central nervous system lymphatic vessels. Nature 523, 337–341. DOI:10.1038/nature14432

Love, M.I., Huber, W., Anders, S., 2014. Moderated estimation of fold change and dispersion for RNA-seq data with DESeq2. Genome Biol. 15, 550. DOI:10.1186/s13059-014-0550-8

Ludwig, C., Gunther, U.L., 2011. MetaboLab - advanced NMR data processing and analysis for metabolomics. BMC Bioinformatics 12, 366. DOI:10.1186/1471-2105-12-366

MacAulay, N., Zeuthen, T., 2010. Water transport between CNS compartments: contributions of aquaporins and cotransporters. Neuroscience 168, 941–956. DOI:10.1016/J.NEUROSCIENCE.2009.09.016

Maffei, M., Halaas, J., Ravussin, E., Pratley, R.E., Lee, G.H., Zhang, Y., Fei, H., et al., 1995. Leptin levels in human and rodent: Measurement of plasma leptin and ob RNA in obese and weight-reduced subjects. Nat. Med. 1, 1155–1161. DOI:10.1038/nm1195-1155

Mahendroo, M.S., Cala, K.M., Russell, D.W., 1996. 5 alpha-reduced androgens play a key role in murine parturition. Mol. Endocrinol. 10, 380–392. DOI:10.1210/mend.10.4.8721983

Malm, J., Kristensen, B., Markgren, P., Ekstedt, J., 1992. CSF hydrodynamics in idiopathic intracranial hypertension: a long-term study. Neurology 42, 851–8. DOI:10.1212/WNL.42.4.851

Malmström, R., Taskinen, M.-R., Karonen, S.-L., Yki-Järvinen, H., 1996. Insulin increases plasma leptin concentrations in normal subjects and patients with NIDDM. Diabetologia 39, 993–996. DOI:10.1007/BF00403921

Manolopoulos, K.N., Karpe, F., Frayn, K.N., 2010. Gluteofemoral body fat as a determinant of metabolic health. Int. J. Obes. 34, 949–959. DOI:10.1038/ijo.2009.286

March, W.A., Moore, V.M., Willson, K.J., Phillips, D.I.W., Norman, R.J., Davies, M.J., 2010. The prevalence of polycystic ovary syndrome in a community sample assessed under contrasting diagnostic criteria. Hum. Reprod. 25, 544–551. DOI:10.1093/humrep/dep399

Markey, K.A., Mollan, S.P., Jensen, R.H., Sinclair, A.J., 2016a. Understanding idiopathic intracranial hypertension: Mechanisms, management, and future directions. Lancet Neurol. 15, 78–91. DOI:10.1016/S1474-4422(15)00298-7

Markey, K.A., Ottridge, R., Mitchell, J.L., Rick, C., Woolley, R., Ives, N., Nightingale, P., et al., 2017. Assessing the Efficacy and Safety of an 11β-Hydroxysteroid Dehydrogenase Type 1 Inhibitor (AZD4017) in the Idiopathic Intracranial Hypertension Drug Trial, IIH:DT: Clinical Methods and Design for a Phase II Randomized Controlled Trial. JMIR Res. Protoc. 6, e181. DOI:10.2196/resprot.7806

Markey, K.A., Uldall, M.S., Botfield, H.F., Cato, L.D., Miah, M.A.L., Hassan-Smith, G., Jensen, R.H., et al., 2016b. Idiopathic intracranial hypertension, hormones, and 11β-hydroxysteroid dehydrogenases. J. Pain Res. 9, 223–232. DOI:10.2147/JPR.S80824

Martin, M., 2011. Cutadapt removes adapter sequences from high-throughput sequencing reads. EMBnet.journal 17, 10. DOI:10.14806/ej.17.1.200

Masuzaki, H., Ogawa, Y., Hosoda, K., Miyawaki, T., Hanaoka, I., Hiraoka, J., Yasuno, A., et al., 1997. Glucocorticoid Regulation of Leptin Synthesis and Secretion in Humans: Elevated Plasma Leptin Levels in Cushing's Syndrome [1]. J. Clin. Endocrinol. Metab. 82, 2542–2547. DOI:10.1210/jcem.82.8.4128

Masuzaki, H., Paterson, J., Shinyama, H., Morton, N.M., Mullins, J.J., Seckl, J.R., Flier, J.S., 2001. A transgenic model of visceral obesity and the metabolic syndrome. Science (80-.). 294, 2166–2170. DOI:10.1126/science.1066285

Maus, T.L., Larsson, L.-I., McLaren, J.W., Brubaker, R.F., 1997. Comparison of Dorzolamide and Acetazolamide as Suppressors of Aqueous Humor Flow in Humans. Arch. Ophthalmol. 115, 45. DOI:10.1001/archopht.1997.01100150047008

McLaren, L., 2007. Socioeconomic Status and Obesity. Epidemiol. Rev. 29, 29–48. DOI:10.1093/epirev/mxm001

Miller, W.L., Auchus, R.J., 2011. The molecular biology, biochemistry, and physiology of human steroidogenesis and its disorders. Endocr. Rev. 32, 81–151. DOI:10.1210/er.2010-0013

Mitchell, S.E., Nogueiras, R., Morris, A., Tovar, S., Grant, C., Cruickshank, M., Rayner, D.V., et al., 2009. Leptin receptor gene expression and number in the brain are regulated by leptin level and nutritional status. J. Physiol. 587, 3573–3585. DOI:10.1113/jphysiol.2009.173328

Mokdad, A.H., Ford, E.S., Bowman, B.A., Dietz, W.H., Vinicor, F., Bales, V.S., Marks, J.S., 2003. Prevalence of Obesity, Diabetes, and Obesity-Related Health Risk Factors, 2001. JAMA 289, 76–79. DOI:10.1001/jama.289.1.76

Mollan, S.P., Aguiar, M., Evison, F., Frew, E., Sinclair, A.J., 2018a. The expanding burden of Idiopathic Intracranial Hypertension. Eye 1. DOI:10.1038/s41433-018-0238-5

Mollan, S.P., Ali, F., Hassan-Smith, G., Botfield, H.F., Friedman, D.I., Sinclair, A.J., 2016. Evolving evidence in adult idiopathic intracranial hypertension: Pathophysiology and management. J. Neurol. Neurosurg. Psychiatry 87, 982–992. DOI:10.1136/jnnp-2015-311302

Mollan, S.P., Davies, B., Silver, N.C., Shaw, S., Mallucci, C.L., Wakerley, B.R., Krishnan, A., et al., 2018b. Idiopathic intracranial hypertension: consensus guidelines on management. J. Neurol. Neurosurg. Psychiatry 89, 1088–1100. DOI:10.1136/jnnp-2017-317440

Montague, C.T., Farooqi, I.S., Whitehead, J.P., Soos, M.A., Rau, H., Wareham, N.J., Sewter, C.P., et al., 1997. Congenital leptin deficiency is associated with severe early-onset obesity in humans. Nature 387, 903–908. DOI:10.1038/43185

Mootha, V.K., Lindgren, C.M., Eriksson, K.-F., Subramanian, A., Sihag, S., Lehar, J., Puigserver, P., et al., 2003. PGC-1α-responsive genes involved in oxidative phosphorylation are coordinately downregulated in human diabetes. Nat. Genet. 34, 267–273. DOI:10.1038/ng1180

Morgan, S.A., McCabe, E.L., Gathercole, L.L., Hassan-Smith, Z.K., Larner, D.P., Bujalska, I.J., Stewart, P.M., et al., 2014. 11β-HSD1 is the major regulator of the tissue-specific effects of circulating glucocorticoid excess. Proc. Natl. Acad. Sci. U. S. A. 111, E2482-91. DOI:10.1073/pnas.1323681111

Mortazavi, M.M., Romeo, A.K., Deep, A., Griessenauer, C.J., Shoja, M.M., Tubbs, R.S., Fisher, W., 2012. Hypertonic saline for treating raised intracranial pressure: literature review with meta-analysis. J. Neurosurg. 116, 210–221. DOI:10.3171/2011.7.JNS102142

Mulla, Y., Markey, K.A., Woolley, R.L., Patel, S., Mollan, S.P., Sinclair, A.J., 2015. Headache determines quality of life in idiopathic intracranial hypertension. J. Headache Pain 16, 521. DOI:10.1186/s10194-015-0521-9

Nam, S.-Y., Kratzsch, J., Wook Kim, K., Rae Kim, K., Lim, S.-K., Marcus, C., 2001. Cerebrospinal Fluid and Plasma Concentrations of Leptin, NPY, andα -MSH in Obese Women and Their Relationship to Negative Energy Balance. J. Clin. Endocrinol. Metab. 86, 4849–4853. DOI:10.1210/jcem.86.10.7939

Nilsson, C., Ståhlberg, F., Thomsen, C., Henriksen, O., Herning, M., Owman, C., 1992. Circadian variation in human cerebrospinal fluid production measured by magnetic resonance imaging. Am. J. Physiol. 262, R20-4. DOI:10.1152/ajpregu.1992.262.1.R20

O'Reilly, M.W., House, P.J., Tomlinson., J.W., 2014. Understanding androgen

action in adipose tissue. J. Steroid Biochem. Mol. Biol. 143, 277–284. DOI:10.1016/j.jsbmb.2014.04.008

O'Reilly, M.W., Kempegowda, P., Walsh, M., Taylor, A.E., Manolopoulos, K.N., Allwood, J.W., Semple, R.K., et al., 2017. AKR1C3-Mediated Adipose Androgen Generation Drives Lipotoxicity in Women With Polycystic Ovary Syndrome. J. Clin. Endocrinol. Metab. 102, 3327–3339. DOI:10.1210/jc.2017-00947

O'Reilly, M.W., Westgate, C.S.J., Hornby, C., Botfield, H., Taylor, A.E., Markey, K., Mitchell, J.L., et al., 2019. A unique androgen excess signature in idiopathic intracranial hypertension is linked to cerebrospinal fluid dynamics. JCI Insight 4, e125348. DOI:10.1172/jci.insight.125348

Oie, S., Matsuzaki, K., Yokoyama, W., Tokunaga, S., Waku, T., Han, S.I., Iwasaki, N., et al., 2014. Hepatic rRNA Transcription Regulates High-Fat-Diet-Induced Obesity. Cell Rep. 7, 807–820. DOI:10.1016/j.celrep.2014.03.038

Orefice, G., Celentano, L., Scaglione, M., Davoli, M., Striano, S., 1992. Radioisotopic cisternography in benign intracranial hypertension of young obese women. A seven-case study and pathogenetic suggestions. Acta Neurol. (Napoli). 14, 39–50.

Oshio, K., Watanabe, H., Song, Y., Verkman, A.., Manley, G., 2004. Reduced cerebrospinal fluid production and intracranial pressure in mice lacking choroid plexus water channel Aquaporin-1. FASEB J. 19, 76–78. DOI:10.1096/fj.04-1711fje

Ottridge, R., Mollan, S.P., Botfield, H.F., Frew, E., Ives, N.J., Matthews, T., Mitchell, J., et al., 2017. Randomised controlled trial of bariatric surgery versus a community weight loss programme for the sustained treatment of idiopathic intracranial hypertension: the Idiopathic Intracranial Hypertension Weight Trial (IIH:WT) protocol. BMJ Open 7, e017426. DOI:10.1136/bmjopen-2017-017426

Panagopoulos, G.N., Deftereos, S.N., Tagaris, G.A., Gryllia, M., Kounadi, T., Karamani, O., Panagiotidis, D., et al., 2007. Octreotide: a therapeutic option for idiopathic intracranial hypertension. Neurol. Neurophysiol. Neurosci. 1.

Patsouris, D., Li, P.-P., Thapar, D., Chapman, J., Olefsky, J.M., Neels, J.G., 2008. Ablation of CD11c-positive cells normalizes insulin sensitivity in obese insulin resistant animals. Cell Metab. 8, 301–9. DOI:10.1016/j.cmet.2008.08.015

Pelleymounter, M.A., Cullen, M.J., Baker, M.B., Hecht, R., Winters, D., Boone, T., Collins, F., 1995. Effects of the obese gene product on body weight regulation in ob/ob mice. Science 269, 540–3. DOI:10.1126/SCIENCE.7624776

Piper, R.J., Kalyvas, A. V., Young, A.M.H., Hughes, M.A., Jamjoom, A.A.B., Fouyas, I.P., 2015. Interventions for idiopathic intracranial hypertension. Cochrane Database Syst. Rev. 2015. DOI:10.1002/14651858.CD003434.pub3

Pollay, M., 2010. The function and structure of the cerebrospinal fluid outflow system. Cerebrospinal Fluid Res. 7, 9. DOI:10.1186/1743-8454-7-9

Pollay, M., Hisey, B., Reynolds, E., Tomkins, P., Stevens, A.F., Smith, R., 1985. Choroid Plexus Na+/K+-activated Adenosine Triphosphatase and Cerebrospinal Fluid Formation. Neurosurgery 17, 768–772. DOI:10.1227/00006123-198511000-00007

Praetorius, J., 2007. Water and solute secretion by the choroid plexus. Pflügers Arch. - Eur. J. Physiol. 454, 1–18. DOI:10.1007/s00424-006-0170-6

Praetorius, J., Nielsen, S., 2006. Distribution of sodium transporters and aquaporin-1 in the human choroid plexus. Am. J. Physiol. Physiol. 291, C59–C67. DOI:10.1152/ajpcell.00433.2005

Quinkler, M., Sinha, B., Tomlinson, J.W., Bujalska, I.J., Stewart, P.M., Arlt, W., 2004. Androgen generation in adipose tissue in women with simple obesity - A site-specific role for 17β-hydroxysteroid dehydrogenase type 5. J. Endocrinol. 183, 331–342. DOI:10.1677/joe.1.05762

Rask, E., Walker, B.R., Söderberg, S., Livingstone, D.E.W., Eliasson, M., Johnson, O., Andrew, R., et al., 2002. Tissue-Specific Changes in Peripheral Cortisol Metabolism in Obese Women: Increased Adipose 11β-Hydroxysteroid Dehydrogenase Type 1 Activity. J. Clin. Endocrinol. Metab. 87, 3330–3336. DOI:10.1210/jcem.87.7.8661

Rauz, S., Walker, E.A., Shackleton, C.H.L., Hewison, M., Murray, P.I., Stewart, P.M., 2001. Expression and Putative Role of 11-Hydroxysteroid Dehydrogenase Isozymes within the Human Eye. Invest. Ophthalmol. Vis. Sci. 42, 2037–2042.

Reddy, D.S., 2010. Neurosteroids: endogenous role in the human brain and therapeutic potentials. Prog. Brain Res. 186, 113–37. DOI:10.1016/B978-0-444-53630-3.00008-7

Ricci, G., Volpi, L., Pasquali, L., Petrozzi, L., Siciliano, G., 2009. Astrocyte-neuron interactions in neurological disorders. J. Biol. Phys. 35, 317–36. DOI:10.1007/s10867-009-9157-9

Riley, M. V., Kishida, K., 1986. ATPases of ciliary epithelium: Cellular and subcellular distribution and probable role in secretion of aqueous humor. Exp. Eye Res. 42, 559–568. DOI:10.1016/0014-4835(86)90046-1

Riveros-McKay, F., Mistry, V., Bounds, R., Hendricks, A., Keogh, J.M., Thomas, H., Henning, E., et al., 2019. Genetic architecture of human thinness compared to severe obesity. PLOS Genet. 15, e1007603.

DOI:10.1371/journal.pgen.1007603

Rodahl, K., Moore, T., 1943. The vitamin A content and toxicity of bear and seal liver. Biochem. J. 37, 166–8.

Rosen, E.D., Spiegelman, B.M., 2014. What we talk about when we talk about fat. Cell 156, 20–44. DOI:10.1016/j.cell.2013.12.012

Rosenthal, J., Angel, A., Farkas, J., 1974. Metabolic fate of leucine: a significant sterol precursor in adipose tissue and muscle. Am. J. Physiol. Content 226, 411–418. DOI:10.1152/ajplegacy.1974.226.2.411

Rui, L., 2014. Energy Metabolism in the Liver, in: Comprehensive Physiology. John Wiley & Sons, Inc., Hoboken, NJ, USA, pp. 177–197. DOI:10.1002/cphy.c130024

Samancl, B., Samancl, Y., Tüzün, E., Altlokka-Uzun, G., Ekizoglu, E., Içöz, S., Sahin, E., et al., 2017. Evidence for potential involvement of pro-inflammatory adipokines in the pathogenesis of idiopathic intracranial hypertension. Cephalalgia 37, 525–531. DOI:10.1177/0333102416650705

Schiffer, L., Arlt, W., Storbeck, K.-H.H., 2018. Intracrine androgen biosynthesis, metabolism and action revisited. Mol. Cell. Endocrinol. 465, 4–26. DOI:10.1016/j.mce.2017.08.016

Schiffer, L., Kempegowda, P., Arlt, W., O'Reilly, M.W., 2017. Mechanisms in endocrinology: The sexually dimorphic role of androgens in human metabolic disease. Eur. J. Endocrinol. DOI:10.1530/EJE-17-0124

Schwalie, P.C., Dong, H., Zachara, M., Russeil, J., Alpern, D., Akchiche, N., Caprara, C., et al., 2018. A stromal cell population that inhibits adipogenesis in mammalian fat depots. Nature 559, 103–108. DOI:10.1038/s41586-018-0226-8

Schwartz, M.W., Peskind, E., Raskind, M., Boyko, E.J., Porte, D., 1996. Cerebrospinal fluid leptin levels: Relationship to plasma levels and to adiposity in humans. Nat. Med. 2, 589–593. DOI:10.1038/nm0596-589

Scotton, W.J., Botfield, H.F., Westgate, C.S.J., Mitchell, J.L., Yiangou, A., Uldall, M.S., Jensen, R.H., et al., 2018a. Topiramate is more effective than acetazolamide at lowering intracranial pressure. Cephalalgia 033310241877645. DOI:10.1177/0333102418776455

Scotton, W.J., Mollan, S.P., Walters, T., Doughty, S., Botfield, H.F., Markey, K., Yiangou, A., et al., 2018b. Characterising the patient experience of diagnostic lumbar puncture in idiopathic intracranial hypertension: a cross-sectional online survey. BMJ Open 8, e020445. DOI:10.1136/bmjopen-2017-020445

Shirai, Y., Yaku, S., Suzuki, M., 2004. Metabolic regulation of leptin production in adipocytes: A role of fatty acid synthesis intermediates. J. Nutr. Biochem.

15, 651–656. DOI:10.1016/J.JNUTBIO.2004.10.002

Sinclair, A.J., Burdon, M.A., Nightingale, P.G., Ball, A.K., Good, P., Matthews, T.D., Jacks, A., et al., 2010a. Low energy diet and intracranial pressure in women with idiopathic intracranial hypertension: prospective cohort study. BMJ 341, c2701–c2701. DOI:10.1136/bmj.c2701

Sinclair, A.J., Onyimba, C.U., Khosla, P., Vijapurapu, N., Tomlinson, J.W., Burdon, M.A., Stewart, P.M., et al., 2007. Corticosteroids, 11β-hydroxysteroid dehydrogenase isozymes and the rabbit choroid plexus. J. Neuroendocrinol. 19, 614–620. DOI:10.1111/j.1365-2826.2007.01569.x

Sinclair, A.J., Walker, E.A., Burdon, M.A., Van Beek, A.P., Kema, I.P., Hughes, B.A., Murray, P.I., et al., 2010b. Cerebrospinal fluid corticosteroid levels and cortisol metabolism in patients with idiopathic intracranial hypertension: A link between 11β-HSD1 and intracranial pressure regulation? J. Clin. Endocrinol. Metab. 95, 5348–5356. DOI:10.1210/jc.2010-0729

Skurk, T., Alberti-Huber, C., Herder, C., Hauner, H., 2007. Relationship between Adipocyte Size and Adipokine Expression and Secretion. J. Clin. Endocrinol. Metab. 92, 1023–1033. DOI:10.1210/jc.2006-1055

Smith, S.R., Lovejoy, J.C., Greenway, F., Ryan, D., deJonge, L., de la Bretonne, J., Volafova, J., et al., 2001. Contributions of total body fat, abdominal subcutaneous adipose tissue compartments, and visceral adipose tissue to the metabolic complications of obesity. Metabolism 50, 425–435. DOI:10.1053/META.2001.21693

Speake, T., Freeman, L.J., Brown, P.D., 2003. Expression of aquaporin 1 and aquaporin 4 water channels in rat choroid plexus. Biochim. Biophys. Acta - Biomembr. 1609, 80–86. DOI:10.1016/S0005-2736(02)00658-2

Spector, R., Johanson, C.E., 2014. The nexus of vitamin homeostasis and DNA synthesis and modification in mammalian brain. Mol. Brain 7, 3. DOI:10.1186/1756-6606-7-3

Spector, R., Keep, R.F., Robert Snodgrass, S., Smith, Q.R., Johanson, C.E., 2015. A balanced view of choroid plexus structure and function: Focus on adult humans. Exp. Neurol. 267, 78–86. DOI:10.1016/J.EXPNEUROL.2015.02.032

Steffensen, A.B., Oernbo, E.K., Stoica, A., Gerkau, N.J., Barbuskaite, D., Tritsaris, K., Rose, C.R., et al., 2018. Cotransporter-mediated water transport underlying cerebrospinal fluid formation. Nat. Commun. 9, 2167. DOI:10.1038/s41467-018-04677-9

Sterling, D., Reithmeier, R.A., Casey, J.R., 2001. A transport metabolon. Functional interaction of carbonic anhydrase II and chloride/bicarbonate exchangers. J. Biol. Chem. 276, 47886–94. DOI:10.1074/jbc.M105959200

Stewart, P.M., Boulton, A., Kumar, S., Clark, P.M.S., Shackleton, C.H.L., 1999.

Cortisol Metabolism in Human Obesity: Impaired Cortisone→Cortisol Conversion in Subjects with Central Adiposity [1]. J. Clin. Endocrinol. Metab. 84, 1022–1027. DOI:10.1210/jcem.84.3.5538

Stoffel-Wagner, B., Watzka, M., Steckelbroeck, S., Ludwig, M., Clusmann, H., Bidlingmaier, F., Casarosa, E., et al., 2003. Allopregnanolone serum levels and expression of 5α-reductase and 3α-hydroxysteroid dehydrogenase isoforms in hippocampal and temporal cortex of patients with epilepsy. Epilepsy Res. 54, 11–19. DOI:10.1016/S0920-1211(03)00036-6

Subramanian, A., Tamayo, P., Mootha, V.K., Mukherjee, S., Ebert, B.L., Gillette, M.A., Paulovich, A., et al., 2005. Gene set enrichment analysis: a knowledge-based approach for interpreting genome-wide expression profiles. Proc. Natl. Acad. Sci. U. S. A. 102, 15545–50. DOI:10.1073/pnas.0506580102

Subramanian, P.S., Goldenberg-Cohen, N., Shukla, S., Cheskin, L.J., Miller, N.R., 2004. Plasma ghrelin levels are normal in obese patients with idiopathic intracranial hypertension (pseudotumor cerebri). Am. J. Ophthalmol. 138, 109–113. DOI:10.1016/J.AJO.2004.02.014

Sun, K., Kusminski, C.M., Scherer, P.E., 2011. Adipose tissue remodeling and obesity. J. Clin. Invest. 121, 2094–101. DOI:10.1172/JCI45887

Taksali, S.E., Caprio, S., Dziura, J., Dufour, S., Calí, A.M.G., Goodman, T.R., Papademetris, X., et al., 2008. High visceral and low abdominal subcutaneous fat stores in the obese adolescent: a determinant of an adverse metabolic phenotype. Diabetes 57, 367–71. DOI:10.2337/db07-0932

Tantama, M., Martínez-François, J.R., Mongeon, R., Yellen, G., 2013. Imaging energy status in live cells with a fluorescent biosensor of the intracellular ATP-to-ADP ratio. Nat. Commun. 4, 2550. DOI:10.1038/ncomms3550

Taponen, S., Martikainen, H., Järvelin, M.-R., Laitinen, J., Pouta, A., Hartikainen, A.-L., Sovio, U., et al., 2003. Hormonal Profile of Women with Self-Reported Symptoms of Oligomenorrhea and/or Hirsutism: Northern Finland Birth Cohort 1966 Study. J. Clin. Endocrinol. Metab. 88, 141–147. DOI:10.1210/jc.2002-020982

Toker, E., Yenice, O., Temel, A., 2003. Influence of serum levels of sex hormones on intraocular pressure in menopausal women. J. Glaucoma 12, 436–40.

Tomlinson, J.W., Moore, J., Cooper, M.S., Bujalska, I., Shahmanesh, M., Burt, C., Strain, A., et al., 2001. Regulation of Expression of 11β-Hydroxysteroid Dehydrogenase Type 1 in Adipose Tissue: Tissue-Specific Induction by Cytokines [1]. Endocrinology 142, 1982–1989. DOI:10.1210/endo.142.5.8168

Tomlinson, J.W., Sinha, B., Bujalska, I., Hewison, M., Stewart, P.M., 2002.

Expression of 11β-Hydroxysteroid Dehydrogenase Type 1 in Adipose Tissue Is Not Increased in Human Obesity. J. Clin. Endocrinol. Metab. 87, 5630–5635. DOI:10.1210/jc.2002-020687

Toscano, V., Sancesario, G., Bianchi, P., Cicardi, C., Casilli, D., Giacomini, P., 1991. Cerebrospinal fluid estrone in pseudotumor cerebri: A change in cerebral steroid hormone metabolism? J. Endocrinol. Invest. 14, 81–86. DOI:10.1007/BF03350271

Uldall, M.S., Botfield, H.F., Jansen-Olesen, I., Sinclair, A.J., Jensen, R., 2017. Acetazolamide lowers intracranial pressure and modulates the cerebrospinal fluid secretion pathway in healthy rats. Neurosci. Lett. 645, 33–39. DOI:10.1016/j.neulet.2017.02.032

Uldall, M.S., Juhler, M., Skjolding, A.D., Kruuse, C., Jansen-Olesen, I., Jensen, R., 2014. A novel method for long-term monitoring of intracranial pressure in rats. J. Neurosci. Methods 227, 1–9. DOI:10.1016/j.jneumeth.2014.01.036

Vates, T.S., Bonting, S.L., Oppelt, W.W., 1964. Na-K activated adenosine triphosphatase formation of cerebrospinal fluid in the cat. Am. J. Physiol. Content 206, 1165–1172. DOI:10.1152/ajplegacy.1964.206.5.1165

Visser, M., Bouter, L.M., McQuillan, G.M., Wener, M.H., Harris, T.B., 1999. Elevated C-Reactive Protein Levels in Overweight and Obese Adults. JAMA 282, 2131. DOI:10.1001/jama.282.22.2131

Vogh, B.P., Langham, M.R., 1981. The effect of furosemide and bumetanide on cerebrospinal fluid formation. Brain Res. 221, 171–183. DOI:10.1016/0006-8993(81)91071-4

Wagshul, M.E., Eide, P.K., Madsen, J.R., 2011. The pulsating brain: A review of experimental and clinical studies of intracranial pulsatility. Fluids Barriers CNS 8, 5. DOI:10.1186/2045-8118-8-5

Walker, A.E., Adamkiewicz, J.J., 1964. Pseudotumor Cerebri Associated With Prolonged Corticosteroid Therapy. JAMA 188, 779–784. DOI:10.1001/jama.1964.03060350005001

Wall, M., McDermott, M.P., Kieburtz, K.D., Corbett, J.J., Feldon, S.E., Friedman, D.I., Katz, D.M., et al., 2014. Effect of Acetazolamide on Visual Function in Patients With Idiopathic Intracranial Hypertension and Mild Visual Loss. Jama 311, 1641. DOI:10.1001/jama.2014.3312

Walter, B.A., Valera, V.A., Takahashi, S., Ushiki, T., 2006. The olfactory route for cerebrospinal fluid drainage into the peripheral lymphatic system. Neuropathol. Appl. Neurobiol. 32, 388–396. DOI:10.1111/j.1365-2990.2006.00737.x

Warner, J.E.A., Larson, A.J., Bhosale, P., Digre, K.B., Henley, C., Alder, S.C., Katz, B.J., et al., 2007. Retinol-Binding Protein and Retinol Analysis in

Cerebrospinal Fluid and Serum of Patients With and Without Idiopathic Intracranial Hypertension. J. Neuro-Ophthalmology 27, 258–262. DOI:10.1097/WNO.0b013e31815b9af0

Wasinger, V.C., Zeng, M., Yau, Y., 2013. Current status and advances in quantitative proteomic mass spectrometry. Int. J. Proteomics 2013, 180605. DOI:10.1155/2013/180605

Wibroe, E.A., Yri, H.M., Jensen, R.H., Wibroe, M.A., Hamann, S., 2016. Osmolality of Cerebrospinal Fluid from Patients with Idiopathic Intracranial Hypertension (IIH). PLoS One 11, e0146793. DOI:10.1371/journal.pone.0146793

Yiangou, A., Mitchell, J., Markey, K.A., Scotton, W.J., Nightingale, P., Botfield, H.F., Ottridge, R., et al., 2018. Therapeutic lumbar puncture for headache in idiopathic intracranial hypertension: Minimal gain, is it worth the pain? Cephalalgia 033310241878219. DOI:10.1177/0333102418782192

Yri, H.M., Fagerlund, B., Forchhammer, H.B., Jensen, R.H., 2014a. Cognitive function in idiopathic intracranial hypertension: A prospective case-control study. BMJ Open 4, e004376. DOI:10.1136/bmjopen-2013-004376

Yri, H.M., Rönnbäck, C., Wegener, M., Hamann, S., Jensen, R.H., 2014b. The course of headache in idiopathic intracranial hypertension: A 12-month prospective follow-up study. Eur. J. Neurol. 21, 1458–1464. DOI:10.1111/ene.12512

Zada, G., Tirosh, A., Kaiser, U.B., Laws, E.R., Woodmansee, W.W., 2010. Cushing's Disease and Idiopathic Intracranial Hypertension: Case Report and Review of Underlying Pathophysiological Mechanisms. J. Clin. Endocrinol. Metab. 95, 4850–4854. DOI:10.1210/jc.2010-0896

Zheng, W., Zhao, Q., 2002. Establishment and characterization of an immortalized Z310 choroidal epithelial cell line from murine choroid plexus. Brain Res. 958, 371–380. DOI:10.1016/S0006-8993(02)03683-1

Zlokovic, B. V., Jovanovic, S., Miao, W., Samara, S., Verma, S., Farrell, C.L., 2000. Differential Regulation of Leptin Transport by the Choroid Plexus and Blood-Brain Barrier and High Affinity Transport Systems for Entry into Hypothalamus and Across the Blood-Cerebrospinal Fluid Barrier [1]. Endocrinology 141, 1434–1441. DOI:10.1210/endo.141.4.7435